Role of DDX1 in Embryonic Development

By

Yixiong Wang

A thesis submitted in partial fulfillment of the requirements for the degree of

Doctor of Philosophy

In

Cancer Sciences

Department of Oncology

University of Alberta

© Yixiong Wang, 2021

Abstract

DEAD Box 1 (DDX1) is a member of the DEAD box protein family of RNA helicases involved in all aspects of RNA metabolism. Although several DEAD box proteins have been well characterized, the biochemical activity of the majority of DEAD box proteins remains to be studied. DDX1 is mostly localized in the nucleus of most cell types analysed; however, it is also abundant in the cytoplasm of tumours in which it is overexpressed. DDX1 plays a variety of roles ranging from RNA transport to the repair of DNA double stranded breaks. *Ddx1* knockout results in abnormal development with reduced body size and aberrant gametogenesis in *Drosophila*, and embryonic lethality in mouse.

My PhD research project is focused on the characterization of DDX1 in early developmental stages of mouse embryos. In Chapter 2, we report that DDX1 forms large cytoplasmic aggregates that do not co-localize with any known organelle or cytoplasmic granule markers in embryos, with the exception of stress granule markers TIA-1 and TIAR. We also show that *Ddx1*$^{-/-}$ mouse embryos stall at the 2- to 4-cell stages *in vitro*. Given that DDX1 is an RNA binding protein, and maternal RNAs are essential for early embryonic development, we pursued a possible relationship between DDX1 aggregates and RNAs. Using RNase A treatment, we obtained evidence that the role of DDX1 in mouse embryos is RNA dependent. By carrying out DDX1-RNA immunoprecipitation and qPCR analysis, we found that

DDX1 binds to a subset of maternal RNAs that are critical for early-stage embryonic development.

In Chapter 3, we further characterized the role of DDX1 in early-stage mouse embryos using electron microscopy (EM) and Stimulated Emission Depletion (STED) microscopy. The latter provides greatly enhanced resolution compared to conventional confocal microscopy. With STED microscopy, we showed that DDX1 forms aggregates at the subplasmalemmal cytoplasm of 2-cell embryos and forms ring-like clusters. With EM, we discovered that DDX1 localizes to previously uncharacterized membrane bound vesicles. These vesicles contain an electron dense RNA core as well as Ca^{2+}. We named these vesicles MARVs (Membrane Associated RNA-containing Vesicles). In *Ddx1*$^{-/-}$ embryos, we observe greatly reduced numbers of MARVs and misregulation of Ca^{2+}, which results in the upregulation of reactive oxygen species (ROS) in mitochondria, as well as increased nuclear and mitochondrial fragmentation. Given that DDX1 binds to maternal RNAs in 2-cell embryos, and Ca^{2+} indirectly regulates the phosphorylation of cytoplasmic polyadenylation factor CPEB1, we examined whether cytoplasmic polyadenylation factors were present in MARVs. Intriguingly, we found that two cytoplasmic polyadenylation factors, CPEB1 and CPSF2, co-localize with DDX1. Because CPEB1 and CPSF2 are critical for the initiation of the cytoplasmic polyadenylation process, our results suggest that MARVs may be hubs for cytoplasmic polyadenylated RNAs, with DDX1 either protecting these RNAs until they are required or playing a role in polyadenylation.

In Chapter 4, we address the importance of DDX1 in early embryonic development. We show that, in contrast to our *in vitro* work, *Ddx1*$^{-/-}$ embryos do not survive past the 1-cell stage *in vivo*. To further characterize DDX1-binding RNAs, we carried out DDX1 RNA-immunoprecipitation using lysates prepared from 2-cell embryos, followed by HiSeq analysis. Surprisingly, approximately 20% of the transcripts identified by RIP-seq were processed pseudogenes and ~24% were long non-coding RNAs. As pseudogenes and long non-coding RNAs are important in the generation of endogenous siRNAs in early embryonic development, we propose that DDX1 may function with these pseudogenes in the protection or processing of RNAs.

These studies reveal critical roles for DDX1 and MARVs in early mouse embryonic development. Future work will focus on the mechanism of action of DDX1 and MARVs vis-a-vis Ca^{2+} regulation, cytoplasmic RNA polyadenylation and endogenous siRNAs, all of which are essential for early embryonic development. Given that in yeast and human cells DEAD box proteins also regulate RNA-containing phase-separated structures, which are now known to be membrane-less organelles, future work will address whether the RNA cores that reside in MARVs are phase-separated RNA droplets that control the fate of maternal RNAs during early embryonic development.

Preface

This thesis is original work by Yixiong Wang.

This work received research ethics approval from the Cross Cancer Institute Animal Care Committee, #BC11185.

A version of chapter 2 has been published as Hildebrandt MR*, Wang Y*, Li L, Yasmin L, Glubrecht DD, Godbout R. Cytoplasmic aggregation of DDX1 in developing embryos: Early embryonic lethality associated with *Ddx1* knockout. Dev Biol. 2019 Nov 15;455(2):420-433. doi: 10.1016/j.ydbio.2019.07.014. *These authors contributed equally to this work. Immunohistochemistry was performed by Darryl Glubrecht. RNA immunoprecipitation and western blot were performed by Dr. Lei Li. I was responsible for data analysis and interpretation, PCR, embryo collection, immunofluorescence staining and imaging, and writing the manuscript. Dr. Matthew Hildebrandt assisted with data analysis, immunofluorescence staining and imaging and writing the manuscript. Dr. Lubna Yasmin assisted with embryo collection and immunofluorescence staining. Dr. Roseline Godbout was involved in all stages of the project and in writing the manuscript.

Acknowledgement

The work presented in this thesis would not have been possible without the help and support of a number of people during both my undergraduate and graduate studies at the University of Alberta. Above all, I would like to express my greatest thanks to my mentor and supervisor, Dr. Roseline Godbout. Over the years of me being her project student as well as graduate student, I have received an enormous amount of support and guidance that I needed to successfully complete my Ph.D. program. We had our differences in terms of ideas, experimental approaches. Thank you Roseline for putting up with me and continuously showing me what it requires to become a Ph.D. I would also like to thank Dr. George Owttrim for his support and guidance when I was a lost undergraduate student seeking direction and opportunities.

I'm very fortunate to be part of Dr. Godbout's lab with a group of focused and talented researchers in the Experimental Oncology division. There are several members that I would like to thank specifically for their assistance: Dr. Lei Li, with whom I have worked closely during my time in the lab and who has been a valuable resource for technical support and discussions; Dr. Matthew Hildebrandt, for teaching me many of the embryo manipulation techniques I needed for the completion of this work; Dr. Lubna Yasmin, for being the only other member that knows embryo manipulation and working closely with me during the final years of the completion of my Ph.D. I would also like to thank other members of the

Godbout lab for their support over the years: Stanley, Liz, Darryl, Devon, Rongzong, Saket, Kevin, Daniel, Mansi, Miranda, Xia, David, and Lucy.

I would also like to give special thanks to our advanced imaging facility and the well-trained staff: Dr. Xuejun Sun, Gerry Barron, Dr. Guobin Sun and Priscilla Gao for all my imaging work which made up 90% of this thesis. Without them, none of my work would have been possible.

Finally, this Ph.D. would not have been possible without the love and continuous support of my family, especially my wife Qi (Cherry). She has been with me through the great, the bad, the laugh and the tears. She's always there to give me the strength I need to get through the tough times. I would also like to thank my Mom and Dad for their support through my studies and for providing me a safe harbor that I needed when I needed to escape. Moreover, I need to thank my uncle (Xiao), who inspired me in doing experiments during my childhood, for the idea of calcium. Lastly, I am also thankful for my dog, Dading, who is always there for a cozy therapy.

Table of Contents

List of Figures

List of Tables

Abbreviations

$\Delta\Psi_m$	Mitochondrial inner membrane potential
ADP	Adenosine diphosphate
ATP	Adenosine triphosphate
Ago	Argonaute
β-ME	β-mercaptoethanol
β-gal	β-galactosidase
Ca^{2+}	Calcium
cDNA	Complementary DNA
CPEB	Cytoplasmic polyadenylation element binding protein
CPSF	Cleavage and polyadenylation specificity factor
CstF	Cleavage stimulation factor
DAPI	4’,6-diamidino-2-pheylindole
DDX	DEAD box
DNA	Deoxyribonucleic acid
ds	Double-strand
DTT	Dithiothreitol
E	Embryonic day
ECL	Enhanced chemiluminescence
EDTA	Ethylenediaminetetraacetic acid
eEF	Eukaryotic elongation factor
EFTEM	Energy filtered transmission electron microscopy
eIF	Eukaryotic initiation factor
ER	Endoplasmic reticulum
ES	Embryonic stem
EtOH	Ethanol

Exo1	Exonuclease 1
FBS	Fetal bovine serum
Gy	Gray
H2AX	Histone 2A isoform X
HIV	Human immunodeficiency virus
HR	Homologous recombination
HRP	Horseradish peroxidase
IF	Immunofluorescence
IHC	Immunohistochemistry
IR	Ionizing radiation
kb	Kilobases
kDa	Kilodalton
LSM	Laser scanning microscope
LLPS	Lipid-lipid phase separation
M	Molar
µM	Micromolar
mM	Millimolar
µg	Microgram
mg	Milligram
µl	Microliter
ml	Milliliter
µm	Micrometer
MRN	Mre11, Rad50 and Nbs1 complex
mRNA	Messenger RNA
mt	Mitochondria
mtROS	Mitochondrial reactive oxygen species
MZT	Maternal to zygotic transition

MARV	Membrane Associated RNA-containing Vesicle
nM	Nanomolar
ng	Nanogram
nm	Nanometer
NHEJ	Non-homologous end joining
P	Postnatal
PAGE	Polyacrylamide gel electrophoresis
PB	Processing bodies
PBS	Phosphate-buffered saline
PCR	Polymerase chain reaction
PM	Plasma membrane
RISC	RNA induced silencing complex
RNA	Ribonucleic acid
RNase	Ribonuclease
RNP	Ribonucleoprotein
rRNA	Ribosomal RNA
ROS	Reactive oxygen species
RT	Reverse transcription
SCA	Subcortical aggregates
SG	Stress granule
siRNA	Small interfering RNA
SMN	Survival motor neuron
SPRY	Dual specific kinase sp1a of *Dictyostelium* and rabbit ryanodine receptors
STED	Stimulated emission depletion
TEM	Transmission electron microscopy
TIA-1	T-cell intracytoplasmic antigen

TIAR	TIA1 related
tRNA	Transfer RNA
UV	Ultraviolet
WT	Wildtype
Zar	Zygote arrest
ZGA	Zygotic gene activation

Chapter 1.

Introduction

1.1 DEAD box protein family

RNA helicases are enzymes found in all three domains of life. They use ATP/ADP to modify RNA secondary structures and are involved in all aspects of RNA metabolism, from transcription to mRNA decay (Linder, Lasko et al. 1989, Abdelhaleem 2005, Linder 2006, Li, Monckton et al. 2008, Gustafson and Wessel 2010, Jankowsky and Putnam 2010, Pan and Russell 2010, Jarmoskaite and Russell 2011, Linder and Jankowsky 2011, Pyle 2011, Liu, Putnam et al. 2014, Kellner, Reinstein et al. 2015, Linder and Fuller-Pace 2015, Li, Germain et al. 2016). Although RNAs can encode proteins, they can also affect a variety of other activities, such as enzymatic activity, gene expression, protein translation, gene stability, etc. depending on their secondary structures (Higgs and Lehman 2015, Nelson and Breaker 2017). As RNA secondary structure is essential for the correct RNA functions, alterations in RNA helicase activity may result in the production of RNAs with incorrect functions.

1.1.1 DEAD box protein structures

RNA helicases can be classified into superfamilies based on their conserved sequences (Fairman-Williams, Guenther et al. 2010). The DEAD box family, along with the DEAH and DExH/D RNA helicases, falls within the helicase superfamily 2 **(Fig. 1.1A)**. DEAD box proteins are characterized by 12 conserved motifs: Q, I, Ia, Ib, Ic, II, III, IV, IVa, V, Va and VI, among which is the D-E-A-D motif

(Asp-Glu-Ala-Asp) (Gorbalenya and Koonin 1993). Structurally, DEAD box proteins contain two tandem RecA-like domains that can fluctuate between open or closed configurations (Benz, Trachsel et al. 1999, Story, Li et al. 2001). Motifs Q to III belong to the N-terminal RecA-like domain whereas the remaining motifs belong to the C-terminal RecA-like domain. Motifs III and Va primarily function as domain coupling motifs to stabilize the two domains (Hilbert, Karow et al. 2009, Banroques, Doere et al. 2010, Schutz, Karlberg et al. 2010). The Q motif is responsible for the recognition of the adenine base of ATP (Tanner 2003, Cordin, Tanner et al. 2004). Coordinating with motif Q, the ATP binding pocket is formed by motifs I, II, IV and stabilized by a Mg^{2+} ion. Structural modeling of conserved RNA binding motifs in DEAD box proteins has shown that the binding to RNA molecules is almost entirely through the RNA backbone (Bono, Ebert et al. 2006, Sengoku, Nureki et al. 2006). This binding property indicates that DEAD box proteins may not recognize specific RNA sequences. Therefore, the DEAD box proteins are likely to require other protein partners to unwind specific substrates.

1.1.2 DEAD box protein functions

DEAD box proteins can alter RNA secondary structures, dissociate double stranded RNAs, and sometimes RNA/DNA duplexes as well (Rogers, Richter et al. 1999, Chen, Potratz et al. 2008, Li, Monckton et al. 2008, Li, Germain et al. 2016). The DEAD box proteins take part in essentially all aspects of RNA metabolism pathways and in many cases, they play critical roles in these pathways. Like many

other proteins involved in RNA metabolism, the DEAD box proteins function as part of large complexes or structures such as the spliceosome complex, RNA transport complex and stress granules (Jarmoskaite and Russell 2011, Shih, Wang et al. 2012, Shih and Lee 2014, Jongjitwimol, Baldock et al. 2016). In spite of limitations inherent to biochemical assays (i.e. using purified proteins with limited numbers of co-factors), DEAD box proteins have been implicated in a wide range of ATP-dependent and independent activities (reviewed in (Linder and Jankowsky 2011)).

In vitro RNA-RNA and/or RNA-DNA unwinding activity has been documented for a number of DEAD box proteins, such as DDX1, eIF4A (DDX2), An3 (DDX3) and Vasa (DDX4) (Rozen, Edery et al. 1990, Gururajan, Mathews et al. 1994, Liang, Diehl-Jones et al. 1994, Li, Monckton et al. 2008). The binding of DEAD box proteins to their RNA substrates requires a conformational change induced by ATP binding (Andersen, Ballut et al. 2006, Sengoku, Nureki et al. 2006, Mallam, Del Campo et al. 2012). The two globular structures of the DEAD box proteins, i.e. helicase domains I and II, enable them to bind and unwind local RNA structures without translocating or progressively unwinding (Cordin, Banroques et al. 2006, Sengoku, Nureki et al. 2006, Mallam, Del Campo et al. 2012). In keeping with this mode of unwinding, most DEAD box proteins have been shown to unwind duplexes that are 10 or 12 base pairs in length (Rogers, Richter et al. 1999, Chen, Potratz et al. 2008). Although the majority of DEAD box family members are reported to have limited processivity, some DEAD box proteins can unwind longer

duplex structures, for example, DDX1, DDX25 and DDX21 can unwind more than 20 bp structures whereas DDX3, DDX5, DDX17 and DDX43 can even unwind more than 40 bp structures (Hirling, Scheffner et al. 1989, Flores-Rozas and Hurwitz 1993, Tang, Tsai-Morris et al. 1999, Rossler, Straka et al. 2001, Yan, Mouillet et al. 2003, Yedavalli, Neuveut et al. 2004, Li, Monckton et al. 2008, Linley, Mathieu et al. 2012, Mathieu, Miles et al. 2014). However, the exact mechanism by which these DEAD box proteins function remains unknown. The unwinding activity of those DEAD box proteins that can unwind longer duplexes may depend on substrate, protein concentration, reaction time and conditions etc. For example, DDX1 has been reported to unwind both 10 bp and 29 bp structures depending on presence of ATP or ADP (Li, Monckton et al. 2008, Kellner, Reinstein et al. 2015). DDX43 has also been reported to unwind either 13 bp duplex or 40 bp duplex depending on assay conditions (Linley, Mathieu et al. 2012, Mathieu, Miles et al. 2014, Talwar, Vidhyasagar et al. 2017). Although ATP binding is needed for the binding activity of DEAD box proteins to their substrates, most DEAD box proteins may not require ATP hydrolysis for their unwinding activity (Andersen, Ballut et al. 2006, Del Campo, Tijerina et al. 2007, Chen, Potratz et al. 2008, Collins, Karlberg et al. 2009). Instead, ATP hydrolysis may be essential for the release of the substrates from the DEAD box proteins after unwinding (Liu, Putnam et al. 2008). This could be due to the conformational change induced by ATP upon substrate binding.

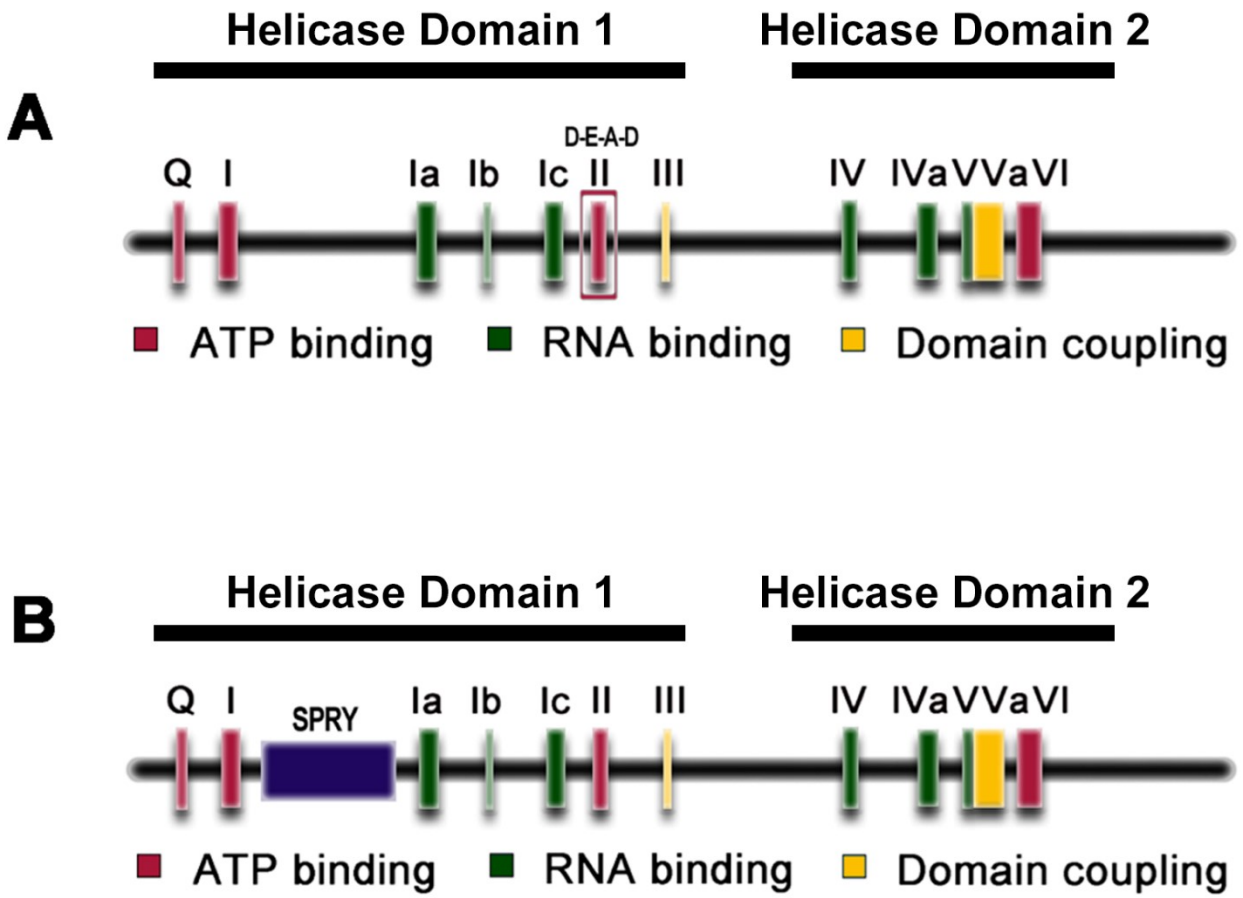
A
Helicase Domain 1
Helicase Domain 2
D-E-A-D
Q I Ia Ib Ic II III IV IVa V VaVI
ATP binding
RNA binding
Domain coupling
B
Helicase Domain 1
Helicase Domain 2
Q I SPRY Ia Ib Ic II III IV IVa V VaVI
ATP binding
RNA binding
Domain coupling

Figure 1.1 Conserved motifs of DEAD box proteins. (A) Motifs shared by the DEAD box family including the ATP binding motif, D(asp)-E(glu)-A(ala)-D(asp). ATP binding motifs are shown in red; RNA binding motifs are shown in green and domain coupling motifs are shown in yellow. (B) DDX1 motifs. In addition to the 12 conserved motifs shared by all members of the DEAD box family, DDX1 has a SPRY domain that has been implicated in protein-protein interaction. Figure adapted from Matthew Hildebrandt's thesis with modifications.

Another important role for DEAD box proteins is remodelling of the RNP complexes. Structural analysis shows that the binding of DEAD box proteins to their substrates is almost entirely based on the RNA backbone, indicating that the binding of DEAD box proteins to their substrate may not be sequence related (Bono, Ebert et al. 2006, Sengoku, Nureki et al. 2006). The DEAD box proteins may be targeting their substrates through interaction with other proteins in the complexes or may be non-specifically binding to RNA substrates simply based on proximity. After binding to the RNA, those DEAD box proteins that take part in the remodeling of RNP complexes often remain bound to RNA duplexes and act as an anchor to recruit other proteins to the complex and/or modulate the binding of proteins to the RNA duplexes (Andersen, Ballut et al. 2006, Bowers, Maroney et al. 2006, Tran, Zhou et al. 2007, Han, Liu et al. 2014).

The binding partners for some of the well-studied DEAD box proteins have been identified. These partner proteins enhance the activities of their partner

DEAD box proteins. For example, eIF4A (DDX2) is a key component of the eukaryotic translation initiation complex (Edery, Humbelin et al. 1983, Seal, Schmidt et al. 1983). Although eIF4A has been shown to unwind DNA-RNA and RNA-RNA duplexes, it has a low affinity for its binding substrates compared to other DEAD box proteins (Rogers, Richter et al. 1999). eIF4G is also involved in eukaryotic translation initiation (Tarun, Wells et al. 1997). When eIF4G binds to eIF4A, the RNA release and ATPase activity of eIF4A is significantly enhanced (Schutz, Bumann et al. 2008). Another example is DEAD box protein Dbp5 (DDX19) which demonstrates enhanced activity when bound to Gle1 (Montpetit, Thomsen et al. 2011). Gle1 and eIF4G have similar structures and bind to similar regions within their partner DEAD box proteins, Dbp5 and eIF4A, respectively (Linder and Jankowsky 2011). Based on these data, one may postulate that other DEAD box proteins may also have similar helper proteins.

1.2 DEAD box 1 (DDX1)

DDX1 was originally cloned from a subtracted retinoblastoma cDNA library prepared from retinoblastoma cell lines in which *DDX1* is amplified (Godbout and Squire 1993). *DDX1* amplification is always accompanied by *MYCN* amplification, with *MYCN* located ~340 kb downstream of *DDX1* on chromosome 2p24 (Kuroda, White et al. 1996, Pandita, Godbout et al. 1997). *DDX1* was subsequently found to also be co-amplified with *MYCN* in neuroblastoma (Squire, Thorner et al. 1995, Godbout, Packer et al. 1998, Godbout, Li et al. 2007) and alveolar

rhabdomyosarcoma (Barr, Duan et al. 2009). Amplification of *DDX1*, along with the fact that DDX1 is over-expressed in the subset of retinoblastoma and neuroblastoma in which it is amplified first suggested a potential role for DDX1 in cancer.

In mammals, DDX1 is expressed in virtually all tissues and cell lines (Godbout and Squire 1993, Godbout, Packer et al. 2002, Fagerberg, Hallstrom et al. 2014). Orthologues of *DDX1* are found in mammals, flies, nematode, amoeba and archaea, but not in yeast or bacteria.

1.2.1 DDX1 structure

In addition to the 12 conserved motifs found in DEAD box proteins, DDX1 has a unique ~150 amino acid SPRY domain located between motifs I and Ia **(Fig. 1.1B)** (Godbout and Squire 1993). SPRY domains are believed to be involved in either protein-protein or protein-RNA interaction (D'Cruz, Babon et al. 2013, Kellner and Meinhart 2015). Furthermore, unlike other DEAD box proteins with unique sequences in the N-terminus, DDX1's Q motif is found immediately after the start codon. The amino acid sequence of the C-terminus of DDX1 is unique, with no homology to other proteins. Thus, the C-terminal domain may be important to DDX1-specific functions or binding partners of DDX1 (Han, Liu et al. 2014).

Crystallization of the entire DDX1 protein has not been successful possibly due to the instability of its two helicase domains. The only domain of DDX1 that

has been successfully crystallized is its isolated SPRY domain (Kellner and Meinhart 2015). The authors found that the DDX1 SPRY domain has a β-sheet structure similar to that observed in other SPRY containing proteins; however, the loop regions of the DDX1 SPRY domain are different from that in other proteins. These loop regions have been proposed to be essential for protein-protein interaction (Woo, Suh et al. 2006, Filippakopoulos, Low et al. 2010). Instead of classic loop regions, the SPRY domain in DDX1 has an area of positively charged amino acids on the protein surface, which may serve as a replacement for loop regions and promote protein-protein interaction through electrostatic surface potential (Kellner and Meinhart 2015). The positively charged surface structure of DDX1 is evolutionarily conserved. Once the binding substrates of DDX1 protein have been identified, it may be possible to stabilize DDX1 configuration allowing crystallization.

1.2.2 SPRY domain

The SPRY domain is named after the kinase spore lysis A in *Dictyostelium* and mammalian ryanodine receptors (RyR) in which it was first identified (Ponting, Schultz et al. 1997, Rhodes, de Bono et al. 2005, Woo, Suh et al. 2006). It is found across all phylogenetic trees, and across all three domains of life (Rhodes, de Bono et al. 2005). The SPRY domain is not defined based on amino acid sequence. Instead, the SPRY domain is classified by its β-sheet sandwich structure (Woo, Suh et al. 2006). SPRY domains have been found at both the N- and C-termini of

proteins, as well as central locations suggesting that the SPRY domain has no positional preference (Ponting, Schultz et al. 1997, Godbout, Packer et al. 2002, Tae, Casarotto et al. 2009). More than 6000 eukaryotic proteins contain SPRY domains based on Genomic SMART database (Letunic, Doerks et al. 2015, Letunic and Bork 2018). Proteins with SPRY domains have been placed in the pathways associated with the following categories based on KEGG pathway analysis: calcium signaling pathway (~45.8% of proteins with SPRY domains; map04020), ubiquitin mediated proteolysis (~25%; map04120), tryptophan metabolism (~12.5%; map00380), cerebellar long-term depression involving a decrease in synaptic strength (Ito 2001, Metzger and Kapfhammer 2003) (~12.5%; map04730) and purine metabolism (~4.2%; map00230) **(Fig. 1.2)**. Notably, these pathways include activation of axonal parallel fibers in the cerebellum, which leads to glutamate release and activation of AMPA receptors and metabotropic glutamate receptors (Daniel, Levenes et al. 1998, Levenes, Daniel et al. 1998), as well as activation of axonal climbing fibers, which opens voltage-gated Ca^{2+} channels (Levenes, Daniel et al. 1998, Metzger and Kapfhammer 2003). In humans, 57 proteins containing SPRY domains have been identified in completely sequenced genomes, with a total of 115 proteins identified in proteomes (SMART database). Of the better known SPRY-containing proteins, RyRs are involved in calcium-release channels on sarcoplasmic reticulum (Ponting, Schultz et al. 1997). As the majority of SPRY domain-containing proteins are involved in calcium

signalling, it is possible that DDX1 plays a role in calcium signalling as well, although an exact role for the DDX1 SPRY domain awaits further studies.

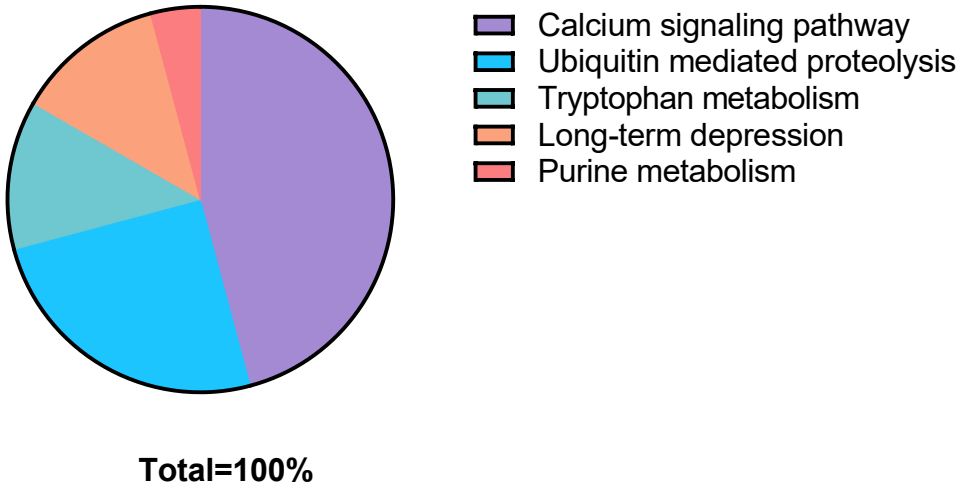

Figure 1.2 Pie chart of SPRY domain containing proteins. SPRY domain containing proteins were identified using SMART database and the metabolism section data was extracted and plotted with Prism.

A domain similar to SPRY, the B30.2 domain, has been identified in human, mouse, chicken and frog (Rhodes, de Bono et al. 2005). The B30.2 domain is ~70 amino acids longer than SPRY and only located at the C-terminus of proteins (Tae, Casarotto et al. 2009). These ~70 amino acids specific to the B30.2 domain are identified as the PRY region which is similar to the N-terminal half of the SPRY domain. B30.2 domains also have a SPRY domain which is located adjacent to and downstream of the PRY region (D'Cruz, Babon et al. 2013). For this reason, the B30.2 domain is also referred to as the PRY/SPRY domain. It is generally

thought that B30.2 and SPRY domains are of the same origin as they share similar amino acid sequences (Tazi-Ahnini, Henry et al. 1997, Henry, Mather et al. 1998). Since SPRY domain is found in all 3 domains of life, it's considered to be more ancient while B30.2 domain likely evolved at later evolutionary stages (Rhodes, de Bono et al. 2005). The B30.2 domain is believed to be evolutionary adapted for immune defense (Rhodes, de Bono et al. 2005).

1.2.3 DDX1 functions

1.2.3.1 DDX1 nuclear bodies

Although DDX1 protein is primarily located in the nucleus of most cell types, it is also found in the cytoplasm (Bleoo, Sun et al. 2001, Fagerberg, Hallstrom et al. 2014). Levels of DDX1 in the cytoplasm are elevated in cell lines and tumours with amplified copies of the *DDX1* gene (Godbout, Li et al. 2007).

DDX1 forms foci in the nucleus throughout the cell cycle with the exception of mitosis (Bleoo, Sun et al. 2001). DDX1 nuclear foci are associated with other nuclear bodies such as Cajal bodies, gems and cleavage bodies (Bleoo, Sun et al. 2001, Li, Roy et al. 2006). These nuclear bodies are dynamic structures that contain protein factors required for pre-mRNA splicing, 3' processing as well as other RNA processing factors (Lamond and Spector 2003). Cajal bodies are often associated with cleavage bodies and have been shown to play parts in RNA processing including pre-mRNA 3' processing, snRNA posttranscriptional

modification, snRNP and snoRNP biogenesis, pre-rRNA processing, tRNA cleavage and histone mRNA processing (Murthy and Manley 1995, Schul, van Der Kraan et al. 1999, Bleoo, Sun et al. 2001, Darzacq, Jady et al. 2002, Jady, Darzacq et al. 2003, Li, Roy et al. 2006, Vitali and Kiss 2019). During S phase, DDX1 nuclear foci (DDX1 bodies) are co-localized with cleavage bodies, which in turn were found to be adjacent to Cajal bodies and gems (Li, Roy et al. 2006). Similar to DDX1, these nuclear bodies (Cajal bodies, gems and cleavage bodies) have not been found during mitosis. The association of DDX1 with these nuclear bodies suggests that DDX1 may play a role in RNA processing (Li, Roy et al. 2006).

Other than the above nuclear bodies, DDX1 has also been found to associate with the microprocessor complex (Han, Liu et al. 2014). The most important components of the microprocessor complex are DROSHA and DGCR8. During pri-miRNA processing by the microprocessor complex, DDX1 has been proposed to bind to a subset of pri-miRNAs in the nucleus and act as an anchor to recruit DROSHA and DGCR8. This recruitment would allow the microprocessor complex to process the pri-miRNAs thereby allowing miRNA biogenesis where the pri-miRNAs are cleaved into precursor miRNAs (pre-miRNAs). In the absence of DDX1, pri-miRNAs accumulate and mature miRNAs decrease indicating the failure of the first step of miRNA biogenesis.

1.2.3.2 DDX1 and cytoplasmic granules

In addition to DDX1's nuclear role, cytoplasmic DDX1 has been observed in mRNA transport complexes found in neurons and in stress granules (SGs) (Kanai, Dohmae et al. 2004, Hirokawa and Takemura 2005, Onishi, Kino et al. 2008, Miller, Blandford et al. 2009, Shih and Lee 2014). In neuronal cells, the transport of proteins to their functional sites through very long axons and dendrites is energy insufficient. Therefore, cells have evolved the ability to transport compact mRNAs through axons and dendrites for local translation (Kanai, Dohmae et al. 2004, Pushpalatha and Besse 2019). The mRNA transport complexes in neuronal cells serve as carriers of mRNAs. The intracellular transport of mRNAs requires functional complexes in both the nucleus and cytoplasm. The hCLE/C14orf166 protein is the main player in this process (Huarte, Sanz-Ezquerro et al. 2001). In the nucleus, hCLE is associated with the spliceosome complex and tRNA ligation complex for the nuclear processing of mRNAs (Rappsilber, Ryder et al. 2002, Popow, Englert et al. 2011). In the cytoplasm, hCLE forms a complex with DDX1, HSPC117 and FAM98B for the transport of mRNAs (Kanai, Dohmae et al. 2004, Perez-Gonzalez, Pazo et al. 2014). There is evidence supporting a role for translation initiation factors such as eIF4E in mRNA transport complexes (Jiang and Schuman 2002), thereby enabling local translation initiation once the mRNAs have reached their destination. Other proteins such as DDX3, Staufen and ALY, which play roles in mRNA export from the nucleus, are also present in mRNA transport complexes and may be involved in RNA processing or resolving the RNA granules upon reaching their destination (Kanai, Dohmae et al. 2004, Hirokawa

2006). In developing brain, RNA transport granules also carry ribosomal proteins to their destination (Elvira, Wasiak et al. 2006).

Stress granules (SGs) are large cytoplasmic aggregates (~100-2000 nm) that form when cells are under induced stress such as hypoxia, heat shock, UV, viral infection, oxidative stress etc. SGs are thought to contain stalled translation initiation complexes bound to RNA binding proteins (Kedersha, Gupta et al. 1999, Kedersha and Anderson 2002, Anderson and Kedersha 2006, Anderson and Kedersha 2008). The initiation step of SG formation is the phosphorylation of eIF2A which prevents the large ribosomal subunit from binding to mRNAs and results in decreased translation (Kedersha, Gupta et al. 1999). This translation stalling event prepares the cell for stress response.

During the stress response, RNAs are only transiently stored in SGs (Mollet, Cougot et al. 2008, Anderson and Kedersha 2009). This transient storage has the advantage of selectively translating proteins required for cells under stress. SGs have been shown to be associated with processing bodies (PBs) which contain proteins associated with miRNA (Ago2, DDX6) and proteins required for RNA degradation (DCP1/2, XRN1 and Lsm) (Kedersha and Anderson 2002, Orban and Izaurralde 2005, Eulalio, Behm-Ansmant et al. 2007, Franks and Lykke-Andersen 2008, Gibbings, Ciaudo et al. 2009, Decker and Parker 2012). PBs are required for cytoplasmic RNA silencing and degradation (Orban and Izaurralde 2005, Franks and Lykke-Andersen 2008). Therefore, these results lead to the

assumption that the transient storage of RNAs in SGs controls the degradation of unwanted RNAs through PBs to limit the use of cellular resources under stress. However, recent studies have shown that PBs serve as storage units for repressed RNAs instead of RNA decay. These RNAs stored in PBs can move rapidly to the translationally active pool and bypass transcription, mRNA processing and nuclear export (Brengues, Teixeira et al. 2005, Eulalio, Behm-Ansmant et al. 2007, Hubstenberger, Courel et al. 2017). DDX1 localizes to SGs in heat-shocked cells, and in cells treated with arsenite as well as H_2O_2 (Onishi, Kino et al. 2008). The role of DDX1 in SGs remains poorly understood but our lab has evidence that it may be involved in the resolution of SGs during the recovery process.

1.2.3.3 DDX1 and the viral role

DDX1 has a well-characterized role in HIV genomic RNA export from the nucleus to the cytoplasm through CRM1 (Fang, Acheampong et al. 2005, Edgcomb, Carmel et al. 2012, Lin, Sivakumaran et al. 2014). In non-infected cells, the export of intron-containing RNAs is tightly controlled (Meshorer and Misteli 2005, Back, Lee et al. 2006, Buckley, Khaladkar et al. 2014, Jurkin, Henkel et al. 2014). While accumulation of some intron-containing RNAs is required for rapid production of mature mRNAs (Moran, Weinberger et al. 2008, Boothby, Zipper et al. 2013, Mauger, Lemoine et al. 2016), these RNAs are either retained in the nucleus or exported to the cytoplasm under very strict control with helper proteins such as DDX3, Staufen, ALY/REF and TAP. The interaction of DDX1 with the HIV

Rev protein was first discovered to play a role in the export of intron-containing HIV genomic RNA from the nucleus (Fang, Acheampong et al. 2005). Rev response element (RRE) undergoes conformational change when bound by DDX1, which is essential for the nuclear export of the RNA through the mammalian export protein CRM1. Intriguingly, not only DDX1, but other DEAD box proteins such as DDX3, DDX5, DDX17, DDX21, DDX56 also bind to RRE and promote the export of HIV genomic RNA (Yedavalli, Neuveut et al. 2004, Naji, Ambrus et al. 2012, Yasuda-Inoue, Kuroki et al. 2013, Ariumi 2014).

DDX1 also affects the replication of other viruses such as JC virus and coronavirus (Sunden, Semba et al. 2007, Sunden, Semba et al. 2007, Xu, Khadijah et al. 2010, Wu, Chen et al. 2014). DDX1 has been reported to regulate JC viral proliferation by binding to the JC viral transcriptional control region. As far as coronavirus, DDX1 was reported to interact with the nonstructural protein 14 (nsp14) of both infectious bronchitis virus (IBV) and severe acute respiratory syndrome coronavirus (SARS-CoV) (Xu, Khadijah et al. 2010). During coronavirus infection, DDX1 relocates from the nucleus to predominant viral replication sites in the cytoplasm of infected cells, potentially promoting viral replication. As DDX1 is naturally attracted to the double stranded RNAs present in the cytoplasm, the role of DDX1 in viral replication may be to hijack the immune response. However, DDX1's exact mechanism of action is still not known.

1.2.3.4 DDX1 in double strand break repair

Cells are continuously exposed to different types of DNA damaging agents such as UV light, reactive oxygen species (ROS) etc. These DNA damaging agents can cause DNA single-strand breaks and double-strand breaks (DSBs). If the DNA damage remains unrepaired, this can lead to genomic instability and potentially cancer. Cells have developed two major pathways to repair DSBs: homologous recombination (HR) and non-homologous end joining (NHEJ) (Davis and Chen 2013, Jasin and Rothstein 2013, Wright, Shah et al. 2018). Repair by HR requires the presence of the sister chromatid serving as the undamaged template strand. Therefore, HR usually occurs during S phase and G2 phase of the cell cycle. Repair by HR is usually error-free. In contrast, NHEJ does not require a template strand as the two ends of the DSB are processed and directly joined together. Thus, NHEJ is usually error-prone and often results the loss of genetic information.

DNA repair by HR is an energy and time-consuming process that requires numerous enzymes working in concert to carry out the correct repair process. When DSBs occur, the MRN complex along with CtIP and hExo1 are recruited to the break sites for 5’ end resection and to generate 3’ ssDNA. The processed strand is then bound by RPA proteins and initiates the invasion of the sister chromatid with Rad51. Once paired with the reverse strand on the sister chromatid, the complementary DNA is synthesized. When the DNA synthesis is done, the resulting Holliday junctions are then resolved. Even though the HR process itself is well-understood, the full complement of players involved in this process remains

to be discovered. When no sister chromatid is present, NHEJ becomes the predominant DSB repair process (Mao, Bozzella et al. 2008). In NHEJ, the DSB sites are bound by KU70/80 heterodimers. The broken ends of the two strands are processed by DNA polymerase Pol λ and Pol μ (Mahajan, Nick McElhinny et al. 2002, Lee, Blanco et al. 2004, Daley, Laan et al. 2005). The processed ends are then ligated by DNA ligase IV along with its cofactor XRCC4 (Wilson, Grawunder et al. 1997). .

There are usually 3-4 DDX1 foci in the nucleus of a cell under normal culture conditions (Bleoo, Sun et al. 2001). When cells are treated with ionizing radiation (IR), the number of foci increases with DDX1 recruited to a subset (~30%) of DSBs (Li, Monckton et al. 2008). Since no change in DDX1 levels are observed post IR, existing DDX1 appears to relocate to DSBs. RNase H treatment of cells treated with IR results in the disappearance of DDX1 from DSBs suggesting that the presence of DNA-RNA duplexes at DSBs recruits DDX1 to these DSB sites (Li, Monckton et al. 2008, Li, Germain et al. 2016). DDX1 knockdown decreases HR repair efficiency which further suggests that DDX1 is promoting HR by the removal of DNA-RNA duplexes from the DSB sites (Li, Monckton et al. 2008, Li, Germain et al. 2016). While yeast does not have a DDX1 homologue, the role of DDX1 in DNA DSB repair by HR in yeast may be replaced by RNase H (Ohle, Tesorero et al. 2016).

1.2.3.5 DDX1 and cancer

As mentioned earlier, DDX1 is co-amplified with *MYCN* in a subset of *MYCN*-amplified neuroblastoma and retinoblastoma cell lines (Godbout and Squire 1993, Squire, Thorner et al. 1995, Godbout, Packer et al. 1998, Godbout, Li et al. 2007). Importantly, there is a strong correlation between *DDX1* gene copy number, mRNA levels and protein levels in retinoblastoma and neuroblastoma cell lines (Godbout, Packer et al. 1998). As amplified genes that do not provide survival advantages are often silenced or mutated, the abundant expression of DDX1 suggests that there may be a growth advantage for cancers with *DDX1* amplification.

Both neuroblastoma and retinoblastoma are childhood cancers. Most retinoblastomas develop before the child is 3 years old. The primary cause of retinoblastoma is mutation of the tumour suppressor gene *RB1* (Dyson 2016). Patients with retinoblastoma are usually cured after their treatment, making it difficult to assess the prognostic significance of *DDX1* amplification.

Neuroblastomas are cancers of neural crest cells that can arise from different tissues with the most common one being the adrenal gland (Nakagawara and Ohira 2004). It has been reported that approximately half neuroblastoma patients with *MYCN* amplification show co-amplification of *DDX1* (Godbout, Li et al. 2007). However, the prognostic significance of *DDX1/MYCN* co-amplification compared to *MYCN*-only amplification remains controversial, with some studies showing a trend towards a worse clinical prognosis in neuroblastomas with MYCN/DDX1 amplification (Squire, Thorner et al. 1995, George, Kenyon et al.

1997) and other studies showing a better prognosis for *MYCN/DDX1* co-amplifed tumours compared to *MYCN*-amplified tumours (Weber, Imisch et al. 2004). Yet other studies show no difference between *MYCN/DDX1* co-amplified and *MYCN*-only amplified tumours (De Preter, Speleman et al. 2005, de Souza, Sanabani et al. 2011). Bioinformatics analysis using the TARGET sequencing database shows that neuroblastoma patients under 18 months with high levels of both *DDX1* and *MYCN* have a significantly lower event free survival rate than high levels of *MYCN* alone. However, this difference in event-free survival disappears when patients are >18 months (**Fig. 1.3;** unpublished data). These data suggest that the role of DDX1 in neuroblastoma is age dependent.

Aside from childhood cancers, our lab has shown that DDX1 is a prognostic marker for early relapse in breast cancer independent of subtype (Germain, Graham et al. 2011). Immunohistochemistry analysis of 120 breast cancer patient tissue microarray revealed that high cytoplasmic levels of DDX1 are associated with poor prognosis and early relapse. This suggests that cytoplasmic DDX1 plays a potential role that's beneficial to tumour growth. In ovarian cancer, DDX1 plays a role in microRNA (miRNA) maturation where DDX1 functions as an anchor to recognize the hairpin structure of the primary miRNA (pri-miRNA) and recruit the microprocessor complex to pri-miRNA for the first step of miRNA biogenesis (Han, Liu et al. 2014).

To summarize, DDX1 has been found to play a variety of cellular roles in different cellular compartments **(Fig. 1.4)**.

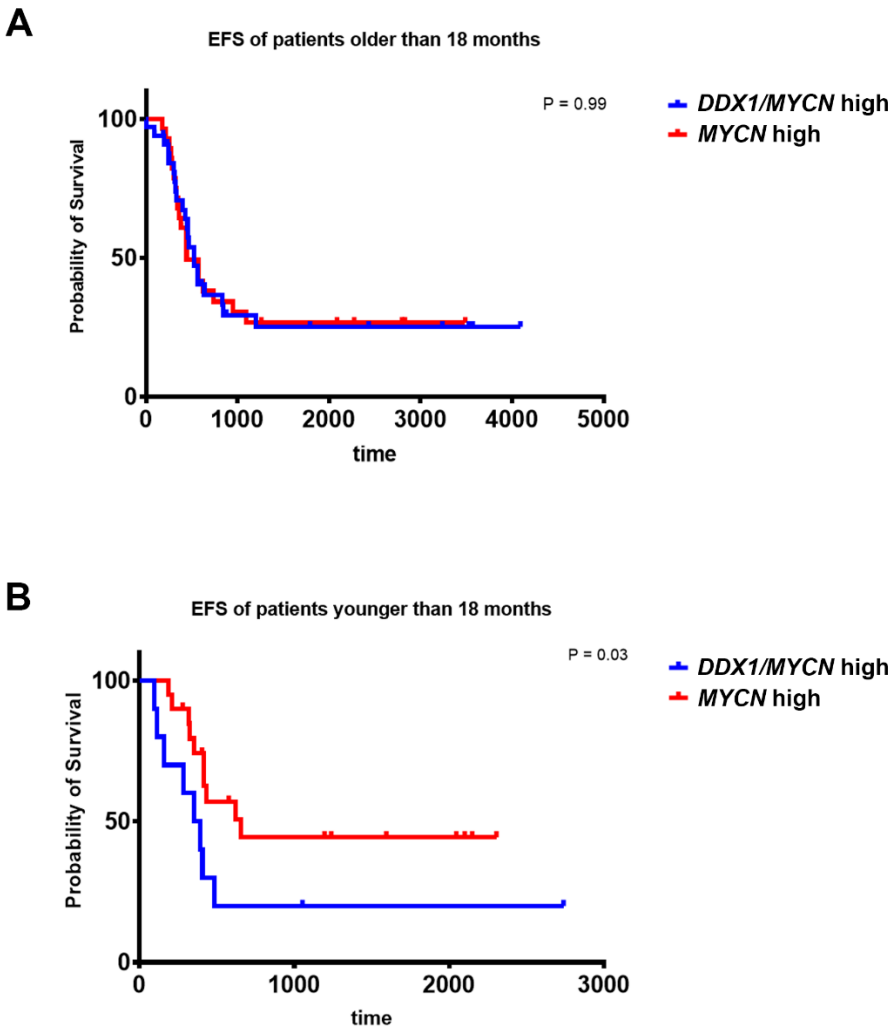

Figure 1.3 Event-free-survival of neuroblastoma patients with *MYCN*-only amplification and *DDX1/MYCN* co-amplification. RNA sequencing data along

with patient age and survival information were obtained from Series GSE62564. Patient samples were grouped based on RNA expression of *MYCN* and *DDX1* using custom R scripts. High levels of *MYCN* and *DDX1* are defined as at least 2-fold higher compared to the mean value of the total mRNA expression levels across all patients. Survival times were plotted with Prism. (A) Event-free-survival of neuroblastoma patients diagnosed before 18 months with high levels of *MYCN* RNA and high levels of both *MYCN* and *DDX1* RNA. No difference was observed between the two groups. (B) When diagnosed after 18 months, event-free-survival of neuroblastoma patients with *MYCN*-only amplification was significantly better than patients with *MYCN/DDX1* co-amplification.

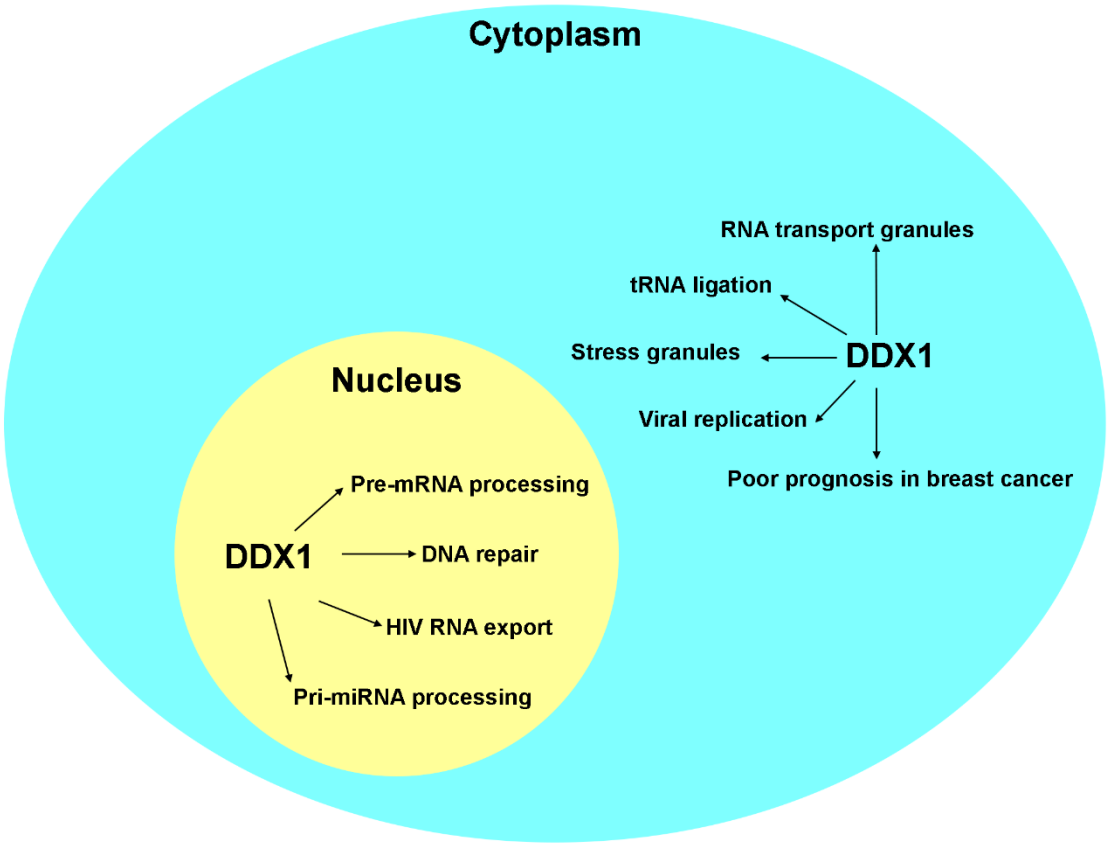

Figure 1.4 Graphical summary of the different cellular roles of DDX1.

1.2.4 DDX1 in development

We have recently shown that DDX1 plays a role in developmental processes with DDX1 knockout resulting in early embryonic lethality in mice and sterility in fruit flies (Germain, Li et al. 2015, Hildebrandt, Germain et al. 2015). Hildebrandt *et al.* showed that *Ddx1*$^{-/-}$ mice are embryonic lethal pre-blastocyst stage suggesting that DDX1 is essential for early mouse embryonic development (Hildebrandt, Germain et al. 2015). Intriguingly, other than embryonic lethality

caused by the absence of DDX1, a transgenic effect was also noted upon crossing *Ddx1*$^{+/-}$ heterozygous mice, with third generation *Ddx1*$^{+/+}$ mice from such crosses showing post-blastocyst lethality. This *Ddx1*$^{+/+}$-associated post-blastocyst lethality was first observed when: 1) *Ddx1*$^{+/-}$ were backcrossed with *Ddx1*$^{+/+}$, 2) the resulting heterozygous progeny were mated to produce second-generation heterozygous offspring, and 3) second-generation heterozygote mice were crossed whereby no *Ddx1*$^{+/+}$ mice were produced. The *Ddx1* wild-type allele in the second generation heterozygous offspring and all subsequent heterozygote crosses has been labelled *Ddx1** **(Fig. 1.5)** (Hildebrandt, Germain et al. 2015). As heterozygote mice have similar levels of DDX1 protein and RNA compared to WT mouse, one possible explanation for the observed wild-type lethality is that compensatory mechanisms are in place to up-regulate DDX1 levels in heterozygote mice; however, up-regulation of DDX1 expression from the *Ddx1** allele results in overexpression of DDX1 in wild-type mice produced from heterozygote crosses. Thus, we are proposing that DDX1 levels must be tightly regulated in developing embryos (Hildebrandt, Germain et al. 2015). The above results suggest that DDX1 is an essential protein during early developmental stages whose levels need to be tightly regulated. Either higher or lower levels of DDX1 during embryonic development will result in early embryonic lethality.

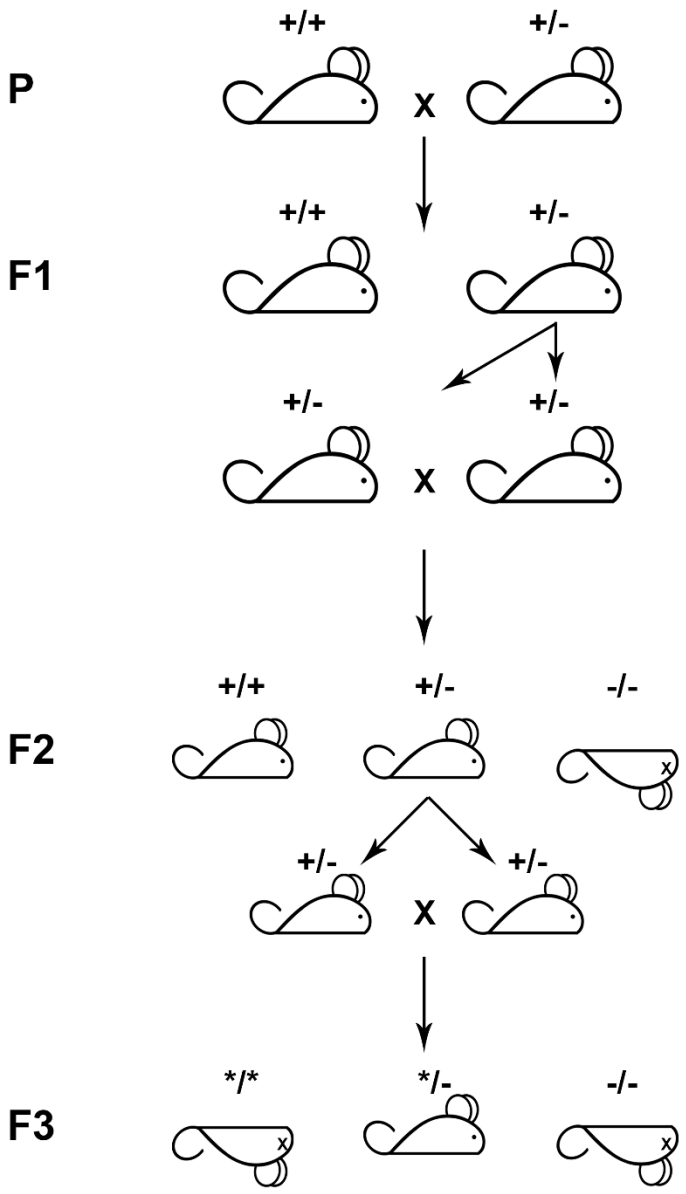

Figure 1.5 Embryonic lethality of *Ddx1** allele. Graphical illustration of the generation and embryonic lethality of *Ddx1*$^{*/*}$ and *Ddx1* knockout. Redrawn from (Hildebrandt, Germain et al. 2015).

Unlike mouse, *Ddx1*$^{-/-}$ adults are viable in *Drosophila*. However, they are sterile due to abnormally developed testis and ovaries (Germain, Li et al. 2015). These *Ddx1 null Drosophila* appear smaller in body size compared to their WT siblings. Germain *et al.* have shown that DDX1 binds to and alters the splicing of starvation-related *Sirup* RNA (Germain, Li et al. 2015). Changes in *Sirup* RNA suggest that the smaller body size and abnormally developed reproductive system observed in *Ddx1*$^{-/-}$ flies are a starvation-like response. Consistent with this hypothesis, *Drosophila* with *Sirup* mutation has also been shown to be sensitive to oxidative stress (Van Vranken, Bricker et al. 2014). These data provide a potential link between cellular metabolism and DDX1. Maternal Ddx1 in *Drosophila* can be detected until the 2nd instar larvae stage whereas maternal DDX1 is degraded much earlier in mouse. This could be the underlying reason for why *Ddx1*$^{-/-}$ mice are embryonic lethal and *Ddx1 null Drosophila* are viable.

1.3 Mouse development

Immediately after fertilization, embryos rely on maternal RNAs and proteins for their development (Tadros and Lipshitz 2009, Marlow 2010). When the zygotic genome is activated (ZGA), the embryos gradually switch from relying on maternal transcripts and proteins to reliance on zygotic materials which is known as the maternal-to-zygotic transition (MZT). With the two waves of zygotic genome activation taking place at 1-cell and 2-cell stages, these are the key developmental time points in the MZT (Nothias, Majumder et al. 1995, Hamatani, Carter et al.

2004, Tadros and Lipshitz 2009, Li, Zheng et al. 2010). As DEAD box proteins are involved in all aspect of RNA metabolism including transcription, translation and RNA degradation (Linder and Jankowsky 2011, Linder and Fuller-Pace 2015), it's very likely that they play a role in early embryonic development, Moreover, other than maternal RNAs and proteins that are essential for early mouse embryonic development, mitochondria are essential for the embryos to develop beyond the 2-cell stage as embryos are believed to rely almost exclusively on the complement of mitochondria received from the oocyte for their energy requirement (Dumollard, Marangos et al. 2004, Dumollard, Duchen et al. 2007, Komatsu, Iwase et al. 2014). As DDX1 is expressed at very early developmental stages and Ddx1 has previously been shown to affect genes involved in mitochondrial function in *Drosophila* (Germain, Li et al. 2015), we postulate that it may be involved in *Ddx1* related mouse embryonic lethality.

1.3.1 Gametogenesis

As embryonic development is a highly regulated process, the health of the embryos depends heavily on the gametes generated by the parents. Hence, generating high quality gametes is an essential first step in embryonic development. This is especially relevant during the very early stages of development when the zygotic genome is not activated, as the development and metabolism of the embryo rely almost entirely on the materials carried by the oocyte and sperm.

In mice, spermatogenesis begins with the mitotic division of spermatogonium in the basal compartment of the seminiferous tubules (Hess and Renato de Franca 2008, Fayomi and Orwig 2018). With this division process, half of the new cell population generated remains as stem cells whereas the other half becomes primary spermatocytes and enters meiosis. The primary spermatocytes will then move to the adluminal compartment of the seminiferous tubules where they undergo DNA duplication which in turn initiates meiosis. At this stage, the primary spermatocytes are still diploid (2N) but contains 2x40 chromatids (4C). After meiosis I, two haploid secondary spermatocytes (1N) are produced from each primary spermatocyte. The secondary spermatocytes, each containing 2x20 chromatids (2C), then undergo spermatidogenesis where each secondary spermatocyte divides once again in meiosis II to generate two haploid spermatids with each containing only one set of chromatids (1C). The division process from the spermatogonium to spermatid stages is incomplete with all the spermatids interconnected by bridges of cytoplasm. This interconnection between spermatids allows transfer of RNAs or proteins to ensure synchronous development. The interconnection between spermatids continues to exist until the spermiogenesis step where the spermatids undergo DNA packaging and morphological changes from round cells to individual elongated spermatozoa (sperm). The further maturation of sperm requires testosterone for the removal of unnecessary cytoplasm and organelles. Soon after, the sperm are released from the protective Sertoli cells into the lumen of the seminiferous tubule. The final step of maturation

occurs when the sperm are transported to the epididymis where they gain motility and are stored for fertilization.

The sole purpose of sperm was originally thought to be delivery of DNA to the oocyte with its mitochondria providing the energy required for motility. However, despite their highly compact nature, sperm is now known to harbor thousands of different RNAs including mRNAs and miRNAs needed for the development of the embryos (Amanai, Brahmajosyula et al. 2006, Dadoune 2009, Fullston, Ohlsson-Teague et al. 2016). Chromosomes are compacted into at least 1/6 the size of the chromosomes in a normal somatic cell undergoing mitosis due to replacement of histones by protamines (Champroux, Torres-Carreira et al. 2016). The dense compaction of the sperm chromosomes leads to transcription stalling and the mRNAs needed for embryonic development are stored in various RNP complexes (Kleene 1993, Braun 1998, Schmidt, Hanson et al. 1999). These mRNAs are believed to be responsible for the genomic imprinting process during early development. In addition to mRNAs, many miRNAs reside in sperm. However, the roles of these miRNAs is not known, although there is evidence supporting a role for sperm miRNAs in the modification of the epigenetic landscape of the embryos (Hosken and Hodgson 2014).

Unlike spermatogonium which can self-renew, oogonium cannot be regenerated once oocytogenesis occurs. The oocytogenesis process is where oogonia become primary oocytes (Gilbert 2000). This process is completed before

or shortly after birth, with primary oocytes stalled at meiosis I. These stalled primary oocytes are called dictyates (Guli and Smyth 1988). Progression through meiosisis controlled by hormone levels and normally resumes upon sexual maturation. As the primary oocytes are diploid (2N) with 4 sets of chromatids (4C), meiosis I of oogenesis results in the generation of a haploid secondary oocyte with 2 sets of chromatids (2C) and the first polar body from a primary oocyte. Usually, there are 4-12 oocytes undergoing meiosis each estrogen cycle in mouse depending on the mouse strain and age (Wang, Ge et al. 2017). Meiosis I division is asymmetric whereby the secondary oocyte retains the majority of the cytoplasm, with the polar body left with a small amount of cytoplasm. Immediately following meiosis I, the secondary oocyte starts to undergo meiosis II. However, this process stalls at metaphase II where the secondary oocyte is stored until fertilization (Horner and Wolfner 2008). Under normal conditions, meiosis II will be completed when fertilization occurs. However, the stalled oocytes can also be released from metaphase II arrest if the oocytes are injected with phospholipase C zeta (PLCξ) (Saunders, Larman et al. 2002, Knott, Kurokawa et al. 2005, Kashir, Konstantinidis et al. 2012), IP_3 (Whitaker 2008) or CaMKIIγ (Backs, Stein et al. 2010). However, the activated eggs are unable to undergo normal development. Without egg activation, the secondary oocyte will disintegrate and be released. Once fertilization occurs, another asymmetric division occurs where a mature oocyte and a secondary polar body is produced. Notably, the oocyte can also be activated in

c-mos deficient mice where the oocyte directly forms pronucleus after first meiosis instead of going through second meiosis (Araki, Naito et al. 1996).

Unlike sperm which all have similar contents, the haploid oocyte retains most of the cytoplasmic materials as the result of polar body formation. Oocyte maturation is accompanied by a large increase in size with accumulation of the maternal RNAs, proteins, mitochondria, etc. required for the development of the newly formed embryo (De Leon, Johnson et al. 1983, Li, Zheng et al. 2010, Nadeau 2017). Cumulus cells surrounding the oocyte have been reported to be connected to the oocyte. Connection of the cumulus cells to oocytes enables the exchange of metabolites and the storage of maternal materials needed for development (Huang and Wells 2010, Gomez-Torres, Garcia et al. 2015).

1.3.2 Cytoplasmic polyadenylation

In eukaryotic cells, the pre-mRNAs transcribed from the genomic DNA need to undergo extensive processing in order to become mature mRNAs which are then transported to the cytoplasm for translation (Proudfoot, Furger et al. 2002). One of these pre-mRNA processing events is 3'-end processing (Proudfoot 2011, Yang and Doublie 2011, Shi and Manley 2015). For most pre-mRNAs, 3'-end processing requires endonucleolytic cleavage at a specific location which resides 10-30 nucleotides downstream of the polyadenylation signal (Proudfoot and

Brownlee 1976, Beaudoing, Freier et al. 2000, Tian, Hu et al. 2005). A long poly(A) tail is then added to the 3'-end of the pre-mRNA.

Cleavage and polyadenylation specificity factor (CPSF) has been reported to play a central role in the 3'-end processing of pre-mRNAs (Bienroth, Wahle et al. 1991, Murthy and Manley 1992). CPSF has 6 subunits including CPSF-160, CPSF-30, WDR33, Fip1, CPSF-73 and CPSF-100 (Sullivan, Steiniger et al. 2009, Schonemann, Kuhn et al. 2014). The first four subunits are essential for polyadenylation signal recognition and polyadenylation whereas the last two form the core cleavage complex for the cleavage reactions (Sullivan, Steiniger et al. 2009, Schonemann, Kuhn et al. 2014). While CPSF-73 has been shown to be an endoribonuclease, different roles for CPSF-100 (as known as CPSF2) have been proposed, none of which involve ribonuclease activity (Mandel, Kaneko et al. 2006). The depletion of CPSF2 by siRNAs results in read-through transcription in *Drosophila* and changes in 3'UTR length in the mouse cell line C2C12 (Li, You et al. 2015, Michalski and Steiniger 2015). CPSF2 mutation has also been reported to affect precise positioning of polyadenylation and transcription termination in *Arabidopsis* embryogenesis (Lin, Xu et al. 2017). Therefore, it is likely that CPSF2 plays a different role than simple cleavage of pre-mRNAs.

Apart from canonical polyadenylation which takes place in the nucleus, cytoplasmic polyadenylation has also been documented. Cytoplasmic polyadenylation was first discovered in oocytes during the maturation process (Fox,

Sheets et al. 1989, McGrew, Dworkin-Rastl et al. 1989). This process is essential for controlling maternal mRNA translation during oocyte growth and maturation as well as early embryonic development (Winata and Korzh 2018). A number of proteins are required for cytoplasmic polyadenylation including cytoplasmic polyadenylation element binding protein (CPEB) and cleavage and polyadenylation specificity factor (CPSF) (Charlesworth, Meijer et al. 2013). The absence of CPSF2 results in reduced cytoplasmic polyadenylation (Dickson, Bilger et al. 1999). mRNAs that undergo cytoplasmic polyadenylation are thought to have a full-length poly(A) tail to allow nuclear export. They then undergo deadenylation by poly(A)-specific ribonuclease (PARN) in the cytoplasm so that their translation can be spatially and temporally controlled (Huarte, Stutz et al. 1992, de Moor and Richter 1999, Richter 1999). Such RNAs are considered to be dormant mRNAs. For the activation of the dormant mRNAs, their poly(A) tails need to be lengthened. Cytoplasmic polyadenylation requires two elements in the 3'UTR: the polyadenylation signal AAUAAA as well as the cytoplasmic polyadenylation element (CPE) (Mendez and Richter 2001). The CPE region in target mRNAs is bound by CPEB which then interacts with the polyadenylation signal-binding protein CPSF (Hodgman, Tay et al. 2001). According to the current model, CPEB is activated by phosphorylation, resulting in poly(A) tail elongation by a poly(A) polymerase such as GLD-2 (Hodgman, Tay et al. 2001, Richter 2007). Once the polyadenylation process is finished, the dormant mRNAs are activated and can be translated.

Dormant RNAs are stored in different cytoplasmic granules in oocytes during oogenesis (Anderson and Kedersha 2009, Voronina, Seydoux et al. 2011, Sengupta and Boag 2012, Courchaine, Lu et al. 2016). In early-stage mouse oocytes arrested at prophase I, P-bodies localize to the perinuclear area as well as the cell cortex (Flemr and Svoboda 2011). These P-bodies disappear during oocyte growth and maturation and the CPEB1 as well as DDX6 form aggregates at the subplasmalemmal cytoplasm (Flemr, Ma et al. 2010). Unlike traditional P-bodies, these aggregates do not contain the decapping protein DCP1 which indicates the function of these aggregates may be mRNA storage and repression rather than degradation. Upon oocyte maturation, these cytoplasmic aggregates also disappear. Three waves of cytoplasmic polyadenylation have been proposed in mouse embryonic development, with the first two waves taking place during oocyte growth and maturation and the third wave taking place after fertilization (Pique, Lopez et al. 2008, Guillen-Boixet, Buzon et al. 2016, Winata and Korzh 2018, Winata, Lapinski et al. 2018). While the first two waves are relatively well understood, involving the phosphorylation of CPEB1 as well as CPEB4 which initiates the polyadenylation process by GLD-2, little is known about the post-fertilization wave of cytoplasmic polyadenylation. As CPEB1/DDX6 aggregates disappear upon oocyte maturation, different factors may be involved in this third wave. However, it's known that the third wave is essential for the embryos to undergo proper MZT (Winata, Lapinski et al. 2018). A better knowledge of the third

wave of cytoplasmic polyadenylation post-fertilization may be essential to our understanding of the maternal regulation of MZT.

1.3.3 Fertilization

Sperm penetration promotes the maturation of the secondary oocyte into ootid and leads to the completion of meiosis II (Horner and Wolfner 2008). After the initial contact with sperm, fertilization by an additional sperm (polyspermy) is blocked by two different of mechanisms (Gardner and Evans 2006, Gardner, Williams et al. 2007). One of them is called membrane block (Horvath, Kellom et al. 1993, Gardner, Williams et al. 2007). In aquatic animals such as frog and zebrafish, the change in oocyte membrane sperm receptivity prevents additional sperm from contacting the oocyte surface. However, the mechanism of the establishment of membrane block in mouse oocyte remains poorly understood. It has been proposed that mouse oocyte membrane block may involve altered membrane actin rearrangement which affects the oocyte-sperm receptivity (Wang, Luo et al. 2017). The other mechanism is known as zona pellucida block which is relatively well conserved across species (Fahrenkamp, Algarra et al. 2020). This process is initiated through the release of cortical granules found adjacent to the oocyte surface to the space between the oocyte surface and the zona pellucida, a glycogen matrix surrounding the oocyte (Wassarman, Chen et al. 1999). The release of cortical granule contents hardens the zona pellucida and increases its resistance to proteolytic digestion (Gwatkin 1964, Gulyas 1980). Electron

microscopy studies of human embryos have suggested that filament bundles on the inner surface of the zona pellucida are fused together and thus lead to increases in density (Familiari, Heyn et al. 2008). Although several processes have been proposed to be responsible for the hardening of the zona pellucida (i.e. ZP2 cleavage (Bleil, Beall et al. 1981), deglycosylation of ZP3 (Bleil and Wassarman 1980, Bleil and Wassarman 1980), glycan cross-linking (Parkening and Chang 1976, Dolci, Bertolani et al. 1991), zinc sparks (Que, Bleher et al. 2015, Que, Duncan et al. 2017)), the exact biochemical modification of the zona pellucida is unknown. At this stage, the genetic material carried by the sperm is unpacked with the removal of protamines resulting in remodelling of compact chromatin into nucleosome structures (Li, Zheng et al. 2010). The fertilized oocyte provides the initial histones for protamine replacement. Within the next few hours, the maternal and paternal pronuclei approach each other with rapid replication of their DNA in order to prepare for the first mitotic division of the zygote. The fusion of the two gametes (syngamy) is completed when the nuclear membranes break down in the first mitosis (Albertini 2018). During this fusion, the maternal and paternal chromosomes are captured by mitotic spindles which leads to the first mitotic division of the embryo.

1.3.4 Calcium wave

Calcium (Ca^{2+}) is a secondary messenger that regulates a number of metabolic responses such as secretion, contraction, gene expression, ROS,

mitochondrial membrane potential ($\Delta\Psi_m$), ATP synthesis and many other cell functions (Szent-Gyorgyi 1975, Johnson, Hill et al. 1997, Brookes, Yoon et al. 2004, Hivelin, Beraud-Dufour et al. 2016). With the initial discovery made in sea urchins, research has shown that Ca^{2+} plays an essential role in fertilization in all the animal species studied to date. The Ca^{2+} wave is triggered by fertilization which releases oocytes from meiosis arrest and activates a variety of pathways (Jones 2005, Ducibella and Fissore 2008). The release of sperm head-associated phospholipase C zeta (PLCξ) during the fusion of sperm-egg plasma membrane causes Ca^{2+} release from the inositol 1,4,5-triphosphate (IP_3) sensitive ER stores (Saunders, Larman et al. 2002, Knott, Kurokawa et al. 2005, Kashir, Konstantinidis et al. 2012). IP_3 seems to be the key component that leads to a Ca^{2+} wave. The microinjection of IP_3 into oocytes initiates oocyte activation while an IP_3 antagonist prevents oocyte activation in various species such as frog, sea urchin, starfish, mouse etc. (Whitaker 2008).

In mouse, the Ca^{2+} wave occurs minutes after sperm-egg fusion starting from the sperm entry point and lasting several hours. The initial release of Ca^{2+} is followed by Ca^{2+} ER reuptake through SERCA pumps and plasma membrane Ca^{2+} extrusion through ATPase pumps. The intracellular Ca^{2+} levels are replenished with influx of extracellular Ca^{2+} (Igusa and Miyazaki 1983, Kline and Kline 1992). In mammalian cells, this process causes repetitive waves of Ca^{2+} signalling. However, except for the first wave, the subsequent Ca^{2+} waves are not restricted

to the sperm entry point (Kline, Mehlmann et al. 1999, Deguchi, Shirakawa et al. 2000). They can be initiated from other regions where ER is enriched.

The early responses of the embryo to Ca^{2+} signals include mitochondrial energy production, cortical granule exocytosis and cell cycle resumption (Abbott and Ducibella 2001, Dumollard, Marangos et al. 2004, Campbell and Swann 2006, Backs, Stein et al. 2010). In normal somatic cells, the mitochondrial uptake of Ca^{2+} is associated with an increased $NADH/NAD^{+}$ ratio and ATP production in mitochondria (Ashby and Tepikin 2001). Uptake of Ca^{2+} by mitochondria is also likely to occur at fertilization (Dumollard, Duchen et al. 2006). Moreover, increased NADH and decreased FAD^{2+} accompanies each Ca^{2+} wave in mouse embryos suggesting increased activity of the TCA cycle and increased ATP production (Campbell and Swann 2006). Chemical inhibitors of mitochondrial function have also been shown to disrupt sperm-induced Ca^{2+} waves in mouse oocytes (Liu, Hammar et al. 2001).

The release of cortical granules can be observed minutes after the first Ca^{2+} wave (Abbott and Ducibella 2001). Multiple waves of cortical granule release coincide with Ca^{2+} waves and most of the cortical granules are gone in pronuclear-stage embryos (Ducibella, Huneau et al. 2002). The failure of cortical granule release can have dramatic effects such as failure to block polyspermy, a consequence of failure to increase the space between zona pellucida and fertilized oocyte membrane.

Ca^{2+} can also contribute to the control of cell cycle resumption through calcium/calmodulin-dependent protein kinase II (CaMKII) (Markoulaki, Matson et al. 2004). The CaMKII undergoes autophosphorylation after Ca^{2+} binding and its activity rises along with the first Ca^{2+} wave (Tombes, Faison et al. 2003). Treatment of fertilized mouse oocytes with CaMKII inhibitors prevents cell cycle progression resulting in failed meiosis (Johnson, Bierle et al. 1998). The knockout of CaMKIIγ, the predominant isoform of CaMKII in mouse oocytes, can cause the complete failure of meiosis resumption despite the fact that these embryos show normal patterns of sperm-induced Ca^{2+} waves and cortical granule exocytosis (Backs, Stein et al. 2010). The failure of cell cycle resumption can also lead to the failure of polar body emission which depends largely on this event (Matson, Markoulaki et al. 2006).

Ca^{2+} waves are essential for mitotic cleavage divisions in mouse, fruit fly, sea urchin, and frog embryos (Poenie, Alderton et al. 1985, Steinhardt and Alderton 1988, Tombes, Simerly et al. 1992, Muto, Kume et al. 1996, Gordo, Kurokawa et al. 2002, Bobinnec, Marcaillou et al. 2003). Live cell imaging of Ca^{2+} in 2-cell mouse embryos reveals high concentrations of Ca^{2+} in microdomains at the subplasmalemmal cytoplasm (Manser and Houghton 2006). These microdomains can be disrupted by inhibiting or uncoupling the electron transport chain of mitochondria suggesting that Ca^{2+} levels may play a role in mitochondrial activity at the 2-cell stage of development (Manser and Houghton 2006).

1.3.5 ER and mitochondria Ca^{2+} buffering

Endoplasmic reticulum (ER) is the largest Ca^{2+} storage compartment in normal cells (Kaufman and Malhotra 2014, Raffaello, Mammucari et al. 2016). The rapid release of Ca^{2+} from ER ensures the sustained cytoplasmic Ca^{2+} needed for specific cell functions. Also, ER Ca^{2+} uptake when cytoplasmic Ca^{2+} levels are high is essential to ensure the maintenance of resting cytoplasmic Ca^{2+} levels (Arnaudeau, Frieden et al. 2002, Gorlach, Klappa et al. 2006).

In normal cells, ER and mitochondrial membranes are partially connected through the mitochondria-associated ER membrane (MAMs). This contact between mitochondria and ER is mediated by a series of proteins such as MFN1/2 and MFN2, Fis1 and BAP31, PTPIP51 and VAPB, and VDAC and IP_3R (Szabadkai, Bianchi et al. 2006, de Brito and Scorrano 2008, Davison, Pennington et al. 2009, Iwasawa, Mahul-Mellier et al. 2011, De Vos, Morotz et al. 2012, Gomez-Suaga, Paillusson et al. 2017). IP_3R on ER membranes forms Ca^{2+} channels that control Ca^{2+} efflux from ER to cytosol and accumulates in MAM (Joseph and Hajnoczky 2007, Patergnani, Suski et al. 2011). VDAC is a mitochondrial membrane protein working together with Mitochondria Calcium Uniporter (MCU) to regulate Ca^{2+} influx (Hoppe 2010). VDAC and IP_3R interact through a cytoplasmic chaperone protein Grp75 (Szabadkai, Bianchi et al. 2006). The IP_3R-Grp75-VDAC-MCU complex enables the proper transfer of Ca^{2+} from ER to mitochondria. The increased Ca^{2+} levels in MAM activates Ca^{2+} influx to mitochondria through the

IP_3R-Grp75-VDAC-MCU complex. When the chaperone protein Grp75 is depleted, a decrease in mitochondrial Ca^{2+} levels is observed (Honrath, Metz et al. 2017).

The transfer of Ca^{2+} from ER to mitochondria can trigger mitochondria energy production as well as apoptosis depending on the levels of Ca^{2+} (Haworth and Hunter 1979, Hansford and Zorov 1998, Rostovtseva, Tan et al. 2005). Upregulation of mitochondrial Ca^{2+} at physiological levels can increase oxidative phosphorylation and mitochondrial potential, as well as facilitate the TCA cycle (Hansford and Zorov 1998). However, abnormally high Ca^{2+} flux from ER to mitochondria can initiate oligomerization of BAX and trigger apoptotic pathways (Rostovtseva, Tan et al. 2005).

1.3.6 Mitochondria in early embryonic development

Mitochondria are the most commonly studied organelle in embryonic development with essential roles in ATP production and Ca^{2+} regulation (Dumollard, Marangos et al. 2004, Dumollard, Duchen et al. 2006, Mishra and Chan 2014). During oocyte maturation, mitochondria undergo progressive replication up to the MII stage, reaching the levels required for the embryos to develop to blastocysts (Piko and Matsumoto 1976, Piko and Taylor 1987). The copy number of mitochondrial DNA per embryo remains constant up to the blastocyst stage when the mitochondria once again undergo active replication. Compared to mitochondria in somatic cells, the mitochondria generated during

oocyte development are smaller, have a different arc-like or ring-like shape with few cristae and appear to be much more electron dense than their somatic counterparts (Reader, Stanton et al. 2017). The functional significance of these mitochondrial morphological changes in embryos is unclear but may be related to the energy state of the mitochondria or the controlled ATP generation required at this stage.

Mitochondria are evenly distributed in germinal vesicle stage oocytes until germinal vesicle breakdown (GVBD) when the mitochondria forms aggregate and move to the perinuclear of the cell during MI stage (Van Blerkom and Runner 1984). After the extrusion of the first polar body, the mitochondria become evenly distributed again (Van Blerkom and Runner 1984). Although mitochondria are evenly distributed in oocyte and early-stage embryos, JC-1 staining, an indicator of mitochondrial membrane potential, shows that the high membrane potential mitochondria accumulate at the subplasmalemmal cytoplasm (Komatsu, Iwase et al. 2014, Shu, Xing et al. 2015). The loss of subplasmalemmal high $\Delta\Psi_m$ mitochondria in embryo blastomeres results in arrested cell division (Komatsu, Iwase et al. 2014). It is thought that the unique distribution of mitochondria with high $\Delta\Psi_m$ in the oocyte and early embryos represents a uniquely spatial requirement for local ATP at these stages (Dumollard, Marangos et al. 2004). However, there are contradictory reports regarding levels of ATP production by mitochondria at this developmental stage, and it has been suggested that ATP

production may not be related to the high $\Delta\Psi_m$ mitochondria identified by JC-1 staining (Van Blerkom, Davis et al. 2003, Dumollard, Marangos et al. 2004).

Interestingly, abnormally elevated levels of cytoplasmic Ca^{2+} were found to be associated with intense J-aggregates, indicative of mitochondria with high membrane potential (Van Blerkom, Davis et al. 2003). Moreover, an increased ratio of high-to-low $\Delta\Psi_m$ mitochondria was shown to be associated with an increased degree of mitochondria fragmentation (Acton, Jurisicova et al. 2004). Therefore, changes in intracellular Ca^{2+} levels can have a severe impact on mitochondrial $\Delta\Psi_m$ which may lead to increased fragmentation.

1.3.7 Maternal to zygotic transition

When the embryos are undergoing ZGA, RNA polymerase II (RNA Pol II) undergoes 'loading', 'pre-configuration' and 'production' at the transition between the minor wave and major wave of ZGA. These sequential RNA Pol II events rely heavily on the proper transition between ZGA waves as the inhibition of the minor wave will result in impaired RNA Pol II pre-configuration and developmental failure (Liu, Xu et al. 2020). Unlike mice, most of the zygotic genome is activated at around 8-cell stage in human and bovines (Telford, Watson et al. 1990, Schultz 2002). Degradation of oocyte-specific transcripts is believed to be the trigger for zygotic genome activation (Piko and Clegg 1982, Schultz 2002).

A large pool of transcripts needed for oocyte and fertilization are generated during oogenesis. Maternal transcripts such as Zygote arrest 1 (*Zar1*) and transcription intermediary factor 1, alpha (*Tif1α*), along with *Mater, Floped* and *Tle6* which encode the subcortical maternal complex (SCMC) are important for embryonic development beyond the 1- to 2-cell stages (Wu, Viveiros et al. 2003, Torres-Padilla and Zernicka-Goetz 2006, Li, Baibakov et al. 2008, Jiao and Woodruff 2013). The degradation of these transcripts is a highly controlled process. Although many transcripts produced by the oocytes are stored for long periods of time, they will all gradually undergo degradation during MZT. In mice, more than 90% of the maternal mRNAs are degraded by the 2-cell stage (Piko and Clegg 1982, Schultz 2002). Transcript degradation in the cytoplasm is associated with the 'RNA induced silencing complex' (RISC) accompanied by endogenous siRNA (Lykke-Andersen, Gilchrist et al. 2008, Stein, Rozhkov et al. 2015). Maternal Argonaute 2 (Ago2) is one of the key components in this pathway with its absence leading to embryonic lethality at the 2-cell stage (Lykke-Andersen, Gilchrist et al. 2008).

Chromatin remodelling is another key component of zygotic genome activation as the embryo must overcome the silencing established during gametogenesis (Li, Zheng et al. 2010). Early embryos undergo extensive demethylation during preimplantation development. In mature oocytes, regions with histone 3 lysine 4 trimethylation (H3K4me3) show up as broad domains instead of sharp peaks as observed in somatic cells (Dahl, Jung et al. 2016). This

indicates a large number of H3K4me3 are present in the oocyte genome. Transcriptional promoter regions bound by histone with H3K4me3 in embryos usually correlates with genes transcribed at the late 2-cell stage (Zhang, Zheng et al. 2016). As H3K4me3 modification usually correlates with activation of transcription in nearby genes, these H3K4me3 domains in oocytes suggest H3K4me3 may be related to recently transcribed gene or genes that will soon be transcribed. After fertilization, H3K4me3 is largely maintained from the zygote to early 2-cell stages (Dahl, Jung et al. 2016, Liu, Wang et al. 2016, Zhang, Zheng et al. 2016). From late 2-cell stage onwards, H3K4me3 levels are dramatically reduced, with histone 3 lysine 27 acetylation (H3K27ac) now occupying genomic regions previously marked by H3K4me3 (Dahl, Jung et al. 2016).

Aside from H3K4me3, the repressive mark histone 3 lysine 27 trimethylation (H3K27me3) also shows up as broad domains in MII stage oocytes and 2-cell stage embryos independent of H3K4me3 (Zheng, Huang et al. 2016). In addition, a number of promoter regions are also marked by H3K27me3 in oocytes which are then removed prior to the major wave of zygotic genome activation (ZGA) (Zheng, Huang et al. 2016). The removal of H3K27me3 also correlates with the activation of the zygotic genome. Unlike the maternal histones, almost all paternal histones are replaced by protamines during chromatin compaction in mouse sperm (Balhorn, Gledhill et al. 1977, Brykczynska, Hisano et al. 2010). The paternal protamines are removed as the result of chromatin remodelling upon fertilization and replaced by histones carried by the oocyte (Li, Zheng et al. 2010). Interestingly, transcription

factors such as Sp1 and Oct-4 only interact with the paternal pronucleus in the zygote suggesting that these transcription factors may only be playing roles in the remodelling of the paternal genome (Worrad, Ram et al. 1994).

1.3.8 Maternal RNA degradation

As mentioned in section 1.3.7, large amounts of maternal RNAs are deposited to oocytes during oocyte growth to sustain oocyte development as well as early embryonic development. These maternal RNAs need to be gradually degraded and replaced by zygotic RNAs (Nothias, Majumder et al. 1995, Hamatani, Carter et al. 2004, Tadros and Lipshitz 2009, Li, Zheng et al. 2010). In fact, the degradation of maternal RNAs is required for zygotic genome activation (Piko and Clegg 1982, Schultz 2002). It has been proposed that maternal RNA degradation may provide a store of ribonucleotides for the transcription of zygotic RNAs (Ma, Fukuda et al. 2015).

Maternal RNAs appear to be degraded using two main pathways: (i) endo-siRNA mediated silencing (Lykke-Andersen, Gilchrist et al. 2008, Kaneda, Tang et al. 2009, Suh, Baehner et al. 2010) and (ii) CCR4-NOT complex mediated RNA decay (Ma, Fukuda et al. 2015, Liu, Lu et al. 2016, Vieux and Clarke 2018). Endo-siRNAs are present in the oocytes and embryos of different species including *Drosophila, Xenopus, C.elegans* as well as mouse. In mouse embryos, the absence of either *Dicer1* or *Ago2* results in the accumulation of maternal RNAs in

oocytes, and embryos stalling at the 1- to 2-cell stages (Tang, Kaneda et al. 2007, Lykke-Andersen, Gilchrist et al. 2008, Philipps, Wigglesworth et al. 2008). Although the absence of the microprocessor complex gene *Dgcr8* results in the depletion of miRNAs, this does not appear to significantly affect maternal RNA degradation (Suh, Baehner et al. 2010). Therefore, it appears that maternal RNAs are degraded in a DGCR8-independent but DICER and AGO2-dependent manner. Interestingly, it has been shown that small RNAs including siRNAs and miRNAs can also undergo polyadenylation (Yang, Lin et al. 2016). During early mouse embryonic development, relatively short poly(A) tails are added to these small RNAs so that they can evade the polyadenylation-dependent RNA degradation event that takes place in 2-cell mouse embryos. These data suggest that endo-siRNA mediated RNA silencing pathways are essential for mouse oogenesis and early embryonic development.

In contrast to endo-siRNA mediated silencing, CCR4-NOT complex mediated RNA decay involves the BTG4 and the CCR4-NOT deadenylase complexes (Ma, Fukuda et al. 2015, Liu, Lu et al. 2016, Vieux and Clarke 2018) which are involved in deadenylation-associated maternal RNA decay. BTG4 and CCR4-NOT associated RNA recognition and degradation involve a number of RNA-binding proteins including eukaryotic initiation factor eIF4E and poly(A) binding protein PABPC1L (Liu, Lu et al. 2016, Yu, Ji et al. 2016). Similar to *Dicer* and *Ago2*, the absence of maternal *Btg4* in mouse embryos results in embryonic

arrest at the 1- to 2-cell stage due ZGA failure (Liu, Lu et al. 2016, Zheng, Zhou et al. 2020).

Although the presence of two different RNA degradation pathways suggests that clearance of maternal RNA is required by ZGA, there is no clear evidence that all maternal RNAs are degraded in early embryonic development. It has been shown that knockout of maternal genes in oocytes can cause abnormal development at later embryonic stages. For example, *Dnmt3l* null oocytes can result in the loss of maternal genomic imprinting at the blastocyst stage (Bourc'his, Xu et al. 2001, Kaneda, Okano et al. 2004), whereas maternal *Nlrp2* RNA starts to degrade at the 2-cell stage but maternal NLRP2 protein is still present at the blastocyst stage (Peng, Chang et al. 2012). Importantly, in human and porcine embryos, several precisely-timed waves of maternal RNA degradations have been documented (Vassena, Boue et al. 2011, Xu, Shen et al. 2012, Sha, Zheng et al. 2020), including one wave at the 4-8 cell stages (during MZT) and another wave at the blastocyst stage (Xu, Shen et al. 2012). Even though these late waves have not been documented in mouse embryos, several studies have demonstrated the presence of maternal RNAs until the blastocyst stage (Bachvarova and De Leon 1980, Crozet 1989, Sato, Fukuda et al. 2008). Based on these combined data, subsets of maternal RNAs may be required until relatively late in early development, up to the blastocyst stage.

1.3.9 Early embryonic lethality

As the maternal RNA is being degraded during MZT, the zygotic genome gets activated. However, maternal transcripts are very important during this transition. The absence of certain maternal mRNAs can cause embryonic lethality with embryos stalling at the 1- to 4-cell stages depending on the mRNA. A number of RNAs have been shown to be associated with failure of important developmental events such as the fusion of pronuclei (i.e. *Zar1*) (Wu, Viveiros et al. 2003), genomic imprinting (i.e. *Dnmt3a, Dnmt3l*) (Bourc'his, Xu et al. 2001, Kaneda, Okano et al. 2004), chromatin remodeling (i.e. *Tif1α*, *Brwd1, Brg1, Npm2*) (Burns, Viveiros et al. 2003, Bultman, Gebuhr et al. 2006, Torres-Padilla and Zernicka-Goetz 2006, Philipps, Wigglesworth et al. 2008), as well as maternal RNA degradation (i.e. *Dicer1, Ago2*) (Tang, Kaneda et al. 2007, Lykke-Andersen, Gilchrist et al. 2008, Philipps, Wigglesworth et al. 2008). During early developmental stages when zygotic genes are not fully activated, development depends mostly on maternal RNAs and proteins. It is therefore not surprising that the absence of maternal mRNAs is tightly associated with early-stage embryonic lethality. Loss of a few zygotic genes also results in embryonic lethality at the 1- to 4-cell stages of mouse development, although their mechanisms of action remain poorly understood. These genes include *Pp2cβ* (a.k.a. *Ppm1b*), *Ddx20*, *Ddx1*, *Profilin 1* as well as *Ercc2* (de Boer, Donker et al. 1998, Witke, Sutherland et al. 2001, Sasaki, Ohnishi et al. 2007, Mouillet, Yan et al. 2008, Hildebrandt, Wang et al. 2019). *Ppm1b* knockout in C57BL/6 mice results in arrest of 2-cell embryos. PPM1B is present in MII-stage oocytes, fertilized oocytes as well as pre-

implantation embryos. Although it has been proposed to be required for 2-cell zygotic genome activation and/or important for enhanced phosphorylation of p38, the exact mechanism behind the 2-cell arrest caused by *Ppm1b* knockout is still unknown. *Ddx20* knockout also results in embryonic lethality at the 2-cell stage. DDX20 has been proposed to play a role in ZGA. *Ddx20* heterozygous mice have reduced levels of *Ddx20* in ovaries. Thus, *Ddx20* expression may be associated with *Ddx20* gene copy number. This is in contrast to *Ddx1* whose expression is similar at both the RNA and protein levels in wild-type and heterozygous mice (Hildebrandt, Germain et al. 2015). As DDX20 interacts with the RNA processing SMN complex, Mouillet *et al.* have proposed that DDX20 may be involved in the processing of maternal RNAs during embryonic development (Charroux, Pellizzoni et al. 1999, Mouillet, Yan et al. 2008). Interestingly, immunostaining analysis indicates that DDX20 localizes to the subplasmalemmal cytoplasm just like DDX1 (Mouillet, Yan et al. 2008, Hildebrandt, Wang et al. 2019). As DDX1 also interacts with SMN, DDX1 and DDX20 may share similar roles during early embryonic development (Li, Roy et al. 2006). *Profilin 1 (Pfn1)* is a cytoskeleton protein whose knockout affects embryonic cleavage. Adult heterozygous *Pfn1* mice show a 50% reduction in PFN1 levels with no apparent abnormality (Witke, Sutherland et al. 2001). *Ercc2* is a DNA helicase involved in the base excision repair pathway (Tirode, Busso et al. 1999). ERCC2 plays a role in the repair of both nuclear and mitochondrial DNA damage (Tirode, Busso et al. 1999, Liu, Fang et al. 2015). XPD/ERCC2 is located in the inner mitochondrial membrane where it plays a role

in the repair of oxidative damage caused by reactive oxygen species (Liu, Fang et al. 2015). Therefore, the *Ercc2* related embryonic lethality may be related to the DNA damage caused by mtROS.

Another cause of 2-cell arrest in mouse embryos is disrupted mitochondrial metabolism at early developmental stages. As introduced in section 1.3.5, abnormal oocyte mitochondria activity is a major factor in early-stage embryonic arrest. One of the maternal genes related to oocyte mitochondrial quality is *Nlrp5* (a.k.a. *Mater*) (Fernandes, Tsuda et al. 2012). *Mater* is a component of the subcortical maternal complex (SCMC). *Mater* has been shown to be associated with oocyte mitochondria quality. In the absence of *Mater*, embryos undergo embryonic arrest due to defective oocyte mitochondrial function. Interestingly, not only can reduced mitochondrial function cause cell death, but increased mitochondrial function as well, as the result of upregulation of mitochondrial reactive oxygen species (mtROS) (Brookes, Yoon et al. 2004, Peng and Jou 2010). The electron transport chain of mitochondria is used for the production of ATP (Peng and Jou 2010). However, if the electron transport chain is leaky, this can also result in increased production of mtROS. Therefore, mitochondrial activity must be controlled within a certain range with lethality associated with either too high or too low activity.

ROS are free radicals that attack DNA in both the mitochondria and the nucleus of the cells. Under normal conditions, these ROS can be tolerated and

neutralized, and the damage they cause can be repaired by DNA repair mechanisms. However, when increased ROS are generated, cells will undergo mitochondria and nuclear fragmentation characteristic of apoptosis (Jezek, Cooper et al. 2018). Embryos undergo rapid division with few zygotic genes activated during very early embryonic developmental stages. Most of the mRNAs that encode DNA double strand break (DSB) repair proteins in rhesus monkey embryos are maternally derived and carried over from oocytes (Zheng, Schramm et al. 2005). As the oocyte matures, overall levels of maternal mRNAs decrease. This decrease of mRNAs carried on until the accumulation of zygotic mRNAs can replace the degraded maternal mRNAs (Zheng, Schramm et al. 2005). Therefore, there may be a stage where mRNAs encoding DNA DSB repair proteins have reached relatively lower levels. With the decrease in DSB repair protein encoding mRNAs and the large increase of ROS generated by active mitochondria, 2-cell embryos may be most vulnerable to ROS attack compared to other embryos stages as DNA repair is not as active in these cells.

1.3.10 Morula and blastocyst stages

Embryos at the 8- to 16-cell stages are called morula. During the morula stage, the blastomeres in the embryo start to form cell-to-cell interactions primarily through E-cadherin (Vestweber, Gossler et al. 1987). E-cadherin is evenly distributed across the plasma membrane of 8-cell stage blastomeres. As embryos progress from the 8-cell stage to the 16-cell stage, they undergo compaction and

polarization with E-cadherins restricted to the cell-to-cell contact sites (Vestweber, Gossler et al. 1987). Compaction is inhibited when E-cadherin is neutralized by antibodies or Ca^{2+} ions are removed (Ducibella and Anderson 1979, Hyafil, Morello et al. 1980, Vestweber, Gossler et al. 1987). However, the role of E-cadherin in compaction remains controversial. Fierro-Gonzalez *et al.* suggested that E-cadherin is needed for the initiation of compaction (Fierro-Gonzalez, White et al. 2013). This group provided evidence for a stage-specific E-cadherin-dependent filopodia being employed by the blastomeres for the attachment of contactless apical domains of neighboring cells. This idea was challenged by Maitre *et al.* who showed that embryo compaction was mainly driven by contractility of the actomyosin cortex (Maitre, Turlier et al. 2016). They proposed that the contractions within the actomyosin cortex are responsible for the generation of increased surface tension between the contactless apical domains whereas E-cadherin reduces the contractility and redirect it away from sites of cell-to-cell contact.

Along with compaction, the establishment of cell polarity is initiated at the 8-cell stage (Johnson and Ziomek 1981). Although the establishment of cell polarity does not depend on the compaction event, cell-to-cell contact is important for this process (Johnson and Ziomek 1981, Johnson, Maro et al. 1986, Fleming, McConnell et al. 1989, Stephenson, Yamanaka et al. 2010). The polarity of the blastomeres determines the cell fate of their daughter cells. When a blastomere undergoes perfect symmetric division, two seemly identical daughter cells are generated. These daughter cells most likely maintain the polarity of the parent

blastomere and occupy the outer positions of the embryo and become the trophectoderm. Asymmetric divisions on the other hand, generate two different daughter cells. The division orientation directly affects the number of inner and outer cells generated by this division. Further divisions increase the number of ICM and trophectoderm cells to 32-cells which is the beginning of blastocyst stage (Morris, Teo et al. 2010). After an additional 24 hours of maturation, the blastocyst is ready for implantation.

1.4 Hypothesis

We propose that DDX1plays a role in the regulation of RNAs that affect the proper functioning of mitochondria, RNA utilization and/or maternal-to-zygotic transition leading to early embryonic arrest.

1.5 Thesis objectives and summaries

1.5.1 Chapter 2: Cytoplasmic DDX1 aggregation in early mouse embryo

Temporally-regulated maternal RNA translation is essential for embryonic development, with defective degradation resulting in stalled 2-cell embryos. The goals of Chapter 2 were to examine: (i) the subcellular distribution of DDX1 in oocytes and early-stage embryos, (ii) the importance of RNA in the subcellular distribution of DDX1, and (iii) identify RNAs that bind to DDX1 in early-stage embryos. We show that DDX1, a DEAD box protein implicated in RNA transport,

may be a key regulator of maternal RNA utilization. DDX1 protein localizes exclusively to cytoplasmic granules in both oocytes and early-stage mouse embryos, with DDX1 requiring RNA for retention at these sites. Homozygous knockout of *Ddx1* causes stalling of mouse embryos at the 2-4 cell stages. These results suggest a maternal RNA-dependent role for DDX1 in the progression of embryos past the 2-4 cell stage. The change in appearance of DDX1-containing granules in developing embryos further supports a role in temporally-regulated degradation of RNAs. We carried out RNA-immunoprecipitations (RNA-IPs) to identify mRNAs bound to DDX1 in 2-cell embryos, focusing on 16 maternal genes previously shown to be essential for embryonic development past the 1- to 2-cell stages. Five of these RNAs were preferentially bound by DDX1: *Ago2*, *Zar1*, *Tle6*, *Floped* and *Tif1α*. We propose that DDX1 controls access to subsets of key maternal RNAs required for early embryonic development.

1.5.2 Chapter 3: Clustering of membrane associated RNA-containing vesicles (MARVs) controls cytoplasmic calcium distribution

DEAD box protein DDX1, previously associated with polyadenylation, forms large aggregates in the cytoplasm of early mouse embryos. DDX1 knockout causes stalling of embryos at the 2-4 cell stages with clear indication of mitochondrial and nuclear fragmentation. The goal of Chapter 3 was to define the structure and composition of the DDX1 aggregates identified in the cytoplasm of early-stage embryos, to get insight into the function of these cytoplasmic

aggregates. By examining DDX1 aggregates in embryos, we discovered a novel calcium-containing vesicle distinguished by an RNA core [Membrane Associated RNA Vesicle (MARV)] located adjacent to subplasmalemmal cytoplasm enriched in high membrane potential mitochondria. We present evidence that DDX1 is required for the formation of MARVs which in turn regulate the spatial distribution of calcium. *Ddx1* knock-out in early embryos disrupts calcium distribution, thereby increasing mitochondria membrane potential and reactive oxygen species. We have also found localization of cytoplasmic polyadenylation proteins CPSF2 and CPEB1 in MARVs suggesting that MARVs may also be hubs for cytoplasmic polyadenylation. Therefore, we propose a role for MARVs in controlled calcium release and RNA polyadenylation essential for embryonic development.

1.5.3 Chapter 4: Identification of DDX1 bound RNAs in 2-cell embryos

Zygotic *Ddx1* is essential in the formation of MARVs during early embryonic development. MARVs are membrane-bound aggregates of DDX1 vesicles which each contain an RNA core structure. As DDX1 belongs to the DEAD box protein family which has been shown to play essential roles in all aspects of RNA metabolism, we propose that DDX1 plays a critical role associated with the RNA cores identified in the DDX1 vesicles. The goals of Chapter 4 were to: (i) further characterize when *Ddx1*$^{-/-}$ embryos die during development, and (ii) use RNA immunoprecipitation followed by RNA sequencing to identify the RNAs bound to DDX1 in early-stage embryos. We show that *Ddx1*$^{-/-}$ embryos are embryonic lethal

at 1-cell stage *in vivo* whereas they can survive to 2-cell stage *in vitro*. We postulate that this early embryonic lethality is due to the immediate requirement for cytoplasmic polyadenylation upon fertilization. Using RNA-immunoprecipitation followed by sequencing (RIP-seq), we found that DDX1 binds to a number of protein-encoding RNAs. Surprisingly, ~20% of the DDX1 bound RNAs were pseudogenes with another ~24% classified as long non-coding RNAs. As pseudogenes and long non-coding RNAs play a role in endogenous siRNA biogenesis, these results suggest that DDX1 may not only be important for processes related to protein-coding RNAs but also for the generation of endogenous siRNAs needed for embryonic development.

Chapter 2.

Cytoplasmic Aggregation of DDX1 in Developing Embryos: Early Embryonic Lethality Associated with Ddx1 Knockout

The goals of this chapter were to examine: (i) the subcellular distribution of DDX1 in oocytes and early-stage embryos, (ii) the importance of RNA in the subcellular distribution of DDX1, and (iii) identify RNAs that bind to DDX1 in early-stage embryos.

A version of chapter 2 has been published as Hildebrandt MR*, Wang Y*, Li L, Yasmin L, Glubrecht DD, Godbout R. Cytoplasmic aggregation of DDX1 in developing embryos: Early embryonic lethality associated with Ddx1 knockout. Developmental Biology. 2019 455(2):420-433. doi: 10.1016/j.ydbio.2019.07.014. *These authors contributed equally to this work. Immunohistochemistry was performed by Darryl Glubrecht. RNA immunoprecipitation and western blot were performed by Dr. Lei Li. I was responsible for data analysis and interpretation, PCR, embryo collection, immunofluorescence staining and imaging, and writing the manuscript. Dr. Matthew Hildebrandt assisted with data analysis, immunofluorescence staining and imaging and writing the manuscript. Dr. Lubna Yasmin assisted with embryo collection and immunofluorescence staining. Dr. Roseline Godbout was involved in all stages of the project and in writing the manuscript.

2.1 Introduction

DEAD box 1 (DDX1) is an RNA helicase involved in cellular processes ranging from RNA transport to the repair of DNA double-strand breaks (Chen, Lin et al. 2002, Kanai, Dohmae et al. 2004, Robertson-Anderson, Wang et al. 2011, Lin, Sivakumaran et al. 2014, Perez-Gonzalez, Pazo et al. 2014, Popow, Jurkin et al. 2014, Li, Poon et al. 2017, Ribeiro de Almeida, Dhir et al. 2018). DDX1 is most often found in the nucleus of the cell where it associates with nuclear bodies involved in RNA processing such as Cajal bodies, gems and cleavage bodies (Bleoo, Sun et al. 2001, Li, Roy et al. 2006). DDX1 is also found in RNA granules located in the cytoplasm of neurons (Kanai, Dohmae et al. 2004, Miller, Blandford et al. 2009). These RNA granules are involved in the transport of RNAs in neuronal cell bodies and processes so that they can be translated where they are needed. When cells are treated with ionizing radiation, DDX1 co-localizes with proteins involved in the repair of DNA double-strand breaks (Li, Monckton et al. 2008, Li, Germain et al. 2016, Li, Poon et al. 2017). There is evidence pointing to a role for DDX1 in the clearance of RNA at DNA double-strand breaks located in transcriptionally active genomic regions (Li, Monckton et al. 2008, Li, Germain et al. 2016, Li, Poon et al. 2017).

The biological role of DDX1 remains poorly understood. *DDX1* cDNA was first cloned from retinoblastoma cell lines carrying amplified copies of the *DDX1* and *MYCN* genes (Godbout and Squire 1993). DDX1 was subsequently found to also be amplified and overexpressed in other pediatric cancers such as

neuroblastoma and alveolar rhabdomyosarcoma (Squire, Thorner et al. 1995, Amler, Schurmann et al. 1996, Noguchi, Akiyama et al. 1996, Godbout, Packer et al. 1998, Akiyama, Akao et al. 1999). More recently, elevated levels of cytoplasmic DDX1 have been shown to correlate with early recurrence in breast cancer, regardless of cancer subtype (Germain, Graham et al. 2011). Intriguingly, levels of DDX1 may be predictive of breast cancer response to chemotherapy and hormone therapy (Balko and Arteaga 2011, Germain, Graham et al. 2011).

Ddx1 knock-out models have been generated in both *Mus musculus* and *Drosophila melanogaster.* Although viable, *Ddx1*-null flies are smaller in size than their wild-type counterparts. Males are sterile due to disrupted spermatogenesis, whereas females show much reduced fertility with egg chambers undergoing autophagy (Germain, Li et al. 2015). In contrast, loss of *Ddx1* function in mice leads to early embryonic lethality, with embryos dying pre-blastocyst (Hildebrandt, Germain et al. 2015). This difference in phenotype between mice and flies may in part be explained by the presence of maternal Ddx1 protein in *Ddx1*-null flies up to the second instar, at 48 h post-egg laying (Germain, Li et al. 2015). Intriguingly, we also observe *Ddx1* wild-type lethality when crossing second generation *Ddx1* heterozygote mice (Hildebrandt, Germain et al. 2015). Our results suggest that transcription of the wild-type *Ddx1* allele is up-regulated in $Ddx1^{+/-}$ mice, leading to lethality when these heterozygote mice are subsequently mated due to overexpression of DDX1 in wild-type mice.

The initial stages of mouse development are dependent on the maternal complement of transcripts and proteins (Tang, Kaneda et al. 2007, Li, Zheng et al. 2010). In mammals, oocytes and surrounding cumulus cells generate the maternal transcripts required by the oocyte and the fertilized zygote. Maternally transcribed genes such as Zygote arrest 1 (*Zar1*) and transcription intermediary factor 1, alpha (*Tif1*α also known as *Trim24*) are important for the progression of the embryo beyond the 1- or 2-cell stage, respectively (Wu, Viveiros et al. 2003, Torres-Padilla and Zernicka-Goetz 2006, Jiao and Woodruff 2013). *Zar1* and *Tif1*α affect pronuclear syngamy and promote the first wave of zygotic genome activation, respectively.

For development to proceed past the initial divisions, the zygote has to undergo genome activation (Schultz 1993, Nothias, Miranda et al. 1996, Zeng and Schultz 2005). The maternal-to-zygotic transition (MZT) occurs just after fertilization and is mostly completed by the 2-cell stage in mice and by the 8-cell stage in humans and bovines (Telford, Watson et al. 1990, Schultz 1993, Schultz 2002). The first component of MZT is the active degradation of oocyte-specific transcripts, a process believed to trigger embryonic transcription (Piko and Clegg 1982, Schultz 2002). Transcript degradation in the cytoplasm is associated with the 'RNA induced silencing complex' (RISC) (Lykke-Andersen, Gilchrist et al. 2008). The endoribonuclease Argonaute 2 (Ago2) encoded by maternal mRNA is one of the key proteins involved in the degradation of maternal transcripts and the loss of the maternal *Ago2* transcripts results in embryonic lethality at the 2-cell

stage (Lykke-Andersen, Gilchrist et al. 2008). Once oocyte-specific degradation occurs, embryonic genes are reprogrammed through chromatin remodeling and embryonic transcription activated (McLay and Clarke 2003, Clapier and Cairns 2009). The large burst of transcription associated with zygotic gene activation does not occur until the 2-cell stage, and there is no delay in the translation of these transcripts (Carter, Hamatani et al. 2003, Hamatani, Carter et al. 2004, Wang, Piotrowska et al. 2004).

We have previously shown that *Ddx1*$^{-/-}$ mouse embryos die prior to the blastocyst stage (Hildebrandt, Germain et al. 2015). Here, we demonstrate that *Ddx1*$^{-/-}$ embryonic development stalls at the 2- to 4-cell stages *in vitro*. Based on immunostaining data, DDX1 is predominantly found in cytoplasmic granules in pre-implantation embryos. Cytoplasmic DDX1 granules are dynamic, changing in size and appearance as development progresses from the zygote to the blastocyst stages. DDX1 granules co-localize with two proteins previously associated with stress granules, TIA-1 and TIAR (Kedersha, Gupta et al. 1999). Our data suggest that DDX1, but not TIAR/TIA-1, accumulation in cytoplasmic granules in early embryos is dependent on the presence of RNA. We propose that DDX1 is part of an essential complex that controls RNA bioavailability early in embryonic development by binding to maternal transcripts that are essential for early embryonic development.

2.2 Materials and Methods

2.2.1 Embryo and oocyte collection

The generation of a *Ddx1* knockout line has been described previously (Hildebrandt, Germain et al. 2015). Naturally mated heterozygote *Ddx1*$^{+/-}$ and C57BL/6 or FVB mice were checked for the presence of a vaginal plug, with plug date designated as embryonic day (E) 0.5. For collection of E0.5 to E2.5 embryos, the oviducts and uterus were removed and placed in prewarmed (37˚C) M2 flush medium (Sigma-Aldrich). Oviducts were flushed using a capillary tube to collect E0.5 to E2.5 embryos. The uterine horns were flushed to collect E3.5 embryos. E0.5 single cell embryos were treated with 300 µg/ml hyaluronidase (Sigma-Aldrich) for 30 seconds to 1 minute to remove the cumulus cells.

To obtain germinal vesical (GV) stage oocytes, ovaries were dissected from adult female mice. Ovaries were placed in prewarmed (37˚C) M2 medium. The ovaries were poked extensively with a fine needle under a dissecting microscope to release oocytes. Cumulus cells were removed with hyaluronidase as described above. For immunostaining, oocytes were placed in PBS and processed as described below for preimplantation embryos. For *in vitro* maturation to meiosis I (MI) (Kidder 2014), oocytes were allowed to mature to meiosis I (MI) by culturing in previously prepared drops of KSOM medium under oil for 24-48 h at 37˚C in 5% CO_2. To obtain MII-arrested oocytes, FVB/N wild-type females were

injected with 5 IU pregnant mare serum gonadotropin (Intervet) followed by 5 IU chorionic gonadotropin (Intervet) approximately 46 h later (Luo, Zuniga et al. 2011). Females were euthanized by cervical dislocation. The oviducts were flushed using a capillary tube to release the oocytes into M2 medium (Sigma-Aldrich) containing 300 µg/ml hyaluronidase to remove the cumulus cells. Oocytes were then rinsed in M2 medium and immunostained as described below for embryos.

2.2.2 Culturing pre-implantation embryos and hatching blastocysts

At least 30 minutes before collecting embryos, M16 or KSOM medium (Sigma-Aldrich) was prepared by placing 25 µl drops covered with embryo-tested mineral oil (Sigma-Aldrich) in a 24-well dish. Three larger (100 µl) drops of medium covered with mineral oil were also prepared for washing the embryos following flushing. The dish was placed in a 5% CO_2 incubator for equilibration. Embryos were collected, rinsed 3X in M16 medium, placed in the 25 µl M16 or KSOM droplets and cultured for the designated times.

For hatching blastocysts, embryos were cultured in high glucose DMEM supplemented with 15% FCS, 0.1 mM β-mercaptoethanol (β-ME), 1X sodium pyruvate (Gibco), 1X non-essential amino acids (Gibco) and penicillin and streptomycin on gelatin-coated wells or coverslips.

2.2.3 Immunostaining embryos

Embryos were transferred from flush medium to PBS and washed 2X in PBS. Embryos were fixed in 4% paraformaldehyde for 15 minutes. The embryos were then washed 3X in PBS + 0.01% Triton-X-100 (PBST), followed by permeabilization in PBS + 0.5% Triton-X-100 for 10 minutes. The embryos were washed 3X in PBST and incubated in primary antibody containing PBST for a minimum of 1 h at room temperature. Following primary antibody incubation, embryos were washed 3X in PBST and transferred to secondary antibody containing PBST for 1 h at room temperature. The plate was wrapped with foil to minimize exposure to light. After washing 3X in PBST, embryos were placed on a slide and mounted in Mowiol (Calbiochem) containing 1 µg/ml 4',6-diamidino-2-phenylindole (DAPI) to stain the DNA. The primary and secondary antibodies used for immunostaining are listed in **Table 2.1.** Anti-DDX1 (2910) was used for all embryo immunostaining. For mitochondria staining, embryos were transferred to M16 droplets containing 100 µM MitoTracker Deep Red (Cell Signaling Technology) and incubated at 37°C for 30 minutes. Embryos were then fixed and permeabilized in methanol:acetone (1:1 ratio) at 4°C for 5 minutes and rehydrated for 30 minutes with PBST. DDX1 immunostaining after permeabilization in methanol:acetone was as described above.

Table 2.1 Antibodies used for immunohistochemistry and immunofluorescence			
Antibody	Host	Dilution	Source
anti-DDX1 (2910)	Rabbit	1:800	In house (batch 2910) (Bleoo, Sun et al. 2001)
anti-DDX1 (2290)	Rabbit	1:500	In house (batch 2290)
anti-CstF64	Mouse	1:100	Dr. James Manley, Columbia University
anti-SMN	Mouse	1:1000	ImmuQuest, Cat. # IQ202
anti-DDX3	Mouse	1:200	Santa Cruz, Cat. # sc-81247
anti-EXOSC5	Mouse	1:100	Abcam, Cat. # ab69699
anti-GW182	Mouse	1:50	Dr. Marvin Fritzler, University of Calgary
anti-RACK1	Mouse	1:400	Transduction Laboratories, Cat. # R20620
anti-FXR1	Goat	1:100	Santa Cruz, Cat. # sc-10554
anti-TIAR	Goat	1:400	Santa Cruz, Cat. # sc-1749
anti-TIA-1	Goat	1:400	Santa Cruz, Cat. # sc-1751
anti-DDX6	Mouse	1:300	Abnova, Cat. # H00001656-M01
anti-Calnexin	Mouse	1:200	Santa Cruz, Cat. # sc-6465
anti-Rabbit Alexa-488	Donkey	1:400	Molecular Probes, Thermofisher
anti-Goat Alexa-488	Donkey	1:400	Molecular Probes, Thermofisher
anti-Mouse Alexa-555	Donkey	1:400	Molecular Probes, Thermofisher
anti-Goat Alexa-555	Donkey	1:400	Molecular Probes, Thermofisher
anti-Rabbit Alexa-555	Donkey	1:400	Molecular Probes, Thermofisher

Embryos were imaged by confocal microscopy using a Zeiss LSM710 laser scanning microscope and a plan-apochromat 40X/1.4 lens to capture single sections. Z-stacks were taken at 0.35 µm intervals. Cytoplasmic DDX1 granules were analysed with Imaris software v7.7.0 (Bitplane). All images were processed with a 3x3x1 median filter followed by surface analysis. Surfaces were not smoothed and an absolute threshold of 200 voxels (3D pixels) was used to define surfaces. A minimum threshold of 200 voxels was used to define the minimum aggregate size. Six to ten embryos were analysed for each developmental stage and the volumes of the DDX1 granules were compared using a box and whisker plot (Prism). Statistical analysis was by one-way ANOVA.

2.2.4 Acridine orange staining embryos and RNase A treatment

Acridine orange (2 µM; Sigma-Aldrich) was used to stain RNA in embryos. For RNase treatment, embryos were collected and transferred to warm DMEM + 5 mM HEPES (pH 7.5) in a 24 well dish. The embryos were transferred to PBS + 0.1% saponin for 6 minutes at room temperature then incubated in PBS containing 150 µg/ml RNase A for 30 minutes at 37˚C. Embryos were then washed in PBS twice before immunofluorescence staining. This method was adapted from Li *et al.* (Li, Monckton et al. 2008).

2.2.5 Transcription and translation inhibition

M16 medium (25 µL) containing either 200 µM cordycepin (Sigma-Aldrich) or 150 µg/ml cycloheximide (Sigma-Aldrich) was used for transcription or translation inhibition, respectively. Untreated 2-cell stage embryos served as controls. M16 medium droplets were covered with mineral oil and incubated at 37°C at least 30 minutes before the transfer of embryos. E1.5 embryos were collected from flush medium and washed 3X in M16 medium before transferring to the 25 µl M16 medium droplets.

2.2.6 Immunohistochemistry

OCT and paraffin-embedded tissues were sectioned. OCT-embedded tissue sections were processed for antigen retrieval by heating tissue sections covered with 10 mM citrate buffer containing 0.05% Tween-20 at pH 6.0 to 100°C, followed by microwaving at 750 W for 6 minutes. For paraffin-embedded tissue sections, tissues were first de-waxed by dipping in xylene 3X for 10 minutes each. Tissue sections were then hydrated through a series of ethanol, from 100% ethanol to ddH_2O and TBS. Antigen retrieval was as described above and the slides washed with TBST (0.05% Tween 20) for 5 minutes. From this point, OCT- and paraffin-embedded tissue sections were treated the same. Tissue sections were blocked for 30 minutes to 1 h in 0.5% fish gelatin in TBST (0.1% Tween 20),

followed by an overnight incubation at 4°C with primary antibody diluted in Dako Antibody Diluent. After a series of washes in TBS and TBST (0.05% Tween 20), background peroxidase activity was removed by incubating slides in 3% H_2O_2 in TBS for 15 minutes. Dakocytomation Envision+ System Labelled Polymer HRP secondary antibody was added for 1-2 h. Tissue sections were washed in TBST and DAB chromagen in TBS added, followed by DAKO Liquid DAB+ Substrate Chromagen System. The DAB signal was darkened by incubating the slides in 1% copper (II) sulphate. For counterstaining, slides were incubated in hematoxylin for 1-5 minutes, washed, and incubated in saturated lithium carbonate for ~2 minutes (to obtain a light blue color). Slides were coverslipped with VectaMount AG (Vector Laboratories). Images were captured with an Axioskop 2 Plus microscope with Zeiss 10X/0.3, 20X/0.75 and 40X/1.3 lenses.

2.2.7 RNA isolation and RT-PCR

Total RNA from adult mouse brain tissue was isolated using the TRIzol reagent (Thermo Fisher Scientific). Total RNAs were extracted from either seven (mouse 1) or eight (mouse 2) 2-cell embryos using the RNeasy Plus Micro Kit (Qiagen) following the manufacturer's protocol. RNAs were reverse transcribed using SuperScript IV (Invitrogen) and oligodT. PCR reactions were carried out using the following primers and conditions. For exons 1 to 9 amplification, nested

PCR was carried out using forward primer 5'-CCCGCAGCGGAGGAGTG-3' and reverse primer 5'-TAATTATCAAATTGTTTATTATGAGA-3 for the first round of PCR, and forward primer 5'-AAGATGGCGGCCTTCTCC-3' and reverse primer 5'-TAATTATCAAATTGTTTATTATGAGA-3' for nested PCR. For exons 10 to 16 amplification, we used forward primer 5'-AATTCACTATGCATGATACCATT-3' and reverse primer 5'-AAGTCTTTTCCCATCACACGT-3'. For exons 17 to 21, we used forward primer 5'-TGATTGTTTGCTCTGCTACTC-3' and reverse primer 5'-CATAAGGAACGCCATGGATAT-3'. For exons 22 to 26, we used forward primer 5'-ACCCTGCCTGATGAGAAGC-3' and reverse primer 5'-TATAGTTGTCAAGTTTATTTTCATT-3'. All PCR reactions (including nested PCRs) were performed under the following conditions: pre-PCR (94°C 5 minutes), 40 cycles (94°C 30s, 58°C 30s, 72°C 30s) with a final extension (72°C 7 minutes).

2.2.8 Western blotting

Whole cell lysates were prepared from two hundred 2-cell embryos, mouse R1 embryonic stem cells and adult mouse brain tissue. Embryos were first treated with Acidic Tyrode's solution (Sigma) to dissolve the zona pellucida. They were then washed with 2X PBS and frozen in liquid nitrogen. Embryos, R1 cells and brain tissue were lysed in lysis buffer [50 mM Tris-HCl pH 7.5, 150 mM NaCl, 1% sodium deoxycholate, 1% Triton-X-100, 1 mM EDTA, 0.1% SDS, 1 mM DTT, 1X

PhosStop (Roche) phosphatase inhibitors and 1X Complete (Roche) protease inhibitors]. The entire 2-cell embryo lysate was mixed with loading buffer, boiled and loaded onto a SDS-PAGE gel. For R1 cells, we loaded 2.5, 5, 10 µg of lysate. For comparison of R1 cells and brain tissue, 40 µg of proteins was loaded in each lane. Proteins were transferred to a PVDF membrane and immunoblotted with two different anti-DDX1 antibodies: anti-DDX1 (2910), targeting aa 1-186, and anti-DDX1 (2290), targeting aa 187-740. R1 and mouse brain blots were also immunoblotted with anti-actin antibody.

2.2.9 RNA immunoprecipitation, pre-amplification and RT-qPCR

Embryos were collected in PBS and frozen in liquid N_2 before storing at -80ºC. Three hundred embryos were pooled together and divided into 2 groups (IgG, DDX1). 150 embryos per group were lysed in lysis buffer [50 mM Tris-HCl, pH 7.5, 150 mM NaCl, 1% NP-40, 0.5% deoxycholate, 5 mM EDTA, 2 mM DTT, 1X Complete protease inhibitor (Roche) and 200 unit/ml RNase inhibitor (Invitrogen)]. Lysates were pre-cleared with Protein A beads (GE Healthcare), followed by incubation with either IgG-purified rabbit-anti-DDX1 antibody or pre-immune serum at 4°C for 90 minutes with rotation. Protein A beads were then added and samples were incubated for another 45 minutes. Immunoprecipitates were washed 5 times in wash buffer [50 mM Tris-HCl, pH 7.5, 1 M NaCl, 1% NP-

40, 1% deoxycholate and 5 mM EDTA], followed by one wash in 1X RQ1 DNase buffer (40 mM Tris-HCl, pH 8.0, 10 mM $MgSO_4$, 1 mM $CaCl_2$). Immunoprecipitates were digested with 8 unit/ml of RQ1 DNase (Promega) at 37°C for 30 minutes, followed by digestion with 250 µg/ml of Protease K (Roche) at 37°C for 30 minutes. Co-immunoprecipitated RNAs were extracted with sodium acetate (pH 5.2)-equilibrated phenol (Roche) and precipitated with ethanol. Precipitated RNAs were resuspended in H_2O and reverse-transcribed to cDNA using random hexamers and Superscript IV reverse transcriptase (Invitrogen) following the manufacturer's instructions. cDNAs were then pre-amplified using 16 different primer sets (**Table 2.2**) at a final concentration of 36 nM for each primer. The pre-amplification PCR reaction was using Phusion DNA polymerase (NEB) at 60ºC and 14 cycles of PCR amplification. The pre-amplification steps were adapted and modified from (Andersson, Akrap et al. 2015) and the protocol of Cell-to-CT kits (Thermo Fisher Scientific). The cDNA products were then diluted 8-fold with nuclease-free water. For RT-qPCR, 1 µl of diluted cDNA was used for each 10 µl reaction containing BrightGreen 2X-qPCR MasterMix-ROX (Applied Biological Materials). PCR was performed in 96-well plates using the QuantStudio 6 Flex Real-Time PCR system (Applied Biosystems). The run method was customized as follows: Pre-PCR (Ramp rate 1.9°C/s, 95°C for 10 minutes), 40 cycles PCR (Ramp rate 1.9°C/s, 95°C 15s, Ramp rate 1.9°C/s, 58°C 30s, Ramp rate 1.6°C/s, 72°C 1 minute). Results were exported in Excel, and analyzed with Prism. Ct values above 36 were considered as 36.

Table 2.2 Primers used for RT-qPCR	
Zar1 Fwd	CGATCGGGTTCCTGTCAAC
Zar1 Rev	GAGAGGCCACAGAAGGTCA
Ago2 Fwd	AGAATACGGGTCTGTGGTGAT
Ago2 Rev	GAAGCAGGTCACAAGAAGCG
Tif1α Fwd	TGCTTCTGAGGAAACCGTGT
Tif1α Rev	CATGCACAGGGGACTTCTG
Dicer1 Fwd	TTGCCTGCATTTTCCCGTTG
Dicer1 Rev	AAGCTCTCCTGTGTGTCGG
Brwd1 Fwd	TGCAGTTGGGAAGCTGTGTA
Brwd1 Rev	AGGACCCATCAAGCACATGG
Hr6a Fwd	CCATCCTAACGTCTATGCAG
Hr6a Rev	CCGCTTGTTCTCCTGGTAC
Brg1 Fwd	CCAGCGGGTATGTCAGTGT
Brg1 Rev	CATACACCTGGCAAGGCAA
Bnc1 Fwd	GCAGGATGGCTGAGGCTAT
Bnc1 Rev	TCGAACACCACATTGGACTG
Mater Fwd	AGCAGACATCAGATAATGGAG
Mater Rev	GGTGTGAGGCTGGAAGGTT
Floped Fwd	GCCTGGCACAAAGAAAACGA
Floped Rev	GCCAGCCAGTTTTAGCCCT
Padi6 Fwd	CAACCAGCAGAGCACCAAAC
Padi6 Rev	GGGGCTCCAGTAATCCACA
Tle6 Fwd	GGGGCCTCCCTAACCTCA
Tle6 Rev	ATTTCAGAGACGACGCTGCT
Filia Fwd	AGCTTGGGCTGAGTAAGGC
Filia Rev	CTCTACTCTGTTCTTCCCGA
Zfp36l2 Fwd	AAGCACAACTTTCCGTCCCT
Zfp36l2 Rev	TTTGCCAGGGATTTCTCCGT
Npm2 Fwd	GCAGCGCAAACACAGTGATA
Npm2 Rev	TGTGGCGACTCATGTCGATT
Hsf1 Fwd	TGCTGGACATTCAGGAGCTT
Hsf1 Rev	CTCCCTGTGTCCACAGCAT

2.3 Results

2.3.1 DDX1 expression in adult mouse ovaries and maturing oocytes

We examined the subcellular localization of DDX1 in mouse ovaries. DDX1 was highly expressed in the developing oocytes and the surrounding granulosa cells of the ovaries **(Fig. 2.1A)**. Stromal cells between follicles had low to no expression of DDX1, while the cells of the corpus luteum were positive for nuclear DDX1 with weak diffuse cytoplasmic staining. All oocytes examined, regardless of maturation state, showed a strong DDX1 signal throughout the cytoplasm.

To further examine the subcellular distribution of DDX1 in oocytes, we collected oocytes at the germinal vesicle (GV) stage (immature oocytes) from both C57BL/6 and FVB mice. GV oocytes were immunostained with anti-DDX1 antibody and z-stacks were used to generate maximum intensity projections of DDX1 localization. Imaris software was used to reconstruct 3D structures from the z-stacks. DDX1 granules averaging 1.2 μm^3 in volume were found throughout the cytoplasm with ~7000 granules per GV oocytes **(Figs. 2.1B, C)**. No DDX1 was detected in the nucleus based on examination of single optical sections. Similar results were obtained in meiosis I (MI) and meiosis II (MII) oocytes, except that there were fewer DDX1 granules per oocyte and DDX1 granules were smaller in size **(Figs. 2.1B, C)**.

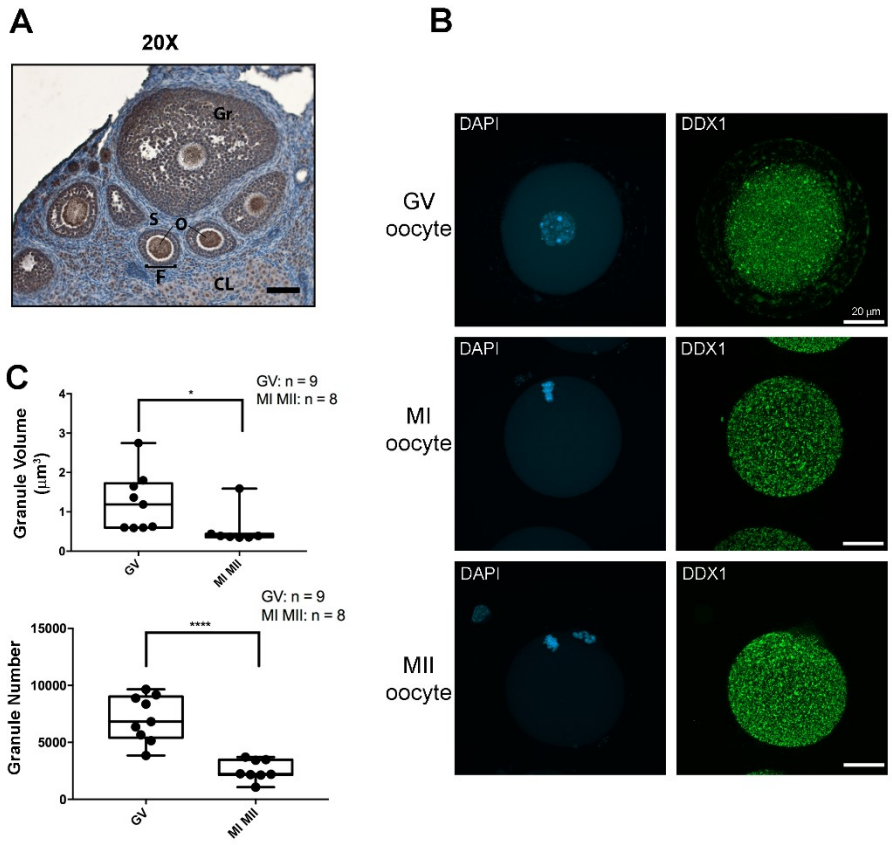

Figure 2.1 DDX1 expression in mouse ovaries and oocytes. (A) Sections of adult mouse ovaries were immunostained with anti-DDX1 antibody. Gr: Granulosa cells; O: Oocytes; F: Follicles; S: Stromal cells; CL: Corpus luteum. (B) Germinal vesicle oocytes, MI (meiosis I) oocytes and MII oocytes were immunostained with anti-DDX1 antibody and counterstained with DAPI for nucleus detection. Oocytes are displayed as 2D projections of Z-stacks imaged by confocal microscopy. Scale bars = 20 µm. (C) Surface rendering by Imaris software was used to calculate the number and volume of DDX1 granules. Statistical differences were calculated by Welch's t test using Prism software (*P<0.05; **** P<0.0001).

2.3.2 DDX1 expression in pre-implantation embryos

Analysis of single-cell RNA sequencing data (Biase, Cao et al. 2014) revealed significant increases in *Ddx1* RNA levels from the zygote to the 4-cell stage, with an ~2-fold increase from zygote to 2-cell stage, and a further 3-fold increase from the 2-cell to 4-cell stage (**Fig. 2.2**). These results suggest that *Ddx1* is one of the few zygotic genes activated during the minor wave of the MZT starting at zygote stage. We therefore examined DDX1 distribution in early stage embryos. In 1-cell stage embryos, the DDX1 immunostaining pattern was similar to that observed in unfertilized oocytes, with numerous granules found throughout the cytoplasm of the embryo (**Fig. 2.3A**). There was no detectable DDX1 in the nucleus of 1-cell stage embryos. DDX1 remained abundant in 2-cell and 4-cell embryos, with numerous DDX1-containing granules observed throughout the cytoplasm. By the 4-cell stage, fewer DDX1 granules were present; however, they appeared larger and less circular. By the 8-cell stage, DDX1 granules were variable in size and shape with what appeared to be aggregates (or clumps) of DDX1 granules throughout the cytoplasm. This trend towards aggregation was even more obvious in blastocysts, with fewer, but larger granules observed. Aggregates were unevenly distributed in blastocyst cells, and were mostly found surrounding the nucleus.

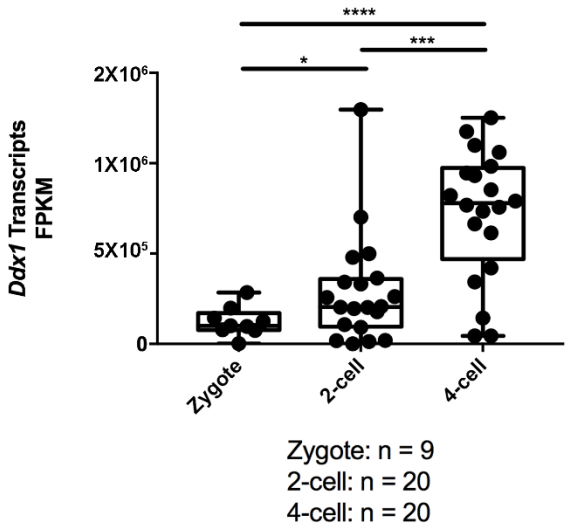

Figure 2.2 *Ddx1* RNA in embryos. Single cell sequencing data for zygotes, 2-cell and 4-cell stage embryos were obtained from Biase et al. (Biase, Cao et al. 2014). Data were merged with custom R scripts and rsqlite package. DDX1 expression profiles were extracted and plotted with Prism. Unpaired t-test between 2- and 4-cell embryos, Welch's t test between zygote and 2-cell, and Welch's t test between zygote and 4-cell were performed using Prism software (*P<0.05; ***P<0.001; **** P<0.0001).

We quantified the gradual decrease in the number of DDX1 granules from the 1-cell (zygote) stage to the blastocyst stage **(Figs. 2.3B, C)**. In 1-cell embryos, there was an average of ~3200 granules per embryo and the average granule size was 0.9 μm^3. In 2-cell embryos, there was an average of ~1700 granules with an average volume of 2.6 μm^3. In 4-cell stage embryos, there were ~600 DDX1

granules per embryo with an average volume of ~9 μm^3. There was one outlier with elevated granule numbers in the 4-cell embryo sample group, but this may have been an early 4-cell embryo in which the smaller DDX1 granules were still transitioning to larger granules. By the 8-cell stage, DDX1 granules had again increased in size to ~12 μm^3 although there was significant variation in granule volume. There were only ~200 large granules per 8-cell embryo. Large DDX1 aggregates with variable appearance were observed at the early (32-cell) blastocyst stage. While the total number of distinct aggregates was low (~50), these varied in volume from 15 to 60 μm^3. There was no significant difference in either the numbers or appearance of DDX1 aggregates in the inner cell mass (ICM) and trophoblast cells of early blastocysts.

As mentioned earlier, DDX1 is primarily found in the nucleus of post-embryonic cells. To determine when the transition from a primarily cytoplasmic localization to a primarily nuclear localization takes place during development, we immunostained later stage blastocysts cultured from 1-cell embryos. A reduction in cytoplasmic DDX1, accompanied by an increase in nuclear DDX1, was observed as blastocysts transitioned from early (**Fig. 2.3A**, bottom panels) to late stages **(Fig. 2.4A)**. DDX1 subcellular distribution was similar in the ICM and trophoblast cells of later stage embryos (magnified in **Fig. 2.4A).** To examine DDX1 subcellular distribution in hatched blastocysts, we cultured E3.5 blastocysts for 48 and 72 h. Hatched blastocysts at 48 h showed weak DDX1 immunostaining in the nucleus of trophoblast cells **(Fig. 2.4B)**. By 72 h in culture, the majority of

DDX1 was found in the nucleus of trophoblast cells **(Fig. 2.4B)**. The thickness of the ICM in hatched embryos precluded detailed analysis of DDX1 subcellular distribution. Overall, these results suggest different roles for DDX1 in embryos compared to post-embryonic tissues.

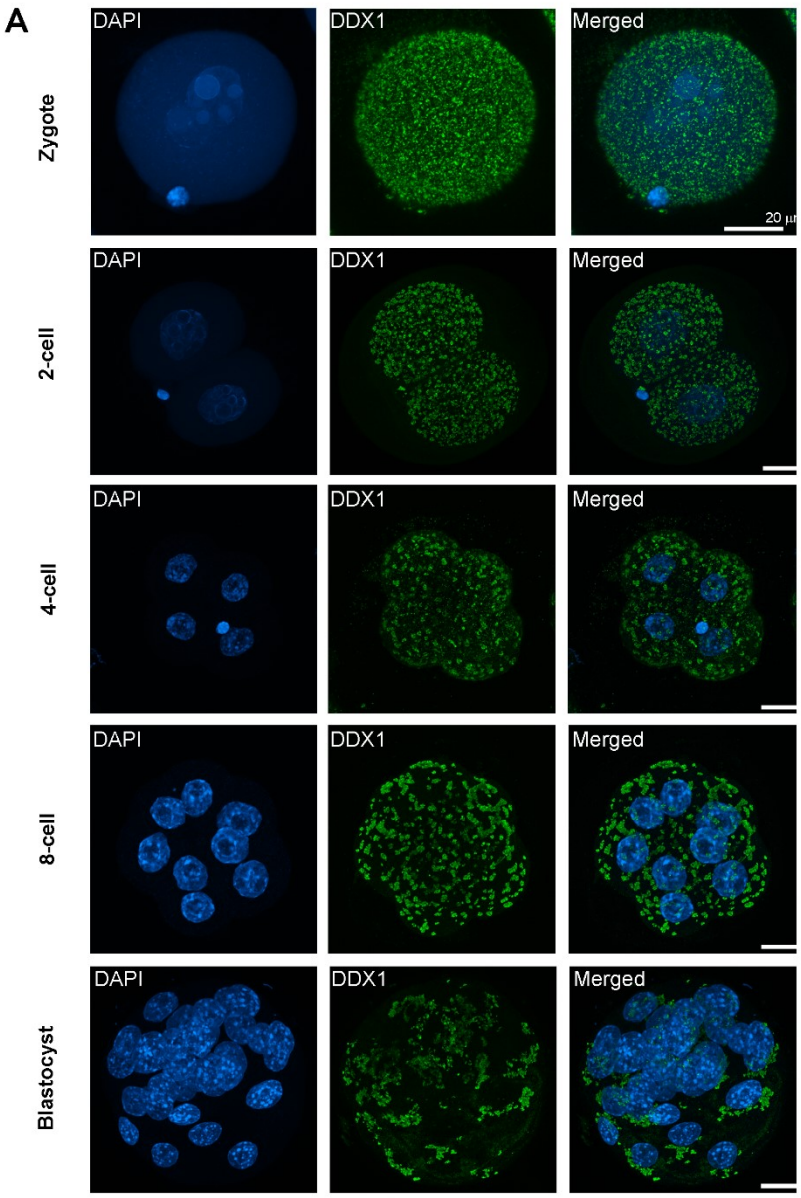
A
DAPI
DDX1
Merged
Zygote
2-cell
4-cell
8-cell
Blastocyst

B

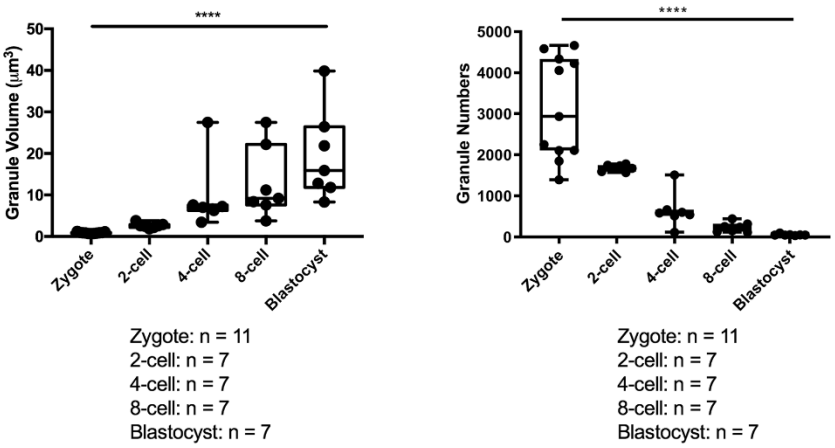

Zygote: n = 11
2-cell: n = 7
4-cell: n = 7
8-cell: n = 7
Blastocyst: n = 7

Zygote: n = 11
2-cell: n = 7
4-cell: n = 7
8-cell: n = 7
Blastocyst: n = 7

C

Average	Volume (μm³)	Numbers
Zygote	0.9	3137
2-cell	2.6	1678
4-cell	9.4	648
8-cell	12.8	235
Blastocyst	19.6	55

Figure 2.3 DDX1 localization in pre-implantation embryos. (A) Embryos at stages E0.5 (zygote or 1-cell), 1.5 (2-cell), 2 (4-cell), 2.5 (8-cell) and 3.5 (blastocyst) were immunostained with anti-DDX1 antibody and counterstained with DAPI for nucleus detection. DDX1 granules were observed exclusively in the cytoplasm. Embryos are displayed as 2D projections of Z-stacks imaged by confocal microscopy. Scale bars = 20 μm. (B, C) Surface rendering by Imaris software was used to calculate the number (B) and volume (C) of DDX1 granules

at each embryonic stage. Statistical differences were calculated by one-way ANOVA using Prism software. (**** indicates P<0.0001).

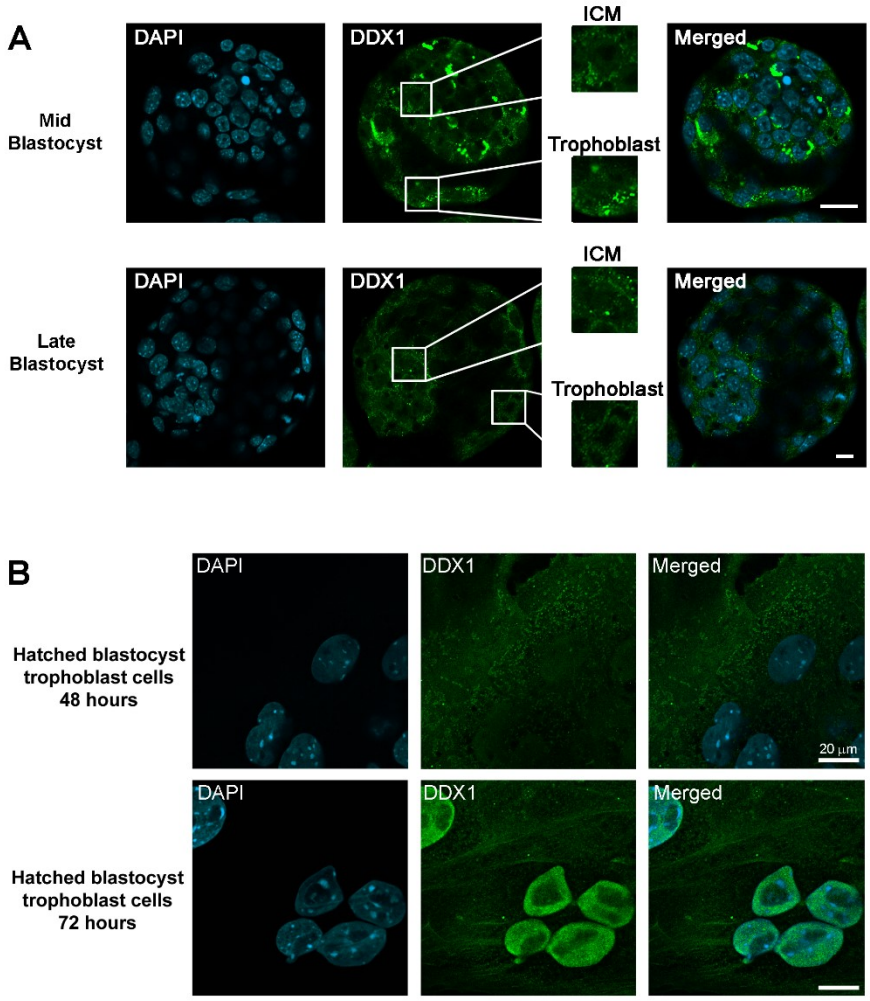

Figure 2.4 DDX1 relocates to the nucleus in late blastocysts. (A) 1-cell stage embryos were cultured in M16 medium to the blastocyst stage. Mid and late pre-hatched blastocyst stages were selected based on blastocyst size and cell numbers, and immunostained with anti-DDX1 antibody. Cytoplasmic DDX1

granules gradually disappeared with blastocyst development. The DDX1 signal is purposely saturated to more clearly show the presence of DDX1 in the nucleus. A magnification of the inner cell mass (ICM) and trophoblast cells is shown on the right. (B) E3.5 embryos were cultured for either 48 h or 72 h and hatched blastocysts immunostained with anti-DDX1 antibody. DAPI was used to stain the nuclei. An increase in the relative amount of DDX1 in the nucleus of trophoblasts in hatched blastocysts was observed at 48 h compared to pre-hatched blastocysts. By 72 h, most of the DDX1 was found in the nucleus of trophoblasts. The ICM of hatched blastocysts was too thick to allow accurate visualization of DDX1 subcellular patterns. Scale bars = 20 μm.

To determine whether there are different forms of DDX1 in embryos versus post-embryonic cells, we first examined single-cell RNA sequencing data (GSE57249) from 1-cell, 2-cell, 4-cell, 8-cell and blastocyst embryos (Biase, Cao et al. 2014). All exons were present in these early stage embryos (data not shown). Although 90% of the single cell sequencing data from 2- cell and 4-cell stages showed identical *DDX1* RNA sequencing patterns to that of post-embryonic RNA, we noted that a small percentage of 2-cell and 4-cell stage embryos (4/40 embryos), but not ICM or trophoblast cells (0/7), had sequences that mapped to intron 1. To pursue the possibility of alternative splicing in early stage embryos, we extracted RNA from 2 sets of 2-cell stage embryos and used RT-PCR and four sets of primers spanning all known exons of *Ddx1* to examine embryonic *Ddx1*

RNA. Although the signal intensity was weak using primers spanning exons 1 and 9, bands were of the expected sizes and appeared identical to bands obtained using adult mouse brain RNA (**Fig. 2.5A**). Similarly, primers designed to amplify exons 10 to 16, exons 17 to 21 and exons 22 to 26 generated same size bands using 2-cell and adult mouse brain RNA.

To further investigate the possibility of different forms of DDX1 being expressed in early stage embryos versus post-embryonic cells, we carried out western blotting using lysates prepared from two hundred 2-cell stage embryos, R1 mouse embryonic stem cells (E3.5), and adult mouse brain. Similar size DDX1 protein bands were observed in all three samples using two different anti-DDX1 antibodies recognizing the N-terminus (aa 1-186) or C-terminus (aa 187-740) of DDX1 (**Figs. 2.5B, C**). Thus, based on combined RNA sequencing, RT-PCR and western blot analyses, we were unable to find evidence of different forms of DDX1 in early stage embryos versus post-embryonic cells.

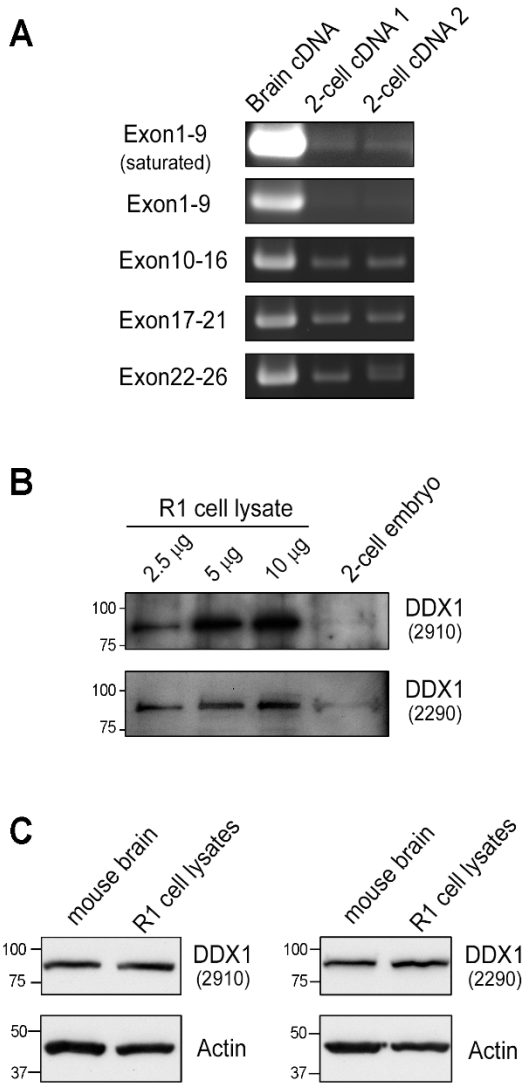

Figure 2.5 DDX1 RNA and protein in 2-cell embryos, R1 cells and mouse brain. (A) (A) Total RNAs were prepared from either seven or eight 2-cell embryos (obtained from two mice), or adult mouse brain tissue. RT-PCR analysis was carried out using 4 sets of primers covering all Ddx1 exons. The signal obtained for exons 1 to 9 was saturated in order to visualize the bands in 2-cell embryos. (B) Whole cell lysates were prepared from 2-cell embryos and R1 cells. Different

amounts of R1 cell lysate (2.5 µg, 5 µg and 10 µg per lane) were loaded to allow comparison with 2-cell embryos. (C) Forty µg whole cell lysates from either adult mouse brain or R1 cells were loaded in each lane. (B, C) Cell lysates were electrophoresed in SDS-PAGE gels and immunoblotted using two different anti-DDX1 antibodies targeting different parts of DDX1 [N-terminal DDX1 (aa 1–186) and C-terminal DDX1 (aa 187-740)]. Size markers are indicated on the left of each blot.

2.3.3 DDX1 granules do not co-localize with proteins associated with RNA decay and RNA processing bodies

As DEAD box proteins are known to be involved in RNA transport, RNA processing and RNA degradation, we co-immunostained 2-cell embryos using antibodies that detect proteins associated with various RNA-related processes: DDX3 **(Fig. 2.6;** with magnification in **Fig. S2.1)**, involved in RNA transport and translational control, and associated with processing (P)-bodies (Lai, Lee et al. 2008, Soto-Rifo, Rubilar et al. 2012, Chahar, Chen et al. 2013); EXOSC5 **(Fig. 2.6;** with magnification in **Fig. S2.2)**, a component of the exosome associated with RNA processing and degradation (Maekawa, Imamachi et al. 2015, Zinder and Lima 2017); GW182 **(Fig. 2.6;** with magnification in **Fig. S2.3)**, associated with miRNA silencing and GW-bodies or P-bodies (Serman, Le Roy et al. 2007); and p54/RCK (DDX6) **(Fig. 2.6;** with magnification in **Fig. S2.4)**, associated with P-bodies

(Tritschler, Braun et al. 2009, Chahar, Chen et al. 2013, Ayache, Benard et al. 2015). There was no co-localization of DDX1 granules with any of these proteins. Similarities in the localization of DDX3, GW182 and DDX6 suggest focused RNA processing/degradation activity at opposite poles near the outer edge of 2-cell embryos. We also examined whether DDX1 was associated with either mitochondria or endoplasmic reticulum (ER). No co-localization was observed between DDX1 granules and either MitoTracker Deep Red, a mitochondria staining dye **(Fig. S2.5)** or calnexin, an ER marker **(Fig. S2.6)**.

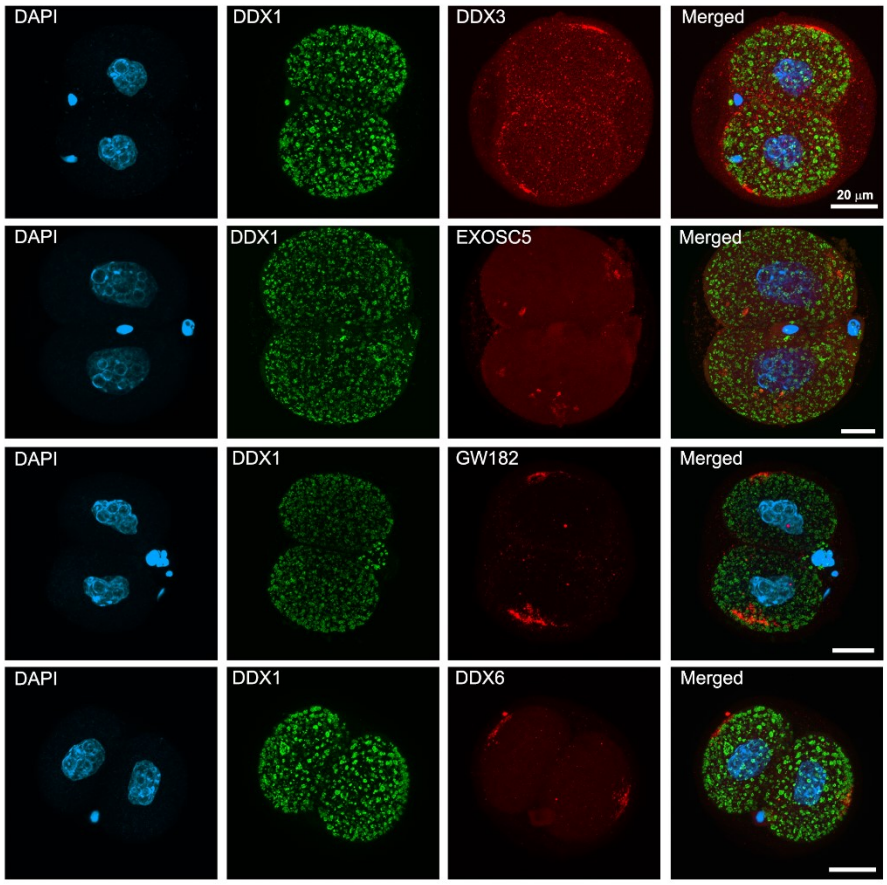

Figure 2.6 DDX1 does not co-localize with RNA processing bodies. Two cell stage embryos were co-immunostained with DDX1 and the following antibodies: anti-DDX3 (P-bodies), anti-EXOSC5 (exosome), anti-GW182 (P-body), and anti-DDX6 (P-body). There was no co-immunostaining of DDX1 with any of these proteins. Embryos are displayed as 2D projections of Z-stacks imaged by confocal microscopy. Scale bar = 20 µm.

2.3.4 DDX1 granules co-localize with TIA-1 and TIAR, proteins normally found in stress granules of somatic cells

DDX1 aggregates in nuclear bodies of mammalian (non-embryonic) cell lines cultured under normal growth conditions. Exposure to stressors such as heat shock and oxidative stress results in aggregation of DDX1 in cytoplasmic stress granules (Onishi, Kino et al. 2008, Kunde, Musante et al. 2011). We therefore co-immunostained early stage embryos with anti-DDX1 antibody as well as antibodies to stress granule markers including TIA-1 and TIAR (Kedersha, Gupta et al. 1999). Co-localization of TIA-1 with DDX1 granules was not observed in 1-cell stage embryos; however, significant co-localization was observed from the 2-cell to blastocyst stages (**Fig. 2.7**). Co-immunostaining of TIAR with DDX1 granules was also observed in embryos, but only from late 2-cell to 8-cell stages (**Fig. S2.7**). In contrast to DDX1 and TIA-1, TIAR expression was restricted to the nucleus at the blastocyst stage. We also examined co-localization of SMN with DDX1 granules, as DDX1 nuclear bodies reside adjacent to or co-localize with gems (SMN-containing nuclear bodies) (Bleoo, Sun et al. 2001, Li, Roy et al. 2006), and SMN is observed in stress granules when mammalian cells are exposed to stress-inducing agents. There was no clear co-localization of SMN with DDX1 granules in 2-cell stage embryos (**Fig. S2.8**). Similarly, co-immunofluorescence analysis using two other markers of stress granules, FXR1 and RACK1 (Mazroui, Huot et al. 2002, Arimoto, Fukuda et al. 2008, Ohn, Kedersha et al. 2008, Gareau, Houssin et al. 2013, Herman, Vrakas et al. 2018), showed no co-localization with DDX1

granules (**Fig. S2.9**). These results suggest that co-localization of TIA-1 and TIAR with DDX1 granules does not simply represent a reconstruction of stress granule-like structures in embryos but reflects an embryo-specific association between DDX1 granules and TIA-1/TIAR proteins.

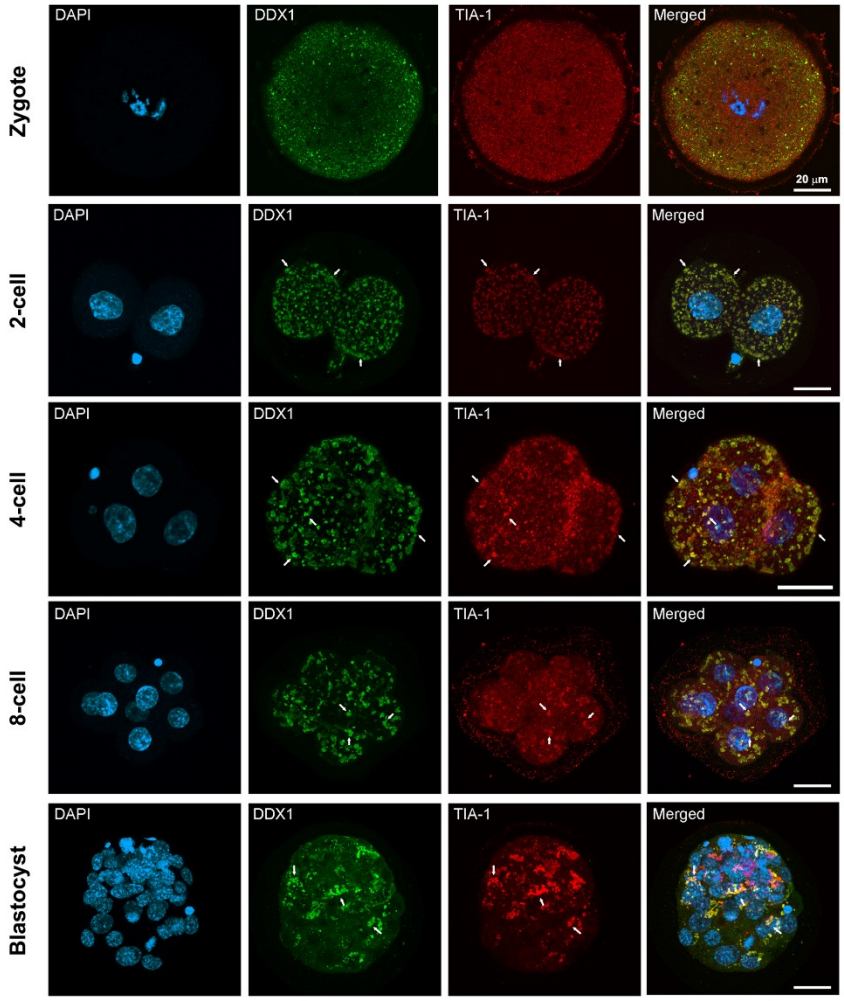

Figure 2.7 DDX1 co-localizes with TIA-1 in pre-implantation embryos. DDX1 co-immunostaining with anti-TIA-1 antibody revealed co-localization of TIA-1 with

DDX1 granules from the zygote to the blastocyst stages. Arrows point to DDX1 granules that co-localize with TIA-1. Embryos are displayed as 2D projections of Z-stacks imaged by confocal microscopy. Scale bar = 20 μm.

As TIA-1 and TIAR are both associated with stress granules in mammalian cell lines, we were interested to see if the number and appearance of DDX1 granules were affected by stress. Embryos were collected and either heat-shocked at 43^{o}C for 45 minutes or incubated at 37^{o}C in KMSO medium for 45 minutes. Embryos were then fixed and immunostained with anti-DDX1 and either anti-TIA-1 or TIAR antibodies. There was no difference between control and heat-shocked embryos in either the immunostaining patterns of DDX1 and TIA-1 or that of DDX1 and TIAR (**Fig. S2.10**). Similar results were observed when we treated 2-cell embryos with 1 mM H_2O_2 for 4 h (data not shown). These results suggest that early stage embryos do not form classic-style stress granules in response to environmental stress.

2.3.5 DDX1 granule formation is dependent on RNA and transcription but not translation

We next asked whether RNA is required for DDX1 granule formation in early embryos. We first stained 2-cell stage embryos with acridine orange (2 μM for 20

minutes) to see if acridine orange could be used to detect RNAs in DDX1 granules. Although numerous small foci, along with a few large foci, were observed in acridine orange-stained cells, there was no apparent co-localization of acridine orange with DDX1 granules **(Fig. 2.8A)**. One possibility is that acridine orange is not able to access the RNAs bound by DDX1.

As a second approach, we treated 2-cell stage embryos with ribonuclease A (RNase A) to examine the effect of RNA removal on the number and appearance of DDX1 granules. Embryos were pre-treated with 0.1% saponin prior to fixation followed by treatment with 150 µg/ml RNase A in PBS. Saponin-treated embryos followed by incubation in PBS served as the negative control. Embryos were then fixed, co-immunostained with anti-DDX1 and anti-TIA-1 antibody, and imaged. Although detergent treatment caused some cell shrinkage, DDX1/TIA-1 granules were still present in control embryos (**Fig. 2.8B**). However, upon RNase A treatment, a significant portion of DDX1 granules disappeared resulting in mostly diffuse cytoplasmic DDX1 immunostaining. Intriguingly, TIA-1 localization to granules was unaffected by RNase A treatment (**Fig. 2.8B**). These data suggest that DDX1 forms a complex with RNA during early embryonic stages, and that RNA is required for retention of DDX1, but not TIA-1, within granules.

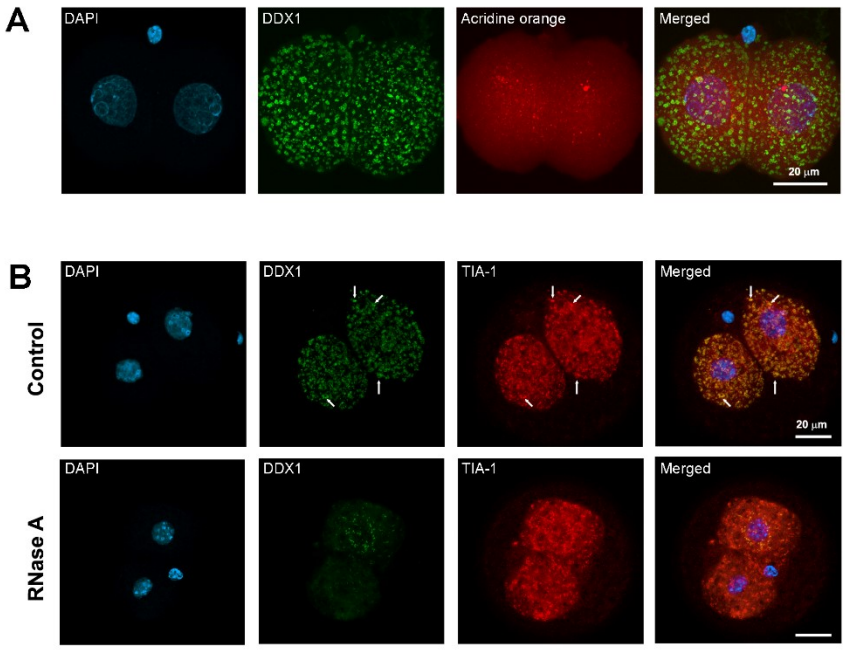

Figure 2.8 DDX1 localization to DDX1 granules depends on the presence of RNA. (A) Embryos were incubated with 2 µM acridine orange for 20 minutes prior to immunostaining with DDX1 antibody. Immunofluorescence analysis revealed no clear pattern of co-localization between RNA detected with acridine orange (red) and DDX1 granules (green). (B) 2-cell stage embryos were treated with 150 µg/mL RNAse A, then immunostained with anti-DDX1 antibody. Fewer DDX1 granules were observed after RNase A treatment. In contrast, the distribution of TIA-1 was not substantially different in control versus RNase A-treated embryos. Embryos are displayed as 2D projections of Z-stacks imaged by confocal microscopy. Scale bar = 20 µm.

We then examined the effect of transcription and translation inhibitors on DDX1 granules. Treatment of 2-cell stage embryos with 100 µg/ml cycloheximide for 8 h (to inhibit translation) had no effect on either the number or appearance of DDX1 granules (**Fig. 2.9A**). However, treatment of 2-cell stage embryos with 200 µM cordycepin for 8 h (to inhibit transcription) resulted in some disruption/clumping of DDX1 granules (**Fig. 2.9B**). These results suggest a role for newly-synthesized RNA but not newly-synthesized protein in maintenance of the DDX1 granules typically observed in 2-cell stage embryos.

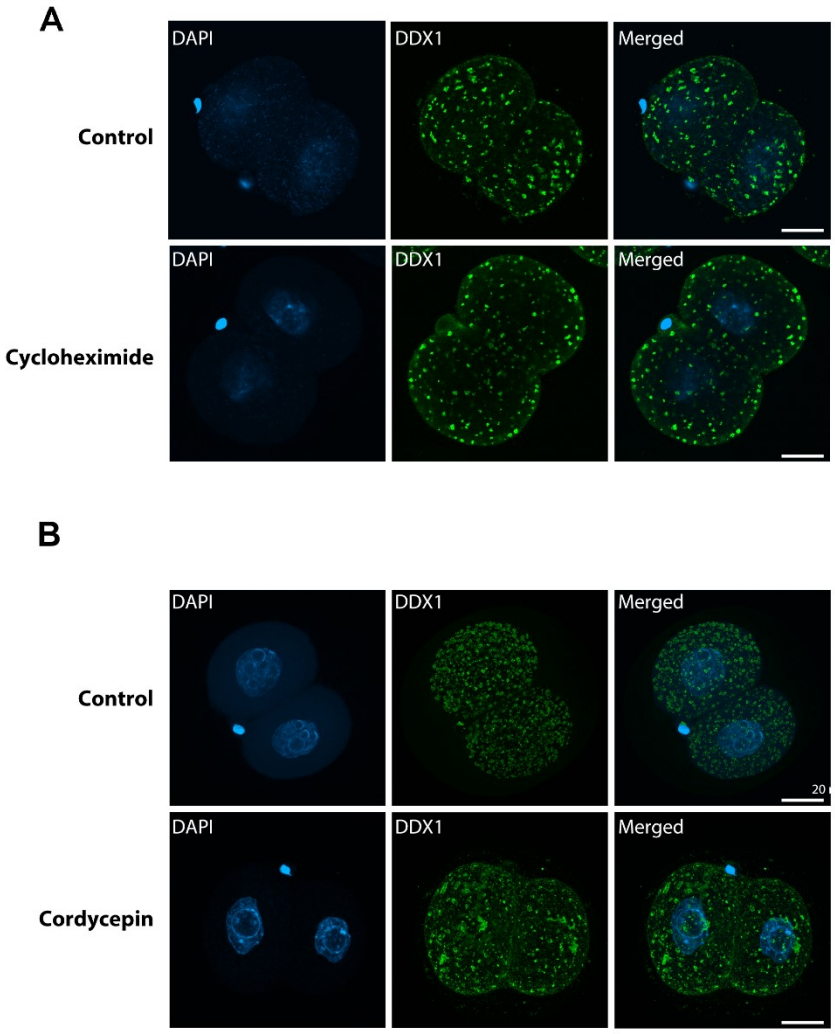

Figure 2.9 Effects of transcription or translation inhibition on DDX1 granules in E1.5 embryos. (A) 2-cell embryos were treated with either 150 μg/ml cycloheximide (inhibition of translation) or (B) 200 μM cordycepin (inhibition of transcription) for 8 h. Untreated 2-cell stage embryos were used as control. The numbers and appearance of DDX1 granules were affected by inhibition of

transcription but not inhibition of translation. Embryos are displayed as 2D projections of Z-stacks imaged by confocal microscopy. Scale bar = 20 μm.

2.3.6 Ddx1$^{-/-}$ embryos stall at the 2- to 4-cell stage

Genotyping analysis revealed loss of *Ddx1*$^{-/-}$ embryo prior to the blastocyst stage. To further address when *Ddx1*$^{-/-}$ embryos die, E0.5 embryos from either wild-type or first generation *Ddx1*$^{+/-}$ X *Ddx1*$^{+/-}$ intercrosses were collected and allowed to develop *in vitro* in microdrops of KMSO culture medium. The embryos were examined for their developmental progression every 24 h. For wild-type crosses, we found the expected progression from 2- to 4- to 8-cell stages at 24 h, 48 h and 72 h, respectively. Of the 17 wild-type embryos analysed, 94% (16/17) reached the 8-cell stage by 72 h, with one embryo stalled at the 1-cell stage for the duration of the experiment (**Table 2.3**). For heterozygous intercrosses, 92% (134/146) of the embryos reached 2-cell stage by 24 h. However, only 99 embryos (68%) and 94 embryos (64%) reached 4- and 8-cell stages by 48 h and 72 h, respectively (**Table 2.3**). Thirty-five embryos (24%) were still at the 2-cell stage at 48 h, while 24 embryos (16%) and 16 embryos (11%) were at the 2-cell and 4-cell stage, respectively, at 72 h. Thus, 16% of intercross embryos failed to progress past the 2-cell stage, and an additional 11% failed to progress past the 4-cell stage after 72 h. Twelve embryos (8%) remained at the one-cell stage throughout the

time analysed. In comparison, 1/17 (5%) of wild-type embryos remained at the one-cell stage.

Table 2.3 Stalling of embryos generated from heterozygous intercrosses prior to blastocyst stage.
This work was done by Dr. Matthew Hildebrandt.

Starting material E0.5 embryos		24 h	48 h	72 h
Wild-type intercrosses (2 crosses)	1-cell	2 (12%)	1 (5%)	1 (5%)
	2-cell	15 (88%)	0	0
	4-cell	-	16 (94%)	0
	8-cell	-	-	16 (94%)
	Total embryos	17	17	17
Heterozygote intercrosses (17 crosses)	1-cell	12 (8%)	12 (8%)	12 (8%)
	2-cell	134 (92%)	35 (24%)	24 (16%)
	4-cell	-	99 (68%)	16 (11%)
	8-cell	-	-	94 (64%)
	Total embryos	146	146	146

To determine whether the stalled embryos were *Ddx1*$^{-/-}$, we cultured embryos from both wild-type and first generation *Ddx1*$^{+/-}$ intercrosses for 72 h, fixed and immunostained the embryos with anti-DDX1 antibody. 2- and 4-cell stage embryos from wild-type crosses showed abundant DDX1 granules throughout the cytoplasm (**Fig. 2.10A**). In contrast, stalled 2-cell and 4-cell stage embryos from

Ddx1$^{+/-}$ intercrosses had an abnormal number of nuclei and virtually no DDX1 immunostaining (**Fig. 2.10B**).

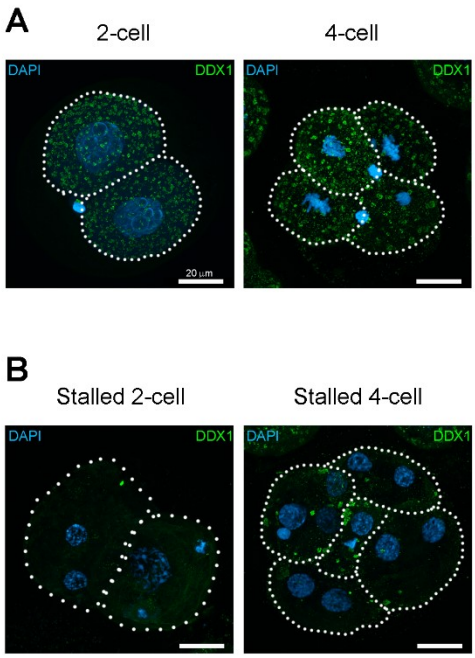

Figure 2.10 Embryos from *Ddx1*$^{+/-}$ intercrosses stall at the 2- to 4-cell stages. (A) Wild-type embryos were collected and immunostained with anti-DDX1 antibody. Nuclei were visualized with DAPI. (B) Embryos from first generation heterozygote intercrosses were collected at E0.5 and cultured at 37^{o}C for 72 h. After 72 h, embryos should be at the 8-16 cell stages. Instead, some of the embryos were stalled at the 2- and 4-cell stages. DDX1 immunostaining of these stalled embryos revealed significantly reduced DDX1 levels throughout the cytoplasm. Embryos are displayed as 2D projections of Z-stacks imaged by confocal microscopy. Scale bar = 20 µm.

2.3.7 DDX1 RNA-immunoprecipitation of 2-cell stage embryos

Like other members of the DEAD box family, DDX1 binds RNA (Chen, Lin et al. 2002, Li, Monckton et al. 2008, Han, Liu et al. 2014, Li, Germain et al. 2016). To address DDX1's role in embryonic development, we carried out RNA-DDX1 immunoprecipitation to identify RNAs bound to DDX1. We collected three hundred 2-cell stage embryos and divided them into 2 groups: control immunoprecipitation with IgG and experimental immunoprecipitation with DDX1 antibody. To identify potential RNA targets of DDX1, we carried out RT-qPCR of 16 genes whose maternal absence causes stalling of embryo development at 1- to 2- or 2- to 4-cell stages. Included in our set of 16 genes were *Ago2* (Lykke-Andersen, Gilchrist et al. 2008), *Bnc1* (Ma, Zeng et al. 2006), *Brg1* (Griffin, Brennan et al. 2008, Singh, Foley et al. 2016), *Brwd1* (Philipps, Wigglesworth et al. 2008, Pattabiraman, Baumann et al. 2015), *Dicer1* (Murchison, Stein et al. 2007, Tang, Kaneda et al. 2007), *Floped* (Li, Baibakov et al. 2008), *Hr6*α (Roest, Baarends et al. 2004), *Mater* (Tong, Gold et al. 2000), *Padi6* (Yurttas, Vitale et al. 2008, Xu, Shi et al. 2016), *Tle6* (Li, Baibakov et al. 2008), *Tif1*α (Torres-Padilla and Zernicka-Goetz 2006), *Zar1* (Wu, Viveiros et al. 2003), *Filia* (Ohsugi, Zheng et al. 2008), *Hsf1* (Christians, Davis et al. 2000, Bierkamp, Luxey et al. 2010), *Npm2* (Kim and Lee 2014, Ogushi, Yamagata et al. 2017), *Zfp36l2* (Ramos, Stumpo et al. 2004, Li, Zheng et al. 2010).

Three independent pre-amplifications from each of the IgG and DDX1 immunoprecipitations were carried out to generate sufficient material for RT-qPCR analysis. Although a significant amount of variation was observed between the three technical replicates, 8/16 RNAs (*Ago2, Brwd1, Dicer1, Floped, Tle6, Tif1α, Zar1* and *Zfp3612*) showed close to 10-fold increases compared to IgG control. Of these 8 RNAs, 2 RNAs (*Ago2* and *Zar1*) showed differences of 2-fold or higher in 2 pre-amplifications and 3 (*Tle6, Floped* and *Tif1α*) showed differences of 2-fold or higher in all 3 pre-amplifications (**Fig. 2.11**).

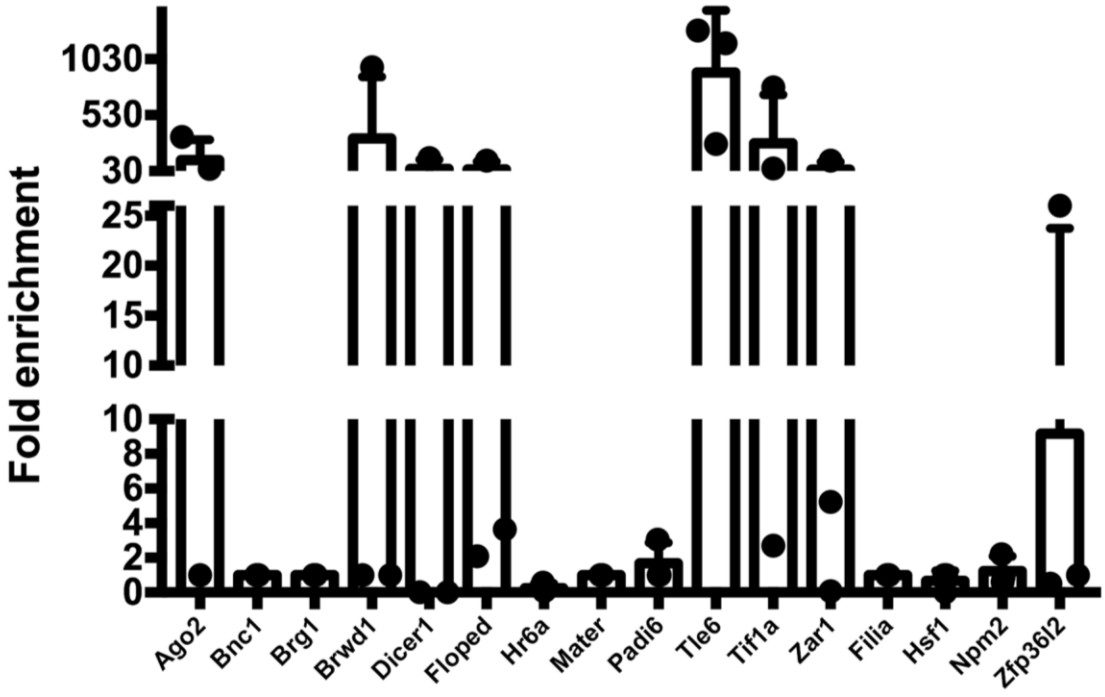

Figure 2.11 DDX1-bound RNAs in 2-cell mouse embryos. DDX1 with its bound RNAs was immunoprecipitated from 2-cell stage embryos using anti-DDX1 antibody (or IgG as control). RT-qPCR analysis was carried out using primers to

16 genes essential for mouse embryo development. Pre-amplifications (n=3) were carried out to generate sufficient cDNA for analysis. The average fold enrichment (anti-DDX1 antibody over IgG) in 3 pre-amplification reactions is shown for each gene.

2.4 Discussion

DDX1 is widely expressed in cell lines and tissues, with a primarily nuclear distribution (Bleoo, Sun et al. 2001, Godbout, Packer et al. 2002, Godbout, Li et al. 2007). In general, proliferating cells and cells of neuroectodermal origin express the highest levels of DDX1 (Fagerberg, Hallstrom et al. 2014). We observed differences in the localization of DDX1 within ovaries, with cortical stroma cells and granulosa cells in follicles showing both nuclear and cytoplasmic DDX1. Cells of the theca externa (cells directly surrounding the follicles) showed either low or no DDX1 expression. Oocytes within each follicle also had very high levels of DDX1, but in contrast to granulosa cells, DDX1 was exclusively found in the cytoplasm. The cytoplasmic distribution of DDX1 observed after fertilization (1-cell to blastocyst stages) suggests related roles for DDX1 in oocytes and early stage embryos.

The appearance of cytoplasmic DDX1 granules underwent a dramatic change over time. In oocytes and 1-cell embryos, DDX1 was found in small granules throughout the cytoplasm, in keeping with the reported uniform distribution of maternal RNAs in oocytes and early embryos (Xie, Timme et al. 2018). After fertilization, the number of DDX1 granules gradually decreased while increasing in size, seemingly aggregating with each other in blastocysts. As DDX1 granules are already present in maturing oocytes, and RNA is required for DDX1 aggregation in granules, an explanation for the changes in DDX1 distribution

patterns is that DDX1's binding targets are maternal RNAs which are progressively getting degraded. It has been estimated that ~100 picograms of maternal RNAs are stored in developing oocytes (Piko and Clegg 1982, Clarke 2012, Eckersley-Maslin, Alda-Catalinas et al. 2018). These RNAs play key roles in embryonic development and undergo highly-regulated programs of translational activation and degradation. Mechanisms underlying their protection versus translation versus degradation remain poorly understood. We propose that DDX1 either protects or regulates the availability of maternal mRNAs during early embryonic development. As the need for maternal RNAs decreases and maternal RNAs are degraded, DDX1 binds to fewer RNAs resulting in larger aggregates as the result of clustering of DDX1 with the remaining maternal RNAs. In this regard, it is interesting that the localization of DDX1 granules within embryos changes over time, shifting from throughout the cytoplasm to large aggregates primarily located on one side of the nucleus. The latter may represent positioning of DDX1 for rapid entry into the nucleus once the proper signals are in place. In keeping with this idea, analysis of DDX1 subcellular localization in cultured blastocysts shows that DDX1 begins to move into the nucleus of ICM and trophoblast cells at the later blastocyst stages.

Development-dependent alterations in the subcellular localization of DDX1 could be driven by a number of factors, including alternative splicing giving rise to different DDX1 isoforms, post-translational modifications such as phosphorylation, as well as DDX1 protein interactors. To our knowledge, there are no reports of DDX1 alternative splicing in the literature although RNA sequencing databases

reveal the presence of intronic regions in some cell types. Of specific relevance to our study, single cell sequencing of early stage mouse embryos (Biase, Cao et al. 2014) indicates the presence of DDX1 intron 1 sequences in a small percentage (~10%) of embryos. However, we were not able to confirm the presence of intron 1 sequences, or obtain evidence of alternative splicing, in 2-cell stage embryos based on RT-PCR. Similarly, there are a number of reports indicating that DDX1 can be phosphorylated (Li, Monckton et al. 2008, Han, Liu et al. 2014) as well as ubiquitinated (Oshikawa, Matsumoto et al. 2012). Again, we were not able to obtain evidence of post-translational modification of 2-cell stage embryos based on western blotting. As not all post-translational modifications cause a shift detectable by western blotting, additional strategies (e.g. 2D gel electrophoresis) will be required to further investigate the nature of DDX1 in early stage embryos compared to later-stage cells. Whether DDX1 is post-translationally modified or not in early stage embryos, it seems likely that protein interactors play a key role in the mobilization and subcellular localization of DDX1 during development.

DDX1 has previously been reported to associate with cytoplasmic RNA-containing granules, including RNA transport granules in neuronal cells and stress granules in mammalian cells exposed to environmental stressors such as heat shock (Kanai, Dohmae et al. 2004, Onishi, Kino et al. 2008, Miller, Blandford et al. 2009). Although various RNA-binding protein (RNP) complexes have been described in early stage mouse embryos, including P-bodies (Spiegelman and Bennett 1973, Clark and Eddy 1975, Lue, Hikim et al. 1999, Chuma, Hosokawa et

al. 2006, Pepling, Wilhelm et al. 2007, Flemr, Ma et al. 2010, Voronina, Seydoux et al. 2011, Kim, Cooke et al. 2012), DDX1 granules appear to be distinct from these as we observed no co-immunostaining with DDX1 and DDX3, GW182 or DDX6 (markers for P-bodies and germ cell granules). Intriguingly, we found co-localization of DDX1 granules with two RNA-binding proteins, TIA-1 and TIAR, normally associated with stress granules in mammalian cells exposed to environmental stressors such as heat-shock and oxidative stress (Kedersha, Gupta et al. 1999, Gilks, Kedersha et al. 2004, McDonald, Aulas et al. 2011, Arimoto-Matsuzaki, Saito et al. 2016). This association was found as early as 2-cell stage embryos.

Stress granules are sites of RNA triage, and contain messenger ribonucleoproteins stalled in translation initiation (Anderson and Kedersha 2008, Protter and Parker 2016). TIA-1 and TIAR play structural and functional roles in stress granules, acting as recruitment sites for other proteins as well as transcripts (Kedersha, Gupta et al. 1999, Gilks, Kedersha et al. 2004, Bley, Lederer et al. 2015). DDX1 and TIA-1 co-immunostaining was observed from the 2-cell to blastocyst stages, as well as in cultured blastocysts. In contrast, there was little co-immunostaining between DDX1 and TIAR by the 8-cell stage, with TIAR showing a primarily nuclear distribution pattern in 8-cell embryos and blastocysts. Unlike DDX1 granules which were affected by RNase A treatment, the distribution pattern of TIA-1 in granules did not change when 2-cell embryos were treated with RNase A. These results suggest that whereas RNA is required for the retention of DDX1

in granules, this is not the case for TIA-1. As TIA-1 has previously been associated with transport of RNAs to stress granules (Gilks, Kedersha et al. 2004), it's possible that TIA-1 is also involved in the transport of RNAs within the early stage embryos. Of note, none of the other components of stress granules tested, including FXR1 and RACK1 co-localized with DDX1 granules. Therefore, although they contain RNA, DDX1 granule formation in embryos may not be related to stress granule formation per se, but may co-opt components of stress granules for their specialized roles in embryos.

Ddx1 knockout embryos die pre-blastocyst, whereas both *Tia-1* and *Tiar* knockout mice display lethality post-blastocyst, with some knockout mice surviving to adulthood with normal lifespans (Beck, Miller et al. 1998, Piecyk, Wax et al. 2000). Based on our embryo cultures, $Ddx1^{-/-}$ embryo die between the 2- and 4-cell stages. Our results thus suggest an essential cytoplasmic role for DDX1 in pre-implantation development, likely involving maternal RNAs. Upon fertilization, embryos must shift from reliance on maternal RNAs and protein to zygotic transcription and translation. One of the key processes in this transition is the controlled degradation of maternal RNAs (Nothias, Majumder et al. 1995, Schultz 2002, Li, Zheng et al. 2010). The absence of certain maternal mRNAs such as *Zar1*, *Ago2* and *Tif1*α results in embryonic lethality at the 1 to 2 cell stages (Wu, Viveiros et al. 2003, Torres-Padilla and Zernicka-Goetz 2006, Lykke-Andersen, Gilchrist et al. 2008, Stein, Rozhkov et al. 2015).

Analysis of DDX1-bound RNAs in 2-cell embryos reveal preferential binding of DDX1 to *Tle6, Floped* and *Tif1*α., and likely *Ago2* and *Zar1*. These maternal mRNAs have all been shown to play essential roles in early embryonic development. AGO2 is required for degradation of maternal RNAs prior to transcriptional activation of the zygotic genome. TIF1α has been identified as one of a few factors responsible for activating zygotic genes (Torres-Padilla and Zernicka-Goetz 2006). FLOPED and TLE6 are two of the four proteins found in the subcortical maternal complex (SCMC) (Li, Baibakov et al. 2008). The SCMC is essential for embryonic development beyond the 2-cell stage. In mice, ZAR1 is known to be critical for pronuclear syngamy of the embryo (Wu, Viveiros et al. 2003). In *Xenopus*, Zar1 regulates the translation of mRNAs involved in the cell cycle of oocytes (Yamamoto, Cook et al. 2013). We propose that spatial-temporal dysregulation of these maternal mRNAs resulting from loss of DDX1 underlies embryonic stalling at the 2- to 4-cell stages.

In summary, we show that DDX1 is an essential protein in embryonic development, with DDX1 knockout causing embryos to stall at the 2- to 4-cell stages. DDX1 forms large granules in the cytoplasm of early-stage embryos, with stress granule markers TIA-1 and TIAR co-localizing with DDX1 in these granules. RNA is required for retention of DDX1, but not TIA-1, in these granules. RNA-DDX1 immunoprecipitation analysis indicates that DDX1 binds to maternal RNAs previously shown to play key roles in embryonic development beyond the 2-cell

stage. We postulate that DDX1 plays a critical role in the temporal-spatial protection of maternal RNAs required for early embryonic development.

2.5 Acknowledgments

We are grateful to Kacie Norton and Dr. Heather McDermid for their help with dissections and superovulation. We thank Dr. James Manley, Columbia University, for the anti-CstF64 antibody and Dr. Marvin Fritzler, University of Calgary, for the anti-GW182 antibody. This work was supported by grants from the Canadian Institutes of Health Research - grant number 162157.

2.6 Competing interests

The authors declare that they have no competing interests.

2.7 References

Akiyama, K., Y. Akao, M. Yokoyama, Y. Nakagawa, T. Noguchi, K. Yagi and Y. Nishi (1999). "Expression of two dead box genes (DDX1 and DDX6) is independent of that of MYCN in human neuroblastoma cell lines." Biochem Mol Biol Int 47(4): 563-568.

Amler, L. C., J. Schurmann and M. Schwab (1996). "The DDX1 gene maps within 400 kbp 5' to MYCN and is frequently coamplified in human neuroblastoma." Genes Chromosomes Cancer 15(2): 134-137.

Anderson, P. and N. Kedersha (2008). "Stress granules: the Tao of RNA triage." Trends Biochem Sci 33(3): 141-150.

Andersson, D., N. Akrap, D. Svec, T. E. Godfrey, M. Kubista, G. Landberg and A. Stahlberg (2015). "Properties of targeted preamplification in DNA and cDNA quantification." Expert Rev Mol Diagn 15(8): 1085-1100.

Arimoto-Matsuzaki, K., H. Saito and M. Takekawa (2016). "TIA1 oxidation inhibits stress granule assembly and sensitizes cells to stress-induced apoptosis." Nat Commun 7: 10252.

Arimoto, K., H. Fukuda, S. Imajoh-Ohmi, H. Saito and M. Takekawa (2008). "Formation of stress granules inhibits apoptosis by suppressing stress-responsive MAPK pathways." Nat Cell Biol 10(11): 1324-1332.

Ayache, J., M. Benard, M. Ernoult-Lange, N. Minshall, N. Standart, M. Kress and D. Weil (2015). "P-body assembly requires DDX6 repression complexes rather than decay or Ataxin2/2L complexes." Mol Biol Cell 26(14): 2579-2595.

Balko, J. M. and C. L. Arteaga (2011). "Dead-box or black-box: is DDX1 a potential biomarker in breast cancer?" Breast Cancer Res Treat 127(1): 65-67.

Beck, A. R., I. J. Miller, P. Anderson and M. Streuli (1998). "RNA-binding protein TIAR is essential for primordial germ cell development." Proc Natl Acad Sci U S A 95(5): 2331-2336.

Biase, F. H., X. Cao and S. Zhong (2014). "Cell fate inclination within 2-cell and 4-cell mouse embryos revealed by single-cell RNA sequencing." Genome Res 24(11): 1787-1796.

Bierkamp, C., M. Luxey, A. Metchat, C. Audouard, R. Dumollard and E. Christians (2010). "Lack of maternal Heat Shock Factor 1 results in multiple cellular and developmental defects, including mitochondrial damage and altered redox

homeostasis, and leads to reduced survival of mammalian oocytes and embryos." Dev Biol 339(2): 338-353.

Bleoo, S., X. Sun, M. J. Hendzel, J. M. Rowe, M. Packer and R. Godbout (2001). "Association of human DEAD box protein DDX1 with a cleavage stimulation factor involved in 3'-end processing of pre-MRNA." Mol Biol Cell 12(10): 3046-3059.

Bley, N., M. Lederer, B. Pfalz, C. Reinke, T. Fuchs, M. Glass, B. Moller and S. Huttelmaier (2015). "Stress granules are dispensable for mRNA stabilization during cellular stress." Nucleic Acids Res 43(4): e26.

Carter, M. G., T. Hamatani, A. A. Sharov, C. E. Carmack, Y. Qian, K. Aiba, N. T. Ko, D. B. Dudekula, P. M. Brzoska, S. S. Hwang and M. S. Ko (2003). "In situ-synthesized novel microarray optimized for mouse stem cell and early developmental expression profiling." Genome Res 13(5): 1011-1021.

Chahar, H. S., S. Chen and N. Manjunath (2013). "P-body components LSM1, GW182, DDX3, DDX6 and XRN1 are recruited to WNV replication sites and positively regulate viral replication." Virology 436(1): 1-7.

Chen, H. C., W. C. Lin, Y. G. Tsay, S. C. Lee and C. J. Chang (2002). "An RNA helicase, DDX1, interacting with poly(A) RNA and heterogeneous nuclear ribonucleoprotein K." J Biol Chem 277(43): 40403-40409.

Christians, E., A. A. Davis, S. D. Thomas and I. J. Benjamin (2000). "Maternal effect of Hsf1 on reproductive success." Nature 407(6805): 693-694.

Chuma, S., M. Hosokawa, K. Kitamura, S. Kasai, M. Fujioka, M. Hiyoshi, K. Takamune, T. Noce and N. Nakatsuji (2006). "Tdrd1/Mtr-1, a tudor-related gene, is essential for male germ-cell differentiation and nuage/germinal granule formation in mice." Proc Natl Acad Sci U S A 103(43): 15894-15899.

Clapier, C. R. and B. R. Cairns (2009). "The biology of chromatin remodeling complexes." Annu Rev Biochem 78: 273-304.

Clark, J. M. and E. M. Eddy (1975). "Fine structural observations on the origin and associations of primordial germ cells of the mouse." Dev Biol 47(1): 136-155.

Clarke, H. J. (2012). "Post-transcriptional control of gene expression during mouse oogenesis." Results Probl Cell Differ 55: 1-21.

Eckersley-Maslin, M. A., C. Alda-Catalinas and W. Reik (2018). "Dynamics of the epigenetic landscape during the maternal-to-zygotic transition." Nat Rev Mol Cell Biol 19(7): 436-450.

Fagerberg, L., B. M. Hallstrom, P. Oksvold, C. Kampf, D. Djureinovic, J. Odeberg, M. Habuka, S. Tahmasebpoor, A. Danielsson, K. Edlund, A. Asplund, E. Sjostedt, E. Lundberg, C. A. Szigyarto, M. Skogs, J. O. Takanen, H. Berling, H. Tegel, J. Mulder, P. Nilsson, J. M. Schwenk, C. Lindskog, F. Danielsson, A. Mardinoglu, A. Sivertsson, K. von Feilitzen, M. Forsberg, M. Zwahlen, I. Olsson, S. Navani, M. Huss, J. Nielsen, F. Ponten and M. Uhlen (2014). "Analysis of the human tissue-specific expression by genome-wide integration of transcriptomics and antibody-based proteomics." Mol Cell Proteomics 13(2): 397-406.

Flemr, M., J. Ma, R. M. Schultz and P. Svoboda (2010). "P-body loss is concomitant with formation of a messenger RNA storage domain in mouse oocytes." Biol Reprod 82(5): 1008-1017.

Gareau, C., E. Houssin, D. Martel, L. Coudert, S. Mellaoui, M. E. Huot, P. Laprise and R. Mazroui (2013). "Characterization of fragile X mental retardation protein recruitment and dynamics in Drosophila stress granules." PLoS One 8(2): e55342.

Germain, D. R., K. Graham, D. D. Glubrecht, J. C. Hugh, J. R. Mackey and R. Godbout (2011). "DEAD box 1: a novel and independent prognostic marker for early recurrence in breast cancer." Breast Cancer Res Treat 127(1): 53-63.

Germain, D. R., L. Li, M. R. Hildebrandt, A. J. Simmonds, S. C. Hughes and R. Godbout (2015). "Loss of the Drosophila melanogaster DEAD box protein Ddx1 leads to reduced size and aberrant gametogenesis." Dev Biol 407(2): 232-245.

Gilks, N., N. Kedersha, M. Ayodele, L. Shen, G. Stoecklin, L. M. Dember and P. Anderson (2004). "Stress granule assembly is mediated by prion-like aggregation of TIA-1." Mol Biol Cell 15(12): 5383-5398.

Godbout, R., L. Li, R. Z. Liu and K. Roy (2007). "Role of DEAD box 1 in retinoblastoma and neuroblastoma." Future Oncol 3(5): 575-587.

Godbout, R., M. Packer and W. Bie (1998). "Overexpression of a DEAD box protein (DDX1) in neuroblastoma and retinoblastoma cell lines." J Biol Chem 273(33): 21161-21168.

Godbout, R., M. Packer, S. Katyal and S. Bleoo (2002). "Cloning and expression analysis of the chicken DEAD box gene DDX1." Biochim Biophys Acta 1574(1): 63-71.

Godbout, R. and J. Squire (1993). "Amplification of a DEAD box protein gene in retinoblastoma cell lines." Proc Natl Acad Sci U S A 90(16): 7578-7582.

Griffin, C. T., J. Brennan and T. Magnuson (2008). "The chromatin-remodeling enzyme BRG1 plays an essential role in primitive erythropoiesis and vascular development." Development 135(3): 493-500.

Hamatani, T., M. G. Carter, A. A. Sharov and M. S. Ko (2004). "Dynamics of global gene expression changes during mouse preimplantation development." Dev Cell 6(1): 117-131.

Han, C., Y. Liu, G. Wan, H. J. Choi, L. Zhao, C. Ivan, X. He, A. K. Sood, X. Zhang and X. Lu (2014). "The RNA-binding protein DDX1 promotes primary microRNA maturation and inhibits ovarian tumor progression." Cell Rep 8(5): 1447-1460.

Herman, A. B., C. N. Vrakas, M. Ray, S. E. Kelemen, M. J. Sweredoski, A. Moradian, D. S. Haines and M. V. Autieri (2018). "FXR1 Is an IL-19-Responsive RNA-Binding Protein that Destabilizes Pro-inflammatory Transcripts in Vascular Smooth Muscle Cells." Cell Rep 24(5): 1176-1189.

Hildebrandt, M. R., D. R. Germain, E. A. Monckton, M. Brun and R. Godbout (2015). "Ddx1 knockout results in transgenerational wild-type lethality in mice." Sci Rep 5: 9829.

Jiao, Z. X. and T. K. Woodruff (2013). "Detection and quantification of maternal-effect gene transcripts in mouse second polar bodies: potential markers of embryo developmental competence." Fertil Steril 99(7): 2055-2061.

Kanai, Y., N. Dohmae and N. Hirokawa (2004). "Kinesin transports RNA: isolation and characterization of an RNA-transporting granule." Neuron 43(4): 513-525.

Kedersha, N. L., M. Gupta, W. Li, I. Miller and P. Anderson (1999). "RNA-binding proteins TIA-1 and TIAR link the phosphorylation of eIF-2 alpha to the assembly of mammalian stress granules." J Cell Biol 147(7): 1431-1442.

Kidder, B. L. (2014). "In vitro maturation and in vitro fertilization of mouse oocytes and preimplantation embryo culture." Methods Mol Biol 1150: 191-199.

Kim, B., H. J. Cooke and K. Rhee (2012). "DAZL is essential for stress granule formation implicated in germ cell survival upon heat stress." Development 139(3): 568-578.

Kim, K. H. and K. A. Lee (2014). "Maternal effect genes: Findings and effects on mouse embryo development." Clin Exp Reprod Med 41(2): 47-61.

Kunde, S. A., L. Musante, A. Grimme, U. Fischer, E. Muller, E. E. Wanker and V. M. Kalscheuer (2011). "The X-chromosome-linked intellectual disability protein PQBP1 is a component of neuronal RNA granules and regulates the appearance of stress granules." Hum Mol Genet 20(24): 4916-4931.

Lai, M. C., Y. H. Lee and W. Y. Tarn (2008). "The DEAD-box RNA helicase DDX3 associates with export messenger ribonucleoproteins as well as tip-associated protein and participates in translational control." Mol Biol Cell 19(9): 3847-3858.

Li, L., B. Baibakov and J. Dean (2008). "A subcortical maternal complex essential for preimplantation mouse embryogenesis." Dev Cell 15(3): 416-425.

Li, L., D. R. Germain, H. Y. Poon, M. R. Hildebrandt, E. A. Monckton, D. McDonald, M. J. Hendzel and R. Godbout (2016). "DEAD Box 1 Facilitates Removal of RNA and Homologous Recombination at DNA Double-Strand Breaks." Mol Cell Biol 36(22): 2794-2810.

Li, L., E. A. Monckton and R. Godbout (2008). "A role for DEAD box 1 at DNA double-strand breaks." Mol Cell Biol 28(20): 6413-6425.

Li, L., H. Y. Poon, M. R. Hildebrandt, E. A. Monckton, D. R. Germain, R. P. Fahlman and R. Godbout (2017). "Role for RIF1-interacting partner DDX1 in BLM recruitment to DNA double-strand breaks." DNA Repair (Amst) 55: 47-63.

Li, L., K. Roy, S. Katyal, X. Sun, S. Bleoo and R. Godbout (2006). "Dynamic nature of cleavage bodies and their spatial relationship to DDX1 bodies, Cajal bodies, and gems." Mol Biol Cell 17(3): 1126-1140.

Li, L., P. Zheng and J. Dean (2010). "Maternal control of early mouse development." Development 137(6): 859-870.

Lin, M. H., H. Sivakumaran, A. Jones, D. Li, C. Harper, T. Wei, H. Jin, L. Rustanti, F. A. Meunier, K. Spann and D. Harrich (2014). "A HIV-1 Tat mutant protein disrupts HIV-1 Rev function by targeting the DEAD-box RNA helicase DDX1." Retrovirology 11: 121.

Lue, Y. H., A. P. Hikim, R. S. Swerdloff, P. Im, K. S. Taing, T. Bui, A. Leung and C. Wang (1999). "Single exposure to heat induces stage-specific germ cell apoptosis in rats: role of intratesticular testosterone on stage specificity." Endocrinology 140(4): 1709-1717.

Luo, C., J. Zuniga, E. Edison, S. Palla, W. Dong and J. Parker-Thornburg (2011). "Superovulation strategies for 6 commonly used mouse strains." J Am Assoc Lab Anim Sci 50(4): 471-478.

Lykke-Andersen, K., M. J. Gilchrist, J. B. Grabarek, P. Das, E. Miska and M. Zernicka-Goetz (2008). "Maternal Argonaute 2 is essential for early mouse development at the maternal-zygotic transition." Mol Biol Cell 19(10): 4383-4392.

Ma, J., F. Zeng, R. M. Schultz and H. Tseng (2006). "Basonuclin: a novel mammalian maternal-effect gene." Development 133(10): 2053-2062.

Maekawa, S., N. Imamachi, T. Irie, H. Tani, K. Matsumoto, R. Mizutani, K. Imamura, M. Kakeda, T. Yada, S. Sugano, Y. Suzuki and N. Akimitsu (2015). "Analysis of

RNA decay factor mediated RNA stability contributions on RNA abundance." BMC Genomics 16: 154.

Mazroui, R., M. E. Huot, S. Tremblay, C. Filion, Y. Labelle and E. W. Khandjian (2002). "Trapping of messenger RNA by Fragile X Mental Retardation protein into cytoplasmic granules induces translation repression." Hum Mol Genet 11(24): 3007-3017.

McDonald, K. K., A. Aulas, L. Destroismaisons, S. Pickles, E. Beleac, W. Camu, G. A. Rouleau and C. Vande Velde (2011). "TAR DNA-binding protein 43 (TDP-43) regulates stress granule dynamics via differential regulation of G3BP and TIA-1." Hum Mol Genet 20(7): 1400-1410.

McLay, D. W. and H. J. Clarke (2003). "Remodelling the paternal chromatin at fertilization in mammals." Reproduction 125(5): 625-633.

Miller, L. C., V. Blandford, R. McAdam, M. R. Sanchez-Carbente, F. Badeaux, L. DesGroseillers and W. S. Sossin (2009). "Combinations of DEAD box proteins distinguish distinct types of RNA: protein complexes in neurons." Mol Cell Neurosci 40(4): 485-495.

Murchison, E. P., P. Stein, Z. Xuan, H. Pan, M. Q. Zhang, R. M. Schultz and G. J. Hannon (2007). "Critical roles for Dicer in the female germline." Genes Dev 21(6): 682-693.

Noguchi, T., K. Akiyama, M. Yokoyama, N. Kanda, T. Matsunaga and Y. Nishi (1996). "Amplification of a DEAD box gene (DDX1) with the MYCN gene in neuroblastomas as a result of cosegregation of sequences flanking the MYCN locus." Genes Chromosomes Cancer 15(2): 129-133.

Nothias, J. Y., S. Majumder, K. J. Kaneko and M. L. DePamphilis (1995). "Regulation of gene expression at the beginning of mammalian development." J Biol Chem 270(38): 22077-22080.

Nothias, J. Y., M. Miranda and M. L. DePamphilis (1996). "Uncoupling of transcription and translation during zygotic gene activation in the mouse." EMBO J 15(20): 5715-5725.

Ogushi, S., K. Yamagata, C. Obuse, K. Furuta, T. Wakayama, M. M. Matzuk and M. Saitou (2017). "Reconstitution of the oocyte nucleolus in mice through a single nucleolar protein, NPM2." J Cell Sci 130(14): 2416-2429.

Ohn, T., N. Kedersha, T. Hickman, S. Tisdale and P. Anderson (2008). "A functional RNAi screen links O-GlcNAc modification of ribosomal proteins to stress granule and processing body assembly." Nat Cell Biol 10(10): 1224-1231.

Ohsugi, M., P. Zheng, B. Baibakov, L. Li and J. Dean (2008). "Maternally derived FILIA-MATER complex localizes asymmetrically in cleavage-stage mouse embryos." Development 135(2): 259-269.

Onishi, H., Y. Kino, T. Morita, E. Futai, N. Sasagawa and S. Ishiura (2008). "MBNL1 associates with YB-1 in cytoplasmic stress granules." J Neurosci Res 86(9): 1994-2002.

Oshikawa, K., M. Matsumoto, K. Oyamada and K. I. Nakayama (2012). "Proteome-wide identification of ubiquitylation sites by conjugation of engineered lysine-less ubiquitin." J Proteome Res 11(2): 796-807.

Pattabiraman, S., C. Baumann, D. Guisado, J. J. Eppig, J. C. Schimenti and R. De La Fuente (2015). "Mouse BRWD1 is critical for spermatid postmeiotic transcription and female meiotic chromosome stability." J Cell Biol 208(1): 53-69.

Pepling, M. E., J. E. Wilhelm, A. L. O'Hara, G. W. Gephardt and A. C. Spradling (2007). "Mouse oocytes within germ cell cysts and primordial follicles contain a Balbiani body." Proc Natl Acad Sci U S A 104(1): 187-192.

Perez-Gonzalez, A., A. Pazo, R. Navajas, S. Ciordia, A. Rodriguez-Frandsen and A. Nieto (2014). "hCLE/C14orf166 associates with DDX1-HSPC117-FAM98B in a novel transcription-dependent shuttling RNA-transporting complex." PLoS One 9(3): e90957.

Philipps, D. L., K. Wigglesworth, S. A. Hartford, F. Sun, S. Pattabiraman, K. Schimenti, M. Handel, J. J. Eppig and J. C. Schimenti (2008). "The dual bromodomain and WD repeat-containing mouse protein BRWD1 is required for normal spermiogenesis and the oocyte-embryo transition." Dev Biol 317(1): 72-82.

Piecyk, M., S. Wax, A. R. Beck, N. Kedersha, M. Gupta, B. Maritim, S. Chen, C. Gueydan, V. Kruys, M. Streuli and P. Anderson (2000). "TIA-1 is a translational silencer that selectively regulates the expression of TNF-alpha." EMBO J 19(15): 4154-4163.

Piko, L. and K. B. Clegg (1982). "Quantitative changes in total RNA, total poly(A), and ribosomes in early mouse embryos." Dev Biol 89(2): 362-378.

Popow, J., J. Jurkin, A. Schleiffer and J. Martinez (2014). "Analysis of orthologous groups reveals archease and DDX1 as tRNA splicing factors." Nature 511(7507): 104-107.

Protter, D. S. W. and R. Parker (2016). "Principles and Properties of Stress Granules." Trends Cell Biol 26(9): 668-679.

Ramos, S. B., D. J. Stumpo, E. A. Kennington, R. S. Phillips, C. B. Bock, F. Ribeiro-Neto and P. J. Blackshear (2004). "The CCCH tandem zinc-finger protein Zfp36l2 is crucial for female fertility and early embryonic development." Development 131(19): 4883-4893.

Ribeiro de Almeida, C., S. Dhir, A. Dhir, A. E. Moghaddam, Q. Sattentau, A. Meinhart and N. J. Proudfoot (2018). "RNA Helicase DDX1 Converts RNA G-Quadruplex Structures into R-Loops to Promote IgH Class Switch Recombination." Mol Cell 70(4): 650-662 e658.

Robertson-Anderson, R. M., J. Wang, S. P. Edgcomb, A. B. Carmel, J. R. Williamson and D. P. Millar (2011). "Single-molecule studies reveal that DEAD box protein DDX1 promotes oligomerization of HIV-1 Rev on the Rev response element." J Mol Biol 410(5): 959-971.

Roest, H. P., W. M. Baarends, J. de Wit, J. W. van Klaveren, E. Wassenaar, J. W. Hoogerbrugge, W. A. van Cappellen, J. H. Hoeijmakers and J. A. Grootegoed (2004). "The ubiquitin-conjugating DNA repair enzyme HR6A is a maternal factor essential for early embryonic development in mice." Mol Cell Biol 24(12): 5485-5495.

Schultz, R. M. (1993). "Regulation of zygotic gene activation in the mouse." Bioessays 15(8): 531-538.

Schultz, R. M. (2002). "The molecular foundations of the maternal to zygotic transition in the preimplantation embryo." Hum Reprod Update 8(4): 323-331.

Serman, A., F. Le Roy, C. Aigueperse, M. Kress, F. Dautry and D. Weil (2007). "GW body disassembly triggered by siRNAs independently of their silencing activity." Nucleic Acids Res 35(14): 4715-4727.

Singh, A. P., J. F. Foley, M. Rubino, M. C. Boyle, A. Tandon, R. Shah and T. K. Archer (2016). "Brg1 Enables Rapid Growth of the Early Embryo by Suppressing Genes That Regulate Apoptosis and Cell Growth Arrest." Mol Cell Biol 36(15): 1990-2010.

Soto-Rifo, R., P. S. Rubilar, T. Limousin, S. de Breyne, D. Decimo and T. Ohlmann (2012). "DEAD-box protein DDX3 associates with eIF4F to promote translation of selected mRNAs." EMBO J 31(18): 3745-3756.

Spiegelman, M. and D. Bennett (1973). "A light- and electron-microscopic study of primordial germ cells in the early mouse embryo." J Embryol Exp Morphol 30(1): 97-118.

Squire, J. A., P. S. Thorner, S. Weitzman, J. D. Maggi, P. Dirks, J. Doyle, M. Hale and R. Godbout (1995). "Co-amplification of MYCN and a DEAD box gene (DDX1) in primary neuroblastoma." Oncogene 10(7): 1417-1422.

Stein, P., N. V. Rozhkov, F. Li, F. L. Cardenas, O. Davydenko, L. E. Vandivier, B. D. Gregory, G. J. Hannon and R. M. Schultz (2015). "Essential Role for endogenous siRNAs during meiosis in mouse oocytes." PLoS Genet 11(2): e1005013.

Tang, F., M. Kaneda, D. O'Carroll, P. Hajkova, S. C. Barton, Y. A. Sun, C. Lee, A. Tarakhovsky, K. Lao and M. A. Surani (2007). "Maternal microRNAs are essential for mouse zygotic development." Genes Dev 21(6): 644-648.

Telford, N. A., A. J. Watson and G. A. Schultz (1990). "Transition from maternal to embryonic control in early mammalian development: a comparison of several species." Mol Reprod Dev 26(1): 90-100.

Tong, Z. B., L. Gold, K. E. Pfeifer, H. Dorward, E. Lee, C. A. Bondy, J. Dean and L. M. Nelson (2000). "Mater, a maternal effect gene required for early embryonic development in mice." Nat Genet 26(3): 267-268.

Torres-Padilla, M. E. and M. Zernicka-Goetz (2006). "Role of TIF1alpha as a modulator of embryonic transcription in the mouse zygote." J Cell Biol 174(3): 329-338.

Tritschler, F., J. E. Braun, A. Eulalio, V. Truffault, E. Izaurralde and O. Weichenrieder (2009). "Structural basis for the mutually exclusive anchoring of P body components EDC3 and Tral to the DEAD box protein DDX6/Me31B." Mol Cell 33(5): 661-668.

Voronina, E., G. Seydoux, P. Sassone-Corsi and I. Nagamori (2011). "RNA granules in germ cells." Cold Spring Harb Perspect Biol 3(12).

Wang, Q. T., K. Piotrowska, M. A. Ciemerych, L. Milenkovic, M. P. Scott, R. W. Davis and M. Zernicka-Goetz (2004). "A genome-wide study of gene activity reveals developmental signaling pathways in the preimplantation mouse embryo." Dev Cell 6(1): 133-144.

Wu, X., M. M. Viveiros, J. J. Eppig, Y. Bai, S. L. Fitzpatrick and M. M. Matzuk (2003). "Zygote arrest 1 (Zar1) is a novel maternal-effect gene critical for the oocyte-to-embryo transition." Nat Genet 33(2): 187-191.

Xie, F., K. A. Timme and J. R. Wood (2018). "Using Single Molecule mRNA Fluorescent in Situ Hybridization (RNA-FISH) to Quantify mRNAs in Individual Murine Oocytes and Embryos." Sci Rep 8(1): 7930.

Xu, Y., Y. Shi, J. Fu, M. Yu, R. Feng, Q. Sang, B. Liang, B. Chen, R. Qu, B. Li, Z. Yan, X. Mao, Y. Kuang, L. Jin, L. He, X. Sun and L. Wang (2016). "Mutations in PADI6 Cause Female Infertility Characterized by Early Embryonic Arrest." Am J Hum Genet 99(3): 744-752.

Yamamoto, T. M., J. M. Cook, C. V. Kotter, T. Khat, K. D. Silva, M. Ferreyros, J. W. Holt, J. D. Knight and A. Charlesworth (2013). "Zar1 represses translation in Xenopus oocytes and binds to the TCS in maternal mRNAs with different characteristics than Zar2." Biochim Biophys Acta 1829(10): 1034-1046.

Yurttas, P., A. M. Vitale, R. J. Fitzhenry, L. Cohen-Gould, W. Wu, J. A. Gossen and S. A. Coonrod (2008). "Role for PADI6 and the cytoplasmic lattices in ribosomal storage in oocytes and translational control in the early mouse embryo." Development 135(15): 2627-2636.

Zeng, F. and R. M. Schultz (2005). "RNA transcript profiling during zygotic gene activation in the preimplantation mouse embryo." Dev Biol 283(1): 40-57.

Zinder, J. C. and C. D. Lima (2017). "Targeting RNA for processing or destruction by the eukaryotic RNA exosome and its cofactors." Genes Dev 31(2): 88-100.

2.8 Supplementary Figures

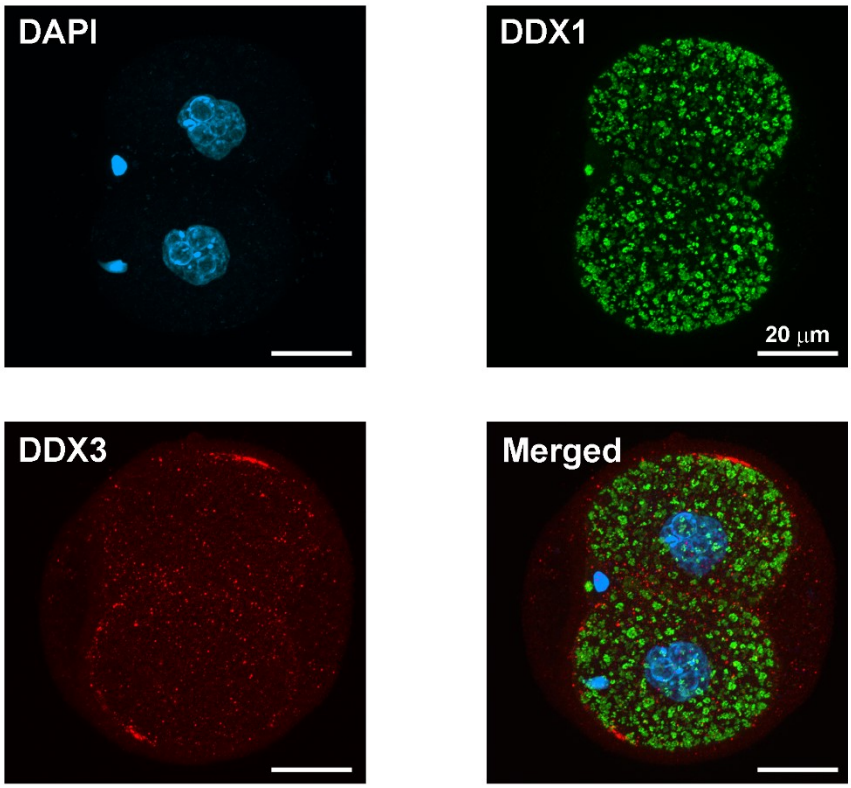

Figure S2.1 DDX1 does not co-immunostain with DDX3 (Magnification of Figure 2.6). Two-cell embryos were co-immunostained with anti-DDX1 antibody and an antibody to the P-body marker DDX3. DDX3 did not co-localize with DDX1 granules. Embryos are displayed as 2D projections of Z-stacks imaged by confocal microscopy. Scale bar = 20 μm.

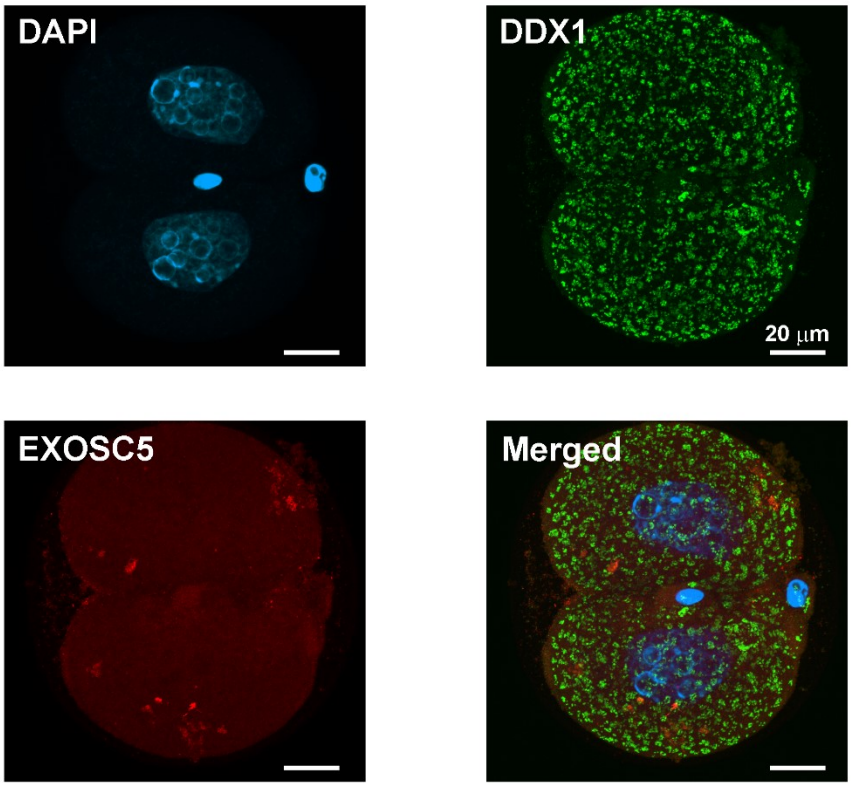

Figure S2.2 DDX1 does not co-immunostain with exosome (Magnification of Figure 2.6). Two-cell embryos were co-immunostained with anti-DDX1 antibody and an antibody to the exosome marker EXOSC5. EXOSC5 did not co-localize with DDX1 granules. Embryos are displayed as 2D projections of Z-stacks imaged by confocal microscopy. Scale bar = 20 μm.

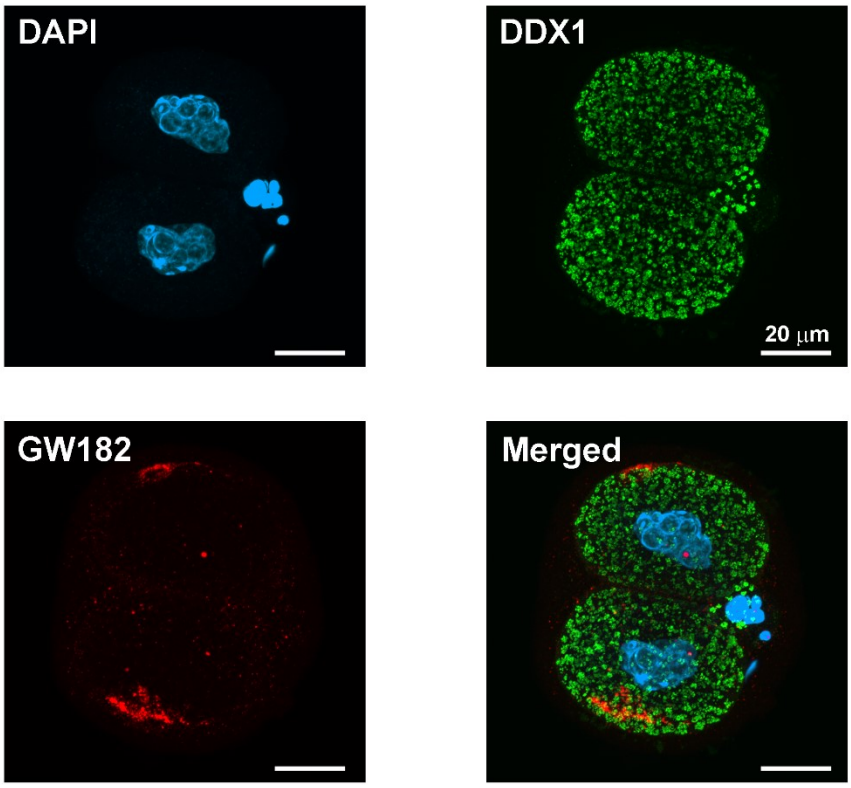

Figure S2.3 DDX1 does not co-immunostain with GW182 (Magnification of Figure 2.6). Two-cell embryos were co-immunostained with anti-DDX1 antibody and anti-GW182, an antibody to P-bodies and germ granules. GW182 did not co-localize with DDX1 granules. Embryos are displayed as 2D projections of Z-stacks imaged by confocal microscopy. Scale bar = 20 µm.

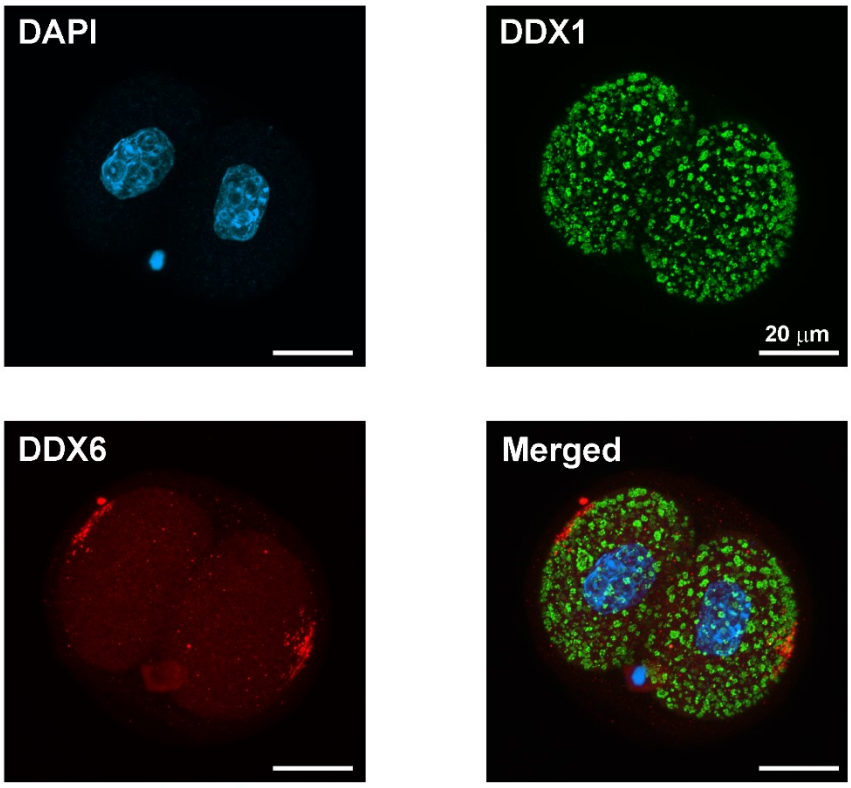

Figure S2.4 DDX1 does not co-immunostain with DDX6 (Magnification of Figure 2.6). Two-cell embryos were co-immunostained with anti-DDX1 antibody and an antibody to P-bodies and germ granule markers DDX6. DDX6 did not co-localize with DDX1 granules. Embryos are displayed as 2D projections of Z-stacks imaged by confocal microscopy. Scale bar = 20 µm.

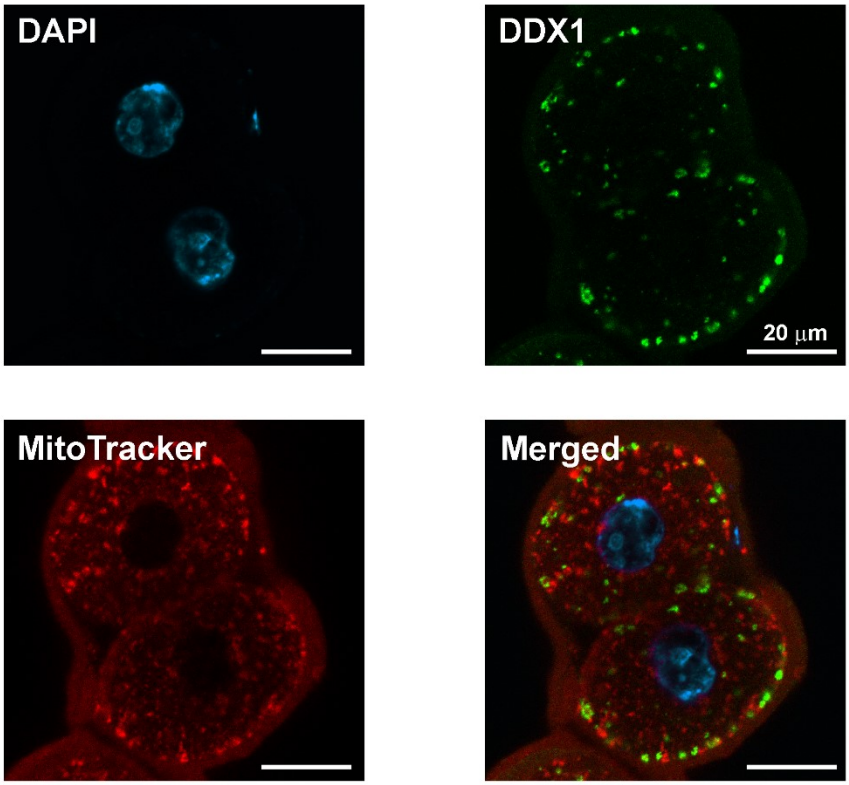

Figure S2.5 DDX1 does not co-localize with mitochondria. Two-cell embryos were stained with MitoTracker Deep Red for 30 minutes at 37°C. The embryos were then fixed and immunostained with anti-DDX1 antibody. MitoTracker Deep Red did not co-localize with DDX1 granules. Scale bar = 20 μm.

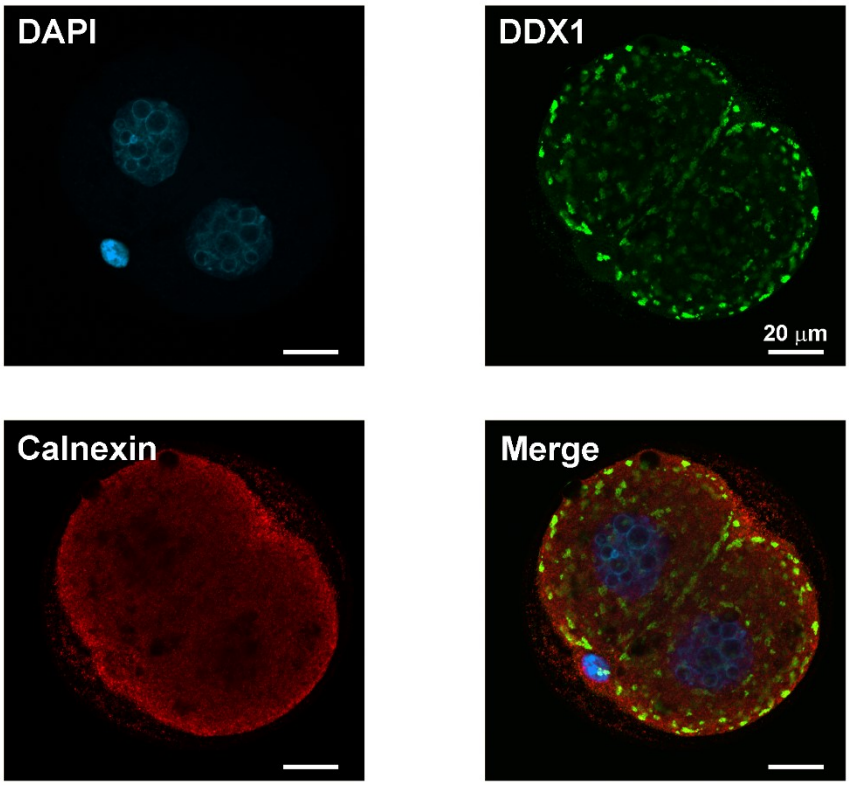

Figure S2.6 DDX1 does not co-localize with endoplasmic reticulum. Two-cell embryos were co-immunostained with anti-DDX1 antibody and an antibody to endoplasmic reticulum marker calnexin. Calnexin did not co-localize with DDX1 granules. Scale bar = 20 μm.

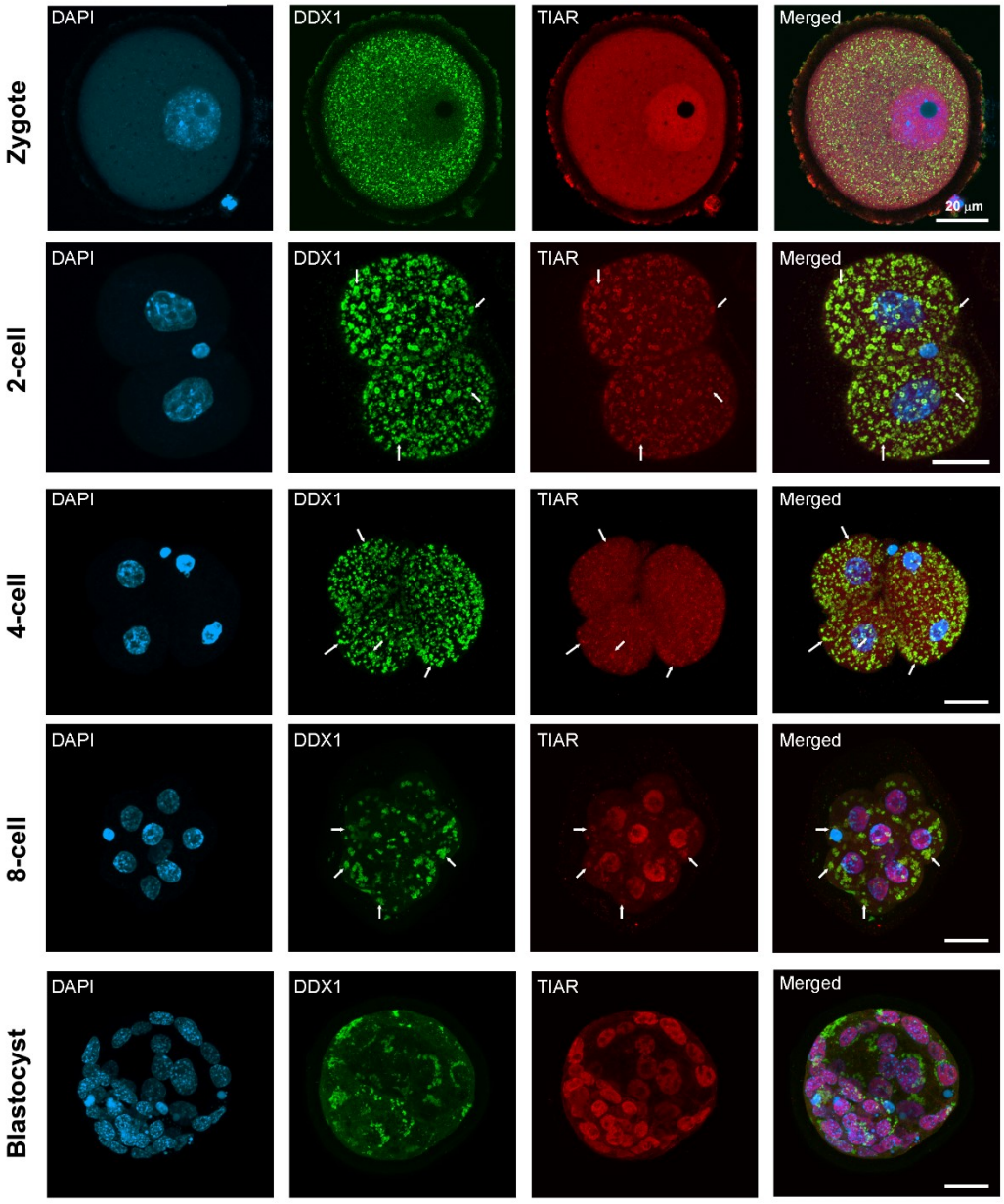

Figure S2.7 DDX1 co-localizes with TIAR in pre-implantation embryos. DDX1 co-immunostaining with anti-TIAR antibody revealed co-localization of TIAR with DDX1 granules from the zygote to the blastocyst stages. Arrows point to DDX1

granules that co-localize with TIAR. Embryos are displayed as 2D projections of Z-stacks imaged by confocal microscopy. Scale bar = 20 μm.

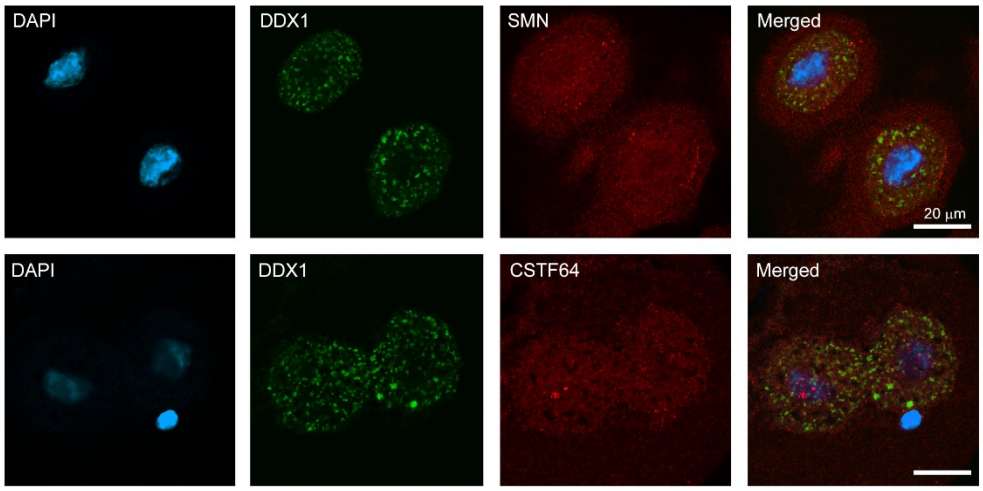

Figure S2.8 DDX1 does not co-immunostain with Cajal and cleavage bodies markers. Two-cell embryos were co-immunostained with anti-DDX1 antibody and antibodies to either SMN (Cajal body marker) or CstF64 (cleavage body marker). Neither SMN nor CstF64 co-localized with DDX1 granules. Scale bar = 20 µm.

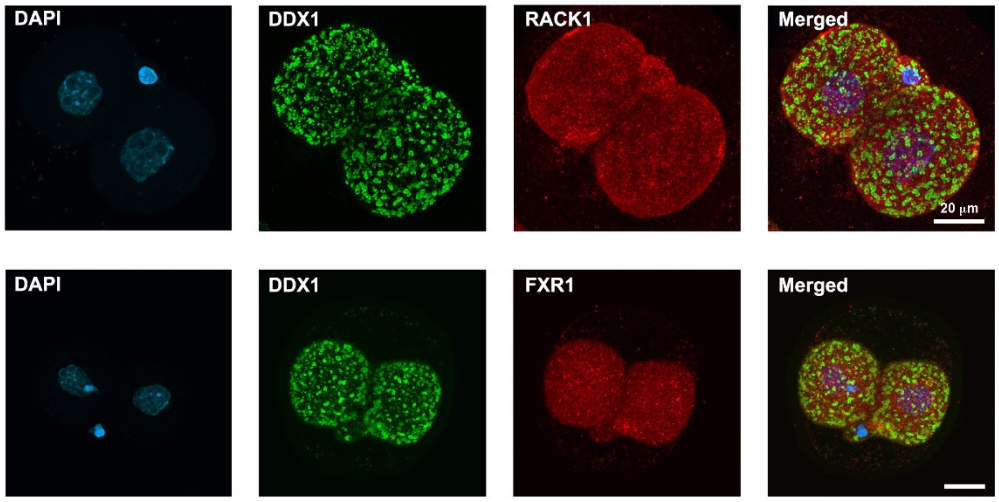

Figure S2.9 FXR1 and RACK1 stress granule markers do not co-localize with DDX1 aggregates. Two-cell embryos were co-immunostained with anti-DDX1 antibody and antibodies to stress granule markers (FXR1 or RACK1). Neither FXR1 nor RACK1 co-localized with DDX1 granules. Embryos are displayed as 2D projections of Z-stacks imaged by confocal microscopy. Scale bar = 20 µm.

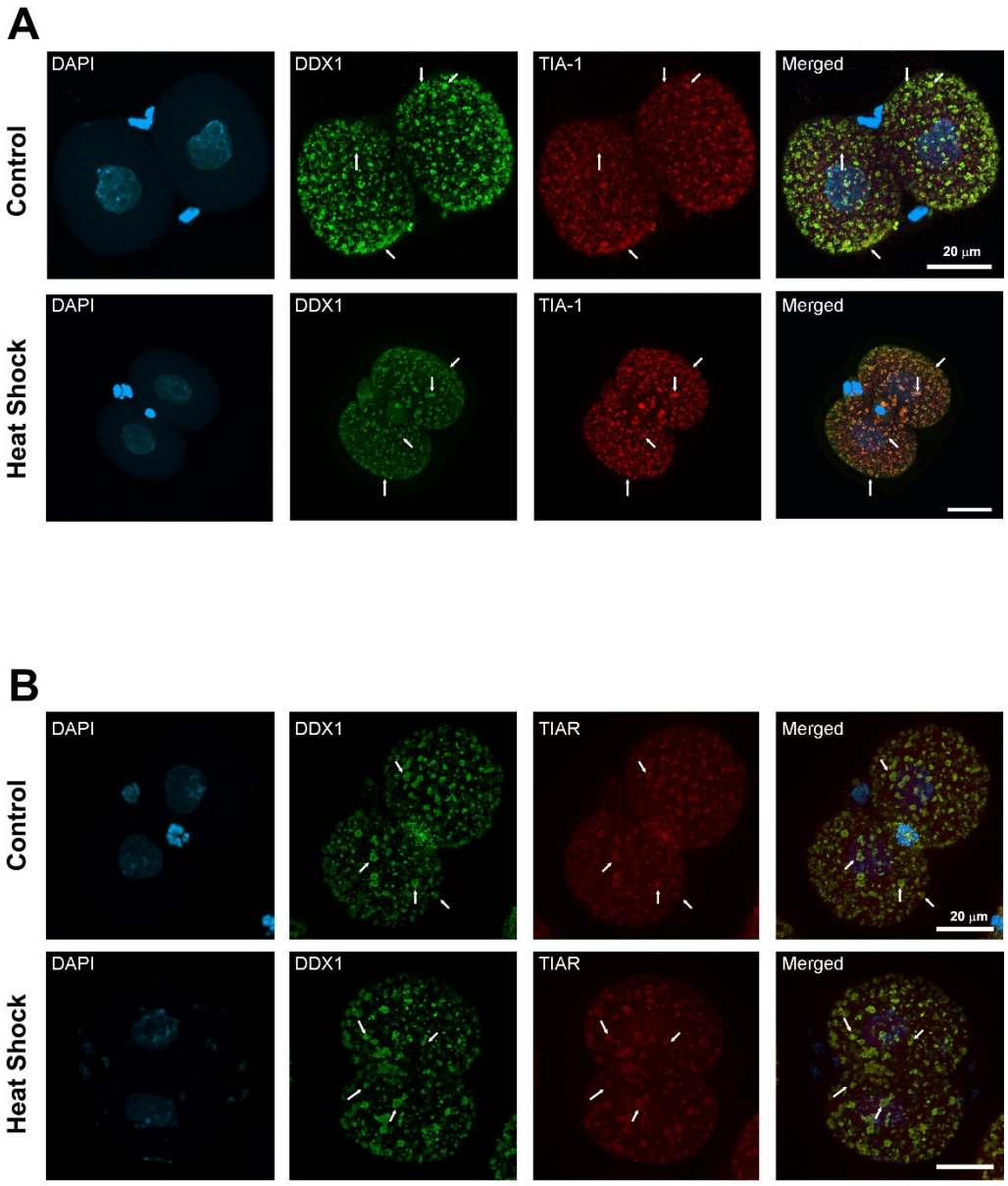

Figure S2.10 Heat shock does not affect the co-localization pattern of DDX1 and TIA-1 and TIAR. Two-cell embryos were co-immunostained with anti-DDX1 antibody and antibodies to TIA-1 or TIAR after the embryos were incubated for 45 minutes at either 37°C (control) or 43°C (heat shock). No significant change in the

distribution of DDX1 and TIA-1 (A) or TIAR (B) was observed after heat-shock. Arrows point to a subset of granules showing DDX1 and TIA-1 (or TIAR) co-immunostaining. Embryos are displayed as 2D projections of Z-stacks imaged by confocal microscopy. Scale bar = 20 μm.

Chapter 3.

Aggregates of Cytoplasmic DDX1 Vesicles Control Calcium-dependent Mitochondrial Activity in Early Mouse Embryos

The goal of this chapter was to define the structure and composition of the DDX1 aggregates identified in the cytoplasm of early-stage embryos, to get insight into the function of these cytoplasmic aggregates.

3.1 Introduction

There are two waves of zygotic genome activation during early-stage development: a minor wave at the 1-cell stage and a major wave at the 2-cell stage (Schultz 2002). The majority of the zygotic genome is activated after these two waves of zygotic genome activation, at which time most of the maternal RNA are degraded (Li, Zheng et al. 2010). Maternal RNAs and proteins are essential to development pre-zygotic genome activation.

The causes underlying the majority of 2-cell arrests are related to maternal factors such as the absence of maternal mRNA or protein needed for zygotic genome activation, genomic imprinting, or abnormal mitochondria resulting from maternal genetic mutations (Li, Zheng et al. 2010, Fernandes, Tsuda et al. 2012). There is much less known about zygotic genes involved in early embryonic development. In addition to *Ddx1*, zygotic genes associated with early embryonic lethality include *Pp2cβ* (a.k.a. *Ppm1b*), *Ddx20*, *Profilin 1* as well as *Ercc2* (de Boer, Donker et al. 1998, Witke, Sutherland et al. 2001, Sasaki, Ohnishi et al. 2007, Mouillet, Yan et al. 2008, Hildebrandt, Wang et al. 2019).

Another cause of 2-cell arrest in mouse embryos involves disruption of cellular metabolism in either oocytes or fertilized eggs (Van Blerkom, Davis et al. 2002, Van Blerkom, Davis et al. 2003, Acton, Jurisicova et al. 2004, Van Blerkom 2004, Van Blerkom and Davis 2006, Komatsu, Iwase et al. 2014). The

considerable energy needs of early mouse embryos are almost exclusively met by mitochondria (Benos and Balaban 1983, Bentov, Yavorska et al. 2011). The total number of mitochondria per embryo remains unchanged from the 1-cell to the blastocyst stages, with numbers of mitochondria halved at each cell division, suggesting a need for increased mitochondrial function as development progresses towards blastocyst stage (Piko and Matsumoto 1976, Piko and Taylor 1987). However, increased mitochondrial function can also result in cell death through upregulation of mitochondrial reactive oxygen species (mtROS) (Brookes, Yoon et al. 2004, Peng and Jou 2010). While ROS production is essential for embryonic development (Han, Ishibashi et al. 2018), excessive production of ROS results in mitochondria and nuclear fragmentation (Jezek, Cooper et al. 2018). Thus, a fine balance must be maintained in early embryos so that sufficient energy is produced without overwhelming the embryo's ability to process and utilize ROS productively. Calcium (Ca^{2+}) signaling is essential for embryonic development and plays an important role in mitochondrial function and ATP production (Ashby and Tepikin 2001, Brookes, Yoon et al. 2004, Dumollard, Marangos et al. 2004, Campbell and Swann 2006, Miao and Williams 2012). Thus, Ca^{2+} may play a key role in regulating mitochondrial function during early embryonic development.

DEAD box 1 (DDX1) is an RNA binding/unwinding protein that is usually found in the nucleus of somatic cells. However, DDX1 is primarily found in the cytoplasm of early-stage embryos, from zygote to the blastocyst stages, where it forms large aggregates (Hildebrandt, Wang et al. 2019). DDX1 aggregates do not

co-compartmentalize with markers for P-bodies or germ cell granules, although they do co-compartmentalize with TIA-1 and TIAR, proteins classically associated with stress granules (Kedersha, Gupta et al. 1999, Hildebrandt, Wang et al. 2019). *Ddx1*-null *Drosophila melanogaster* are infertile, with smaller body sizes compared to their wild-type counterparts, suggesting a potential link between *Ddx1* and metabolism (Germain, Li et al. 2015). Furthermore, RNA sequencing analysis revealed a possible role for DDX1 in upregulating the unspliced variant of *Sirup*, the homolog of succinate dehydrogenase SDHAF4 which promotes mitochondrial succinate dehydrogenase activity (Van Vranken, Bricker et al. 2014, Cox, Thummel et al. 2017). These data suggest a possible role for DDX1 in the maintenance of optimum embryonic mitochondrial function.

We show that DDX1 cytoplasmic aggregates in 2-cell embryos consist of membrane-bound vesicles that contain RNA and Ca^{2+}. Loss of DDX1 is associated with considerably-reduced numbers of membrane-bound vesicles and disruption of Ca^{2+} cytoplasmic distribution, events that are accompanied by increased mtROS and nuclear fragmentation suggesting a role for DDX1 vesicles in Ca^{2+} regulation. Intriguingly, in addition of DDX1, membrane-bound vesicles contain the cytoplasmic polyadenylation factors CPEB1 and CPSF2 based on our immunostaining data. As DDX1 has previously been shown to interact with pre-mRNA 3' processing factor CstF64 which plays a role in pre-mRNA 3' processing (Bleoo, Sun et al. 2001), we propose that DDX1 plays a dual role in Ca^{2+}-dependent mitochondrial regulation and the formation of DDX1 vesicles that serve

as sites for the storage, processing and/or utilization of RNAs prior to their translation. We have named the aggregates of DDX1 vesicles MARVs, for membrane associated RNA-containing vesicles.

3.2 Materials and methods

3.2.1 Embryo and oocyte collection

All embryos used in our experiments were obtained under natural-mating conditions in the FVB/N background. For embryo cultures, M16 medium (Sigma-Aldrich) was allowed to equilibrate overnight in a 37°C incubator with 5% CO_2. The generation of the *Ddx1* mouse knockout line in the FVB/N background has been described previously (Hildebrandt, Germain et al. 2015). For timed pregnancies, females were tested for the presence of vaginal plugs, with plugged date labelled as embryonic day (E) 0.5. For collection of E0.5 to E2.5 embryos, oviducts were removed and placed in 35mm tissue culture dishes where they were flushed with equilibrated (37°C) M16 medium using capillary tubes (World Precision Instruments). E0.5 embryos were treated with 300 µg/ml hyaluronidase (Sigma-Aldrich) to remove cumulus cells. For collection of E3.5 embryos, the uterus was removed and placed in 35mm tissue culture dishes. Uterine horns were flushed with equilibrated (37°C) M16 medium using 18G needles.

To obtain meiosis II arrested (MII-arrested) oocytes, FVB/N wildtype mice were injected with 5 IU pregnant mare serum gonadotropin (MSD Animal Health) followed by 5 IU human chorionic gonadotropin (MSD Animal Health) 48 h later. The oviducts were then removed and flushed with M16 medium using capillary

tubes. MII stage oocytes were treated with 300 μg/ml hyaluronidase for the removal of cumulus cells.

3.2.2 Culturing embryos

M16 medium was allowed to equilibrate overnight in a 37°C incubator with 5% CO_2. The humidifier culture chamber is an adaption from Gasperin *et al.* (Gasperin, Barreta et al. 2010). As illustrated in **Figure 3.1**, all gaps between each well of 96-well plates were filled with 150 μl autoclaved ddH_2O and the centermost 3*3 wells were filled with 50 μl/well of equilibrated M16 medium. After the embryos were collected, they were washed 3X in the first 3 wells of M16 medium and placed in the center well of the 3*3 matrix and cultured for the designated times in a 37°C incubator with 5% CO_2.

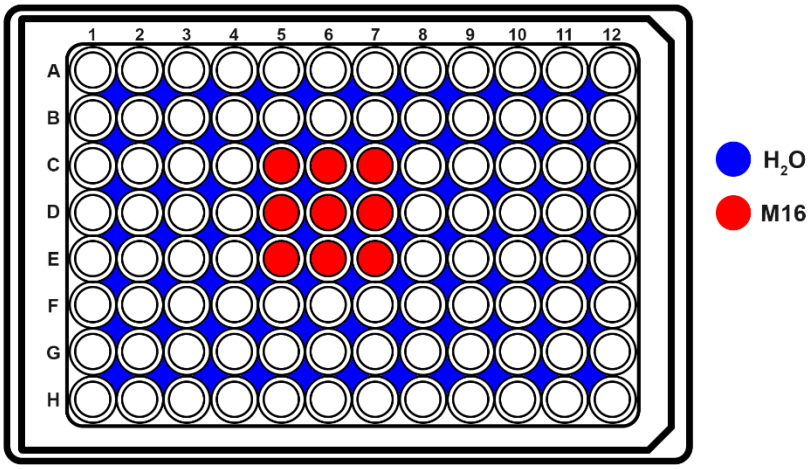

Figure 3.1 Humidification chamber for pre-implantation stage embryo cultures. Graphical demonstration of customized humidification chamber. 150 µl of H_2O was placed into each gap between wells. Nine wells in the centre of the plate contain 50 µl of M16 medium each.

3.2.3 Primary antibody conjugation

The specificity of the anti-DDX1 antibody used for our experiments has been previously described (Bleoo, Sun et al. 2001), and used for mouse embryo immunostaining (Hildebrandt, Germain et al. 2015, Hildebrandt, Wang et al. 2019). For direct conjugation of anti-DDX1 antibody to Atto 550, one ml of anti-DDX1 antibody was IgG-purified with a Melon Gel IgG Spin Purification Kit (ThermoFisher) and concentrated to 1 mg/ml. The purified anti-DDX1 antibody was then

conjugated to Atto 550 using the Atto 550 Protein Labeling Kit (Sigma-Aldrich) following the manufacturer's protocol.

3.2.4 Immunofluorescence staining

Embryos were flushed from oviducts using PBS or transferred from culture M16 medium to PBS and fixed in 4% paraformaldehyde for 15 min. The embryos were then washed 3X with PBS + 0.01% Triton-X-100 (PBST) and permeabilized with PBS + 0.5% Triton-X-100 for 15 min. Next, the embryos were incubated in 0.5% fish gelatin blocking solution for 30 min, and incubated for 1 h in PBST-diluted anti-DDX1 antibody. The immunostaining plate was wrapped in aluminum foil to protect the antibody from light. For immunostaining of other proteins, embryos were treated as described above for DDX1 immunostaining, then washed 3X with PBST and incubated with secondary antibody for 1 h. After washing 3X with PBST, embryos were placed on a slide and mounted with Mowiol (Calbiochem) without 4',6-diamidino-2-phenylindole (DAPI). The antibodies used are listed in **Table 3.1**.

For super resolution images, embryos were imaged using a Leica TCS SP8 STED super resolution microscope and 100X/NA1.4 oil lens to capture single sections. As whole mount embryos are relatively thick for super resolution microscope, the embryos were imaged at the sections that were the closest to the

cover slip. For confocal Z-stacks, the embryos were imaged with a Leica TCS SP8 microscope and 100X/NA1.4 oil lens without the depletion laser.

A subset of immunostained embryos was imaged using a Zeiss Laser Scanning Confocal microscope (LSM710) mounted on an inverted microscope (Axio Observer). Embryos were mounted with Mowiol (Calbiochem) containing DAPI. Images were taken with a 40X/NA1.3 oil lens as previously descripted (Hildebrandt, Wang et al. 2019).

3.2.5 Inhibition of global and mitochondrial translation

M16 medium (50 µl) containing either 150 µg/ml cycloheximide (Sigma-Aldrich) or 200 µg/ml chloramphenicol (Sigma-Aldrich) was used for global or mitochondrial translation inhibition, respectively. For collection of E0.5 embryos, oviducts were flushed (at 10:00) with equilibrated M16 medium and embryos treated with 300 µg/ml hyaluronidase to remove cumulus cells. The embryos were then washed 3X with equilibrated M16 medium and incubated at 37°C until 16:00 the same day. The embryos were transferred to M16 medium with cycloheximide or chloramphenicol and incubated at 37°C for 8 h. Control embryos were incubated in M16 medium without inhibitors. Embryos were then fixed in 4% paraformaldehyde and processed for immunofluorescence staining.

3.2.6 Saponin Treatment

The detergent-like saponin permeabilizes plasma membranes without destroying them (Jacob, Favre et al. 1991). When used at high concentrations (0.1 to 0.2 mg/ml), saponin also permeabilizes internal organelles (Wassler, Jonasson et al. 1987). E1.5 embryos were incubated in equilibrated M16 medium containing 0.1% saponin for 6 min at room temperature. Control embryos were incubated in equilibrated M16 medium without saponin (Sigma-Aldrich). The embryos were washed 3X in equilibrated M16 medium and incubated in equilibrated M16 medium for an additional 30 min and processed for immunofluorescence staining or immunogold labelling.

3.2.7 Live cell imaging

For JC-1, MitoSOX, ER-Tracker and MitoTracker Deep Red staining, E0.5 or E1.5 embryos were incubated for 30 min in equilibrated M16 medium containing 10 µg/ml JC-1 dye (ThermoFisher Scientific), 2 µM MitoSOX (ThermoFisher Scientific), 200 nM ER-Tracker Red (ThermoFisher Scientific), or 100 nM MitoTracker Deep Red (Cell Signaling Technology). The embryos were washed 3X in equilibrated M16 medium and transferred to ultrathin bottom 96-well plates

(Grenier bio-one Cat. 6550900) containing 50 µl equilibrated M16 medium and processed for imaging with LSM 710. For saponin treatment, the embryos were incubated in equilibrated M16 medium with or without 0.1% saponin before incubation with MitoTracker Deep Red. For Ca^{2+} staining, the embryos were incubated for 30 min in equilibrated M16 medium containing 5 µM Fluo-4 AM dye. The embryos were washed 3X in equilibrated M16 medium, followed by incubation in 50 µl of equilibrated M16 medium for 30 min to remove nonspecifically-bound dye. For live cell co-staining with other dyes, the embryos were transferred to equilibrated M16 medium containing the dye of interest for 30 min and imaged in ultrathin bottom 96-well plates containing 50 µl equilibrated M16 medium. Live cell imaging was carried out using a Zeiss LSM710 laser scanning microscope and a 20X/NA0.8 lens.

3.2.8 Co-staining for calcium and DDX1

Fluo-4 AM stained 2-cell mouse embryos were fixed and permeabilized using -20°C methanol-acetone (1:1) for 5 min at 4°C. For co-staining with Fluo-4 AM and Atto 550-conjugated anti-DDX1 antibody, methanol-acetone fixed embryos were first incubated in PBST (10 min X3) for rehydration followed by incubation with primary antibody. Stained embryos were placed in ultrathin bottom

96-well plates (to minimize signal loss) and imaged using a Zeiss LSM710 microscope.

3.2.9 Imaging analysis

Images were imported to ImageJ. Regions of interest were drawn with iPad Pro (Apple) and Apple pencil 2 using duet display. Mean intensity values of different channels were used for JC-1 and MitoSOX statistical analysis. Coloc2 ImageJ co-localization analysis plugin was used for the analysis of mitochondria and Ca^{2+} with and without saponin treatment. Point spread function (PSF) was set to 3.0 and Costes randomisation was set to 100. Pearson correlations for each image were marked for statistical analysis with Prism. T-test was performed with Prism.

For mitochondria fragmentation analysis, Particle Analysis plug-in in ImageJ was used. The images were first adjusted with Auto Local Threshold using Midgrey method with a radius of 30 to best represent the particles. Particles with size of 10 $pixel^2$ and above were recorded. Custom Python script was used to summarize count particles within different size ranges and convert to μm^2. Data were then plotted with Prism.

3.2.10 Immunogold labelling

Ultralow melt agarose (SeaPrep) (4%) was prepared and melted at 60°C, then placed in a 37°C water bath. Embryos at different developmental stages were collected and fixed in 4% paraformaldehyde in 0.1M phosphate buffer for 1 h at room temperature. The embryos were transferred to a 250-µL tube and immersed in 5 µl of 4% agarose. The embryos were placed at 4°C to allow the agarose to solidify.

The agarose-embedded embryos were rinsed in 0.1 M phosphate buffer pH 7.3 followed by H_2O. The embryos were dehydrated in series of pre-cooled ethanol solutions (30%, 50% and 70% 15 min each and 95% and 100% ETOH 10 min each). For embedding, the embryos were placed in LR white resin-100% ethanol (2:1) for 2 h at 4°C and pure LR white resin overnight. LR white was polymerized under UV for 96 h at 4°C. Samples were cut into 100-nm sections with a Leica EM UC6 ultramicrotome and the sections were collected on 400 mesh nickel grids.

For immunogold labeling, the grids were immersed in 50 mM of NH_4Cl for 1 min at room temperature and then blocked with 0.5% fish gelatin in PBS for 45 min at room temperature. The grids were incubated with anti-DDX1 antibody (1:1000 dilution) in PBS for 3 h at room temperature, followed by 20 - 1X PBS washes. The grids were then incubated in goat anti-rabbit 10 nm nano-gold (Electron Microscopy Sciences) in PBS for 1 h **(Table 3.1)**. The grids were washed in 0.05%

fish gelatin in PBS, followed by PBS and H_2O. The samples were fixed again in 2% paraformaldehyde + 2.5% glutaraldehyde for 15 min at room temperature, rinsed in H_2O and treated with 1% OsO_4 for 10 min at room temperature. The samples were washed in H_2O and stained with 1% uranyl acetate 25-30 min at room temperature and 1% lead citrate for 3 min at room temperature. Images were obtained with a JEOL JEM-2100 transmission electron microscope at 200 kV.

Table 3.1 Antibodies used for immunofluorescence and immunogold labelling.

Antibody	Host	Dilution	Source
Anti-DDX1 (2910)	Rabbit	1:1000	In house (batch 2910)
Atto 550-conjugated anti-DDX1 (2910)	Rabbit	1:400	Anti-DDX1 (2910) conjugated with Atto 550 (Sigma-Aldrich)
Anti-RPS6	Mouse	1:50	Santa Cruz, Cat #sc-13007
Anti-MRPS27	Mouse	1:100	Santa Cruz, Cat #sc-390396
Anti-MRPL42	Mouse	1:100	Santa Cruz, Cat #sc-515820
Anti-MRPL44	Mouse	1:100	Santa Cruz, Cat #sc-515503
Anti-TIA-1	Goat	1:400	Santa Cruz, Cat #sc-1751
Anti-CPEB1	Mouse	1:50	Santa Cruz, Cat #sc-514688
Anti-CPSF2	Goat	1:100	Santa Cruz, Cat #sc-26658
Anti-Mouse Alexa 647	Donkey	1:400	Molecular Probes, Thermofisher
Anti-Goat Alexa 647	Donkey	1:400	Molecular Probes, Thermofisher

Gold conjugated 10 nm goat anti-rabbit	Goat	1:100	Electron Microscope Sciences, Cat #25109

3.2.11 OsO_4/uranyl acetate staining

The embryos were fixed in 2% paraformaldehyde + 2.5% glutaraldehyde in 0.1M phosphate buffer (pH7.3) for 1 h at room temperature and placed in low melt agarose as described under immunogold labelling, washed in 0.1 M phosphate buffer pH 7.3, and post-fixed in 0.1 M phosphate buffer containing 1% OsO_4 for 35 min at room temperature. The embryos were then incubated in freshly made 1% carbohydrazide solution (in H_2O) at room temperature for 5 min and quickly rinsed with ddH_2O. This was followed by incubation in 0.1 M phosphate buffer with 1% OsO_4 for 15 min and washed with ddH_2O.

The samples were dehydrated in 30% and 50% ethanol solutions (10 min each). The samples were then further dehydrated in 70% ethanol overnight at room temperature (if uranyl acetate was used, 1% uranyl acetate was added to the 70% ethanol), followed by 95% ethanol for 10 min and 3X 100% ethanol (10-15 min each). A series of resin infiltrations were performed using Spurr's resin [Spurr's:100% ethanol (1:4) for 1 h and 40 min, Spurr's:100% ethanol (1:1) for 1 h and 35 min, Spurr's:100% ethanol (3:1) for 2 h]. The samples were then embedded

in pure Spurr's resin for 1 h, overnight and 2 h. The infiltrated embryos were polymerized in a 65°C oven for 21 h. The samples were then cut into 100 nm sections. If uranyl acetate was used in the experiment, samples were final-stained in 1% uranyl acetate for 15 min followed by 1% lead citrate for 4 min.

3.2.12 Energy Filtered Transmission Electron Microscopy (EFTEM)

A Gatan GIF UltraScan 1000 camera (Gatan, CA, USA) mounted on a JEOL 200kv TEM (JEM 2100) with a Lab6 filament was used for EFTEM elemental mapping of phosphate and nitrogen. For phosphate mapping, embryos were stained with OsO_4 (no uranyl acetate) and analysed using three window EFTEM. Pre-edge images were obtained at 122eV and 127eV, and the post-edge image was obtained at 155eV. The energy-selecting window was set at 5eV. For nitrogen mapping, embryos were DDX1 immunogold-labelled. No OsO_4/uranyl acetate was used in nitrogen mapping to avoid interference of osmium with nitrogen. Pre-edge images were obtained at 368eV and 388eV, and the post-edge image was obtained at 411eV. The energy-selecting window was set at 20eV.

3.3 Results

3.3.1 DDX1 aggregates consist of large membrane bound vesicles

We used stimulated emission depletion (STED) super-resolution microscopy combined with Atto 550-conjugated anti-DDX1 antibody to better resolve the structure of DDX1 aggregates in mouse embryos. We discovered that each DDX1 aggregate in 2-cell embryos consists of a ring-like cluster **(Fig. 3.2)**. These ring-like clusters gradually become larger, denser, and less ring-like as the embryo matures **(Fig. 3.3)**. Interestingly, DDX1 aggregates are primarily found in the subplasmalemmal cytoplasm, spatially located immediately next to the plasma membrane **(Fig. 3.4)**. Staining with JC-1, a mitochondrial potential indicator dye, showed that mitochondria with high membrane potential ($\Delta\Psi_m$), which are generally associated with high levels of mitochondrial activity, also localize to the subplasmalemmal cytoplasm **(Fig. 3.5)** (Van Blerkom, Davis et al. 2003).

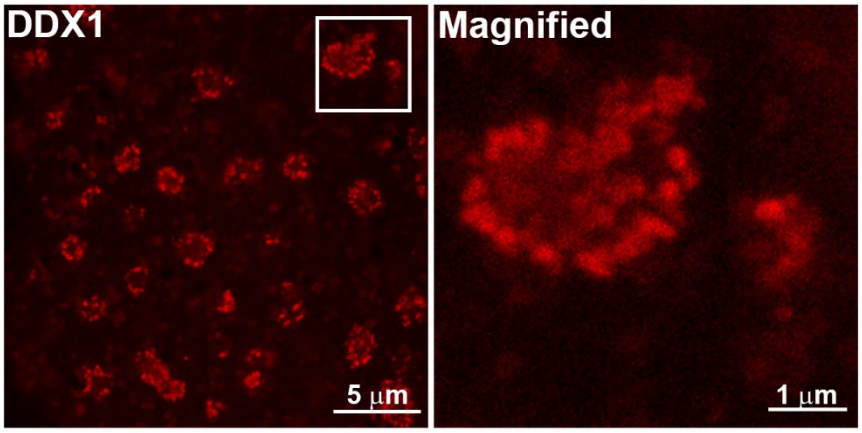

Figure 3.2 DDX1 form ring-like structures in 2-cell embryos. 2-cell embryos were fixed in 4% paraformaldehyde and immunostained with Atto 555-conjugated anti-DDX1 antibody. Images were obtained by STED microscopy (Leica SP8) using a 100X lens. The white square is magnified in the panel on the right. Scale bar = 10 μm. Magnified image scale bar = 1 μm.

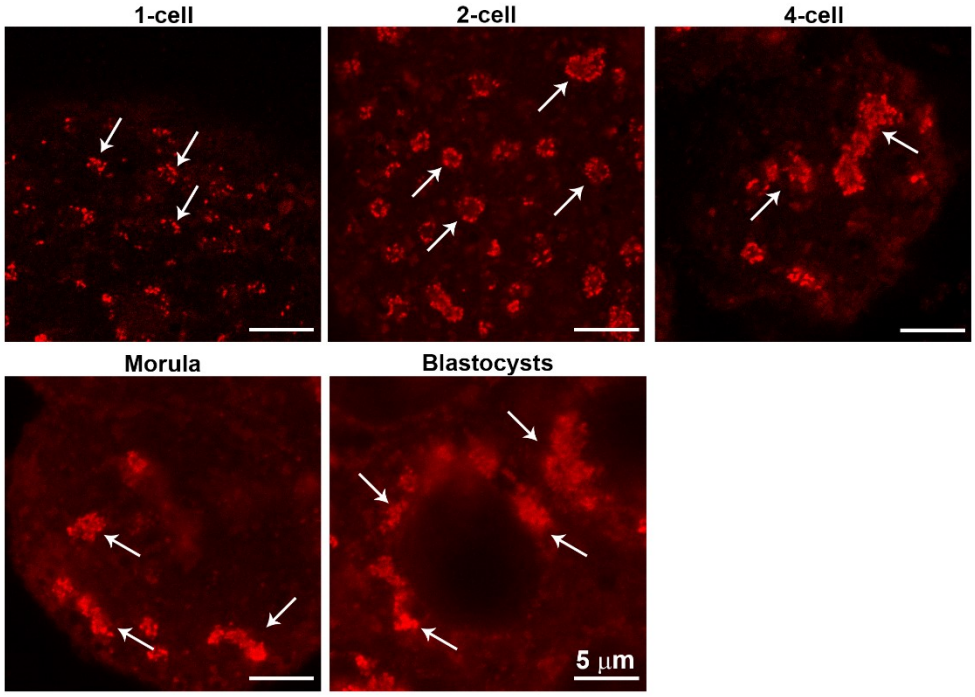

Figure 3.3 Images of DDX1 aggregates in embryos from 1-cell to blastocyst stages using STED super resolution microscopy. Embryos were fixed in 4% paraformaldehyde and immunostained with anti-DDX1 antibody. DDX1 aggregates formed ring-like structures at the 2-cell stage. These structures became larger, denser and less ring-like with embryonic development. The DDX1 aggregates were mostly observed around the nucleus at the blastocyst stage. Images were acquired with a 100X lens using a Leica SP8 STED microscope and a 660 nm STED depletion laser. Scale bar = 10 μm. Arrows point to a subset of DDX1 aggregates.

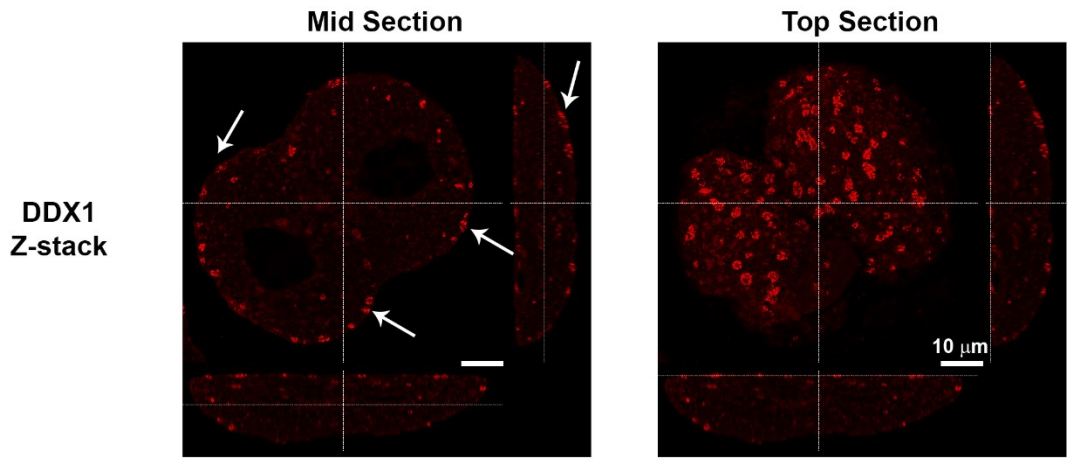

Figure 3.4 DDX1 localizes to the subplasmalemmal cytoplasm in 2-cell embryos. Two-cell embryos were fixed in 4% paraformaldehyde and immunostained with anti-DDX1 antibody. The DDX1 aggregates were mostly found at the subplasmalemmal cytoplasm. Z-stack images were acquired with a 100X lens using a Leica SP8 confocal microscope. Orthogonal image sections of both mid and top sections are shown to demonstrate the subplasmalemmal cytoplasmic DDX1 distribution from the X and Y axis of a 3D-reconstructed 2-cell stage embryo. Scale bar = 10 μm. Arrows point to DDX1 aggregates at the subplasmalemmal cytoplasm.

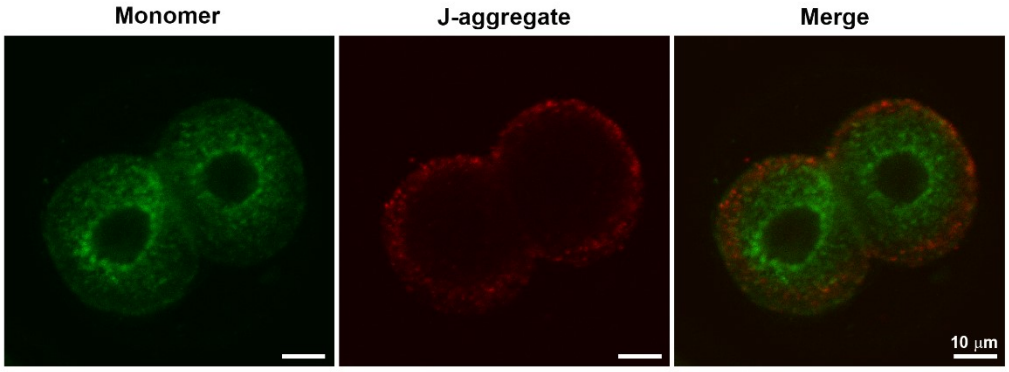

Figure 3.5 Mitochondria with high membrane potential ($\Delta\Psi_m$) are located at the subplasmalemmal cytoplasm in 2-cell embryos. JC-1 forms J-aggregates, indicative of molecular self-aggregation, under high membrane potential condition, and monomers under low membrane potential condition, characterized by red and green fluorescence emissions, respectively. 2-cell embryos were incubated in M16 medium with 10 μg/ml of JC-1 for 30 min and imaged using a Zeiss LSM 710 microscope and 20X lens. Scale bar = 10 μm.

To further study the structure of DDX1 aggregates, we carried out transmission electron microscopy (TEM) with DDX1-immunogold-labelled 2-cell embryos. In agreement with our STED data, DDX1-containing aggregates localized to the subplasmalemmal cytoplasm, with many aggregates located next to mitochondria **(Fig. 3.6A)**. Intriguingly, we found that each DDX1 aggregate consists of several large membrane-bound vesicles (~200 - 400 nm) loosely structured in a ring (**Fig. 3.6A; B)**. Based on manual counting of gold particles

within vesicles and outside vesicles, we estimate that ~84.2% ± 3.2% of DDX1-immunogold-labelled particles are located in membrane-bound vesicles. The number of particles located inside the vesicles could potentially be underestimated due to differences in the number of particles in different sections of the embryos, as well as obstruction caused by the size of the primary and secondary antibodies (~15 nm each) and the size of the gold particles (10 nm). Analysis of oocytes and different stage embryos revealed that DDX1 vesicles are absent in MII oocytes, but present in 1-cell embryos, disappearing by the blastocyst stage **(Fig. 3.7)**. Thus, a single DDX1 aggregate observed by confocal microscopy consists of multiple membrane-bound DDX1 vesicles that first appear in 1-cell embryos.

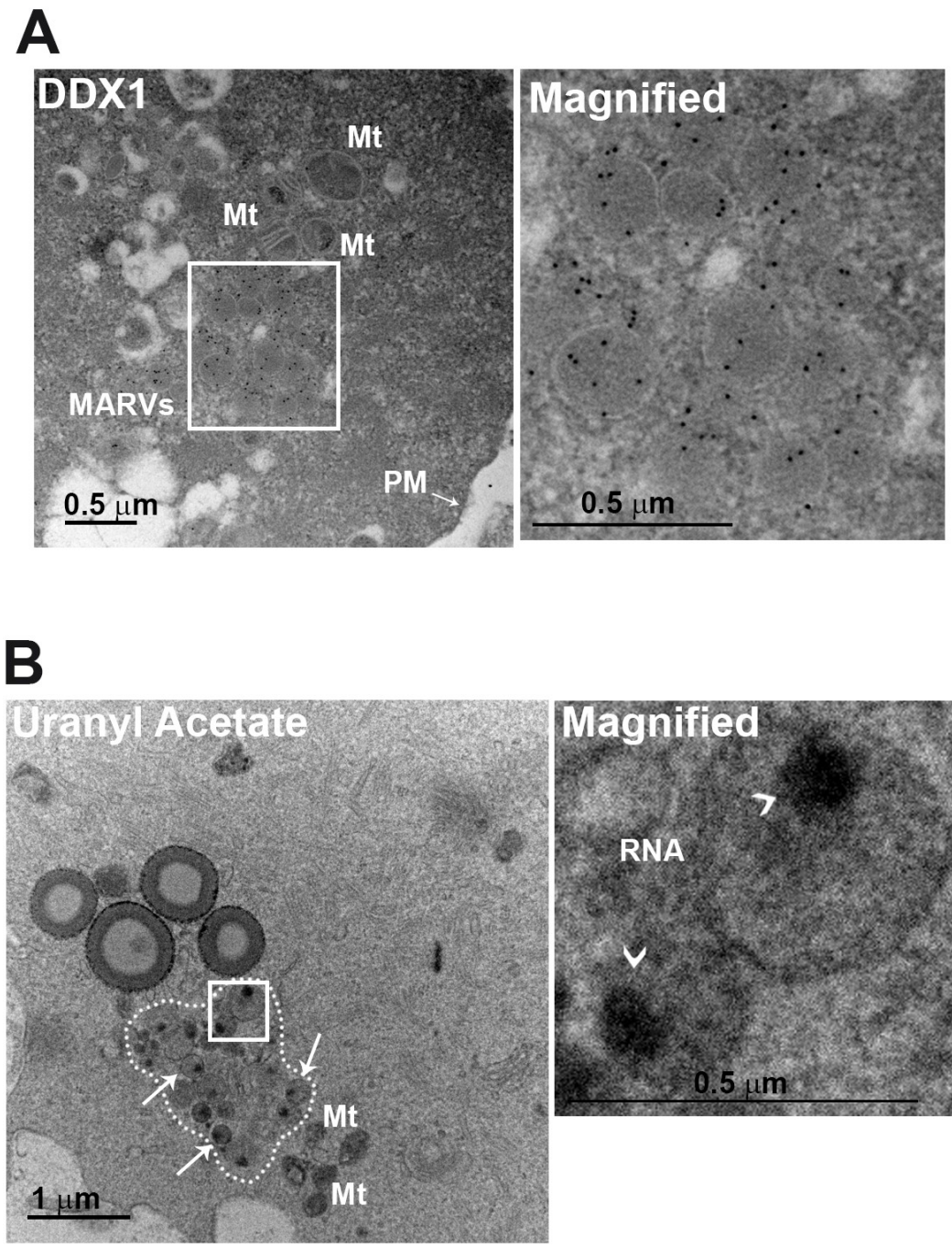
A
DDX1
Mt
Mt
Mt
MARVs
PM
0.5 μm
Magnified
0.5 μm
B
Uranyl Acetate
Mt
Mt
1 μm
Magnified
RNA
0.5 μm

Figure 3.6 DDX1 aggregates form ring-like structures with regionalized RNAs in 2-cell embryos. (A) TEM image of a 2-cell embryo labelled with rabbit anti-DDX1 antibody followed by anti-rabbit 10 nm nanogold particles. A DDX1 aggregate consisting of several DDX1 vesicles is shown in the square magnified on the right. Scale bar = 0.5 μm. (B) TEM image of a 2-cell embryo stained with OsO_4/uranyl acetate. Arrows point to a subset of DDX1 vesicles within a DDX1 aggregate. Regions containing RNA are indicated by arrowheads. Scale bar = 1 μm. Magnified image scale bar = 0.5 μm. Mt: mitochondria.

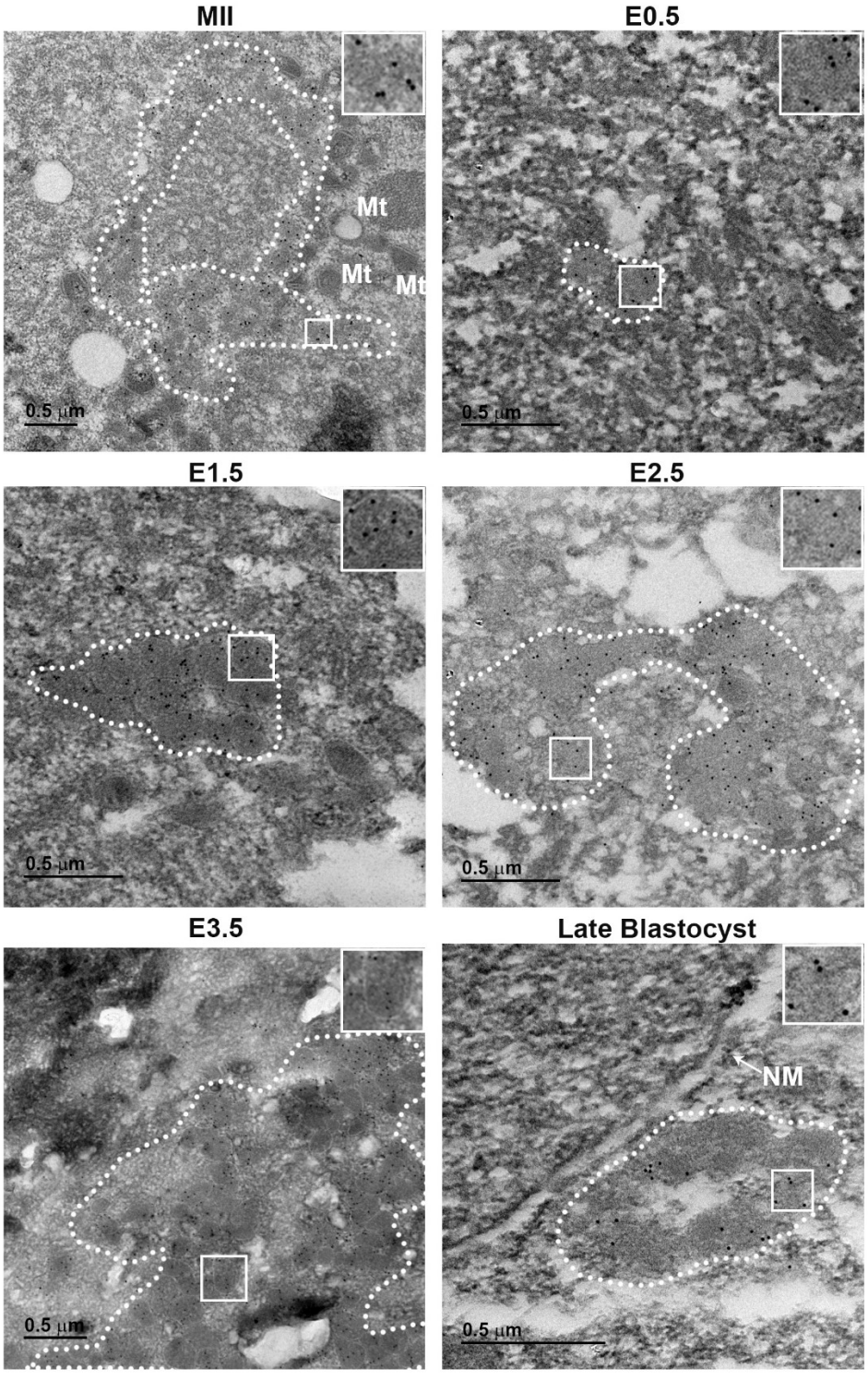
MII
Mt
Mt
Mt
0.5 μm
E0.5
0.5 μm
E1.5
0.5 μm
E2.5
0.5 μm
E3.5
0.5 μm
Late Blastocyst
NM
0.5 μm

Figure 3.7 TEM images of DDX1 vesicles in MII oocytes and embryos at different stages. Oocytes and embryos were fixed in 4% paraformaldehyde for 1 h and labelled with unconjugated anti-DDX1 antibody followed by 10 nm goat anti-rabbit gold nanoparticles. Membrane bound DDX1-containing vesicles were first visualized in 1-cell embryos, but could no longer be identified at the blastocyst stage when aggregates of DDX1 were observed surrounding the nucleus. DDX1 aggregates (MII stage and blastocyst) and MARVs (E0.5 to E3.5) are indicated by the dotted lines. The square in each panel is magnified in the right-hand corner. The images were acquired with a JEOL JEM-2100 TEM at 200 kV. NM: Nuclear membrane. Mt: Mitochondria. Scale bar = 0.5 μm.

DDX1 is a member of the DEAD box family of RNA binding/unwinding/restructuring proteins (Godbout and Squire 1993). We have previously shown that digestion of 2-cell embryos with RNase A causes disaggregation of DDX1 (Hildebrandt, Wang et al. 2019). To visualize where the RNA is located in DDX1 vesicles, we used electron microscopy and OsO_4/uranyl acetate staining which stabilizes nucleic acids and increases electron density. We observed intense staining in a distinct patch within each vesicle **(Fig. 3.6B)** (Brodie, Huie et al. 1982). We next used energy-filtered transmission electron microscopy (EFTEM) for elemental mapping of nitrogen (indicative of proteins) and phosphate (indicative of nucleic acids) in 2-cell embryos (Longo, Twesten et al. 2014). Similar to what was observed with OsO_4/uranyl acetate staining, phosphate was enriched in a small compartment within each vesicle of each DDX1 aggregate **(Fig. 3.8)**.

Combined with our previous RNase A data, these results suggest that RNA occupies a distinct compartment within each vesicle, suggesting a requirement for compaction, organization and/or localization of RNAs at these sites. To our knowledge, compartmentalized RNA-containing membrane–bound vesicles have not been described previously, we named these vesicles Membrane Associated RNA-containing Vesicles (MARVs) **(Fig. 3.9)**.

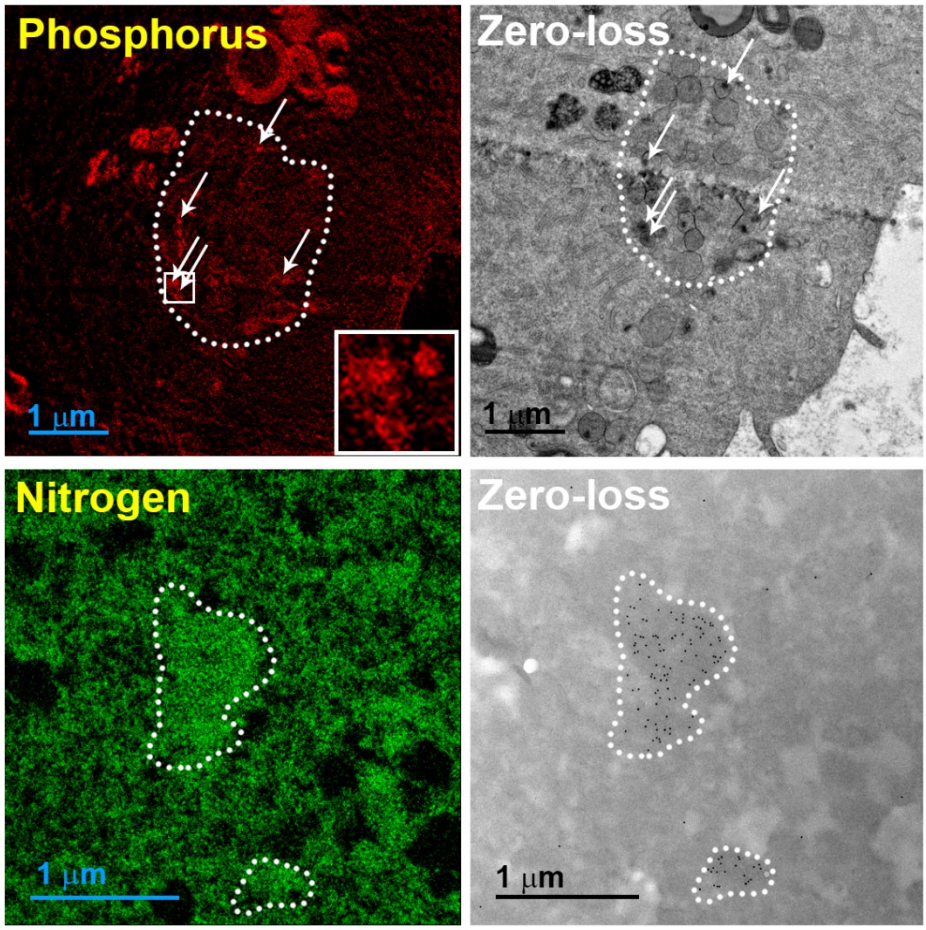

Figure 3.8 DDX1 aggregates contain nucleic acid and protein. For phosphorus, 2-cell embryos were fixed and stained with OsO_4. For nitrogen, 2-cell embryos were fixed and DDX1 immunogold-labelled (without OsO_4 or uranyl acetate staining) for better contrast. Zero-loss images are also shown. DDX1 aggregates are circled with dotted lines.

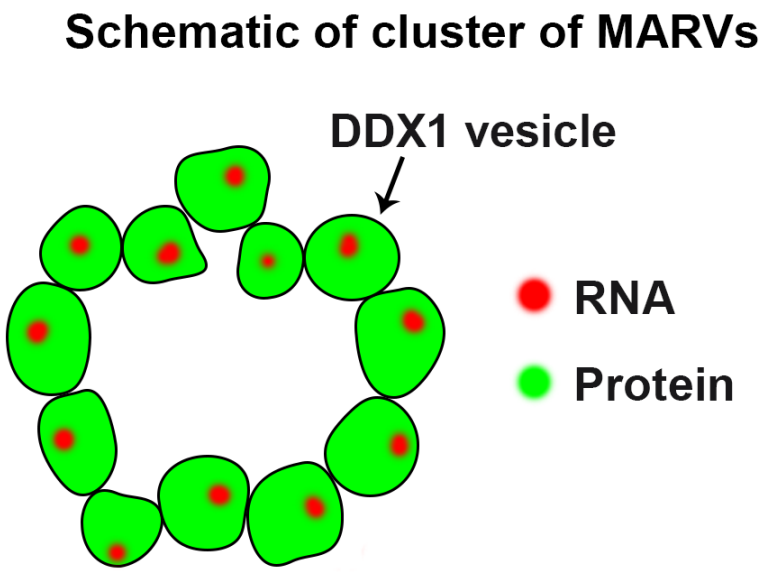

Figure 3.9 Graphical demonstration of MARVs. Graphical demonstration of a cluster of MARVs.

3.3.2 Aggregates of DDX1 vesicles show no association with mitochondrial translation

Embryos undergoing rapid cell division require a continuous supply of energy. The total number of mitochondria per embryo remains unchanged from the 1-cell to early blastocyst stages, with numbers of mitochondria halved at each cell division, suggesting a need for increased mitochondrial function to compensate for their reduced numbers (Piko and Matsumoto 1976, Piko and

Taylor 1987). Our immunofluorescence (IF) data and TEM data indicate that DDX1 vesicles are located at the subplasmalemmal cytoplasm where mitochondria with high $\Delta\Psi_m$ are located. It is generally accepted that mitochondria with high membrane potential produce elevated levels of ATP. We therefore asked whether RNA in MARVs might be specifically required for translation of proteins for mitochondrial function. We co-immunostained 2-cell embryos with anti-DDX1 antibody and antibodies to cytoplasmic ribosomal protein (RPS6), or mitoribosomal proteins MRP-L42, MRP-L44 or MRP-S27. DDX1 did not co-localize with any of these proteins (**Figs. 3.10 and 3.11**). Notably, RPS6 does not show staining in the nucleolus, the site of ribosome biogenesis. This could be due to the highly condensed nature of the nucleoli at this developmental stage. Next, we treated 1-cell embryos in culture with cycloheximide for 8 h, a global inhibitor of protein synthesis. STED microscopy revealed decreased DDX1 aggregates (**Fig. 3.12**). Thus, clustering of MARVs may be dependent on active translation. Conversely, treatment with chloramphenicol, an inhibitor of mitochondrial translation, for 8 h did not affect the abundance of DDX1 within DDX1 aggregates in 1-cell embryos, suggesting a potential link between MARVs and cytoplasmic, rather than mitochondrial, protein translation **(Fig. 3.12)**.

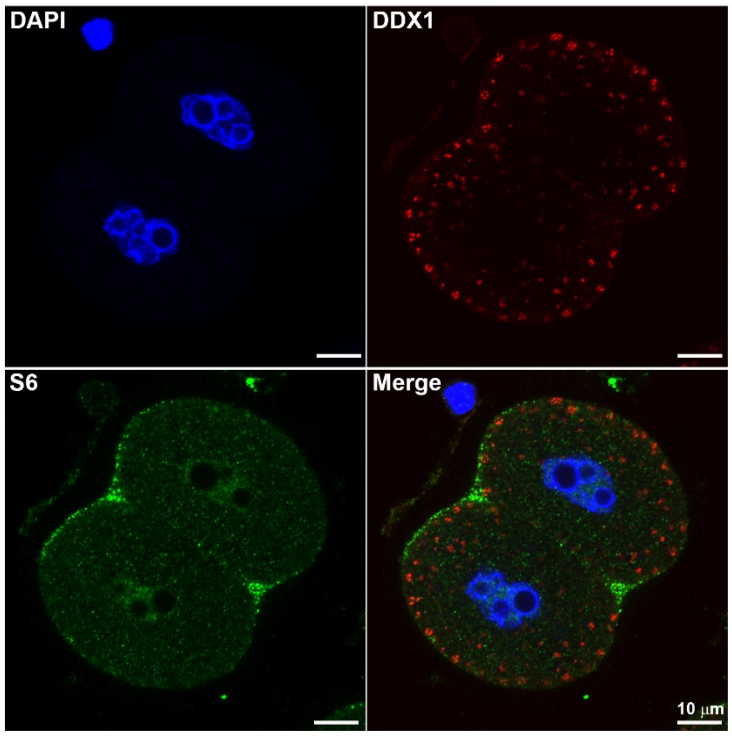

Figure 3.10 DDX1 does not co-immunostain with cytoplasmic ribosomal protein RPS6. Two-cell embryos were co-immunostained with antibodies to DDX1 and ribosomal protein RPS6. RPS6 did not co-localize with DDX1 in 2-cell embryos. Embryos were imaged using a Zeiss LSM710 confocal microscopy and a 40X lens. Scale bar = 10 μm.

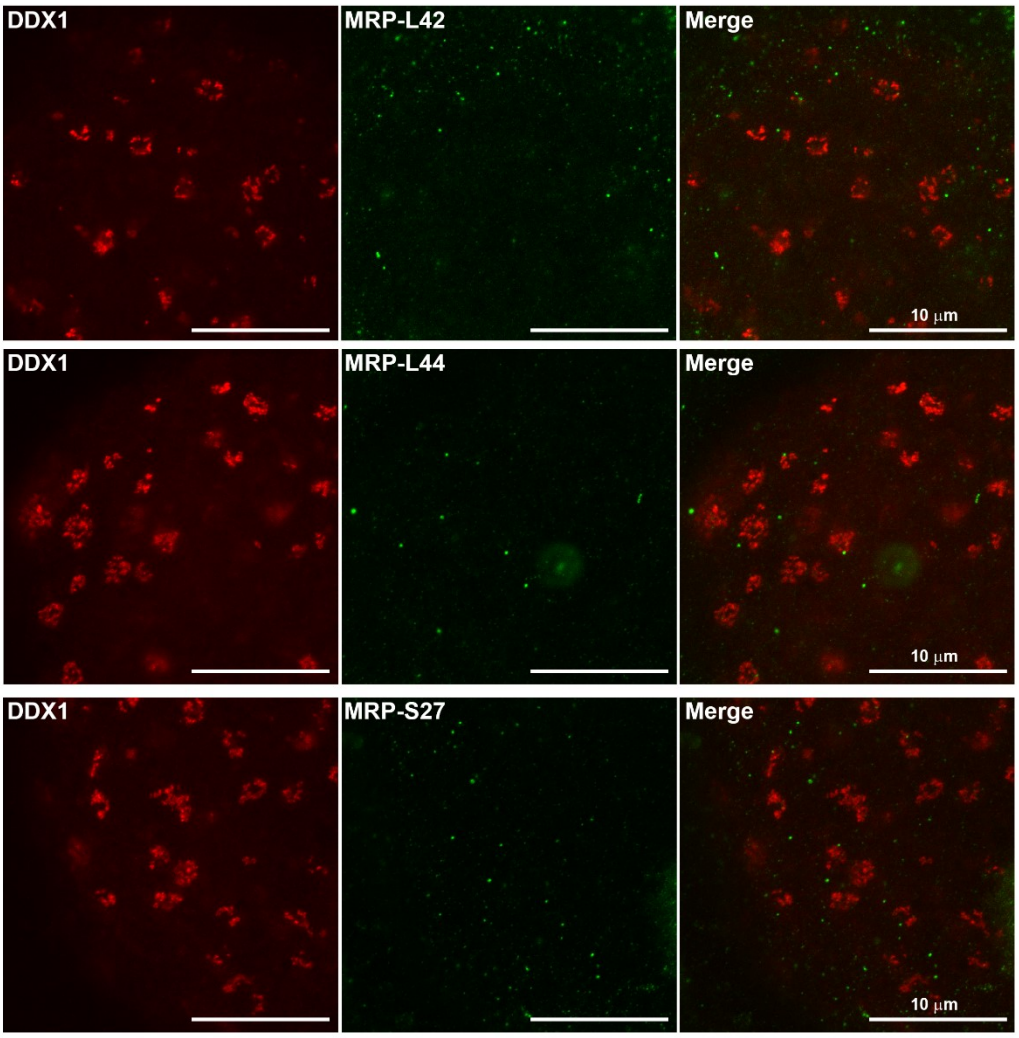

Figure 3.11 DDX1 does not co-localize with mitochondrial ribosomal proteins. 2-cell stage embryos were fixed in 4% paraformaldehyde and co-immunostained with Atto 550-conjugated anti-DDX1 antibody and antibodies targeting mitochondrial ribosomal protein MRP-L42, MRP-L44 or MRP-S27, followed donkey anti-mouse Alexa 647 secondary antibody for mitochondrial ribosomal proteins. Scale bar = 10 μm.

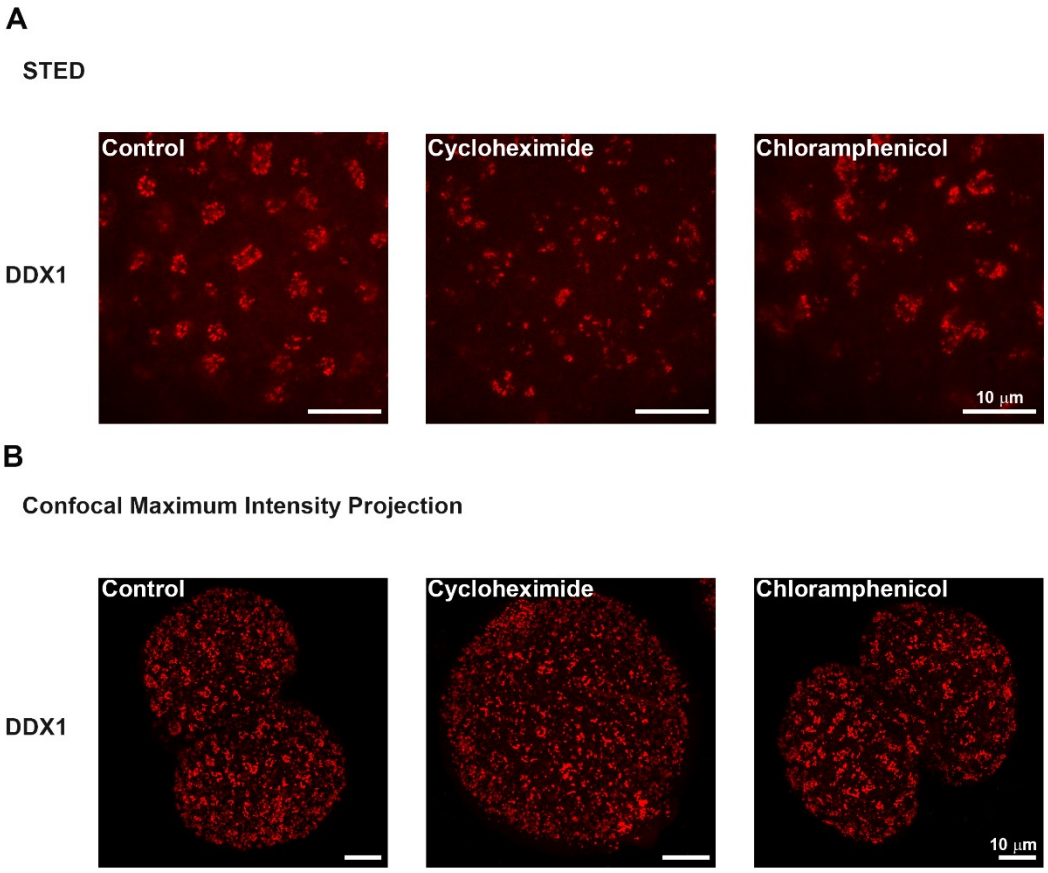

Figure 3.12 MARVs are disrupted when embryos are treated with cycloheximide but not chloramphenicol. (A) E0.5 embryos were cultured for 8 h in 150 μg/ml cycloheximide or 200 μg/ml chloramphenicol. The embryos were then fixed in 4% paraformaldehyde and immunostained with anti-DDX1 antibody. Images shown are single section images acquired with a Leica SP8 STED microscope. DDX1 ring-like structures are disrupted when embryos are treated with cycloheximide, with no obvious effect observed when embryos are treated with chloramphenicol. (B) Z-stack images of embryos treated with cycloheximide and chloramphenicol for 8 h are shown in maximum intensity projection. Note that embryos treated with cycloheximide did not progress to the 2-cell stage. Images

were acquired with a Leica SP8 confocal microscope with a 100X lens. Scale bar = 10 μm.

3.3.3 Ca^{2+} signal co-localizes with DDX1 vesicles

Ca^{2+} signaling triggers the events required for embryonic development after fertilization including regulation of mRNA translation (Miao and Williams 2012). Mitochondria located along with the endoplasmic reticulum control Ca^{2+} release upon fertilization (Miao and Williams 2012). We used the calcium indicator Fluo-4 AM to study the distribution of Ca^{2+} in 2-cell embryos in relation to that of mitochondria and DDX1 aggregates. As previously reported, Ca^{2+} was particularly abundant in subplasmalemmal cytoplasm, with a similar distribution pattern to that of DDX1 aggregates **(Fig. 3.13)** (Manser and Houghton 2006). Next, we investigated the relationship between Ca^{2+} aggregates and mitochondria using Fluo-4 AM and MitoTracker Deep Red (Giorgi, Marchi et al. 2018). We observed Ca^{2+} aggregates next to mitochondria located at the subplasmalemmal cytoplasm **(Fig. 3.14)**. As predicted based on these results, co-localization was observed when 2-cell embryos were co-stained with anti-DDX1 antibody and Fluo-4 AM (**Fig. 3.15**). Although our ER pattern is similar with previously reported by other researches (Watanabe, Thayil et al. 2010, Zhang, Qian et al. 2013), Fluo-4 AM did not co-localize with ER-Tracker in 2-cell embryos, indicating that Ca^{2+}/DDX1-

containing vesicles are unlikely to be ER, the reported location of Ca^{2+} in oocytes (**Fig. 3.16**) (Kline, Mehlmann et al. 1999). Our combined results are thus in line with Ca^{2+}/DDX1-containing vesicles serving as reservoirs for rapid mobilization of Ca^{2+} and RNAs required for early embryonic development.

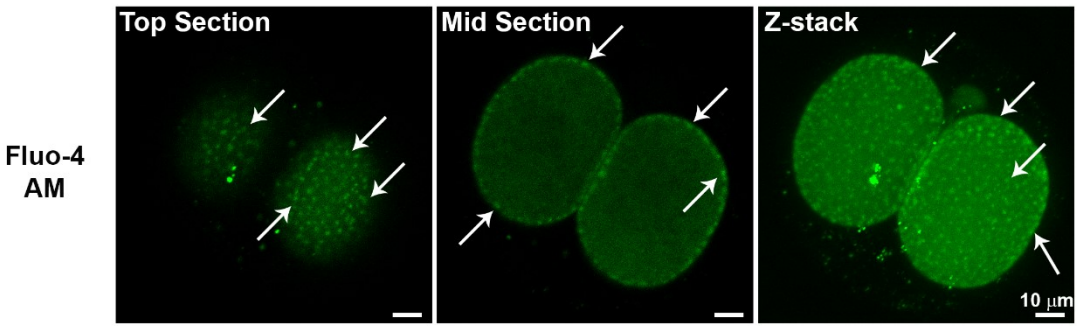

Figure 3.13 Ca^{2+} microdomains are located at the subplasmalemmal cytoplasm in 2-cell embryos. 2-cell embryos were incubated in M16 medium containing 5 μM Fluo-4 AM for 1 h and destained for 30 min. Images were acquired with a Zeiss LSM 710 confocal microscope using a 20X lens. Single section images and maximum intensity projection of Z-stack images are shown. Scale bar = 10 μm. Arrows are pointing to a subset of Ca^{2+} microdomains.

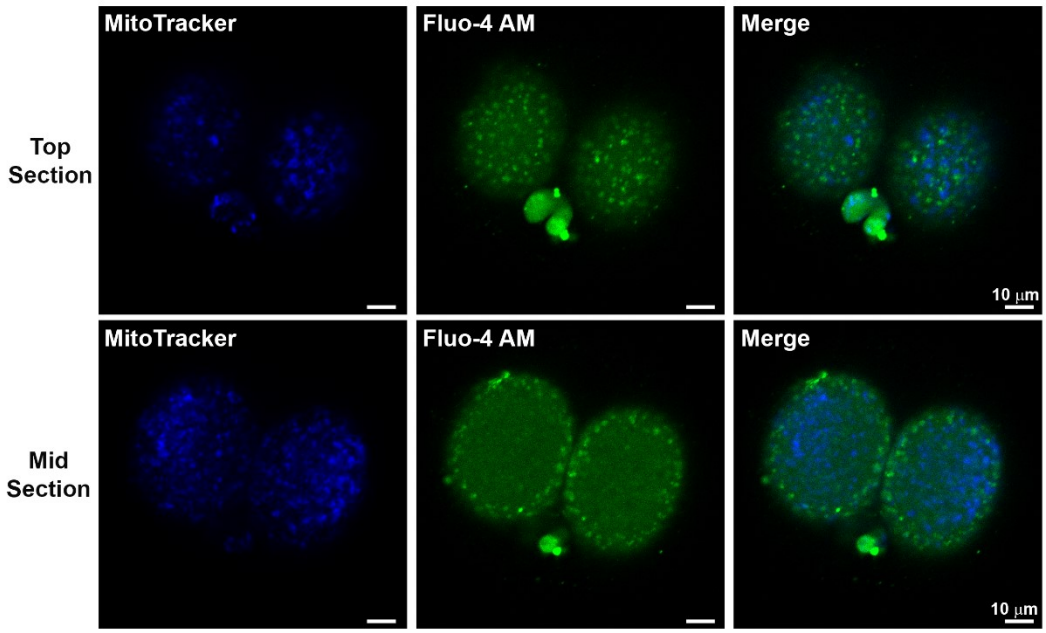

Figure 3.14 Ca^{2+} microdomains (Fluo-4, green) do not co-localize with MitoTracker Deep Red (Blue). 2-cell embryos were incubated with M16 medium containing 100 nM MitoTracker Deep Red for 30 min followed by M16 medium containing 5 µM Fluo-4 AM for 1 h. The embryos were then destained for 30 min and imaged using a Zeiss LSM 710 confocal microscope and a 20X lens. Top section (closest to the coverslip) and mid sections are shown. Scale bar = 10 µm.

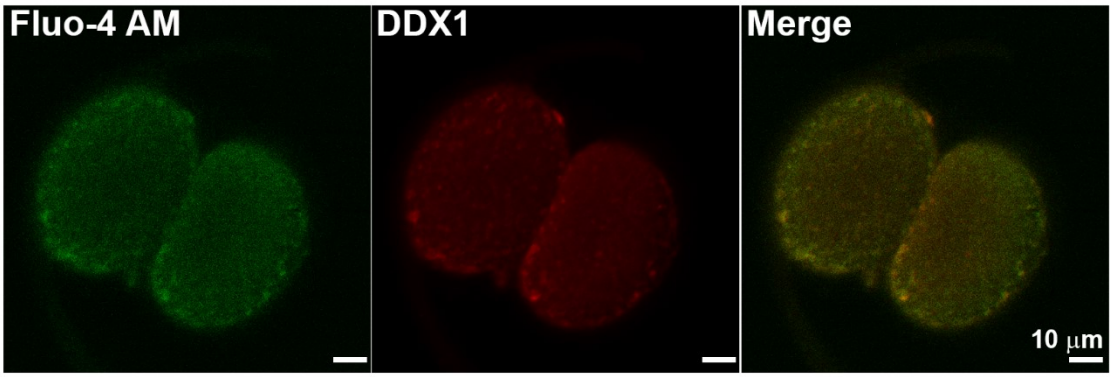

Figure 3.15 Co-localization of Ca^{2+} and DDX1 in MARVs. 2-cell embryos were first stained with Fluo-4 AM for 1 h and destained for 30 min. The embryos were immediately fixed with methanol-acetone (1:1) and immunostained with Atto 550-conjugated anti-DDX1 antibody. Embryos were imaged with a Zeiss LSM 710 confocal microscope using 20X objective lens. Scale bar = 10 μm.

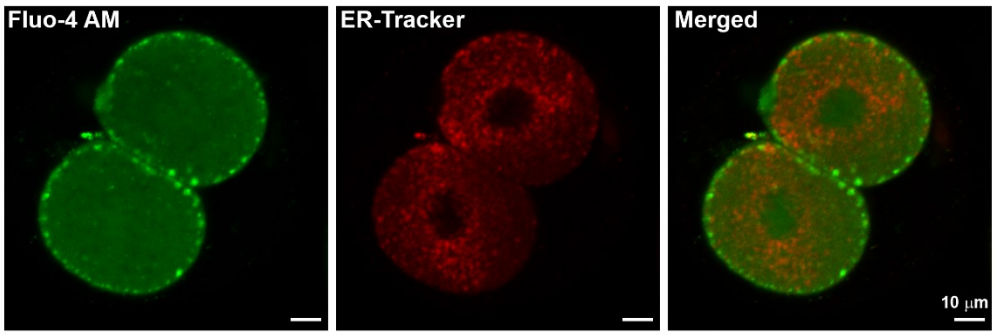

Figure 3.16 Calcium microdomains (Fluo-4, green) do not co-localize with ER (ER-tracker, red). 2-cell embryos were incubated with M16 medium containing 5 μM Fluo-4 AM for 30 min and transferred to M16 medium containing 200 nM ER-Tracker. Scale bar = 10 μm.

3.3.4 Ca^{2+} relocates to mitochondria when embryos are treated with saponin

To further understand the link between MARVs and Ca^{2+} release during embryonic development, we treated 2-cell embryos with 0.1% saponin, a mild detergent used for live cell permeabilization (Hildebrandt, Wang et al. 2019). Saponin permeabilizes plasma membrane as well as organelle membranes (Bangham, Horne et al. 1962). Staining of saponin-permeabilized embryos with Fluo-4 AM showed disruption of Ca^{2+} subplasmalemmal microdomains, with Ca^{2+} moving to the inner cytoplasm **(Fig. 3.17A)**. Upon co-staining with Fluo-4 AM and MitoTracker Deep Red, we found co-localization of Fluo-4 AM and MitoTracker Deep Red, indicating that Ca^{2+} had migrated to inner cytoplasm mitochondria upon saponin permeabilization **(Figs. 3.17A, B)**. As the vesicle membrane seemed to be intact and DDX1 was still present in the vesicles of saponin-permeabilized embryos based on immunogold-labeling TEM, it appears that Ca^{2+} may have leaked out of these vesicles upon saponin treatment to be taken up by mitochondria **(Fig. 3.18)**.

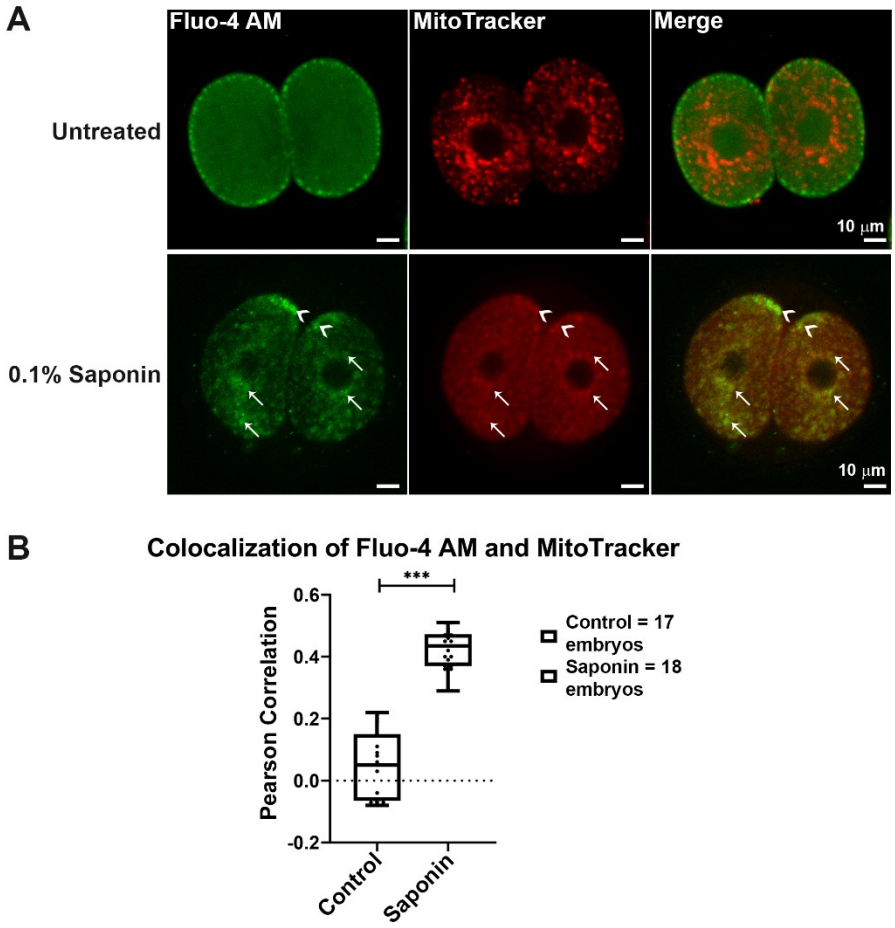

Figure 3.17 Redistribution of Ca^{2+} to mitochondria upon saponin treatment. (A) Embryos were treated with 5 μM Fluo-4 AM as described above, then transferred to M16 medium containing 100 nM MitoTracker Deep Red for 30 min. Embryos were then incubated in M16 medium (control) or M16 medium containing 0.1% saponin for 6 min and imaged. Arrows and arrowheads point to Fluo-4 AM and Mitotracker co-localization at the inner and subplasmalemmal cytoplasm, respectively. Scale bar = 10 μm. (B) 2-cell embryos obtained from three pairs of wildtype natural-matings were cultured in M16 medium containing 5 μM Fluo-4 AM

for 30 min and transferred to M16 medium containing 100 nM MitoTracker Deep Red. Mid-stacks of each embryo were imaged and Coloc2 ImageJ plugin was used to calculate Pearson Correlation. Data were plotted with Prism. *** indicates P < 0.001.

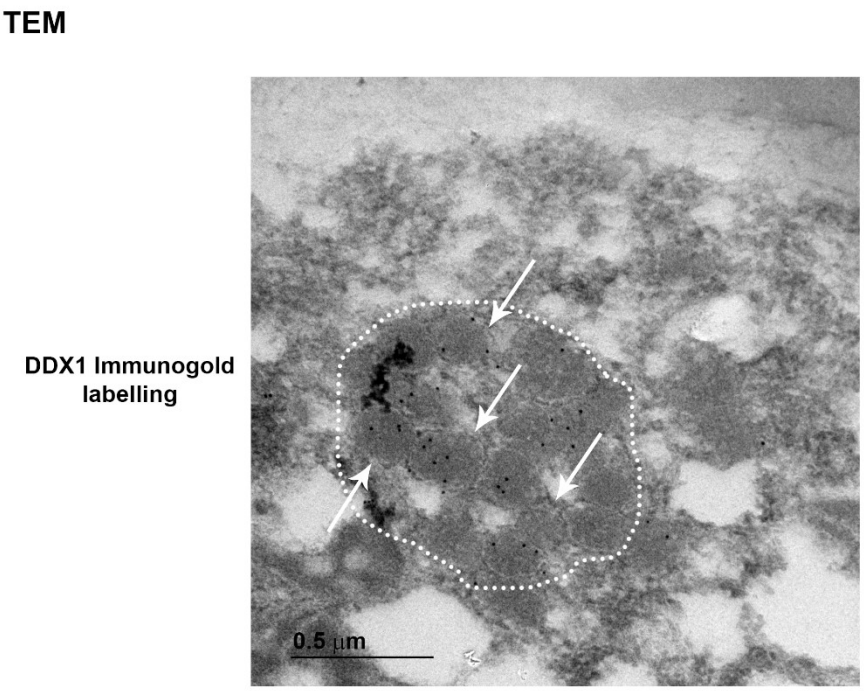

Figure 3.18 DDX1 remains in MARVs after 0.1% saponin treatment. 2-cell embryos were treated with 0.1% saponin for 6 min, then fixed in 4% paraformaldehyde for 1 h. The embryos were labelled with unconjugated anti-DDX1 antibody followed by 10 nm goat anti-rabbit gold nanoparticles. The images were acquired with a JEOL JEM-2100 TEM at 200 kV. Arrows point to MARVs. An aggregate of MARVs is circled by the dotted line. Scale bar = 0.5 µm.

3.3.5 Ddx1$^{-/-}$ embryos have elevated mitochondrial $\Delta\Psi_m$ and mtROS with absence of Ca^{2+} microdomains at the subplasmalemmal cytoplasm

The above results point to MARVs playing a role in the spatial distribution of Ca^{2+} in 2-cell embryos. We have previously shown that *Ddx1*$^{-/-}$ embryos stall at 2- to 4-cell stages with nuclear fragmentation *in vitro* (Hildebrandt, Wang et al. 2019). However, the mechanism behind this embryonic arrest is still unknown. We therefore cultured 1-cell embryos from *Ddx1*$^{+/-}$ intercrosses to address the effect of DDX1 knockdown on Ca^{2+} distribution and mitochondria. Analysis of 14 pairs of *Ddx1*$^{+/-}$ intercrosses revealed the expected ~25% (25/98) stalled embryos (presumably *Ddx1*$^{-/-}$) at the 2- to 4-cell stages after 72 h (Hildebrandt, Wang et al. 2019)**.** Stalled embryos were used for the following analyses: Fluo-4 AM and mitochondria fragmentation (5 embryos), JC-1 (13 embryos), and MitoSOX (7 embryos). Wild-type 2-cell embryos and cultured embryos that had proceeded to the compaction stage after 72 h were used for comparison. We found little evidence of subplasmalemmal cytoplasmic Ca^{2+} microdomains in stalled embryos compared to wild-type embryos **(Fig. 3.19)**. Intriguingly, staining with JC-1 revealed higher mitochondrial membrane potential in stalled embryos compared to wild-type 2-cell or compacted embryos **(Fig. 3.20A, B)**, with stalled embryos showing both mitochondria and nuclei fragmentation **(Fig. 3.21A, B)**. Using MitoSOX, we found increased levels of mtROS in stalled embryos **(Fig. 3.22A, B)**.

We next immunostained embryos with anti-TIA-1 antibody as a DDX1 surrogate marker for MARV aggregates (Hildebrandt, Wang et al. 2019). Few aggregates were observed in *Ddx1*$^{-/-}$ embryos, with TIA-1 co-localizing with residual DDX1 **(Fig. 3.23)**. The presence of high potential mitochondria as well as high levels of mtROS in stalled embryos suggests that these embryos are still metabolically active. These results suggest that a key role for DDX1 in early embryonic development may involve the formation/retention of vesicles which control Ca^{2+} distribution in early embryos.

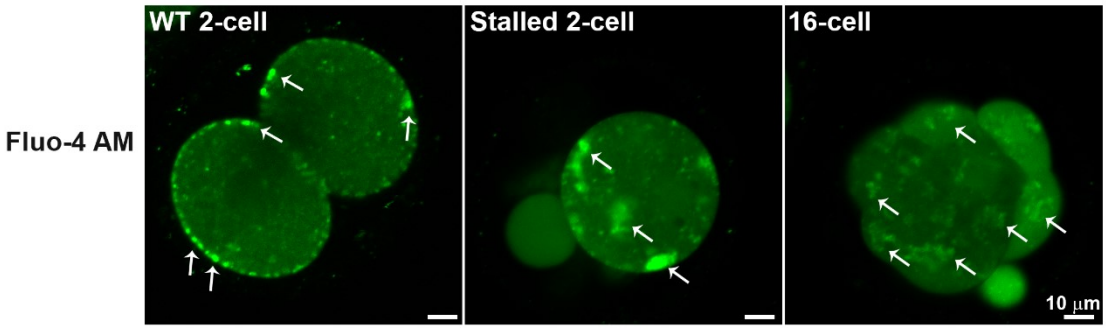

Figure 3.19 Loss of *Ddx1* disrupts calcium distribution. 1-cell embryos were cultured for 72 h. Embryos were then incubated in M16 medium containing 5 μM Fluo-4 AM for 30 min and destained in regular M16 medium for 30 min. Arrows point to Ca^{2+} distribution in different stage embryos. Scale bar = 10 μm.

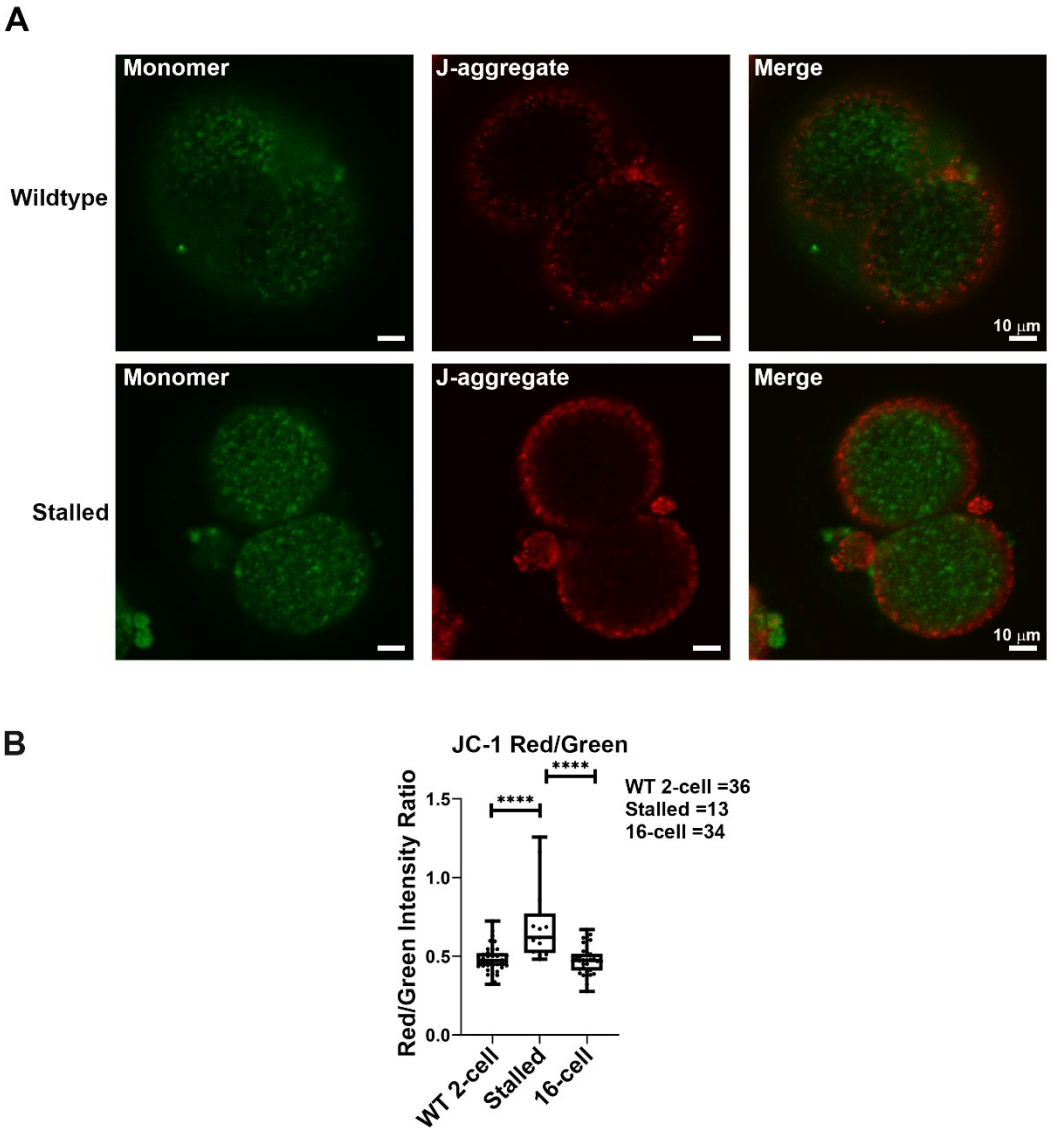

Figure 3.20 Loss of Ddx1 leads to increased mitochondrial membrane potential. (A) Stalled embryos were incubated in M16 medium containing 10 μg/ml JC-1 for 30 min. Embryos were then washed 3X in prewarmed M16 medium and transferred to ultrathin bottom 96-well plates for imaging using a Zeiss LSM710 microscope and 20X lens. Wildtype 2-cell embryos were used as controls. Stalled embryos had a stronger J-aggregate signal compared to wildtype embryos

indicating that the mitochondrial membrane potential is higher in stalled embryos. Scale bar = 10 μm. (B) 1-cell embryos from four pairs of heterozygous natural matings were cultured for 72 h in M16 medium supplemented with 10 μg/ml JC-1 for 30 min. Z-stacks were used for fluorescence intensity calculations. Wildtype 2-cell embryos were used for comparison. Mean intensity values were plotted with Prism. **** indicates $P < 0.0001$.

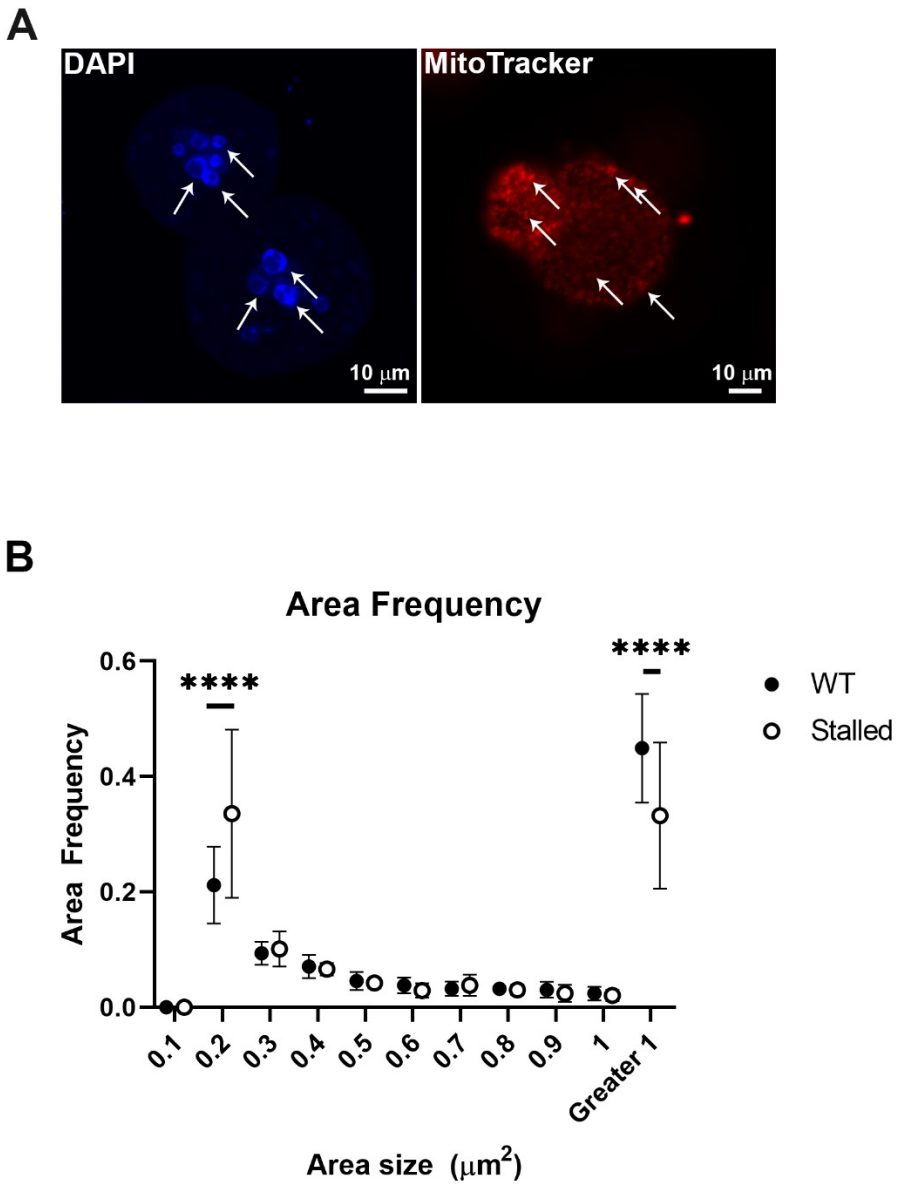

Figure 3.21 Nuclear and mitochondrial fragmentation in stalled embryos. (A) Stalled embryos were either fixed in 4% paraformaldehyde and stained with DAPI (left panel) or incubated in M16 medium containing 100 nM MitoTracker for 30 min (right panel). Scale bar = 10 μm. Arrows point to fragmented nuclei as well as fragmented mitochondria. (B) E0.5 embryos from three pairs of heterozygous

natural matings were cultured for 72 h in a 37°C incubator, followed by 30 min in M16 medium containing 100 nM MitoTracker Deep Red. Mid-stack sections of each embryo were imaged using a confocal microscope, and ImageJ Particle Analysis was used to summarize numbers of areas within a certain range of area size (μm^2). The reduced size of MitoTracker Deep Red aggregates suggests fragmentation of mitochondria. Wildtype 2-cell embryos were used as controls. Data were plotted with Prism. **** indicates P < 0.0001.

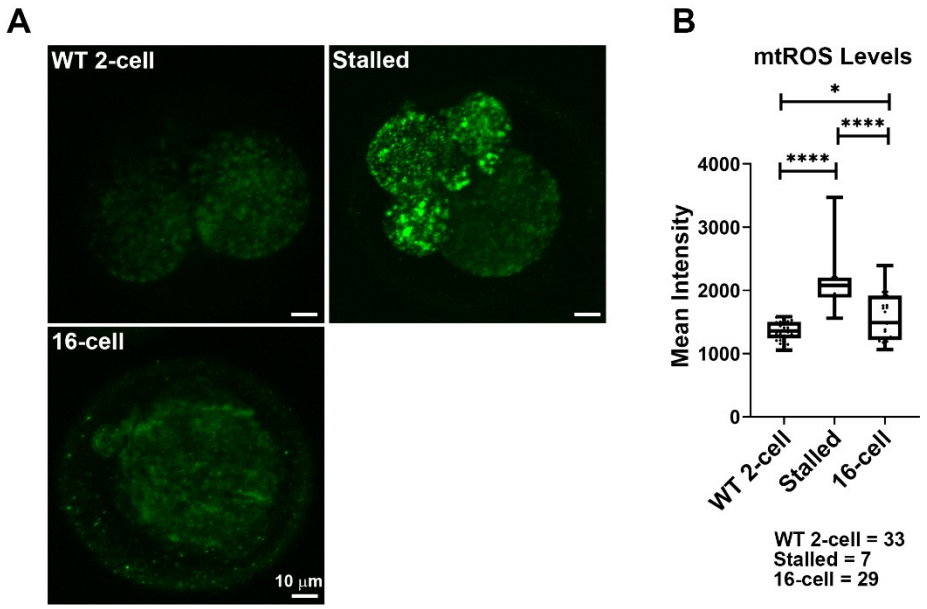

Figure 3.22 Loss of Ddx1 leads to increased mitochondrial ROS. (A) Same as Figure 3.20 except that embryos were cultured in medium supplemented with 2 μM MitoSOX for 30 min. (B) Data obtained from (A) were plotted with Prism. **** indicates P < 0.0001, * indicates P < 0.05.

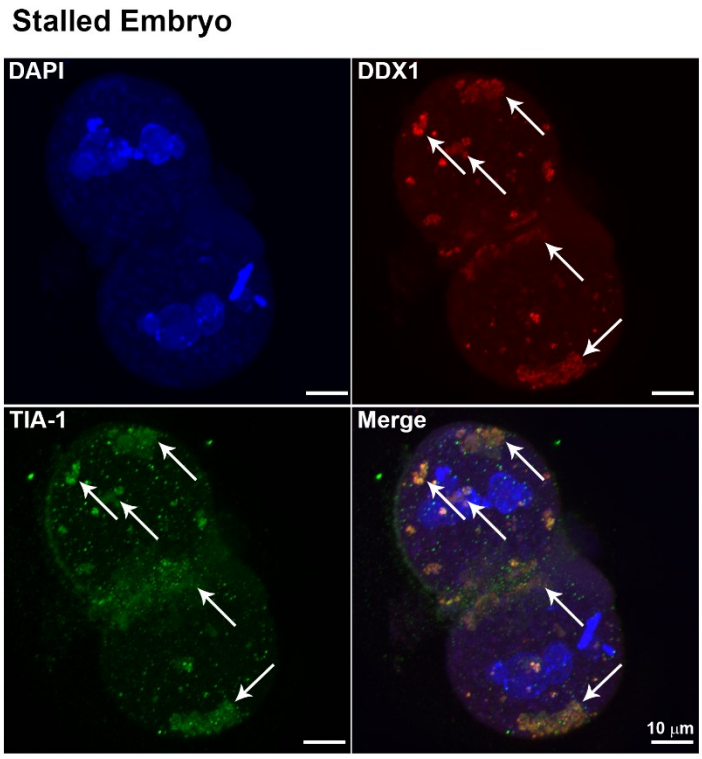

Figure 3.23 TIA-1 co-localizes with residual DDX1 signal. Stalled embryos were fixed in 4% paraformaldehyde and immunostained with DDX1 and TIA-1 antibodies. Nuclei were labelled with DAPI. Both the TIA-1 and DDX1 signals are reduced in stalled embryos with TIA-1 co-localizing with residual DDX1. Embryos were imaged using a Zeiss LSM710 microscope and 40X lens. Scale bar = 10 μm. Arrows point DDX1 and TIA-1 co-localization.

3.3.6 Cytoplasmic polyadenylation factors localized in MARVs

Maternal RNAs are critical for development of the fertilized egg, with dormant mRNAs in oocytes characterized by short poly(A) tails (Winata and Korzh 2018). The cytoplasmic polyadenylation element binding proteins (CPEB) and cleavage and polyadenylation specificity factors (CPSF) are required for cytoplasmic polyadenylation in mouse oogenesis (Hodgman, Tay et al. 2001, Winata and Korzh 2018). Ca^{2+} has long been known to activate CPEB1 through the phosphorylation of CAMKII in mouse neuronal cells (Atkins, Nozaki et al. 2004). Given the essential function of CPEB1 and Ca^{2+} in early embryonic development (Paillard, Maniey et al. 2000, Jones 2005, Jones 2007, Vishnu, Sumaroka et al. 2011), it's very likely that Ca^{2+} may also play a role in the activation of CPEB1 in embryos.

DDX1 has previously been associated with RNA processing in mammalian cell lines, with DDX1 shown to interact with polyadenylation factor CstF64 and co-localizing with both CstF64 and CPSF2 (Bleoo, Sun et al. 2001, Li, Roy et al. 2006). In light of our previous work showing that DDX1 binds to a subset of RNAs essential for embryonic development, we further investigated the localization of the cytoplasmic polyadenylation factors CPSF2 and CPEB1 in 2-cell embryos. In addition to their expected nuclear localization, both CPSF2 and CPEB1 co-localized with DDX1 in the cytoplasm of 2-cell embryos **(Fig. 3.24A and B)**. Although CPSF2 and DDX1 appear to have higher Pearson's correlation coefficients compared to CPEB1 and DDX1, the difference is not statistically

significant. The appearance of a stronger correlation between CPSF2 and DDX1 may be due to the relatively lower expression levels of CPEB1 compared to CPSF2. Co-localization of CPSF2 and CPEB1 with DDX1 supports the possibility that MARVs function as sites of cytoplasmic polyadenylation after fertilization.

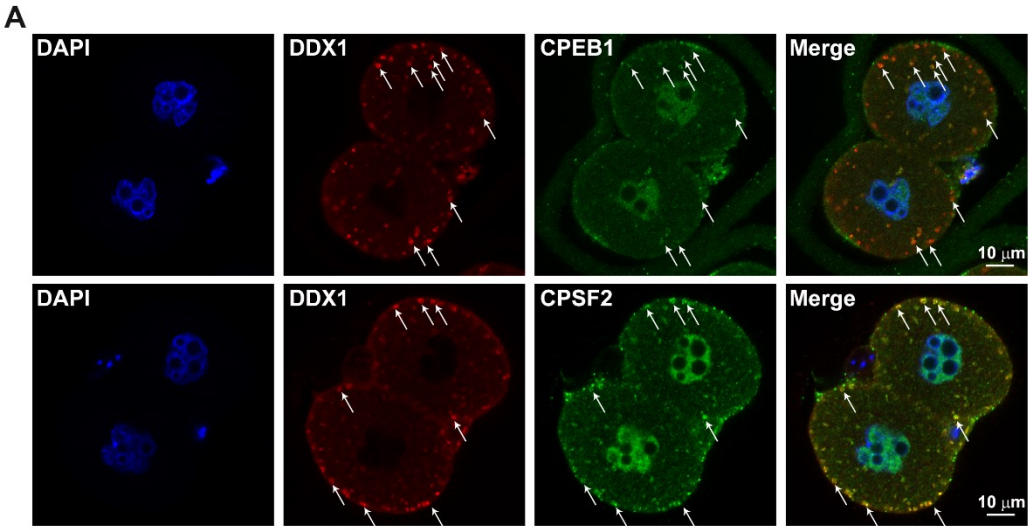

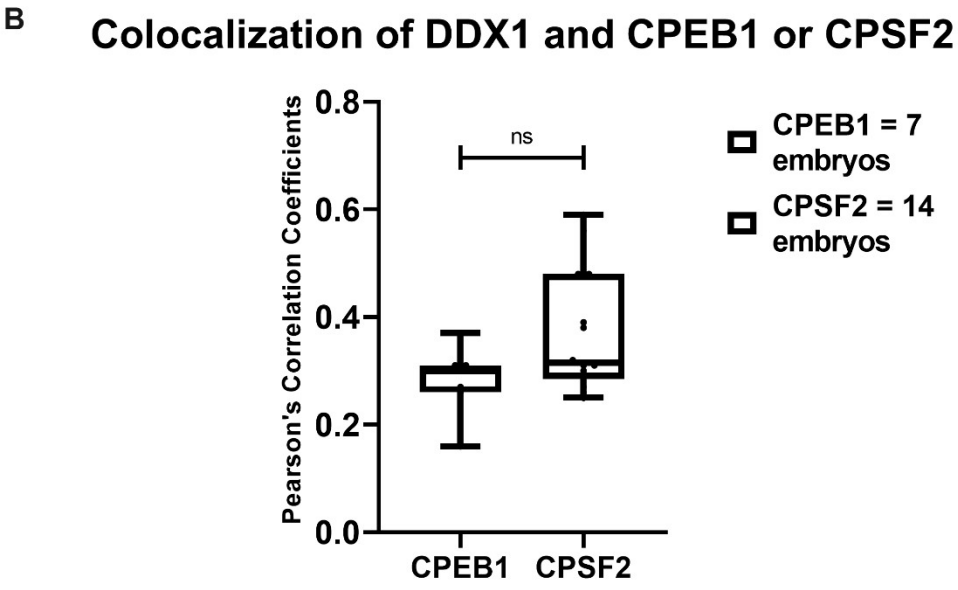

Figure 3.24 CPEB1 and CPSF2 localize with DDX1 in MARVs. 2-cell embryos were fixed in 4% paraformaldehyde and immunostained with DDX1 and CPEB1 or CPSF2 antibodies. Nuclei were labelled with DAPI. Both CPEB1 and CPSF2 co-localize with DDX1. (A) Embryos were imaged using a Zeiss LSM710 microscope and 40X lens. Scale bar = 10 μm. Arrows point a subset of co-localizing signals. (B) Images from (A) were used to calculate Pearson Correlation with Coloc2 ImageJ plugin. Data were plotted with Prism. ns indicates $P > 0.05$.

3.4 Discussion

We have previously reported that DDX1 forms large cytoplasmic aggregates in early-stage mouse embryos, with loss of *Ddx1* resulting in embryonic arrest at the 2- to 4-cell stages (Hildebrandt, Wang et al. 2019). In this paper, we show that 84.2% ± 3.2% of DDX1 localizes to membrane bound vesicles (200-400 nm in size) which we have named Membrane Associated RNA-containing Vesicles (MARVs). MARVs are preferentially located at subplasmalemmal cytoplasm, and contain Ca^{2+}, RNA and cytoplasmic polyadenylation factors. Loss of *Ddx1* in early-stage mouse embryos is associated with a large decrease in the number of MARVs, which accompanying increased mitochondria membrane potential and ROS formation, and increased nuclear and mitochondrial fragmentation **(Figure 3.25)**. We propose that the role of MARVs is to regulate cytoplasmic polyadenylation of RNAs needed for controlled translation in a mitochondrial dependent manner in early-stage embryos.

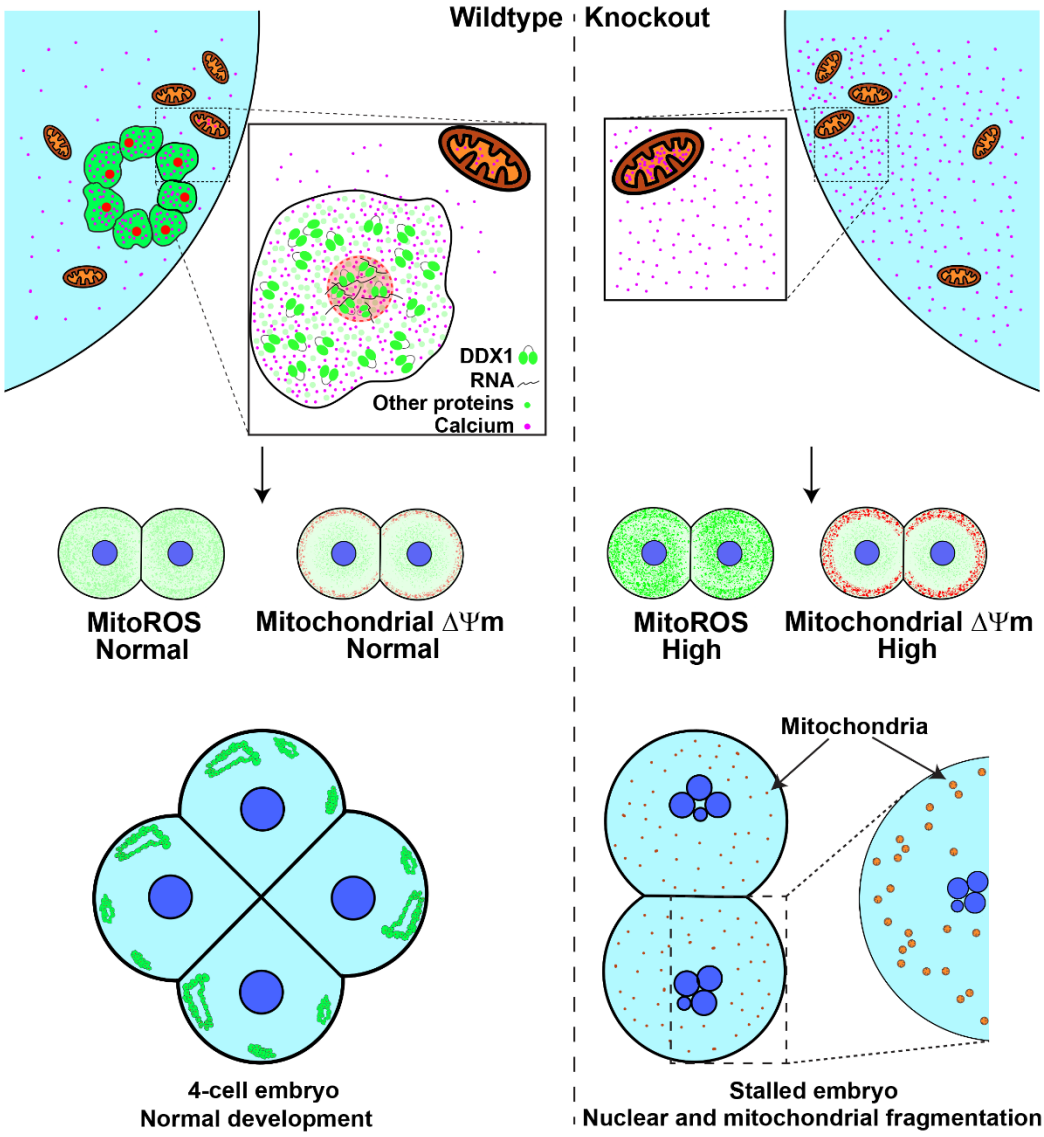

Figure 3.25 Schematic depiction of DDX1 and MARV function. Wildtype embryos develop normally when MARVs are present. However, absence of MARVs in DDX1 knockout embryos results in disrupted Ca^{2+} distribution which causes upregulation of mitochondrial activity and increased mitochondrial ROS, leading to nuclear and mitochondrial fragmentation.

A large number of cytoplasmic RNA-containing bodies have been described in oocytes and embryos, including P granules, Balbiani bodies, polar granules, germinal granules and subcortical aggregates (Kloc, Bilinski et al. 2001, Kobayashi, Sato et al. 2005, Flemr, Ma et al. 2010, Parker, Winkenbach et al. 2020). In contrast to the more classically known membrane-bound organelles such as ER, mitochondria and lysosomes, these cytoplasmic bodies are not delineated by a membrane but are compartmentalized as the result of liquid-liquid phase separation (Brangwynne, Eckmann et al. 2009, Buchan 2014). A distinguishing feature of membrane-bound organelles (in particular mitochondria, ER and lysosomes) is that they can serve as storage and controlled release sites for intracellular Ca^{2+} (Kline, Mehlmann et al. 1999, Hoppe 2010, Patergnani, Suski et al. 2011, Raffaello, Mammucari et al. 2016). Our imaging data indicate that MARVs are the main site for Ca^{2+} storage in 2-cell mouse embryos. When the membranes of early-stage embryos were permeabilized with 0.1% saponin, we observed extensive disruption of intracellular Ca^{2+} distribution, underlining the importance of membranes in the retention of Ca^{2+} within MARVs. Ca^{2+} regulation has mostly been studied in the context of the fertilization process when Ca^{2+} oscillations are required for oocyte activation. (Wakai, Zhang et al. 2013). Little is known about Ca^{2+} function in the pre-compaction stage of embryonic development. In 2-cell mouse embryos, Ca^{2+} has been shown to form microdomains/speckles at the subplasmalemmal cytoplasm (Manser and Houghton 2006, Nagaraj, Sharpley et al. 2017). These Ca^{2+} microdomains did not co-localize with either caveolae or

cortical granules. Manser and Houghton concluded that Ca^{2+} microdomains may affect nitric oxide production, leading to mitochondrial-related apoptosis. Our results indicating that Ca^{2+} co-compartmentalizes with DDX1 in membrane-bound vesicles is thus in keeping with the need to control Ca^{2+} distribution in early-stage embryos. In this regard, it is important to note that MARVs do not exist in oocytes, but are first observed in 1-cell embryos. These results suggest a specialized need for MARVs post-fertilization, perhaps related to mitochondrial ATP production or protection from the high levels of ROS produced by high membrane potential mitochondria (Dumollard, Marangos et al. 2004). It is also worth noting that an extensive review of previously published TEM images of 2-cell mouse embryos failed to reveal MARV-like structures. Membrane-bound structures such as lipid droplets and lysosomes do not show similar distribution as MARVs in embryos. Reasons for these structures not being previously reported include: (i) the vesicles first form in 1-cell embryos and are no longer apparent post-blastocyst, and (ii) the vesicles are concentrated at the subplasmalemmal cytoplasm of the embryos. Therefore, specific markers (such as DDX1 or TIA-1) and TEM sections in the right location are needed to identify these vesicles. Furthermore, although previous publications have reported that Ca^{2+} localizes to mitochondria in 2-cell embryos (Manser and Houghton 2006, Nagaraj, Sharpley et al. 2017), the location of the concentrated Ca^{2+} signal could easily have been mistaken for mitochondria, thereby requiring further investigation.

A key feature of MARVs is that they are made up of a ring of DDX1 vesicles in 2-cell embryos, each containing a nucleic acid core believed to be RNA based on RNase digestion (Hildebrandt, Wang et al. 2019). As DDX1 is an RNA binding/unwinding protein, we postulate that at least some of the RNAs found at the core of each DDX1 vesicle can be bound and structurally remodelled by DDX1. In addition, TIA-1, TIAR and CPEB1 also co-localize with DDX1 in early embryos (Hildebrandt, Wang et al. 2019). TIA-1, TIAR, CPEB1 and DDX1 have all been shown to localize to stress granules when mammalian cells are exposed to environmental stress (Gilks, Kedersha et al. 2004, Onishi, Kino et al. 2008). Although our previous work indicates that TIA-1/TIAR/DDX1-containing vesicles in 2-cell embryos are not related to stress in the classic sense, there may be functional similarities between DDX1 vesicles and stress granules (Hildebrandt, Wang et al. 2019). Stress granules are membrane-less organelles that serve as sites of RNA recruitment when cells are under stress. Recruited RNAs are mostly repressed although recent data indicate that specific transcripts undergo translation at stress granules (Mateju, Eichenberger et al. 2020). These data, combined with well-demonstrated roles for members of the DEAD box protein family in translation (Linder and Jankowsky 2011, Hondele, Sachdev et al. 2019), suggest that MARVs may serve as sites of translation. However, despite the fact that we did observe that aggregation of DDX1 in 2-cell embryos was affected by inhibition of global translation, we were not able to obtain evidence for the presence of either mitochondrial or cytoplasmic ribosomal proteins in MARVs

based on immunofluorescence and TEM analysis. Thus, unlike stress granules, MARVs may not be sites of active translation.

It has long been known that oocytes store large quantities of maternal RNAs that are required for early embryonic development (Olszanska and Borgul 1993). Zygotic genes are activated shortly after fertilization with two waves of zygotic genome activation (ZGA) with a major wave occurring at the 2-cell stage (Nothias, Majumder et al. 1995, Hamatani, Carter et al. 2004, Tadros and Lipshitz 2009, Li, Zheng et al. 2010). DDX1 aggregates are readily apparent in the cytoplasm of mouse oocytes from the germinal vesicle (GV) stage onwards (Hildebrandt, Wang et al. 2019); however, it is only after fertilization that DDX1 and RNA become enclosed within a membrane. These results suggest a link between utilization of maternal RNAs and MARVs after fertilization. Thus, MARVs may serve as sites of RNA degradation, sites of RNA storage, or sites of active RNA processing prior to translation.

Maternal mRNAs are degraded through two main pathways including endogenous siRNA-mediated degradation (Lykke-Andersen, Gilchrist et al. 2008, Kaneda, Tang et al. 2009, Suh, Baehner et al. 2010) and CCR4-NOT deadenylase complex mediated mRNA decay (Ma, Fukuda et al. 2015, Liu, Lu et al. 2016, Vieux and Clarke 2018). However, we (unpublished data) and others have shown that the immunostaining pattern of Ago2 is different from that of MARVs (Lykke-Andersen, Gilchrist et al. 2008, Zhang, Hou et al. 2020), indicating that MARVs do

not serve as Ago2-mediated RNA degradation sites. As well, the immunostaining pattern of a subset of players in the CCR4-NOT complex including CNOT3 (Zheng, Yang et al. 2016), CNOT7 as well as BTG4 (Yu, Ji et al. 2016) have immunostaining patterns that are different from that of DDX1 suggesting that MARVs may not be involved in CCR4-NOT mediated mRNA decay. In agreement with these data, we have previously shown that DDX1 does not co-localize with RNA degradation markers such as markers for P-bodies (DDX6, DDX3, GW182), GW-bodies (GW182), and exosomes (Exosc5) (Hildebrandt, Wang et al. 2019). Together, these data suggest that MARVs may serve as sites for RNA storage or processing rather than degradation.

During oogenesis and early embryonic development, maternal RNAs are stored and repressed prior to their temporally-controlled activation by stage-specific RNA processing (Winata and Korzh 2018). Therefore, activation of RNA processing may occur in a continuum in developing embryos. While a number of RNA-containing germ granules that serve as RNA storage sites have been identified in oocytes and embryos (Voronina, Seydoux et al. 2011), none of these granules have the appearance of MARVs nor have they been shown to be membrane-bound. Furthermore, while germ granules have been identified in *Drosophila, C. elegans, Xenopus, Danio rerio*, they have yet to be reported in mammalian embryos (Voronina, Seydoux et al. 2011, Kulkarni and Extavour 2017). Intriguingly, we have found key cytoplasmic polyadenylation factors (CPEB1 and CPSF2) in DDX1 vesicles, suggesting that MARVs may play similar roles to that

of germ granules in mammals, and may serve as sites of translation repression (RNA storage) and/or cytoplasmic polyadenylation (RNA processing) (de Moor and Richter 1999, Pique, Lopez et al. 2008, Charlesworth, Meijer et al. 2013). Cytoplasmic deadenylation is a common strategy used in different species to control the activation of maternal mRNAs in oocytes and embryos (Charlesworth, Meijer et al. 2013). When required, these deadenylated maternal RNAs must be polyadenylated, a process that occurs in the cytoplasm (Huarte, Stutz et al. 1992, de Moor and Richter 1999, Richter 1999, Paillard, Maniey et al. 2000, Vishnu, Sumaroka et al. 2011). In addition to the classic polyadenylation signal (PAS) required for nuclear polyadenylation, cytoplasmic polyadenylation also requires the cytoplasmic polyadenylation element (CPE) (Mendez and Richter 2001). The cytoplasmic polyadenylation factors CPEB1 and CPSF2 bind to CPE and PAS, respectively (Dickson, Bilger et al. 1999, Charlesworth, Meijer et al. 2013). In *Xenopus* 2-cell embryos, CPEB1 and CPSF2 are locally concentrated (Vishnu, Sumaroka et al. 2011), possibly by liquid-liquid phase separation, to carry out their cytoplasmic polyadenylation functions. However, membrane-less compartments do not have the ability to retain concentrated levels of Ca^{2+} which may be especially important for cytoplasmic polyadenylation in 2-cell mouse embryos. Therefore, MARVs may not only serve to compartmentalize RNAs and proteins but also the Ca^{2+}. As Ca^{2+} has been shown to be responsible for the phosphorylation and activation of the essential cytoplasmic polyadenylation factor CPEB1 (Atkins,

Nozaki et al. 2004), it seems likely that the CPEB1 in MARVs is activated. Thus, MARVs may be sites for controlled cytoplasmic polyadenylation **(Fig. 3.26A)**.

It is noteworthy that the appearance of MARVs changes dramatically as the embryos mature, becoming larger and denser, finally encircling the nuclei of blastocysts. As DDX1 is an RNA helicase that alters RNA structure in an ATP/ADP-dependent manner (Li, Monckton et al. 2008, Kellner, Reinstein et al. 2015), and MARVs contain Ca^{2+} that may be essential to stimulate the mitochondria TCA cycle and oxidative phosphorylation for ATP production (Brookes, Yoon et al. 2004, Peng and Jou 2010), the change in MARVs may reflect increased local concentration of Ca^{2+} which stimulates ATP production in the vicinity of MARVs, in turn modulating DDX1 RNA binding/remodeling function **(Fig. 3.26B)**.

In conclusion, we have discovered a potential role for DDX1 in the formation of previously unreported clusters of membrane-bound RNA-containing DDX1 vesicles, which we have named MARVs. MARVs first appear in 1-cell embryos and are hubs of DDX1, cytoplasmic polyadenylation factors, RNAs and Ca^{2+} which reside in the vicinity of high membrane potential mitochondria. *Ddx1* knockout results in disruption of MARVs and is accompanied by release of Ca^{2+} and increased mitochondrial activity. We propose that MARVs not only regulate mitochondrial function in a Ca^{2+} dependent manner, but also play an essential role in the temporal regulation of maternal RNA polyadenylation required during early embryonic development.

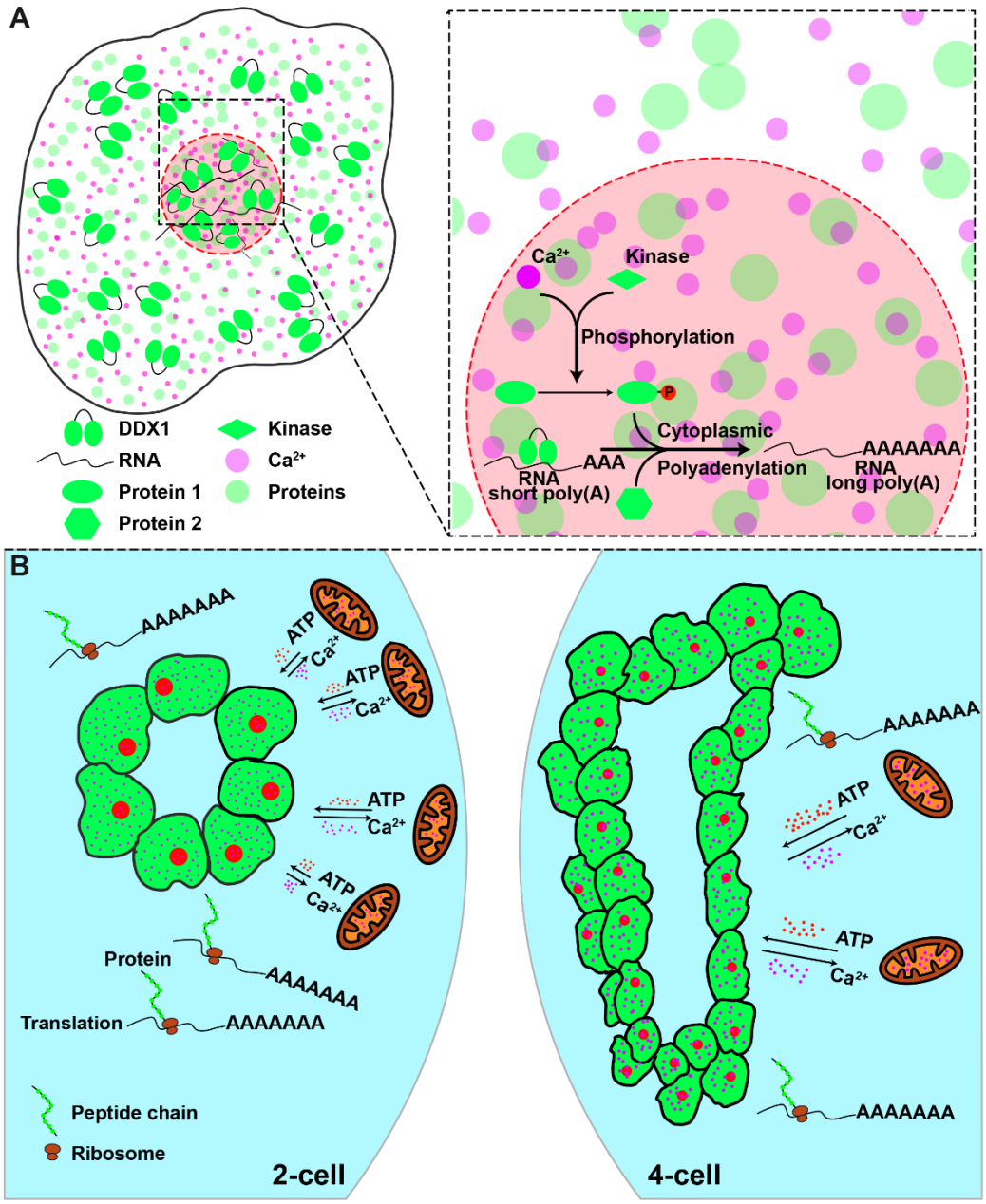

Figure 3.26 Proposed role for MARVs in early embryonic development. (A) Proposed role for MARVs in polyadenylation of cytoplasmic mRNAs. MARVs formed upon fertilization are hubs of Ca^{2+} and proteins (including DDX1, CPEB1, CPSF2) required for cytoplasmic polyadenylation. CPEB1 is activated by the high

levels of Ca^{2+} in MARVs, initiating the series of events required for the production of translation-ready cytoplasmic mRNAs. (B) As numbers of mitochondria do not increase in the developing embryo until the blastocyst stage, the increased aggregation of DDX1 vesicles to form larger MARVs observed as development progresses from 2-cell to blastocyst stages may reflect the need for increased concentrations of Ca^{2+} to hyper-activate a smaller number of mitochondria as well as polyadenylation factors.

3.5 Acknowledgments

We thank Dan McGinn and Cheryl Santos for their help with the mouse experiments. We are also grateful for the support of Gerry Barron, Xuejun Sun and the Cross Cancer institute Cell Imaging Facility. We would like to thank Dr. Lei Li for advice on experimental design and reading the manuscript. This work was supported by a grant from the Canadian Institutes of Health Research – grant number 162157.

3.6 Competing interests

The authors declare no conflict of interest.

Chapter 4.

Identification of DDX1-bound RNAs in 2-cell embryos

The goals of this chapter were to: (i) further characterize when *Ddx1*$^{-/-}$ embryos die during development, and (ii) use RNA immunoprecipitation followed by RNA sequencing to identify the RNAs bound to DDX1 in early-stage embryos.

4.1 Introduction

DEAD box 1 (DDX1) is an RNA helicase involved in different cellular processes from stress response, to repair of DNA double-strand breaks (Li, Monckton et al. 2008, Edgcomb, Carmel et al. 2012, Li, Germain et al. 2016). DDX1 is mostly found in the nucleus of mature somatic cells; however, DDX1 is also abundant in the cytoplasm of cells overexpressing DDX1 such as *DDX1/MYCN* co-amplified neuroblastoma and retinoblastoma cells (Godbout and Squire 1993, Godbout, Packer et al. 1998, Fagerberg, Hallstrom et al. 2014). There is evidence that DDX1 plays a role in unwinding RNA-DNA hybrids located at DNA double strand breaks in transcriptionally active genomic regions (Li, Germain et al. 2016).

The role of DDX1 in embryonic development has been studied in *Drosophila melanogaster* and *Mus musculus* (Germain, Li et al. 2015, Hildebrandt, Germain et al. 2015, Hildebrandt, Wang et al. 2019). *Ddx1*-null *Drosophila* have a smaller body size at the pupal and adult stages with severely affected reproductive systems. In contrast, *Ddx1* knockout in mice leads to very early lethality with embryos stalling at the 2- to 4-cell stages *in vitro*. This difference may be explained in part by the presence of maternal Ddx1 protein in *Ddx1*-null *Drosophila* up to the 2nd instar, in contrast to maternal DDX1 protein in mouse embryos which is likely to be degraded at the 2- to 4-cell stages (Germain, Li et al. 2015, Hildebrandt, Wang et al. 2019). We have discovered that zygotic *Ddx1* is associated with the

formation/retention of aggregates of DDX1 vesicles (called MARVs – Chapter 3) which control the subplasmalemmal cytoplasmic distribution of Ca^{2+} in early mouse embryos. In the absence of zygotic DDX1, cytoplasmic Ca^{2+} distribution is disrupted and few subplasmalemmal cytoplasmic Ca^{2+} microdomains are observed. The disruption of Ca^{2+} microdomains correlates with increased mitochondrial activity and production of reactive oxygen species (mtROS), which may lead to nuclear and mitochondrial fragmentation. These results point to embryonic DDX1 playing an essential role in early embryonic metabolism and development.

The main function of DEAD box proteins is to bind and remodel RNA. As such, DDX1 may be subjected to conformational changes when bound by RNAs (Sengoku, Nureki et al. 2006, Mallam, Del Campo et al. 2012). We already know based on transmission electron microscopy and RNase digestion experiments that DDX1 vesicles contain RNAs (Chapters 2 and 3). As Ca^{2+} is required for the localization of maternal poly(A)$^{+}$ RNAs in oocytes (Larabell and Capco 1988), and DDX1 is an RNA binding/RNA remodeling RNA helicase, one possibility is that MARVs serve as storage sites for maternal RNAs. However, as cytoplasmic polyadenylation factors have also been identified in MARVs, another possibility is that MARVs can also serve as sites for cytoplasmic polyadenylation of maternal RNAs in early embryonic development.

Mouse embryos rely on maternal materials, including proteins and RNAs, to develop past the maternal-to-zygotic transition (MZT) stage (Schultz 2002, Li, Zheng et al. 2010). In order to control maternal RNA utilization, the maternal RNAs are deadenylated during oogenesis. When the RNAs need to be translated after fertilization, they undergo cytoplasmic polyadenylation (Winata and Korzh 2018). Three waves of cytoplasmic polyadenylation have been described during oogenesis and early embryonic development. The first two waves of cytoplasmic polyadenylation take place during oogenesis. These two waves are relatively well characterized. However, the third wave of cytoplasmic polyadenylation, which takes place after fertilization, still remains poorly understood. Apart from the cytoplasmic polyadenylation element binding protein (CPEB1), little is known about the proteins involved in the third wave of cytoplasmic polyadenylation (Winata and Korzh 2018). What is known is that Ca^{2+} plays an important role in the phosphorylation of CPEB1 which is believed to initiate the cytoplasmic polyadenylation process (Atkins, Nozaki et al. 2004). CPEB1 interacts with cleavage and polyadenylation specificity factor (CPSF) which is a nuclear polyadenylation factor in non-embryonic somatic cells (Hodgman, Tay et al. 2001). Notably, CPSF2 has been reported to play a role in cytoplasmic polyadenylation in embryos (Dickson, Bilger et al. 1999, Hodgman, Tay et al. 2001, Vishnu, Sumaroka et al. 2011). DDX1 is an ATP/ADP binding DEAD box protein that interacts with polyadenylation factor Cstf64 and co-localizes with both Cstf64 and CPSF2 in human cell lines (Bleoo, Sun et al. 2001, Li, Roy et al. 2006). Thus, an

interesting possibility is that MARVs may bring together the cytoplasmic polyadenylation machinery required for the third wave of cytoplasmic polyadenylation during early embryonic development.

We have previously reported that *Ddx1*$^{-/-}$ mouse embryos fail to develop Ca^{2+} subplasmalemmal cytoplasmic microdomains which results in an upregulation of mtROS with embryos stalling at the 2- to 4-cell stages *in vitro*. In this chapter, we present evidence that *Ddx1*$^{-/-}$ embryos die prior to the 2-cell stage *in vivo*. As DDX1 vesicles start to form at the 1-cell stage, we propose that zygotic DDX1 may be needed *in vivo* earlier than previously suspected. As the role of the RNAs present in DDX1 vesicles remains unknown, and in order to understand the relationship between DDX1, Ca^{2+} and RNAs, we used stimulated emission depletion (STED) microscopy to examine the co-localization of DDX1 with different nucleic acids (e.g. dsRNA, ssDNA, dsDNA and DNA/RNA duplex). We also carried out RNA-DDX1 immunoprecipitations followed by RNA sequencing (RIP-seq) to identify the RNAs bound to DDX1 in early embryos. We found that ~20% of the transcripts identified by RIP-seq were processed pseudogenes, with an additional ~24% of transcripts representing long non-coding RNAs.

4.2 Materials and methods

4.2.1 DDX1 immunostaining in different stage embryos

The generation of the *Ddx1* knockout mice line has been described previously (Hildebrandt, Germain et al. 2015). All embryos used in these experiments were obtained under natural mating conditions using FVB/N mice. Mice found to have vaginal plugs were considered to be at embryonic day (E) 0.5 of gestation. For collection of E0.5 to E2.5 embryos, the oviducts were removed and placed in 35mm tissue culture dishes where they were flushed with pre-equilibrated (37°C) M16 medium (Sigma-Aldrich) using capillary tubes (World Precision Instruments). E0.5 embryos were treated with 300 µg/ml hyaluronidase (Sigma-Aldrich) for the removal of cumulus cells. Embryos were obtained from heterozygous *Ddx1* intercrosses at different developmental stages starting from the plug date (E0.5). If culturing was required, the embryos were cultured as described in Chapter 3.

4.2.2 Immunofluorescence staining

Immunofluorescence staining was carried out using embryos flushed with PBS from oviducts or embryos cultured in M16 medium and washed 2X with PBS. Embryos were then fixed in 4% paraformaldehyde for 15 min, followed by 3X PBS + 0.01% Tween (PBST) washes and permeabilization with PBS + 0.5% Triton-X-100 for 15 min. The embryos were then incubated in 0.5% fish gelatin blocking

solution for 30 min, and transferred to PBST diluted anti-DDX1 antibody and incubated for 1 h. The immunostaining plate was wrapped with aluminum foil to protect the antibody from light. When secondary antibody was needed, the embryos were washed 3X with PBST and incubated with secondary antibody for 1 h. After washing 3X with PBST, embryos were then placed on a slide and mounted with Mowiol (Calbiochem) without 4',6-diamidino-2-phenylindole (DAPI). The antibodies used in this chapter are listed in **Table 4.1.**

Table 4.1 Antibodies used for immunofluorescent			
Antibody	Host	Dilution	Source
Anti-DDX1 (2910)	Rabbit	1:1000	In house (batch 2910)
Atto 550 conjugated anti-DDX1 (2910)	Rabbit	1:400	Anti-DDX1 (2910) conjugated with Atto 550 (Sigma-Aldrich)
Anti-dsRNA (J2)	Mouse	1:100	Scicons #10010200
Anti-dsDNA	Mouse	1:100	Millipore #MAB1293MI
Anti-ssDNA	Mouse	1:100	Millipore #MAB3034
Anti-RNA-DNA duplex (S9.6)	Mouse	1:100	Gift from Dr. Stephen Leppla, NIH
Anti-Mouse Alexa 647	Donkey	1:400	Molecular Probes, Thermofisher

4.2.3 Single embryo genotyping

E0.5 embryos were digested with 300 μg/ml hyaluronidase to remove cumulus cells and washed 3X with PBS. E1.5 embryos were washed 2X with PBS.

E0.5 and E1.5 embryos were then treated with Acidic Tyrode's solution (Sigma) to dissolve the zona pellucida. Genomic DNA was extracted using the Tissue Genomic DNA extraction kit. The DNA was amplified using nested PCR reactions with the following PCR primers: forward: RG062: GATGGAGACAGTCTCTGGTT; reverse: RG066: CCAAGCTCCACTATTATCCC (*Ddx1*), RG061: GCGCGTACATCGGGCAAATAATATC (*β-gal*). Nested PCR primers were: forward: RG063: ATTAGGAACTGGGCATGTATC; reverse: RG065: AGCACTAGTAAGTACCTACAC (*Ddx1*), RG060: CTGGGGTTCGTGTCCTACAA (*β-gal*). PCR products were analyzed by agarose gel electrophoresis.

4.2.4 Embryonic RNA detection

For detection of *β-gal* RNA, *Ddx1*$^{+/-}$ males were crossed with wildtype females. E0.5 and E1.5 embryos were flushed. Cumulus cells and zona pellucida were removed as described above. Embryos from single females (6-8 embryos per female) were pooled together for RNA extraction. The RNAs were extracted with RNeasy Micro Kit (Qiagen) and reverse transcribed with SuperScript IV Reverse Transcriptase (Invitrogen) following the manufacturers' instructions. The cDNAs were then used for Taqman qPCR reactions (*Ddx1*: Mm00506198_m1, *β-gal*: Mr03987581_mr).

4.2.5 RNA immunoprecipitations and next-generation RNA sequencing

Embryos were collected in PBS and frozen in liquid N_2 before storing at -80ºC. For the first RNA sequencing experiment (MiSeq), 450 embryos were pooled and divided as follows: 150 embryos for control pre-immune serum immunoprecipitations (X1) and 150 embryos each for anti-DDX1 antibody immunoprecipitations (X3). For the second RNA sequencing experiment (HiSeq), 1500 embryos were pooled and divided as follows: 250 embryos each for control pre-immune serum immunoprecipitations (X 3) and 250 embryos each for anti-DDX1 antibody immunoprecipitations (X 3). The embryos were lysed in lysis buffer [50 mM Tris-HCl, pH 7.5, 150 mM NaCl, 1% NP-40, 0.5% sodium deoxycholate, 5 mM EDTA, 2 mM DTT, 1X Complete protease inhibitor (Roche) and 200 unit/ml RNase inhibitor (Invitrogen)]. Lysates were pre-cleared with Protein A beads (GE Healthcare), followed by incubation with either IgG-purified rabbit-anti-DDX1 antibody or pre-immune serum at 4°C for 90 minutes with rotation. Protein A beads were then added and samples were incubated for another 45 minutes. Immunoprecipitates were washed 5 times in wash buffer [50 mM Tris-HCl, pH 7.5, 1 M NaCl, 1% NP-40, 1% sodium deoxycholate and 5 mM EDTA], followed by one wash in 1X RQ1 DNase buffer (40 mM Tris-HCl, pH 8.0, 10 mM $MgSO_4$, 1 mM $CaCl_2$). Immunoprecipitates were digested with 8 units/ml of RQ1 DNase (Promega) at 37°C for 30 minutes, followed by digestion with 250 µg/ml of Protease K (Roche) at 37°C for 30 minutes. Co-immunoprecipitated RNAs were extracted with sodium acetate (pH 5.2)-equilibrated phenol (Roche) and precipitated with ethanol. Precipitated RNAs were resuspended in H_2O and

reverse-transcribed to cDNA using both oligo(dT) and random hexamers and Superscript IV reverse transcriptase (Invitrogen) following the manufacturer's instructions. The cDNAs were then amplified with either PCR following adapter ligation (MiSeq) or QIAseq FX Single Cell RNA Library Kit (QIAGEN, Cat. No. 180733) (HiSeq).

For RNA sequencing analysis, MiSeq was done in collaboration with Dr. Gane Wong and HiSeq was carried out by Novogene (8801 Folsom Blvd #290, Sacramento, CA, US). Both sequencing data were analyzed in two different ways: (1) CLIPSeqTools, and (2) featureCounts followed by DESeq2. For CLIPSeqTools, the raw sequencing data were mapped with STAR aligner using mouse reference genome mm9 provided by CLIPSeqTools (Dobin, Davis et al. 2013, Maragkakis, Alexiou et al. 2016). The read counts on each exon were obtained from CLIPSeqTools (Maragkakis, Alexiou et al. 2016). Upperquantile normalization from R package preprocessCore was used to normalize the read counts for each sample and normalized counts were then used for comparison (Bolstad 2020). For featureCounts/DESeq2, the raw sequencing data were mapped with STAR aligner using Ensembl mouse reference genome GRCm38 (Dobin, Davis et al. 2013). The read counts and genomic distributions were obtained from featureCounts in the Rsubread package (Liao, Smyth et al. 2014, Liao, Smyth et al. 2019). The count table was obtained from featureCounts and further processed by DESeq2 package (Love, Huber et al. 2014).

4.3 Results

4.3.1 Ddx1$^{-/-}$ embryos die pre-2-cell stage in vivo

We have previously reported that *Ddx1*$^{-/-}$ embryos are lost prior to the blastocyst stage *in vivo* and *Ddx1*$^{-/-}$ embryos stall at the 2- to 4-cell stages *in vitro* (Hildebrandt, Wang et al. 2019). To examine embryo stalling under physiological conditions, we next attempted to capture stalled *Ddx1*$^{-/-}$ *in vivo.* Unexpectedly, we failed to find *Ddx1*$^{-/-}$ embryos from the 2-cell (E1.5) to 8-cell (E2.5) stages **(Fig. 4.1A)**. To determine when embryos die *in vivo*, we cultured E0.5 (1-cell stage) and E1.5 (2-cell stage) embryos from six and twelve heterozygote crosses, respectively, up to the blastocyst stage. We found that 18/62 cultured embryos (29%) collected at the E0.5 stage failed to reach the morula to blastocyst stages, similar to what we previously reported. In contrast, we only found a single stalled embryo (1/84) when cultured embryos were collected at the E1.5 (2-cell) stage.

A

No. Embryos	25	18	36	13	12	20
Stages	2-cell	2-cell	2- to 4-cell	2- to 4-cell	4-cell	8-cell
Time Plugged (E0.5)	10am+1	4pm+1	8pm+1	12am+2	6am+2	10am+2

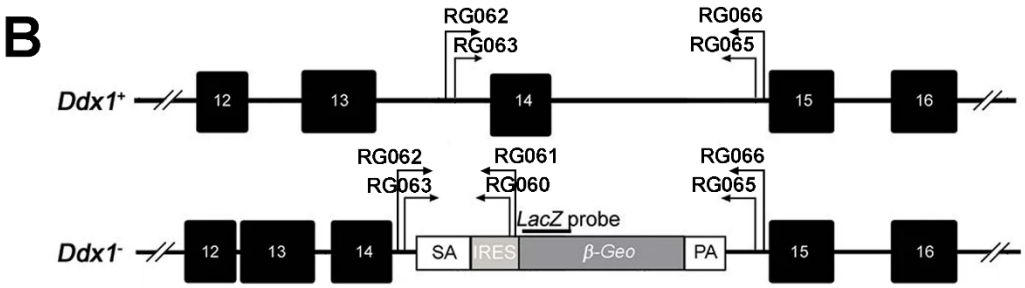

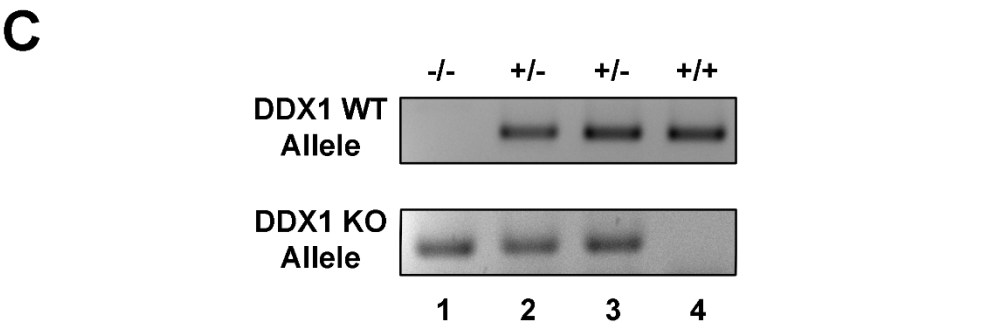

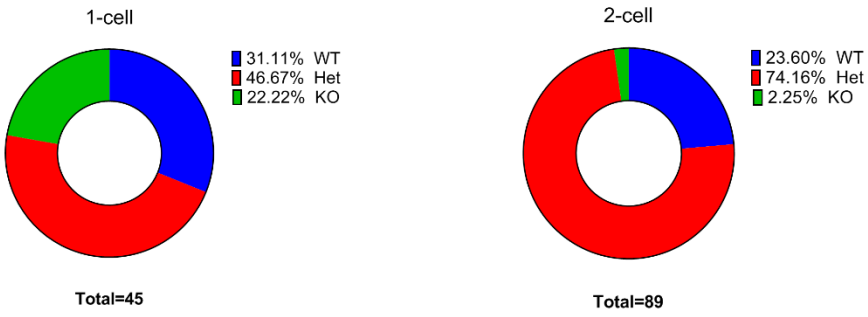

Figure 4.1 Absence of 2-cell *Ddx1*$^{-/-}$ embryos *in vivo.* (A) Embryos were collected at different time points starting from E1.5 (at 10 am on the 2nd day of the

vaginal plug). Embryos were immunostained with anti-DDX1 antibody. No embryos with reduced levels of DDX1 protein were observed. (B) Location of PCR primers with respect to the DDX1 wildtype and knockout alleles. Figure adapted from (Hildebrandt, Germain et al. 2015). (C) Representative PCR results for *Ddx1* wildtype, heterozygous and knockout embryos (top panel). PCR amplification of the wildtype allele was carried out using primer pairs RG062 and RG066 which was then nested with RG063 and RG065. PCR amplification of the knockout allele was carried out using primer pairs RG062 and RG061 which was then nested with RG063 and RG060. Diagrammatic representation of genotype statistics of embryos collected at the 1-cell and 2-cell stages (bottom panel).

To further investigate when *Ddx1*$^{-/-}$ embryos die *in vivo*, we carried out nested PCR on individual embryos collected at the 1-cell and 2-cell stages for genotyping. Of 45 embryos collected at the 1-cell stage from heterozygous crosses, 31% (14/45) were wildtype and ~22% (10/45) were *Ddx1*$^{-/-}$, with the remainder being heterozygotes. In agreement with our *in vitro* data, we obtained ~24% (21/89) wildtype embryos and ~2% (2/89) *Ddx1*$^{-/-}$ embryos when embryos were collected at E1.5 **(Fig. 4.1B)**. These data indicate that very few *Ddx1*$^{-/-}$ embryos reach the 2-cell stage under *in vivo* condition. Thus, differences between *in vitro* and *in vivo* conditions appear to affect when *Ddx1*$^{-/-}$ embryos die.

4.3.2 Zygotic DDX1 is needed for embryos to develop to the 2-cell stage in vivo

We next asked whether zygotic *Ddx1* was one of the few genes activated during the first wave of MZT. In order to avoid interference with maternal *Ddx1* transcripts, we made use of the gene trap (*β-gal* insertion at the *Ddx1* locus) that was used to generate our *Ddx1* knockout mice (Hildebrandt, Germain et al. 2015).

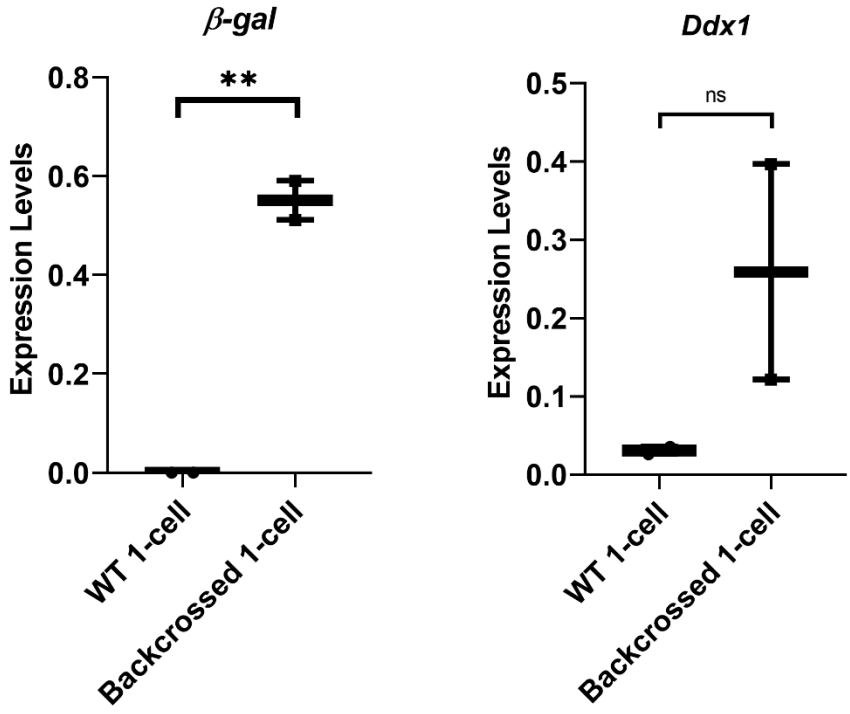

Figure 4.2 *β-gal* mRNA expression in 1-cell embryos. Female wildtype *Ddx1*$^{+/+}$ and male *Ddx1*$^{+/-}$ mice were backcrossed, and 1-cell progeny collected and pooled for RNA extraction. Embryos were also collected from wildtype crosses. RT-qPCR was used to measure *β-gal* and *Ddx1* levels in embryos. ** indicates $P < 0.01$.

Female *Ddx1*$^{+/+}$ mice (negative for *β-gal* mRNA) were crossed with male *Ddx1*$^{+/-}$ to generate *Ddx1*$^{+/+}$ and *Ddx1*$^{+/-}$ embryos. The embryos were collected and pooled for RNA extraction and RT-qPCR analysis. Consistent with our prediction, *β-gal* mRNA was detected in E0.5 (1-cell) embryos. There was no significant difference in *Ddx1* RNA between wildtype and the embryos generated from *Ddx1*$^{+/+}$ X *Ddx1*$^{+/-}$ crosses, although there was wide variation in *Ddx1* RNA levels in the embryos generated from *Ddx1*$^{+/+}$ X *Ddx1*$^{+/-}$ crosses compared to wildtype embryos **(Fig. 4.2)**. These results suggest that zygotic *Ddx1* is expressed in 1-cell stage embryos and is essential for embryonic development past the 1-cell stage *in vivo*.

4.3.3 DNA-RNA hybrids are not detected in MARVs in 2-cell embryos

To further investigate the role of zygotic *Ddx1*, we focused on the nucleic acid binding activity of DDX1. DDX1 has been reported to unwind DNA-RNA duplexes as well as dsRNAs (Li, Monckton et al. 2008, Li, Germain et al. 2016). We therefore used co-immunostaining analysis to investigate whether DDX1 co-localizes with single-strand DNA (ssDNA), double-strand DNA (dsDNA), double-strand RNA (dsRNA), or DNA-RNA hybrids in 2-cell embryos.

Dual colour STED showed no clear co-localization of DDX1 with ssDNA, dsDNA or dsRNA in 2-cell embryos, although some overlap was observed with the DDX1-containing ring-like MARV structures **(Fig. 4.3)**. The signals observed for ssDNA, dsDNA and dsRNA were mostly scattered throughout the embryos.

Results with the DNA-RNA hybrid antibody S9.6 were clearer, showing the MARVs are devoid of RNA-DNA hybrids **(Fig. 4.4)**.

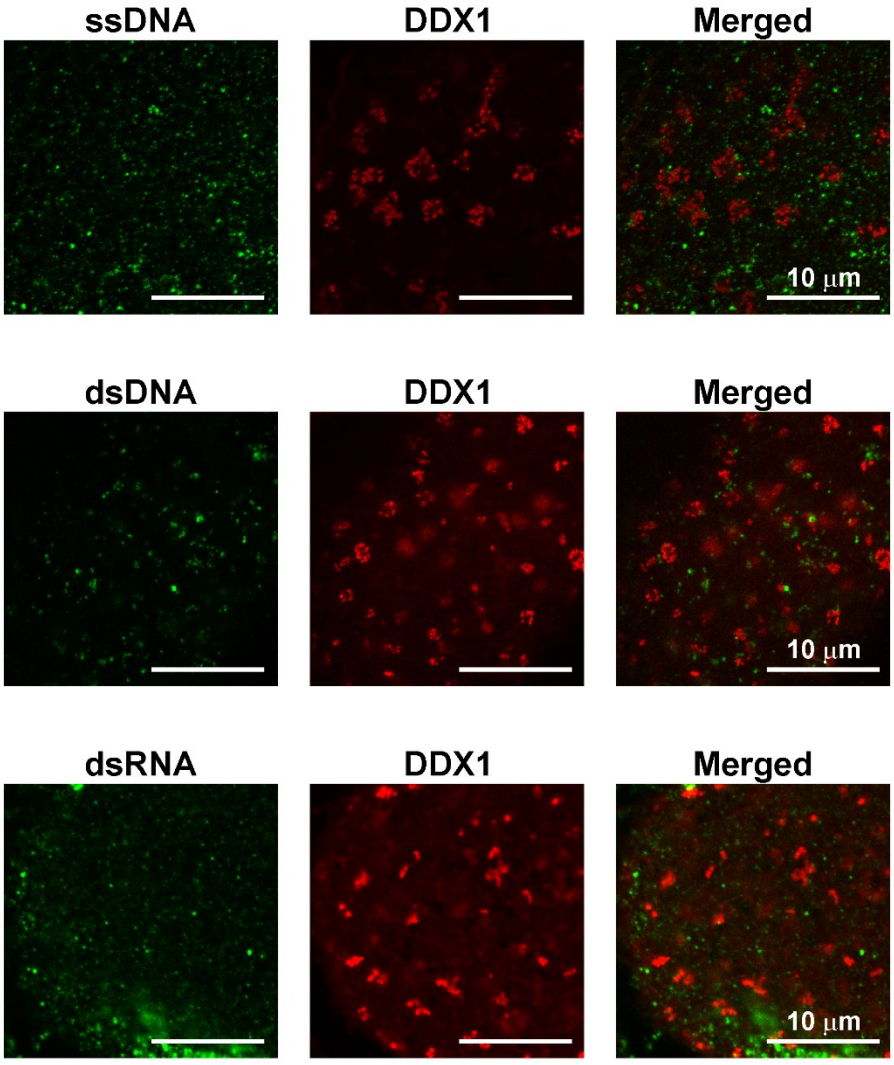

Figure 4.3 MARVs show no co-localization with ssDNA, dsDNA or dsRNA. 2-cell embryos were fixed with 4% paraformaldehyde and immunostained with Atto 550-conjugated anti-DDX1 antibody and mouse antibodies targeting ssDNA, dsDNA and dsRNA followed by Alexa 647-conjugated donkey anti-mouse

secondary antibody. No co-localization between DDX1 antibody and the nucleic acid antibodies was observed. Scale bar = 10 μm.

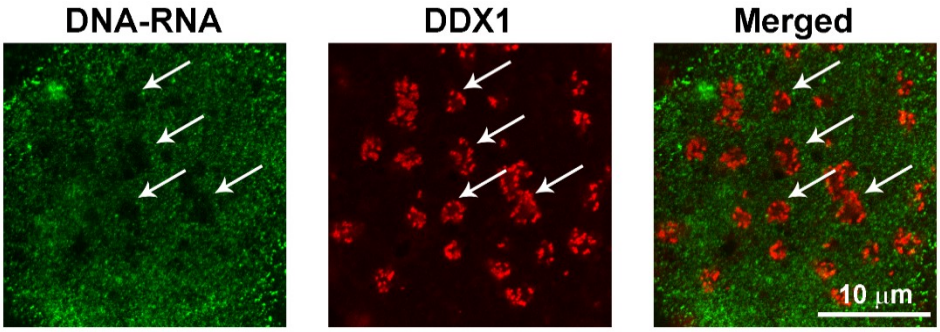

Figure 4.4 Absence of DNA-RNA hybrids in MARVs. 2-cell embryos were fixed with 4% paraformaldehyde and immunostained with Atto 550-conjugated anti-DDX1 antibody and mouse antibodies targeting DNA-RNA hybrids (S9.6 antibody) followed by Alexa 647-conjugated donkey anti-mouse secondary antibody. No co-localization between DDX1 and DNA-RNA hybrids was observed. Scale bar = 10 μm. Arrows indicate the absence of DNA-RNA hybrids in MARVs.

4.3.4 Identification of RNAs bound to DDX1 by RNA-immunoprecipitation followed by sequencing

We carried out RNA-DDX1 immunoprecipitation followed by RNA sequencing (RIP-seq) to identify DDX1 binding targets. Our first experiment

(MiSeq) was carried out using 450 embryos at the 2-cell stage. Embryos were divided into 1 IgG control group (150 embryos) and 2 DDX1 antibody groups (150 embryos each). The raw reads were aligned with STAR aligner followed by CLIPSeqTools with provided mm9 UCSC reference genome to collapse identical reads and extract read counts (Dobin, Davis et al. 2013, Maragkakis, Alexiou et al. 2016). Upperquantile normalized read counts per nucleotide per exon were used to identify the genes with the most abundant DDX1-bound RNAs (Bolstad 2020).

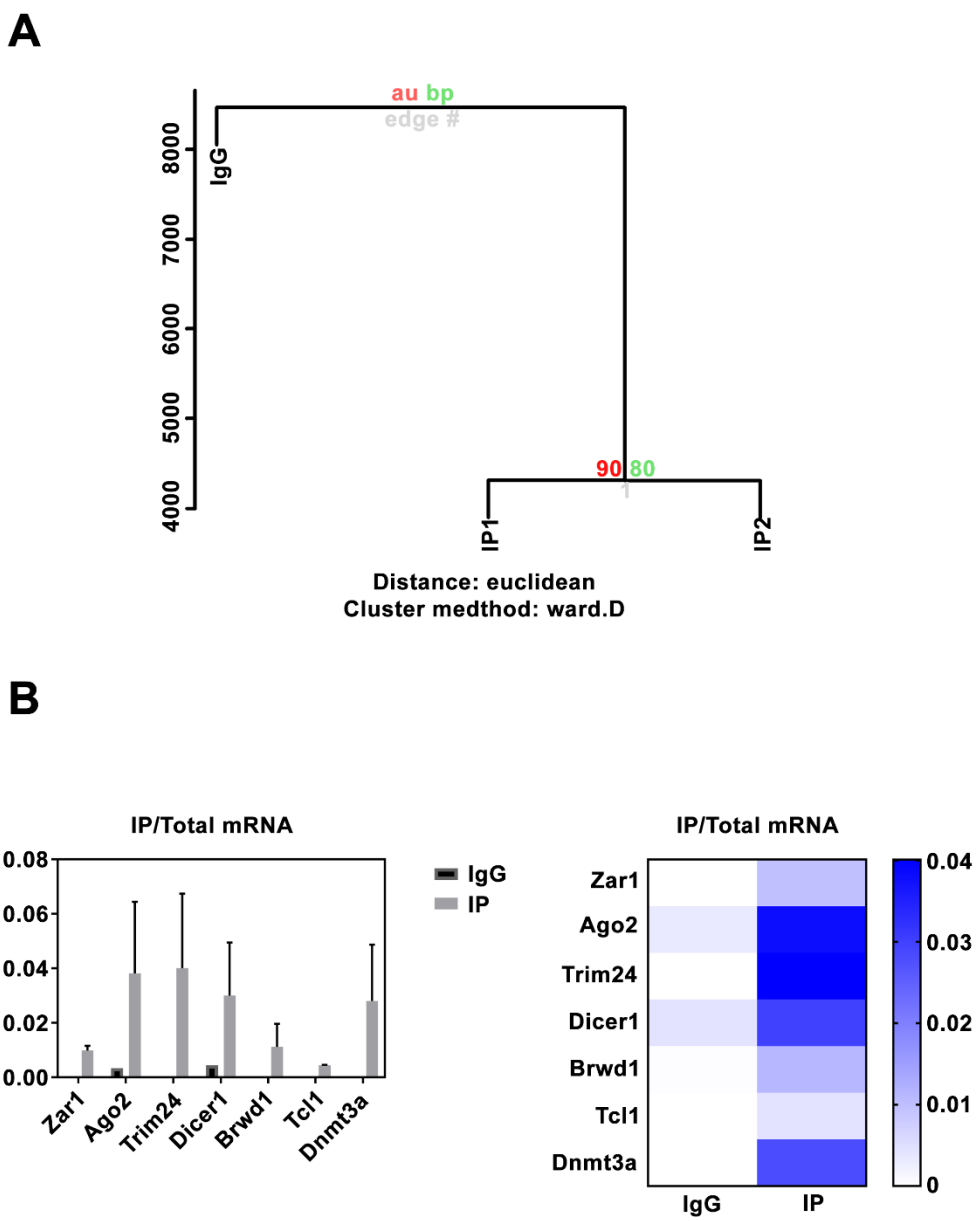

Figure 4.5 Identification of DDX1 bound RNAs by DDX1 RIP-seq. (A) Cluster dendrogram of IgG and DDX1 IP results from RIP-seq analysis was generated with R package pvclust. Approximately Unbiased (au) is labelled in red and Bootstrap Probability (bp) is labelled in green. (B) Histogram and heatmap of seven DDX1

binding targets of interest was normalized with mRNA levels reported by Biase *et al.* for 2-cell single cell sequencing data (Biase, Cao et al. 2014).

After processing, cluster analysis was used to generate the diagram shown in **Fig. 4.5A** (Suzuki and Shimodaira 2006). The two DDX1 antibody RIP groups were clustered together and away from the IgG group. Based on this analysis with CLIPSeqTools, out of the 31900 reference genes from mouse genome, we identified ~3500 genes producing transcripts potentially bound by DDX1. In agreement with Chapter 2, *Ago2, Zar1* and *Trim24* were found in our DDX1 RIP-seq data **(Fig. 4.5B)**. Moreover, of the 27 previously reported maternal genes whose loss results in embryonic lethality pre-implantation, we found an additional four genes not identified in Chapter 2 whose transcripts appear to be bound to DDX1 (*Dicer1, Brwd1, Tcl1* and *Dnmt3α*) (Li, Zheng et al. 2010), XXXI changed this because it made no sense to me **(Fig. 4.5B)**. However, this first RIP-seq analysis was done with only 1 pre-immune control and 2 IP samples which does not permit statistical analysis. Therefore, we performed another RNA sequencing experiment with the HiSeq sequencing analysis. In this second experiment, we divided a total of 1500 embryos into 3 pre-immune controls and 3 IP samples. We identified 558 genes whose transcripts were significantly bound by DDX1 (p-values < 0.01). We found that a subset of genes preferentially bound by DDX1 (IP/control > 1) in our first RIP-seq analysis were also present in the second RIP-seq analysis (IP/control > 1, p-value < 0.01). However, out of the 7 genes stated above (*Ago2, Zar1, Trim24, Dicer1, Brwd1, Tcl1* and *Dnmt3α*), only *Brwd1* had a p-value < 0.01

with the other genes showing no statistical significance (p-values: (IP/control = 0.43, p-value = 0.5), *Zar1* (0.53), *Trim24* (0.47), *Dicer1* (0.25), *Tcl1* (0.5), *Dnmt3α* (0.12)). *Ago2* RNA was not bound to DDX1 based on the second RIP-seq experiment. Of the DDX1 preferentially bound transcripts identified in our first RIP-seq analysis (~3500), 390 were significantly (p-value < 0.01) bound by DDX1 in the second RIP-seq experiment. Significance was established as IP/control > 1, p-values <0.01. As these are preliminary data that require validation, the p-values were calculated with two-tailed unpaired t-test without correction for false discovery rate.

We were not able to use CLIPSeqTools with the most recent reference genome as the UCSC reference genome provided by the CLIPSeqTools package was mm9 which was generated in 2007. Thus, we carried out RIP-seq analysis using a standard RNA sequencing pipeline proposed to be more suitable than CLIP-seq based pipelines as no RNase fragmentation is involved during the immunoprecipitation process (Li, Zhao et al. 2013, Tichy, Pickl et al. 2018). For these analyses, the raw reads were preprocessed with STAR aligner followed by featureCounts to extract read counts (Dobin, Davis et al. 2013, Liao, Smyth et al. 2014, Liao, Smyth et al. 2019). featureCounts identifies genes whose transcripts are preferentially bound by DDX1 in counts per gene which simplifies identification of preferentially bound transcripts in DDX1 IP samples compared to control samples. featureCounts also counts intronic sequences towards the total counts per gene. In regards to the latter, DDX1 has previously been shown to bind to

differentially spliced transcripts in flies (Germain, Li et al. 2015). As well, reads mapping to intronic sequences have been identified in other RNA sequencing analyses (Fang, Acheampong et al. 2005, Edgcomb, Carmel et al. 2012, Yasuda-Inoue, Kuroki et al. 2013, Biase, Cao et al. 2014, Qiao, Ren et al. 2020). DESeq2 was used to identify genes with the most abundant DDX1-bound RNAs (Love, Huber et al. 2014).

As our first RIP-seq experiment only contains 1 control sample and 2 IP samples, we were only able to obtain statistical results for our second RIP-seq experiment. Using the RNA-seq pipeline, we identified >20,000 genes out of the 55,487 reference genes that are preferentially bound by DDX1 (fold change >1) from our first RIP-seq experiment without any statistical criteria for filtering. In our second RIP-seq experiment, we identified >25,000 genes that are preferentially bound by DDX1 (fold change >1) out of the 55,487 reference genes. However, when p-value <0.01 was added for selection purposes, only 384 genes whose transcripts are significantly bound by DDX1 (fold change >1; p-value <0.01) were identified. Although not statistically valid, we decided to cross compare the preferentially bound transcripts from the ~20,000 genes identified in our first RIP-seq experiment with the significantly bound transcripts from the 384 genes identified in our second RIP-seq experiments. This analysis revealed 159 genes common to both RIP-seq experiments **(Table 4.2)**. Notably, ~51% of the identified genes were non-protein-coding, with ~20% classified as pseudogenes and ~24% classified as long non-coding RNAs. As pseudogenes and long non-coding RNAs

have been implicated in the production of endogenous siRNAs that play critical roles during early-stage embryonic development, DDX1's role may be related to the generation of these key siRNAs (Babiarz, Ruby et al. 2008, Yang, Lin et al. 2016, Karlic, Ganesh et al. 2017, Svoboda 2017).

Table 4.2 Transcripts preferentially bound by DDX1. LncRNA: long noncoding RNA; TR_V_gene: immunoglobulin variable chain and T-cell receptor genes; TEC: to be experimentally confirmed. 1st fold change indicates the fold change (IP/IgG) in first RIP-seq experiment and 2nd fold change indicates the fold change (IP/IgG) of the 2nd RIP-seq experiment. Only p-values and adjusted p-values of 2nd RIP-seq are shown.

Gene	Biotype	1st FoldChange	2nd FoldChange	2nd pvalue	2nd padj
Hddc2	protein_coding	1.08	10.30	0.006493922	0.26958265
Alox12	protein_coding	1.27	7.13	0.006376611	0.26720687
Tmem79	protein_coding	1.59	7.17	0.005103923	0.23855389
Trmt1	protein_coding	1.27	3.96	0.000725381	0.07414478
Mmd	protein_coding	1.53	6.22	0.004723752	0.22731619
Nsmf	protein_coding	1.34	3.19	0.00445824	0.21991262
Dqx1	protein_coding	1.07	6.66	0.001472645	0.11395979
Podnl1	protein_coding	1.25	4.48	0.007346642	0.28459346
Crlf3	protein_coding	1.09	2.98	0.000272702	0.03941681
Trim11	protein_coding	1.09	3.24	0.0096151	0.32391404
Rsad2	protein_coding	1.88	16.96	3.60E-09	3.69E-06
Tsen54	protein_coding	1.04	5.47	0.007322608	0.28399774
Zmynd11	protein_coding	1.55	4.85	0.008547657	0.30584206
Amacr	protein_coding	1.40	10.69	0.001019414	0.09089125
Rabl2	protein_coding	2.99	9.74	0.002848074	0.1674017
Slc30a6	protein_coding	1.05	2.61	0.00658209	0.27199615
Pkdcc	protein_coding	1.14	7.39	0.004471061	0.21994002
Cdh2	protein_coding	1.28	2.94	0.006714514	0.27253811
Trim8	protein_coding	1.39	4.37	0.005700057	0.25342084
Igfbp5	protein_coding	1.51	3.75	0.000416136	0.05133022
Nppc	protein_coding	1.76	4.48	0.003660977	0.19250053
Traf1	protein_coding	1.21	13.82	0.002138536	0.14261686
Sord	protein_coding	1.12	25.51	0.000296637	0.04049842
Lrp4	protein_coding	1.37	2.92	0.001934429	0.13504373
Ocstamp	protein_coding	2.04	8.10	0.006659318	0.27253811
Car9	protein_coding	1.51	5.48	0.004993132	0.23450429
Urod	protein_coding	4.32	4.12	0.003822374	0.19831552

Tmem50a	protein_coding	1.24	5.56	0.008288816	0.30018139
Sh3bgrl3	protein_coding	1.75	3.83	0.005836873	0.25565252
Pcyox1	protein_coding	1.16	8.77	0.009746145	0.32531104
Ptms	protein_coding	1.22	9.36	0.001154522	0.09847583
Gabarapl1	protein_coding	1.21	3.51	0.007808315	0.29213069
Dkkl1	protein_coding	1.51	4.70	0.006627535	0.27253811
Serpina7	protein_coding	1.05	21.73	0.002651177	0.1607907
Slc12a3	protein_coding	1.35	3.61	0.001235905	0.10151724
Rac2	protein_coding	1.38	2.94	0.005995242	0.25763316
Tle6	protein_coding	1.34	3.80	0.00886776	0.31218891
Tbxa2r	protein_coding	1.17	13.46	0.002122228	0.14210699
Apln	protein_coding	1.66	4.09	0.005750927	0.25413261
Mfsd2b	protein_coding	1.99	3.57	0.001163739	0.09866525
Flywch1	protein_coding	1.08	8.88	0.002435829	0.15452844
Ggt6	protein_coding	7.99	24.71	9.54E-05	0.01909291
Mfap4	protein_coding	3.32	5.00	1.15E-05	0.00350297
Tbc1d8b	protein_coding	1.80	8.29	0.000854128	0.08242588
Abcb4	protein_coding	1.11	8.61	0.002029536	0.13815585
Dmtf1	protein_coding	1.44	9.82	0.002111579	0.14210699
Pbxip1	protein_coding	1.10	5.42	0.008200127	0.29889062
Aqp6	protein_coding	2.72	9.82	0.002949225	0.17066494
Serpinb3a	protein_coding	6.27	3.05	0.001185265	0.0997173
Calhm6	protein_coding	1.78	3.58	0.002561203	0.15766536
Adam26a	protein_coding	1.81	23.37	0.000949007	0.08642927
Chchd10	protein_coding	1.88	6.13	0.004623583	0.22474723
Fzd2	protein_coding	2.01	3.25	8.64E-05	0.01768047
Oosp2	protein_coding	2.11	3.32	0.008196583	0.29889062
Ptafr	protein_coding	1.07	7.74	4.67E-05	0.0110127
Trim12c	protein_coding	1.56	3.36	0.000193584	0.03191798
Egln2	protein_coding	1.82	4.67	0.008114704	0.29760584
Olfr979	protein_coding	2.02	8.77	0.00671686	0.27253811
Rrs1	protein_coding	1.04	3.52	0.003640074	0.19195013
Tmem151a	protein_coding	1.48	4.02	0.002509457	0.15653574
Trank1	protein_coding	1.23	6.62	0.006499036	0.26958265
Olfr133	protein_coding	1.71	4.23	0.008729489	0.30798202
Scgb3a1	protein_coding	4.07	14.37	0.001259216	0.10277649
Tesl1	protein_coding	1.19	7.03	0.007069255	0.27913434
Vmn2r34	protein_coding	1.39	3.28	0.000719671	0.07402235
Olfr676	protein_coding	2.30	4.77	0.008652987	0.30726531
CN725425	protein_coding	1.13	2.35	0.006022512	0.25763316

Ifit1bl1	protein_coding	2.68	3.25	0.005862004	0.25565252
Mdfic2	protein_coding	1.13	3.48	0.009619388	0.32391404
Gm5916	protein_coding	3.43	3.10	0.003094254	0.17525746
Gm3269	protein_coding	4.81	7.55	0.006579635	0.27199615
Gm8922	protein_coding	2.37	3.23	0.001383	0.10934368
Gm3159	protein_coding	26.93	9.16	0.004343148	0.21526137
Speer1	protein_coding	1.09	2.88	0.004275048	0.2138241
Gm8897	protein_coding	1.09	2.31	0.006020055	0.25763316
Gm3839	protein_coding	1.14	5.87	0.007984531	0.29495735
Gm5767	protein_coding	1.13	9.51	0.000904431	0.0852738
Snhg16	lncRNA	2.70	3.33	0.002919863	0.16956394
H3f3aos	lncRNA	1.47	6.05	0.004303823	0.21413795
Trav14n-3	TR_V_gene	2.45	24.63	0.001721522	0.12571688
Gm3985	lncRNA	1.14	4.11	0.004389762	0.21724358
Gm14061	lncRNA	1.16	4.64	0.008943289	0.31288822
Platr13	lncRNA	2.11	9.13	0.00020971	0.03375985
Platr15	lncRNA	4.41	5.40	0.001980859	0.13711807
Gm11635	lncRNA	1.69	6.99	0.008247548	0.29934766
Gm16638	lncRNA	1.67	7.96	0.000271751	0.03941681
Gm16268	lncRNA	1.26	6.38	0.009204392	0.31790033
Gm6455	lncRNA	3.98	2.32	0.009591047	0.32391404
Gm20507	lncRNA	1.68	6.80	0.000767639	0.07699123
Gm20544	lncRNA	1.19	3.30	0.001909318	0.13386031
Trav14-3	TR_V_gene	7.99	10.27	0.007452863	0.2860069
Trav14n-1	TR_V_gene	1.25	15.63	0.000568527	0.06302008
4933433G15Rik	lncRNA	2.42	8.37	0.000167548	0.02873096
Gm5091	lncRNA	1.73	3.57	0.009148936	0.31665162
Gm26644	lncRNA	2.89	8.73	0.002016356	0.13810231
Gm28271	lncRNA	1.85	6.47	0.000233228	0.03609642
Gm29585	lncRNA	1.35	6.67	0.004778054	0.22953548
Gm28482	lncRNA	1.42	42.32	0.001303795	0.10510095
4930412E21Rik	lncRNA	1.25	3.79	0.000779714	0.07776044
A630035G10Rik	lncRNA	2.16	13.93	0.001640677	0.12234605
Gm37647	TEC	2.37	2.79	0.004290057	0.21392259
Gm44573	TEC	1.94	16.21	0.000340319	0.04378909
Gm42922	TEC	1.63	3.77	0.004313955	0.21413795
Gm42595	lncRNA	2.45	15.24	0.005867128	0.25565252
Gm43077	lncRNA	3.87	5.97	0.007410027	0.2853643
Gm43134	lncRNA	5.91	18.66	0.001489502	0.11499306
Gm43131	lncRNA	2.33	5.19	0.009850489	0.32709163

Gm29811	lncRNA	1.32	4.33	0.005797566	0.2552615
Gm42879	TEC	2.15	33.62	7.03E-05	0.01511884
Gm32914	lncRNA	7.73	16.83	0.001306915	0.10510095
Gm44198	TEC	1.42	14.28	0.000603161	0.06404628
4930448A20Rik	lncRNA	29.88	12.24	0.00051481	0.05804613
Gm45212	TEC	1.60	6.77	0.003264287	0.179975
Gm44707	lncRNA	1.42	3.01	0.009079597	0.31538521
Gm45164	lncRNA	2.20	3.46	0.002910507	0.16932032
Gm44843	TEC	1.41	32.21	0.00947719	0.32166092
Gm32352	lncRNA	1.76	4.01	0.009342658	0.31998117
BC049987	lncRNA	1.02	3.59	0.005811476	0.2552615
Gm47205	TEC	1.27	11.39	0.007047742	0.27913434
Gm47430	lncRNA	1.25	20.78	0.000316646	0.04188361
Gm46440	lncRNA	1.27	9.71	0.00119606	0.09987177
5930438M14Rik	lncRNA	1.47	5.86	0.000239264	0.03685682
1700087I21Rik	lncRNA	5.59	2.72	0.0073828	0.2853643
Gm49492	lncRNA	4.74	4.43	0.007782922	0.29213069
Gm49636	lncRNA	2.59	14.17	0.001766195	0.12708474
Gm49586	lncRNA	1.14	10.44	0.003584105	0.18998074
6330415G19Rik	lncRNA	1.43	4.92	0.002816871	0.16593241
Gm50393	TEC	2.60	4.46	0.004911156	0.23242496
Gm10040	pseudogene	52.47	12.99	0.000303128	0.0409298
Gm4825	processed_pseudogene	1.27	4.04	0.005849846	0.25565252
Gm10319	transcribed_unprocessed_pseudogene	1.02	9.82	0.004705101	0.22702806
Gm41	unprocessed_pseudogene	3.58	5.35	0.000877055	0.08414342
Gm12030	processed_pseudogene	3.43	109.43	0.000103176	0.0201506
Gm11897	processed_pseudogene	1.91	10.73	0.007754213	0.29213069
Gm11927	processed_pseudogene	3.58	7.19	0.001447377	0.11266882
Gm11988	processed_pseudogene	8.85	11.84	0.005888165	0.25622888
Gm14006	processed_pseudogene	1.91	8.16	0.006367539	0.26716794
Gm13193	processed_pseudogene	2.11	61.96	0.004251053	0.21294853
Gm14363	processed_pseudogene	2.45	4.38	0.00499584	0.23450429
Gm12182	processed_pseudogene	5.96	17.07	0.003495777	0.18765454
Alms1-ps2	transcribed_unprocessed_pseudogene	1.35	2.46	0.007807861	0.29213069
Gm6283	processed_pseudogene	1.41	7.33	0.005148819	0.23995987
Gm18848	processed_pseudogene	10.12	7.38	0.0024396	0.15452844
Gm21122	processed_pseudogene	3.57	5.12	0.006398418	0.26743755
Gm29633	transcribed_unprocessed_pseudogene	4.81	12.80	0.000251176	0.03830069
Gm37770	processed_pseudogene	10.12	11.74	0.009624076	0.32391404
Gm37501	processed_pseudogene	48.64	12.26	0.00176045	0.12708474

Gm30652	processed_pseudogene	4.81	18.68	0.008477695	
Gm29754	processed_pseudogene	4.81	12.36	0.004875119	0.23154783
Olfr1285	transcribed_unprocessed_pseudogene	5.73	10.41	0.002597272	0.15928804
Gm17794	processed_pseudogene	5.96	17.23	0.002383321	0.15213842
Gm6353	processed_pseudogene	20.47	8.73	0.003098207	0.17525746
Gm47706	processed_pseudogene	1.85	4.99	0.005804092	0.2552615
Gm18313	processed_pseudogene	4.32	5.25	0.001897511	0.13360347
Gm19222	processed_pseudogene	1.04	11.92	0.000228443	0.03583578
Gm18930	processed_pseudogene	1.91	5.23	0.003825965	0.19831552
Gm4116	processed_pseudogene	5.96	8.02	0.00368499	0.19345315
Zfp520-ps	processed_pseudogene	2.33	12.20	0.001697749	0.12546133
Gm34967	processed_pseudogene	3.58	35.26	0.001232877	0.10151724

4.4 Discussion

In this chapter, we show that, in contrast to our previous *in vitro* results indicating that *Ddx1*$^{-/-}$ embryos stall at the 2-4 cell stage *in vitro*, very few *Ddx1*$^{-/-}$ embryos survive to the 2-cell stage *in vivo* (Hildebrandt, Wang et al. 2019). This conclusion is based on two separate lines of investigations: genotyping data and cultures of 1- and 2-cell embryos. The latter were carried out using both KSOM and M16 culture media, with similar results obtained for both media. Thus, *Ddx1*$^{-/-}$ related embryonic lethality *in vivo* occurs pre-2-cell stage. Unlike other zygotic proteins shown to cause embryonic lethality at the 2-cell stage (e.g. *Ddx20*, *Pp2cβ*, *Pfn1* or *Ercc2*), we detected little to no difference in DDX1 protein levels in heterozygous female oocytes compared to wildtype oocytes (de Boer, Donker et al. 1998, Witke, Sutherland et al. 2001, Sasaki, Ohnishi et al. 2007, Mouillet, Yan et al. 2008, Hildebrandt, Germain et al. 2015, Hildebrandt, Wang et al. 2019). Therefore, these results suggest that the early embryonic lethality caused by the absence of zygotic *Ddx1* may not be related to the malfunction of maternal oocytes. Since it has been reported that two waves of ZGA take place during mouse embryonic development, *Ddx1* transcription may be required during the first wave of ZGA which takes place at the 1-cell stage (Li, Zheng et al. 2010). To validate this idea, we used RT-qPCR to examine the expression of the gene trap *β-gal* in the progeny of wildtype female and heterozygous male crosses. Our results indicate that *β-gal* is expressed in 1-cell embryos suggesting that zygotic *Ddx1* transcription is triggered at the 1-cell stage.

Evidence presented in Chapter 3 suggests that DDX1-containing MARVs are involved in the spatial distribution of Ca^{2+} as well as regulation of mtROS levels. In 1998, Chandel et al. showed that 5% O_2 (physiological conditions) increases ROS production by mitochondria in human Hep3B hepatoma cells (Chandel, Maltepe et al. 1998). Thus, the difference in O_2 levels between *in vivo* (5%) and *in vitro* (20%) conditions, with accompanying increases in ROS levels under low O_2 conditions, may explain why *in vivo* conditions are more detrimental to *Ddx1*$^{-/-}$ embryos. However, we did not observe any stalled 1-cell embryos when embryos from heterozygous crosses were cultured in either 1% oxygen or 5% oxygen (Godbout lab unpublished data), suggesting the absence of 1-cell *Ddx1-/-* embryos. Alternatively, the reported drop in Ca^{2+} in the oviduct observed at E1.5 may place additional stress on *Ddx1*$^{-/-}$ embryos *in vivo* compared to the constant Ca^{2+} levels in culture (Lee and Kendle 1979). Irrespective of exact mechanisms, our results suggest that zygotic *Ddx1* may be required as early as the 1-cell stage.

DDX1 is known to bind RNA and to unwind RNA-RNA and RNA-DNA double-strand structures. As expected, DDX1 did not co-localize with ssDNA and dsDNA based on immunostaining. We were also not able to detect dsRNA co-localization with DDX1 based on immunostaining with the J2 dsRNA antibody. The immunostaining pattern observed with this antibody was similar to that observed with antibodies to DDX3, DDX6 and GW182, indicating that dsRNAs may be related to the potential roles of these proteins in embryonic development (our unpublished data). Thus, our results suggest that the RNA cores in DDX1 vesicles

either do not contain dsRNA, or that dsRNA structures cannot be detected by immunostaining with the J2 antibody.

Interestingly, the immunostaining obtained with the S9.6 RNA-DNA hybrid antibody showed localization throughout the cytoplasm of 2-cell embryos with the exception of MARVs. It is possible that the lack of DNA-RNA hybrids in DDX1 vesicles is due to DDX1's RNA-DNA unwinding activity. RNA-DNA hybrids were originally thought to exist mainly in the nuclei as well as the mitochondria in normal cells. However, in 2015, Koo et al. showed that RNA-DNA hybrids are also present outside the mitochondria in the cytoplasm of several human cell lines (Koo, Kobiyama et al. 2015). These RNA-DNA hybrids have been proposed to be involved in miRNA biogenesis. As DDX1 has been shown to play an essential role in miRNA maturation (Han, Liu et al. 2014), MARVs may serve as sites of RNA-DNA hybrid-related miRNA biogenesis. Moreover, cytoplasmic RNA-DNA hybrids have also been detected in pathogen-infected cells where they play a role in innate immune response (Theofilopoulos, Kono et al. 2011, Jounai, Kobiyama et al. 2012, Kailasan Vanaja, Rathinam et al. 2014, Rigby, Webb et al. 2014). Finally, as genomic imprints are removed at the 2-cell stage in embryos, it is possible that the resulting accumulation of retrotransposons and intermediate RNA/cDNA hybrids triggers a response similar to that of viral infection in early-stage embryos (Bourque, Burns et al. 2018, Yin, Zhou et al. 2018).

Our RIP-seq experiments were designed to identify the RNAs bound by DDX1 in 2-cell embryos. RIP-seq experiments were also used to validate the RT-PCR results presented in Chapter 2. We were faced with a number of challenges in our attempts to identify RNA targets of DDX1 in 2-cell embryos. Notably, there are no designated sequencing pipelines for RIP-seq analysis. We therefore used two surrogate pipelines: CLIPSeqTools (CLIP-seq analysis pipeline) and featureCounts followed by DESeq2 (RNA-seq analysis pipeline). Based on PANTHER database analysis, the genes identified in our RIP-seq experiments did not show any specific patterns with respect to molecular function or biological pathways (Thomas, Campbell et al. 2003, Mi, Muruganujan et al. 2013). As well, our two RIP-seq experiments generated different putative targets. There are many reasons for this discrepancy. (1) Our first RIP-seq experiment was done with only 1 control and 2 DDX1 immunoprecipitations, thereby not allowing p-value filtering. (2) The samples were prepared using different methods. (3) RNA yields from our RNA-immunoprecipitations experiments were extremely low, requiring amplification. In the first experiment, the RNA was amplified by RT-PCR after adapter ligation. In the second experiment, we used a linear amplification method which is less prone to artefacts. (4) We used random hexamer reverse transcription for the first experiment and did not shear either the RNA or the cDNA. In the second experiment where we used a vector-based QIAGEN kit the vectors were sheared followed by adapter ligation, potentially introducing bias as the result of two independent transcripts being ligated together, leading to alignment error.

In spite of differences in protocols, we were able to identify a number of potential RNA targets of DDX1 by comparing both sets of RNA-seq experiments obtained using either the CLIP-seq pipeline (390 genes) or theRNA-seq pipeline (159 genes). Perhaps most noteworthy is the large number of non-protein-coding RNAs identified using the RNA-seq pipeline, with ~40% of the non-protein-coding RNAs identified as transcripts from pseudogenes. Pseudogenes are essential for the biogenesis of endogenous siRNAs involved in the control of retrotransposons and degradation of maternal RNAs during oocyte maturation and zygotic genome activation at 2-cell stage (Babiarz, Ruby et al. 2008, Lykke-Andersen, Gilchrist et al. 2008, Claycomb 2014, Stein, Rozhkov et al. 2015, Kong, Quan et al. 2019). Therefore, MARVs may serve as storage/protection units for pseudogene RNAs until they are processed into endogenous siRNAs.

In conclusion, we have shown that zygotic *Ddx1* is expressed in 1-cell embryos, and that absence of zygotic *Ddx1* can result in embryonic lethality between the 1-cell and 2-cell stages *in vivo*. The results suggest a requirement for zygotic *Ddx1* for embryonic development past the 1-cell stage. Thus, these data push the embryonic lethality caused by $Ddx1^{-/-}$ to an even earlier stage than previously documented *in vitro*. Based on our immunostaining data, neither dsRNA nor RNA-DNA hybrids co-localize with DDX1 vesicles. However, the absence of DNA-RNA hybrids in MARV aggregates in 2-cell embryos, combined with the large number of pseudogene transcripts preferentially bound by DDX1, suggest the interesting possibility that DDX1 and MARVs may play critical roles in

retrotransposon and endogenous siRNA-mediated protection/regulation of maternal RNAs.

Chapter 5.

Discussion and future directions.

5.1 Discussion

As early-stage mouse embryonic development relies heavily on maternal RNA and proteins, the vast majority of contributors to 1- to 4-cell embryonic developmental arrest are of maternal origin (Li, Zheng et al. 2010). The absence of maternal RNA can affect the fusion of pronuclei (Wu, Viveiros et al. 2003), chromatin remodeling (Burns, Viveiros et al. 2003, Bultman, Gebuhr et al. 2006, Torres-Padilla and Zernicka-Goetz 2006, Philipps, Wigglesworth et al. 2008), genomic imprinting (Bourc'his, Xu et al. 2001, Kaneda, Okano et al. 2004), as well as the quality of the mitochondria (Fernandes, Tsuda et al. 2012). So far, knock-out of only a few genes has been shown to cause embryonic arrest at the 1- to 4-cell stages. The results from this thesis indicate that *Ddx1* can be added to the list of genes that results in embryonic lethality at the 1- to 4-cell stages. Our data suggest that DDX1 is responsible for the formation of membrane-bound vesicles that cluster in ring-like structures which we have named Membrane Associated RNA-containing Vesicles (MARVs). MARVs contain proteins, RNAs, as well as Ca^{2+}. The loss of zygotic DDX1 causes a dramatic decrease in MARVs which in turn leads to disruption in Ca^{2+} distribution and upregulation of mitochondrial ROS. Thus, increased production of ROS may underlie the nuclear and mitochondrial fragmentation observed in *Ddx1*$^{-/-}$ embryos. Intriguingly, the RNAs located inside each DDX1-containing vesicle that make up MARVs exist in the form of a core-like structure. This core of RNA may be analogous to that formed by lipid-lipid phase separation (LLPS) associated with stress granules and P-bodies (Hondele,

Sachdev et al. 2019). In addition to DDX1 which has previously been implicated in polyadenylation (Bleoo, Sun et al. 2001), MARVs contain cytoplasmic polyadenylation factors, CPEB1 and CPSF2, suggesting that MARVs may be cellular compartments for cytoplasmic polyadenylation-related processes after fertilization.

5.1.1 MARVs, calcium and mitochondria

Cellular compartments, both membrane-bound organelles and membrane-less compartments, are found in the cytoplasm of eukaryotic cells (Aguilera-Gomez and Rabouille 2017). As these compartments are separated from the bulk cytoplasm, they can provide protected spaces for chemical reactions and toxic metabolic intermediates, as well as improve the efficiency of biologically-related processes. There is accumulating evidence indicating that membrane-less compartments behave like fluid droplets which are formed by liquid-liquid phase separation (LLPS) (Courchaine, Lu et al. 2016). Unlike the formation of membrane-bound organelles which are time and energy consuming (Courchaine, Lu et al. 2016), membrane-less compartments in the cytoplasm tend to be used for shorter-lived cellular compartments such as stress granules and P-bodies in response to certain cellular events, and resolving rapidly upon the termination of such events (Hondele, Sachdev et al. 2019). Although more energy consuming compared to LLPS compartments, membrane-bound organelles serve as much more than “separation” compartments from bulk cytoplasm. Membrane-bound organelles

serve as communication hubs, not only via intracellular signalling through receptors located on the organelle membranes, but also by exchanging materials with small vesicles transporting cargo through intracellular and intercellular networks. Importantly, membranes allow these organelles to confine anions such as Ca^{2+} and act as storage units (Kline, Mehlmann et al. 1999, Hoppe 2010, Patergnani, Suski et al. 2011, Raffaello, Mammucari et al. 2016). The major Ca^{2+} storage units in the cell are membrane-bound ER, mitochondria, as well as lysosomes, with ER being the largest Ca^{2+} storage unit (Raffaello, Mammucari et al. 2016).

Similar to somatic cells, the ER is also the major Ca^{2+} storage unit in oocytes (Dumollard, Duchen et al. 2006, Ducibella and Fissore 2008, Miao and Williams 2012, Wakai, Zhang et al. 2013). During fertilization, sperm trigger Ca^{2+} release from ER resulting in Ca^{2+} oscillation (a.k.a Ca^{2+} waves) in the fertilized mouse oocyte (Kline, Mehlmann et al. 1999, Knott, Kurokawa et al. 2005). However, little is known about the Ca^{2+} storage compartments in 2- to 4-cell stage embryos. In 2006, Manser and Houghton reported that Ca^{2+} forms large aggregates at the subplasmalemmal cytoplasm of early-stage embryos (Manser and Houghton 2006). Even though these aggregates can easily be mistaken for the cortical ER reported in oocytes where Ca^{2+} is stored (Kline, Mehlmann et al. 1999), Manser and Houghton postulated a different location for Ca^{2+} aggregates such as caveolae or cortical granules. Experiments designed to address this possibility showed that Ca^{2+} aggregates do not co-compartmentalize with markers for caveolae and

cortical granules in early-stage embryos (Manser and Houghton 2006). Based on our research, Ca^{2+} aggregates co-localize with MARVs which first appear in late 1-cell mouse embryos and last until early blastocyst. It is noteworthy that we were not able to find co-localization between DDX1 and markers for a variety of cytoplasmic bodies/aggregates/organelles in early-stage embryos. Therefore, the formation of MARVs may be a fertilization dependent event that is specifically needed in early-stage embryos. We find it very interesting that MARVs are membrane-bound organelles as opposed to the more transient LLPS compartments which would be equally effective at compartmentalizing RNAs. We thus propose that MARVs are required for the confinement of Ca^{2+} combined with Ca^{2+}-dependent RNA regulation.

Similar to somatic cells treated with the inhibitor of mitochondrial oxidative phosphorylation FCCP, 2-cell embryos treated with FCCP have increased cytoplasmic Ca^{2+} (Manser and Houghton 2006). FCCP also disrupts Ca^{2+} microdomains at the subplasmalemmal cytoplasm of 2-cell embryos. When combined with our results, these results suggest that FCCP may cause the release of Ca^{2+} from MARVs, similar to what has been observed in somatic cells, except that in somatic cells, the ER is the Ca^{2+} storage unit instead of MARVs (Eaddy and Schnellmann 2011). It is well known that ER-mitochondria interact with each other in somatic cells through the mitochondria-associated membrane (MAM) with multiple tethering complexes to ensure proper signal transduction between the two organelles (Lee and Min 2018). Although both organelles have been shown to play

important roles in cellular Ca^{2+} homeostasis, mitochondria often rely on ER Ca^{2+} transfer through the MAM to stimulate oxidative phosphorylation and the TCA cycle for ATP production or control cell death such as autophagic cell death and apoptosis. (Kaufman and Malhotra 2014). Ca^{2+} transfer between ER and mitochondria is mainly through the IP_3R-Grp75-VDAC complex (introduced in section 1.3.5) where the VDAC forms a Ca^{2+} channel on the outer mitochondrial membrane. After passing though the outer membrane, the Ca^{2+} is then taken up by the mitochondrial calcium uniporter (MCU) located on the inner mitochondrial membrane (Lee and Min 2018). However, it has also been reported that the outer mitochondrial membrane is permeable to small molecules <10 kDa, in contrast to the inner membrane which is completely impermeable even to small molecules (except for O_2, H_2O and CO_2) (Patergnani, Suski et al. 2011). Therefore, Ca^{2+} can pass through the outer membrane while following an ion gradient without VDAC, but can only pass through the inner mitochondrial membrane via the MCU. These results indicate that while IP_3R-Grp75-VDAC may act as a tethering complex to improve Ca^{2+} transfer, VDAC may not be essential for Ca^{2+} entry into the outer mitochondrial membrane. Thus, proximity, along with an ion gradient, may also be important factors in controlling Ca^{2+} transfer from ER to mitochondria. Unlike the close connection between ER and mitochondria which are typically located within 100 nm of each other (minimum of 10-25 nm), MARVs and mitochondria are much further apart (>200 nm) indicating that MARVs may not be close enough to form a similar complex as IP_3R-Grp75-VDAC for Ca^{2+} transfer to mitochondria through

the VDAC tunnel. In agreement with this, a recent study has demonstrated that although MCU is present in oocyte mitochondria, VDAC does not appear to localize to oocyte mitochondria (Wang, Meng et al. 2020).

Mitochondria from oocyte to pre-blastocyst stage have a distinct morphology compared to mitochondria found in somatic cells. The mitochondria in oocyte and early embryos have been described as “immature” as they are smaller in size, more electron dense, have fewer numbers of cristae, and consume less oxygen compared to regular mitochondria (Dumollard, Marangos et al. 2004, Reader, Stanton et al. 2017). In spite of their “immature” mitochondria, oocytes and early embryos rely heavily on mitochondria for their metabolism (Dumollard, Marangos et al. 2004, Dumollard, Duchen et al. 2007). Oocyte mitochondria are abundant but function suboptimally to reduce the production of toxic mtROS (Dumollard, Duchen et al. 2007). With Ca^{2+} being a main stimulator of the TCA cycle and oxidative phosphorylation for energy production, Ca^{2+} distribution needs to be tightly controlled in order to regulate mitochondria function (Brookes, Yoon et al. 2004, Peng and Jou 2010). Thus, the normal Ca^{2+} release from ER to mitochondria may not be suitable or applicable in early-stage embryos. Although more work needs to be done, we propose that the release of Ca^{2+} from MARVs may be controlled by the distance and local concentration of MARVs in relation to mitochondria.

Consistent with our proposed role for MARVs in Ca^{2+} segregation, we showed in Chapter 3 that disruption of MARVs in *Ddx1*$^{-/-}$ embryos results in stalled 2- to 4-cell stage embryos with disrupted Ca^{2+} distribution, upregulation of mitochondrial membrane potential, increased mtROS production, and nuclear and mitochondrial fragmentation. Although we do not know the sequence of these events, we postulate that disruption of Ca^{2+} is the root cause for this series of events. As mentioned above, Ca^{2+} is needed to stimulate mitochondrial ATP production which is accompanied by mtROS production. Therefore, a change in Ca^{2+} balance could have a profound effect on embryonic development. For example, although mtROS is essential for embryonic development (Han, Ishibashi et al. 2018), overproduction of mtROS can lead to oxidative stress and embryonic lethality (Liu, Trimarchi et al. 2000, Dumollard, Duchen et al. 2007). Thus, the relatively smaller isolated MARV units may be more beneficial to the embryos than the interconnected ER, as they allow a more precise control of Ca^{2+} distribution in embryos.

In summary, we propose that MARVs are structures whose purpose is to control the spatial distribution of Ca^{2+} within early-stage embryos such that mitochondria activity is precisely regulated to control ROS production and minimize ROS-induced damage to the embryos.

5.1.2 DDX1, MARVs and RNA regulation

Besides Ca^{2+}, we have also found that MARVs contain RNAs. As the compartmentalization of RNAs and RNA storage can easily be achieved by LLPS, one needs to question whether membrane-bound DDX1 vesicles and the formation of MARVs are required for RNA-related functions associated with these structures. In this regard, it's important to note that the RNA in DDX1 vesicles is not simply being separated from the bulk cytoplasm of the embryos, but that it forms a LLPS-compartment-like core within each DDX1 vesicle suggesting some structural-functional relationship within the vesicles. Proteins associated with LLPS compartments such as stress granules include TIA-1, TIAR, CPEB1, as well as DDX1, all of which are also found in MARVs, further supporting functional similarities between LLPS compartments and the RNA core within the DDX1 vesicles. As DEAD box proteins have been shown to function as scaffold proteins that recruit cofactors for the unwinding of RNA-RNA duplexes, it is possible that DDX1 in MARVs play a role in the temporal disassembly of the RNA cores with ATP/ADP provided by mitochondria. After the disassembly of the RNA cores, these RNAs may undergo additional processes such as cytoplasmic polyadenylation within MARVs prior to their functions in bulk cytoplasm.

In Chapter 4, we used RIP-seq to identify RNAs bound by DDX1 in 2-cell embryos. We found that ~40% of the DDX1-bound RNAs encode proteins. Maternal mRNAs are deadenylated to prevent premature translation. These short-poly(A) tail mRNAs must be activated by cytoplasmic polyadenylation before they can be translated. The presence of CPSF2 along with CPEB1 in MARVs are strong

indicators of cytoplasmic polyadenylation-related events taking place in MARVs. Therefore, we suggest that the protein-encoding mRNAs bound by DDX1 in 2-cell embryos are pre-translation deadenylated mRNAs.

Oocytes store large quantities of maternal RNAs (Olszanska and Borgul 1993). During oocyte maturation and embryonic development, cytoplasmic mRNAs need to be polyadenylated, a process that occurs at different stages to allow for temporally controlled activation of these mRNAs (Winata and Korzh 2018). Oocyte growth is accompanied by the loss of P-bodies and the appearance of subcortical aggregates (SCAs) at the subplasmalemmal cytoplasm of GV oocytes. However, the absence of the decapping protein DCP-1 in the SCAs suggests that these SCAs may be RNA storage units rather than degradation units such as P-bodies (Tang, Kaneda et al. 2007, Lykke-Andersen, Gilchrist et al. 2008, Zhang, Hou et al. 2020). For the first two waves of cytoplasmic polyadenylation that take place during oocyte growth and maturation before fertilization, the presence of CPEB1 in the SCAs suggests a role in cytoplasmic polyadenylation (Suh, Baehner et al. 2010). Interestingly, although thousands of maternal RNAs are polyadenylated during the third and last wave of cytoplasmic polyadenylation which takes place after fertilization (Subtelny, Eichhorn et al. 2014), the SCAs have already disappeared by the MII stage of oocyte maturation (Babiarz, Ruby et al. 2008, Lykke-Andersen, Gilchrist et al. 2008, Claycomb 2014, Stein, Rozhkov et al. 2015, Kong, Quan et al. 2019). This suggests that a different structure/complex may replace SCAs after fertilization to facilitate the last wave of cytoplasmic

polyadenylation required for embryos to undergo maternal-to-zygotic transition (Han, Liu et al. 2014). As CPSF2 and CPEB1 are essential for cytoplasmic polyadenylation (Paillard, Maniey et al. 2000, Vishnu, Sumaroka et al. 2011), for the recognition of the polyadenylation signal and cytoplasmic polyadenylation element, respectively, we suggest that MARVs may replace SCAs during early development.

To obtain further evidence for cytoplasmic polyadenylation in MARVs, we have tested for the presence of two additional proteins needed for cytoplasmic polyadenylation, GLD2 and PARN. GLD2 is a poly(A) polymerase that's needed for cytoplasmic polyadenylation in *Xenopus*, *C. elegans* and *Drosophila*, whereas PARN is a poly(A)-specific ribonuclease needed for the deadenylation of the cytoplasmic mRNAs in *Xenopus* and *C. elegans* (Bourque, Burns et al. 2018). However, we did not observe co-localization of DDX1 with either GLD2 or PARN (data not shown). These results suggest that other polymerases and ribonucleases may be needed for cytoplasmic polyadenylation in mouse oocytes and embryos. Indeed, investigators have shown that although both GLD2 and PARN are found in mouse oocytes, they are not essential for oocyte maturation due to the abundance of a variety of proteins with similar functions (Jachowicz, Bing et al. 2017). In light of the presence of CPEB1 and CPSF2 in MARVs along with our previous finding that DDX1 is associated with polyadenylation (Bleoo, Sun et al. 2001), we propose that MARVs are sites of cytoplasmic polyadenylation during early embryonic development in mouse.

To our surprise, aside from the protein-coding mRNAs, our DDX1 RIP-seq data revealed that –~20% of DDX1 binding RNAs were from processed pseudogenes along with ~24% of long non-coding RNAs (lncRNAs). Pseudogenes have been shown to be important for the generation of endogenous small interfering RNAs (endo-siRNAs) required for the regulation of retrotransposons and maternal RNAs in developing embryos (Huarte, Stutz et al. 1992, de Moor and Richter 1999, Richter 1999). While little is known about endo-siRNA metabolism with respect to cytoplasmic polyadenylation, it has recently been shown that cytoplasmic polyadenylation of lncRNAs contributes to pseudogene-related endo-siRNA biogenesis (Karlic, Ganesh et al. 2017, Svoboda 2017). The significance of this observation is not clear, especially in light of sequencing data showing that endo-siRNAs and miRNAs in 1- to 2-cell embryos undergo cytoplasmic polyadenylation events to evade the massive maternal RNA degradation (Yang, Lin et al. 2016) which takes place in early embryonic development (Radford, Meijer et al. 2008, Flemr, Ma et al. 2010, Stoecklin and Kedersha 2013). Therefore, it's possible that MARVs are hubs not only for the cytoplasmic polyadenylation of maternal protein-coding mRNAs, but also for lncRNAs and small RNAs.

It seems paradoxical that although both MARVs and SCAs are potentially involved in cytoplasmic polyadenylation, the first consists of membrane-bound DDX1 vesicles that first appear after fertilization, whereas the latter are LLPS compartments present in maturing oocytes. We propose that the RNA cores found in MARVs may require an additional layer of control compared to LLPS

compartments. By this, we mean that a barrier must be maintained to separate these RNAs from the bulk cytoplasm. Since MARVs contain Ca^{2+}, and Ca^{2+} is responsible for the phosphorylation and activation of the essential cytoplasmic polyadenylation factor CPEB1 (Subtelny, Eichhorn et al. 2014), we propose the following sequence of events for the cytoplasmic polyadenylation of RNAs in MARVs: (i) DDX1 resolves RNA structures within the RNA cores, thus exposing the RNAs; (ii) Ca^{2+} within MARVs facilitates the phosphorylation of CPEB1; and (iii) CPEB1 and CPSF2 initiate the cytoplasmic polyadenylation and the polyadenylated RNAs are released for downstream processes **(Fig. 5.1)**. Since DDX1 is an RNA helicase which alters RNA structure in an ATP/ADP-dependent manner, the cytoplasmic polyadenylation process which takes place in MARVs likely requires efficient mitochondrial function to ensure an adequate ATP/ADP supply. The need for an adequate ATP/ADP supply could also contribute to the gradual aggregation of MARVs as embryos proceed to the blastocyst stage.

To conclude, we have present evidence that DDX1 is needed for the formation of a new organelle, containing cytoplasmic polyadenylation factors, RNAs and Ca^{2+}, whose absence can result in early embryonic lethality. This discovery can potentially lead to a further understanding of how maternal mitochondria function is regulated during the rapid division of mammalian embryos. Moreover, as no RNA regulating germ cell granules have been discovered in mature mammalian gametes and early-stage mammalian embryos, the discovery

of MARVs may have potential implication in further understanding the similarity in embryonic development between mammalian and other organisms.

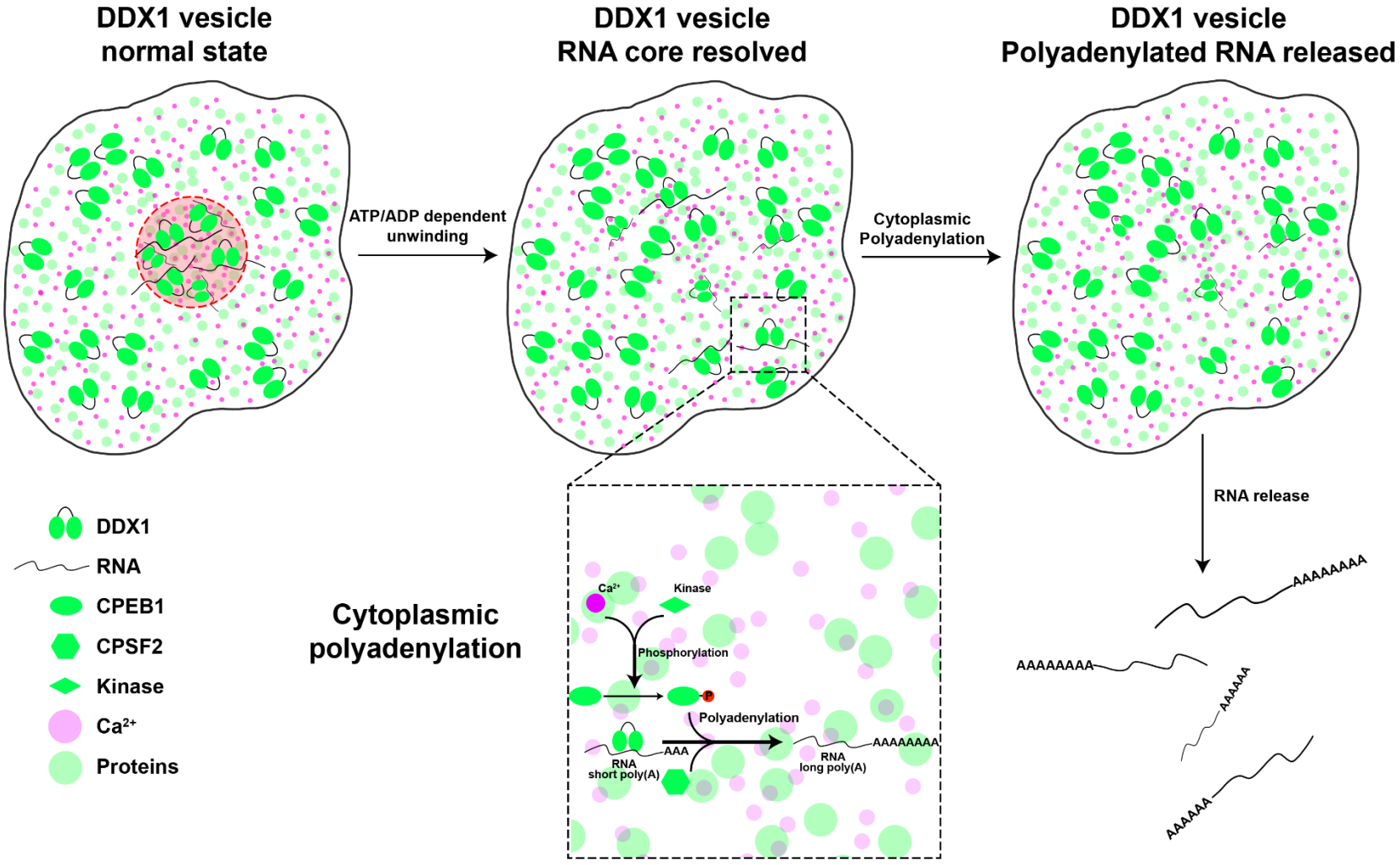
DDX1 vesicle
normal state
ATP/ADP dependent
unwinding
DDX1 vesicle
RNA core resolved
Cytoplasmic
Polyadenylation
DDX1 vesicle
Polyadenylated RNA released
RNA release
DDX1
RNA
CPEB1
CPSF2
Kinase
Ca2+
Proteins
Cytoplasmic
polyadenylation
Ca2+
Kinase
Phosphorylation
P
Polyadenylation
AAA
AAAAAAAA
RNA
short poly(A)
RNA
long poly(A)
AAAAAAAA
AAAAAAAA
AAAAAA
AAAAAA

Figure 5.1 Graphical demonstration of the role of DDX1-containing vesicles in polyadenylation.

5.2 Future directions

5.2.1 Ddx1 transgenic phenotype

Even though not part of this thesis, wild-type *Ddx1*$^{*/*}$ embryos have also been shown to be embryonic lethal albeit at a later developmental stage (post-implantation) (Hildebrandt, Germain et al. 2015). This *Ddx1** allele appears after 2 sequential heterozygous intercrosses. As the levels of DDX1 RNA and protein are essentially the same in *Ddx1*$^{+/+}$ and *Ddx1*$^{+/-}$ mice, we have hypothesized that the *Ddx1** allele may be capable of producing twice the amount of DDX1 normally produced by one allele. Thus, the embryonic lethality associated with *Ddx1*$^{*/*}$ may be caused by excessive production of DDX1 (4X) in the embryos.

The previous chapters have demonstrated that DDX1 may play a role in the formation of MARVs which may be important for maternal RNA cytoplasmic polyadenylation as well as embryonic mitochondrial function. When an excessive amount of DDX1 is produced, these activities may be affected. It has long been known that the number of embryonic mitochondria remains the same from MII stage oocytes to blastocysts, at which time mitochondria start to replicate (Piko and Matsumoto 1976, Piko and Clegg 1982, Piko and Taylor 1987). Since MARVs disappear and DDX1 starts entering the nucleus at the same developmental stage

as mitochondria start replicating (i.e. the blastocyst stage) (Hildebrandt, Wang et al. 2019), there may be an association between MARVs, cytoplasmic DDX1 and mitochondrial replication. To test mitochondrial replication and mitochondrial function in *Ddx1*$^{*/*}$, mitochondrial staining dyes such as MitoTracker and JC-1 could be used to quantify mitochondrial activity in blastocyst embryos.

Another possibility could be that excessive DDX1 in *Ddx1*$^{*/*}$ affects the cytoplasmic polyadenylation and translation of maternal mRNAs. DEAD box proteins have already been shown to play roles in resolving the aggregation of RNAs in LLPS compartments (Hondele, Sachdev et al. 2019). In the presence of excessive amounts of DDX1, maternal RNAs may not be regulated properly during development. For example, excessive DDX1 may result in abnormal unwinding of maternal RNAs leading to improper release of these RNAs at the wrong developmental stages. To systematically address this possibility, single embryo RNA sequencing at different developmental stages needs to be carried out on the pre-implantation embryos from *Ddx1*$^{*/-}$ heterozygous intercrosses.

5.2.2 Identification of the origin of MARVs

In Chapter 3, we identified a new membrane-bound organelle which we named MARVs. Although organelles have been studied since the 1800s, the *de novo* formation of organelles (building organelles from scratch) still remains unclear. The better-known mechanism is to generate membranes through existing

organelles such as ER (Joshi, Zhang et al. 2017). We have found in Chapter 4 that the transcription of zygotic *Ddx1* is needed at the 1-cell stage *in vivo* which is around the same time as the formation of DDX1 vesicles as well as MARVs. This indicates that the formation of MARVs may be related to the newly transcribed *Ddx1* mRNAs or translated DDX1 proteins. Given the role of ER in protein synthesis, organelle biogenesis and Ca^{2+} distribution, we postulate that MARVs may be generated from ER.

To validate this hypothesis, we can perform *in vitro* fertilization where we can trace the embryos through the different developmental stages from MII stage oocyte to 2-cell stage embryos or later. We can visualize the formation of the DDX1 vesicles in two ways. Firstly, we could use Spinning Disk Confocal microscopy to perform live cell imaging as the embryos develop. Briefly, as Fluo-4 AM is not toxic to live cells, we can use this Ca^{2+} marker to see if and how Ca^{2+} directly migrates from ER to MARVs following fertilization. Another approach would be the microinjection of GFP-tagged DDX1. As oocyte *Ddx1* transcripts undergo massive degradation (~3X reduction) upon fertilization, it would be better if we could inject recombinant GFP-tagged DDX1 protein. Secondly, we can also perform TEM to manually trace the IVF embryos at different time points after fertilization. This method would allow better visualization of the budding of DDX1 vesicles and their aggregation into MARVs. However, there are some disadvantages to this method. To perform TEM imaging, the embryos need to be fixed and therefore, we will not be able to trace the formation MARVs in live embryos. Without live cell imaging,

we will need a large number of embryos at different time points to capture the full sequence of events underlying MARV formation. Also, TEM only allows visualize of a section of the embryos at a time. With the combination of both techniques, we may be able to better characterize the origin of MARVs.

5.2.3 The binding targets of DDX1 and cytoplasmic polyadenylation

DDX1 belongs to the DEAD box family of RNA helicases and has been reported to unwind both dsRNAs and RNA/DNA duplexes (Li, Monckton et al. 2008, Kellner, Reinstein et al. 2015, Li, Germain et al. 2016). In Chapter 4, we performed both immunostaining as well as RIP-seq analysis to identify potential DDX1 binding substrates. None of the antibodies tested (i.e. antibodies targeting dsDNA, ssDNA, dsRNA and RNA/DNA hybrids) showed co-localization to DDX1. These data are preliminary and experiments need to be repeated with additional controls. As a positive control, for example, we could include dsDNA and ssDNA staining in ATM-deficient cells which is known to increase levels of fragmented genomic DNA in the cytoplasm (Song, Ma et al. 2019). In addition, we could use different approaches to investigate the presence of different nucleic acid structures in embryos, such as RNase H treatment to specifically degrade the RNA-DNA hybrids, followed by S9.6 antibody staining to ensure the specificity of this antibody. We could also carry out DDX1 antibody DNA-RNA immunoprecipitations (DRIP) followed by PCR or sequencing to detect RNA-DNA hybrids (Halasz, Karanyi et al. 2017). We are particularly interested in the possibility that RNA-DNA hybrids exist

in early embryos because of recently discovered cytoplasmic DNA outside the mitochondria (Asada, Ito et al. 2018). The cGAS-STING pathway has been shown to serve as a sensor for cytoplasmic DNA resulting from DNA damage and viral infection. Although, to our knowledge, no one has shown a connection between early-stage embryos and cGAS-STING (Gamdzyk, Doycheva et al. 2020, Zhang, Liu et al. 2020), it would be interesting to see if there are fragmented DNAs or RNA-DNA hybrids in early-stage embryos resulting from DNA damage or retrotransposon activity (discussed in section 5.2.3).

Further sequencing experiments will be required to resolve the polyadenylation status of the binding targets of DDX1. For example, the progeny of *Ddx1* heterozygous crosses could be used for single embryo sequencing. To determine the poly(A) tail length of the global RNAs in 2-cell embryos, PAIso-seq could be used as it's applicable to small amounts of RNA (Liu, Nie et al. 2019). Once we have a better idea of poly(A) tail length, we can perform cluster analysis to determine if ~25% of the embryos are systematically different from the remaining 75%. Alternatively, if the DDX1 binding targets are identified, the Poly(A) Tail-Length Assay Kit (ThermoFisher) can be used to determine the poly(A) tail length of specific RNAs. These experiments will shed light not only on the binding targets of DDX1 but also the polyadenylation state of its binding targets.

Moreover, we were not able to distinguish between zygotic RNAs and maternal RNAs during early embryonic developmental stages as MZT is a

continuous event of maternal RNA degradation accompanied by zygotic RNA transcription. Based on the cordycepin data, it is possible that the formation/regulation of MARVs may be affected by zygotic transcription. But we were unable to distinguish between the protection/regulation of the RNAs that are already present in the vesicles and the RNAs that are being carried to the vesicles. However, we do not believe that the main function of MARVs is to regulate newly transcribed RNAs as the knockout of *Tia-1/Tiar*, which functions as RNA transporting factors in SGs, causes embryonic lethality at E11.5. If the main function of MARVs were to regulate zygotic RNAs then we would expect *Tia-1/Tiar* knockout to be equally deadly to the embryos. However, we cannot exclude the possibility that the presence of maternal TIA-1 and TIAR can prolong the survival of *Ddx1*$^{-/-}$ embryos. To further address the origin of the RNAs inside MARVs, we could inhibit zygotic transcription with cordycepin or α-amanitin and examine the appearance and abundance of RNA cores inside MARVs. If so, this would support the RNA cores being of zygotic origin. However, a significant disadvantage to transcription blockade is that blocking ZGA may be detrimental to the embryo. Therefore, it may not be possible to obtain meaningful data using this approach. Also, it would be interesting to examine the DDX1 and MARVs distribution in *Tia-1/Tiar* knockout embryos.

5.2.4 Impact of tissue specific Ddx1 knockout

So far, we have only been able to carry out limited analysis of *Ddx1* knockout mice due to the early embryonic lethality. However, *Drosophila* homozygous knockouts are viable, likely because maternal Ddx1 can be detected until the 2nd instar (Germain, Li et al. 2015). Therefore, it would be informative to see the effect of *Ddx1* homozygous knockout in different tissues. To generate tissue-specific knockout mice, we would use a conditional knockout with CRE/LoxP recognition sites partnered with FRT trap (Chaiyachati, Kaundal et al. 2012). We would then use a Flp recombinase system to remove the reporter genes globally, followed by a tissue-specific Cre recombinase system to knockout the *Ddx1* allele in a specific tissue **(Fig. 5.2)**. This conditional knockout could provide valuable insight into the tissue specific function of DDX1 in mice.

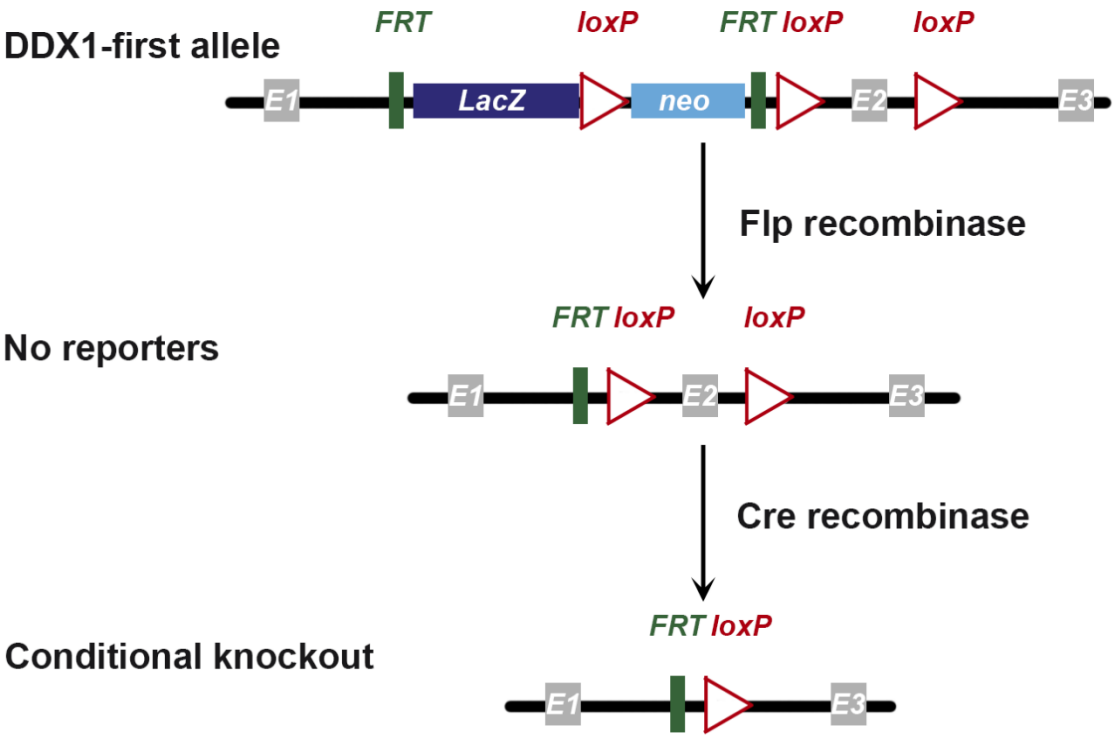

Figure 5.2 Graphical demonstration of possible steps in generating *Ddx1* conditional knockout.

References

Abbott, A. L. and T. Ducibella (2001). "Calcium and the control of mammalian cortical granule exocytosis." Front Biosci **6**: D792-806.

Abdelhaleem, M. (2005). "RNA helicases: regulators of differentiation." Clin Biochem **38**(6): 499-503.

Acton, B. M., A. Jurisicova, I. Jurisica and R. F. Casper (2004). "Alterations in mitochondrial membrane potential during preimplantation stages of mouse and human embryo development." Mol Hum Reprod **10**(1): 23-32.

Aguilera-Gomez, A. and C. Rabouille (2017). "Membrane-bound organelles versus membrane-less compartments and their control of anabolic pathways in Drosophila." Dev Biol **428**(2): 310-317.

Akiyama, K., Y. Akao, M. Yokoyama, Y. Nakagawa, T. Noguchi, K. Yagi and Y. Nishi (1999). "Expression of two dead box genes (DDX1 and DDX6) is independent of that of MYCN in human neuroblastoma cell lines." Biochem Mol Biol Int **47**(4): 563-568.

Albertini, D. F. (2018). "Making sense out of syngamy at the onset of mammalian development." J Assist Reprod Genet **35**(8): 1357-1358.

Amanai, M., M. Brahmajosyula and A. C. Perry (2006). "A restricted role for sperm-borne microRNAs in mammalian fertilization." Biol Reprod **75**(6): 877-884.

Amler, L. C., J. Schurmann and M. Schwab (1996). "The DDX1 gene maps within 400 kbp 5' to MYCN and is frequently coamplified in human neuroblastoma." Genes Chromosomes Cancer **15**(2): 134-137.

Andersen, C. B., L. Ballut, J. S. Johansen, H. Chamieh, K. H. Nielsen, C. L. Oliveira, J. S. Pedersen, B. Seraphin, H. Le Hir and G. R. Andersen (2006). "Structure of the exon junction core complex with a trapped DEAD-box ATPase bound to RNA." Science **313**(5795): 1968-1972.

Anderson, P. and N. Kedersha (2006). "RNA granules." J Cell Biol **172**(6): 803-808.

Anderson, P. and N. Kedersha (2008). "Stress granules: the Tao of RNA triage." Trends Biochem Sci **33**(3): 141-150.

Anderson, P. and N. Kedersha (2009). "RNA granules: post-transcriptional and epigenetic modulators of gene expression." Nat Rev Mol Cell Biol **10**(6): 430-436.

Anderson, P. and N. Kedersha (2009). "Stress granules." Curr Biol **19**(10): R397-398.

Andersson, D., N. Akrap, D. Svec, T. E. Godfrey, M. Kubista, G. Landberg and A. Stahlberg (2015). "Properties of targeted preamplification in DNA and cDNA quantification." Expert Rev Mol Diagn **15**(8): 1085-1100.

Araki, K., K. Naito, S. Haraguchi, R. Suzuki, M. Yokoyama, M. Inoue, S. Aizawa, Y. Toyoda and E. Sato (1996). "Meiotic abnormalities of c-mos knockout mouse oocytes: activation after first meiosis or entrance into third meiotic metaphase." Biol Reprod **55**(6): 1315-1324.

Arimoto-Matsuzaki, K., H. Saito and M. Takekawa (2016). "TIA1 oxidation inhibits stress granule assembly and sensitizes cells to stress-induced apoptosis." Nat Commun **7**: 10252.

Arimoto, K., H. Fukuda, S. Imajoh-Ohmi, H. Saito and M. Takekawa (2008). "Formation of stress granules inhibits apoptosis by suppressing stress-responsive MAPK pathways." Nat Cell Biol **10**(11): 1324-1332.

Ariumi, Y. (2014). "Multiple functions of DDX3 RNA helicase in gene regulation, tumorigenesis, and viral infection." Front Genet **5**: 423.

Arnaudeau, S., M. Frieden, K. Nakamura, C. Castelbou, M. Michalak and N. Demaurex (2002). "Calreticulin differentially modulates calcium uptake and release in the endoplasmic reticulum and mitochondria." J Biol Chem **277**(48): 46696-46705.

Asada, K., K. Ito, D. Yui, H. Tagaya and T. Yokota (2018). "Cytosolic Genomic DNA functions as a Natural Antisense." Sci Rep **8**(1): 8551.

Ashby, M. C. and A. V. Tepikin (2001). "ER calcium and the functions of intracellular organelles." Semin Cell Dev Biol **12**(1): 11-17.

Atkins, C. M., N. Nozaki, Y. Shigeri and T. R. Soderling (2004). "Cytoplasmic polyadenylation element binding protein-dependent protein synthesis is regulated by calcium/calmodulin-dependent protein kinase II." J Neurosci **24**(22): 5193-5201.

Ayache, J., M. Benard, M. Ernoult-Lange, N. Minshall, N. Standart, M. Kress and D. Weil (2015). "P-body assembly requires DDX6 repression complexes rather than decay or Ataxin2/2L complexes." Mol Biol Cell **26**(14): 2579-2595.

Babiarz, J. E., J. G. Ruby, Y. Wang, D. P. Bartel and R. Blelloch (2008). "Mouse ES cells express endogenous shRNAs, siRNAs, and other Microprocessor-independent, Dicer-dependent small RNAs." Genes Dev **22**(20): 2773-2785.

Bachvarova, R. and V. De Leon (1980). "Polyadenylated RNA of mouse ova and loss of maternal RNA in early development." Dev Biol **74**(1): 1-8.

Back, S. H., K. Lee, E. Vink and R. J. Kaufman (2006). "Cytoplasmic IRE1alpha-mediated XBP1 mRNA splicing in the absence of nuclear processing and endoplasmic reticulum stress." J Biol Chem **281**(27): 18691-18706.

Backs, J., P. Stein, T. Backs, F. E. Duncan, C. E. Grueter, J. McAnally, X. Qi, R. M. Schultz and E. N. Olson (2010). "The gamma isoform of CaM kinase II controls mouse egg activation by regulating cell cycle resumption." Proc Natl Acad Sci U S A **107**(1): 81-86.

Balhorn, R., B. L. Gledhill and A. J. Wyrobek (1977). "Mouse sperm chromatin proteins: quantitative isolation and partial characterization." Biochemistry **16**(18): 4074-4080.

Balko, J. M. and C. L. Arteaga (2011). "Dead-box or black-box: is DDX1 a potential biomarker in breast cancer?" Breast Cancer Res Treat **127**(1): 65-67.

Bangham, A. D., R. W. Horne, A. M. Glauert, J. T. Dingle and J. A. Lucy (1962). "Action of saponin on biological cell membranes." Nature **196**: 952-955.

Banroques, J., M. Doere, M. Dreyfus, P. Linder and N. K. Tanner (2010). "Motif III in superfamily 2 "helicases" helps convert the binding energy of ATP into a high-affinity RNA binding site in the yeast DEAD-box protein Ded1." J Mol Biol **396**(4): 949-966.

Barr, F. G., F. Duan, L. M. Smith, D. Gustafson, M. Pitts, S. Hammond and J. M. Gastier-Foster (2009). "Genomic and clinical analyses of 2p24 and 12q13-q14 amplification in alveolar rhabdomyosarcoma: a report from the Children's Oncology Group." Genes Chromosomes Cancer **48**(8): 661-672.

Beaudoing, E., S. Freier, J. R. Wyatt, J. M. Claverie and D. Gautheret (2000). "Patterns of variant polyadenylation signal usage in human genes." Genome Res **10**(7): 1001-1010.

Beck, A. R., I. J. Miller, P. Anderson and M. Streuli (1998). "RNA-binding protein TIAR is essential for primordial germ cell development." Proc Natl Acad Sci U S A **95**(5): 2331-2336.

Benos, D. J. and R. S. Balaban (1983). "Energy metabolism of preimplantation mammalian blastocysts." Am J Physiol **245**(1): C40-45.

Bentov, Y., T. Yavorska, N. Esfandiari, A. Jurisicova and R. F. Casper (2011). "The contribution of mitochondrial function to reproductive aging." J Assist Reprod Genet **28**(9): 773-783.

Benz, J., H. Trachsel and U. Baumann (1999). "Crystal structure of the ATPase domain of translation initiation factor 4A from Saccharomyces cerevisiae--the prototype of the DEAD box protein family." Structure **7**(6): 671-679.

Biase, F. H., X. Cao and S. Zhong (2014). "Cell fate inclination within 2-cell and 4-cell mouse embryos revealed by single-cell RNA sequencing." Genome Res **24**(11): 1787-1796.

Bienroth, S., E. Wahle, C. Suter-Crazzolara and W. Keller (1991). "Purification of the cleavage and polyadenylation factor involved in the 3'-processing of messenger RNA precursors." J Biol Chem **266**(29): 19768-19776.

Bierkamp, C., M. Luxey, A. Metchat, C. Audouard, R. Dumollard and E. Christians (2010). "Lack of maternal Heat Shock Factor 1 results in multiple cellular and developmental defects, including mitochondrial damage and altered redox homeostasis, and leads to reduced survival of mammalian oocytes and embryos." Dev Biol **339**(2): 338-353.

Bleil, J. D., C. F. Beall and P. M. Wassarman (1981). "Mammalian sperm-egg interaction: fertilization of mouse eggs triggers modification of the major zona pellucida glycoprotein, ZP2." Dev Biol **86**(1): 189-197.

Bleil, J. D. and P. M. Wassarman (1980). "Mammalian sperm-egg interaction: identification of a glycoprotein in mouse egg zonae pellucidae possessing receptor activity for sperm." Cell **20**(3): 873-882.

Bleil, J. D. and P. M. Wassarman (1980). "Structure and function of the zona pellucida: identification and characterization of the proteins of the mouse oocyte's zona pellucida." Dev Biol **76**(1): 185-202.

Bleoo, S., X. Sun, M. J. Hendzel, J. M. Rowe, M. Packer and R. Godbout (2001). "Association of human DEAD box protein DDX1 with a cleavage stimulation factor involved in 3'-end processing of pre-MRNA." Mol Biol Cell **12**(10): 3046-3059.

Bley, N., M. Lederer, B. Pfalz, C. Reinke, T. Fuchs, M. Glass, B. Moller and S. Huttelmaier (2015). "Stress granules are dispensable for mRNA stabilization during cellular stress." Nucleic Acids Res **43**(4): e26.

Bobinnec, Y., C. Marcaillou, X. Morin and A. Debec (2003). "Dynamics of the endoplasmic reticulum during early development of Drosophila melanogaster." Cell Motil Cytoskeleton **54**(3): 217-225.

Bolstad, B. (2020). preprocessCore: A collection of pre-processing functions., Bioconductor.

Bono, F., J. Ebert, E. Lorentzen and E. Conti (2006). "The crystal structure of the exon junction complex reveals how it maintains a stable grip on mRNA." Cell **126**(4): 713-725.

Boothby, T. C., R. S. Zipper, C. M. van der Weele and S. M. Wolniak (2013). "Removal of retained introns regulates translation in the rapidly developing gametophyte of Marsilea vestita." Dev Cell **24**(5): 517-529.

Bourc'his, D., G. L. Xu, C. S. Lin, B. Bollman and T. H. Bestor (2001). "Dnmt3L and the establishment of maternal genomic imprints." Science **294**(5551): 2536-2539.

Bourque, G., K. H. Burns, M. Gehring, V. Gorbunova, A. Seluanov, M. Hammell, M. Imbeault, Z. Izsvak, H. L. Levin, T. S. Macfarlan, D. L. Mager and C. Feschotte (2018). "Ten things you should know about transposable elements." Genome Biol **19**(1): 199.

Bowers, H. A., P. A. Maroney, M. E. Fairman, B. Kastner, R. Luhrmann, T. W. Nilsen and E. Jankowsky (2006). "Discriminatory RNP remodeling by the DEAD-box protein DED1." RNA **12**(5): 903-912.

Brangwynne, C. P., C. R. Eckmann, D. S. Courson, A. Rybarska, C. Hoege, J. Gharakhani, F. Julicher and A. A. Hyman (2009). "Germline P granules are liquid droplets that localize by controlled dissolution/condensation." Science **324**(5935): 1729-1732.

Braun, R. E. (1998). "Post-transcriptional control of gene expression during spermatogenesis." Semin Cell Dev Biol **9**(4): 483-489.

Brengues, M., D. Teixeira and R. Parker (2005). "Movement of eukaryotic mRNAs between polysomes and cytoplasmic processing bodies." Science **310**(5747): 486-489.

Brodie, D. A., P. Huie, M. Locke and F. P. Ottensmeyer (1982). "The correlation between bismuth and uranyl staining and phosphorus content of intracellular structures as determined by electron spectroscopic imaging." Tissue and Cell **14**(4): 621-627.

Brookes, P. S., Y. Yoon, J. L. Robotham, M. W. Anders and S. S. Sheu (2004). "Calcium, ATP, and ROS: a mitochondrial love-hate triangle." Am J Physiol Cell Physiol **287**(4): C817-833.

Brykczynska, U., M. Hisano, S. Erkek, L. Ramos, E. J. Oakeley, T. C. Roloff, C. Beisel, D. Schubeler, M. B. Stadler and A. H. Peters (2010). "Repressive and active histone methylation mark distinct promoters in human and mouse spermatozoa." Nat Struct Mol Biol **17**(6): 679-687.

Buchan, J. R. (2014). "mRNP granules. Assembly, function, and connections with disease." RNA Biol **11**(8): 1019-1030.

Buckley, P. T., M. Khaladkar, J. Kim and J. Eberwine (2014). "Cytoplasmic intron retention, function, splicing, and the sentinel RNA hypothesis." Wiley Interdiscip Rev RNA **5**(2): 223-230.

Bultman, S. J., T. C. Gebuhr, H. Pan, P. Svoboda, R. M. Schultz and T. Magnuson (2006). "Maternal BRG1 regulates zygotic genome activation in the mouse." Genes Dev **20**(13): 1744-1754.

Burns, K. H., M. M. Viveiros, Y. Ren, P. Wang, F. J. DeMayo, D. E. Frail, J. J. Eppig and M. M. Matzuk (2003). "Roles of NPM2 in chromatin and nucleolar organization in oocytes and embryos." Science **300**(5619): 633-636.

Campbell, K. and K. Swann (2006). "Ca2+ oscillations stimulate an ATP increase during fertilization of mouse eggs." Dev Biol **298**(1): 225-233.

Carter, M. G., T. Hamatani, A. A. Sharov, C. E. Carmack, Y. Qian, K. Aiba, N. T. Ko, D. B. Dudekula, P. M. Brzoska, S. S. Hwang and M. S. Ko (2003). "In situ-synthesized novel microarray optimized for mouse stem cell and early developmental expression profiling." Genome Res **13**(5): 1011-1021.

Chahar, H. S., S. Chen and N. Manjunath (2013). "P-body components LSM1, GW182, DDX3, DDX6 and XRN1 are recruited to WNV replication sites and positively regulate viral replication." Virology **436**(1): 1-7.

Chaiyachati, B. H., R. K. Kaundal, J. Zhao, J. Wu, R. Flavell and T. Chi (2012). "LoxP-FRT Trap (LOFT): a simple and flexible system for conventional and reversible gene targeting." BMC Biol **10**: 96.

Champroux, A., J. Torres-Carreira, P. Gharagozloo, J. R. Drevet and A. Kocer (2016). "Mammalian sperm nuclear organization: resiliencies and vulnerabilities." Basic Clin Androl **26**: 17.

Chandel, N. S., E. Maltepe, E. Goldwasser, C. E. Mathieu, M. C. Simon and P. T. Schumacker (1998). "Mitochondrial reactive oxygen species trigger hypoxia-induced transcription." Proc Natl Acad Sci U S A **95**(20): 11715-11720.

Charlesworth, A., H. A. Meijer and C. H. de Moor (2013). "Specificity factors in cytoplasmic polyadenylation." Wiley Interdiscip Rev RNA **4**(4): 437-461.

Charroux, B., L. Pellizzoni, R. A. Perkinson, A. Shevchenko, M. Mann and G. Dreyfuss (1999). "Gemin3: A novel DEAD box protein that interacts with SMN, the spinal muscular atrophy gene product, and is a component of gems." J Cell Biol **147**(6): 1181-1194.

Chen, H. C., W. C. Lin, Y. G. Tsay, S. C. Lee and C. J. Chang (2002). "An RNA helicase, DDX1, interacting with poly(A) RNA and heterogeneous nuclear ribonucleoprotein K." J Biol Chem **277**(43): 40403-40409.

Chen, Y., J. P. Potratz, P. Tijerina, M. Del Campo, A. M. Lambowitz and R. Russell (2008). "DEAD-box proteins can completely separate an RNA duplex using a single ATP." Proc Natl Acad Sci U S A **105**(51): 20203-20208.

Christians, E., A. A. Davis, S. D. Thomas and I. J. Benjamin (2000). "Maternal effect of Hsf1 on reproductive success." Nature **407**(6805): 693-694.

Chuma, S., M. Hosokawa, K. Kitamura, S. Kasai, M. Fujioka, M. Hiyoshi, K. Takamune, T. Noce and N. Nakatsuji (2006). "Tdrd1/Mtr-1, a tudor-related gene, is essential for male germ-cell differentiation and nuage/germinal granule formation in mice." Proc Natl Acad Sci U S A **103**(43): 15894-15899.

Clapier, C. R. and B. R. Cairns (2009). "The biology of chromatin remodeling complexes." Annu Rev Biochem **78**: 273-304.

Clark, J. M. and E. M. Eddy (1975). "Fine structural observations on the origin and associations of primordial germ cells of the mouse." Dev Biol **47**(1): 136-155.

Clarke, H. J. (2012). "Post-transcriptional control of gene expression during mouse oogenesis." Results Probl Cell Differ **55**: 1-21.

Claycomb, J. M. (2014). "Ancient endo-siRNA pathways reveal new tricks." Curr Biol **24**(15): R703-715.

Collins, R., T. Karlberg, L. Lehtio, P. Schutz, S. van den Berg, L. G. Dahlgren, M. Hammarstrom, J. Weigelt and H. Schuler (2009). "The DEXD/H-box RNA helicase DDX19 is regulated by an {alpha}-helical switch." J Biol Chem **284**(16): 10296-10300.

Cordin, O., J. Banroques, N. K. Tanner and P. Linder (2006). "The DEAD-box protein family of RNA helicases." Gene **367**: 17-37.

Cordin, O., N. K. Tanner, M. Doere, P. Linder and J. Banroques (2004). "The newly discovered Q motif of DEAD-box RNA helicases regulates RNA-binding and helicase activity." EMBO J **23**(13): 2478-2487.

Courchaine, E. M., A. Lu and K. M. Neugebauer (2016). "Droplet organelles?" EMBO J **35**(15): 1603-1612.

Cox, J. E., C. S. Thummel and J. M. Tennessen (2017). "Metabolomic Studies in Drosophila." Genetics **206**(3): 1169-1185.

Crozet, N. (1989). "Nucleolar structure and RNA synthesis in mammalian oocytes." J Reprod Fertil Suppl **38**: 9-16.

D'Cruz, A. A., J. J. Babon, R. S. Norton, N. A. Nicola and S. E. Nicholson (2013). "Structure and function of the SPRY/B30.2 domain proteins involved in innate immunity." Protein Sci **22**(1): 1-10.

Dadoune, J. P. (2009). "Spermatozoal RNAs: what about their functions?" Microsc Res Tech **72**(8): 536-551.

Dahl, J. A., I. Jung, H. Aanes, G. D. Greggains, A. Manaf, M. Lerdrup, G. Li, S. Kuan, B. Li, A. Y. Lee, S. Preissl, I. Jermstad, M. H. Haugen, R. Suganthan, M. Bjoras, K. Hansen, K. T. Dalen, P. Fedorcsak, B. Ren and A. Klungland (2016). "Broad histone H3K4me3 domains in mouse oocytes modulate maternal-to-zygotic transition." Nature **537**(7621): 548-552.

Daley, J. M., R. L. Laan, A. Suresh and T. E. Wilson (2005). "DNA joint dependence of pol X family polymerase action in nonhomologous end joining." J Biol Chem **280**(32): 29030-29037.

Daniel, H., C. Levenes and F. Crepel (1998). "Cellular mechanisms of cerebellar LTD." Trends Neurosci **21**(9): 401-407.

Darzacq, X., B. E. Jady, C. Verheggen, A. M. Kiss, E. Bertrand and T. Kiss (2002). "Cajal body-specific small nuclear RNAs: a novel class of 2'-O-methylation and pseudouridylation guide RNAs." EMBO J **21**(11): 2746-2756.

Davis, A. J. and D. J. Chen (2013). "DNA double strand break repair via non-homologous end-joining." Transl Cancer Res **2**(3): 130-143.

Davison, E. J., K. Pennington, C. C. Hung, J. Peng, R. Rafiq, A. Ostareck-Lederer, D. H. Ostareck, H. C. Ardley, R. E. Banks and P. A. Robinson (2009). "Proteomic analysis of increased Parkin expression and its interactants provides evidence for a role in modulation of mitochondrial function." Proteomics **9**(18): 4284-4297.

de Boer, J., I. Donker, J. de Wit, J. H. Hoeijmakers and G. Weeda (1998). "Disruption of the mouse xeroderma pigmentosum group D DNA repair/basal transcription gene results in preimplantation lethality." Cancer Res **58**(1): 89-94.

de Brito, O. M. and L. Scorrano (2008). "Mitofusin 2 tethers endoplasmic reticulum to mitochondria." Nature **456**(7222): 605-610.

De Leon, V., A. Johnson and R. Bachvarova (1983). "Half-lives and relative amounts of stored and polysomal ribosomes and poly(A) + RNA in mouse oocytes." Dev Biol **98**(2): 400-408.

de Moor, C. H. and J. D. Richter (1999). "Cytoplasmic polyadenylation elements mediate masking and unmasking of cyclin B1 mRNA." EMBO J **18**(8): 2294-2303.

De Preter, K., F. Speleman, V. Combaret, J. Lunec, J. Board, A. Pearson, A. De Paepe, N. Van Roy, G. Laureys and J. Vandesompele (2005). "No evidence for correlation of DDX1 gene amplification with improved survival probability in patients with MYCN-amplified neuroblastomas." J Clin Oncol **23**(13): 3167-3168; author reply 3168-3170.

de Souza, D. R., S. S. Sanabani, A. C. de Souza, V. Filho Odone, S. Epelman and I. Bendit (2011). "Prognostic impact of MYCN, DDX1, TrkA, and TrkC gene transcripts expression in neuroblastoma." Pediatr Blood Cancer **56**(5): 749-756.

De Vos, K. J., G. M. Morotz, R. Stoica, E. L. Tudor, K. F. Lau, S. Ackerley, A. Warley, C. E. Shaw and C. C. Miller (2012). "VAPB interacts with the mitochondrial protein PTPIP51 to regulate calcium homeostasis." Hum Mol Genet **21**(6): 1299-1311.

Decker, C. J. and R. Parker (2012). "P-bodies and stress granules: possible roles in the control of translation and mRNA degradation." Cold Spring Harb Perspect Biol **4**(9): a012286.

Deguchi, R., H. Shirakawa, S. Oda, T. Mohri and S. Miyazaki (2000). "Spatiotemporal analysis of Ca(2+) waves in relation to the sperm entry site and animal-vegetal axis during Ca(2+) oscillations in fertilized mouse eggs." Dev Biol **218**(2): 299-313.

Del Campo, M., P. Tijerina, H. Bhaskaran, S. Mohr, Q. Yang, E. Jankowsky, R. Russell and A. M. Lambowitz (2007). "Do DEAD-box proteins promote group II intron splicing without unwinding RNA?" Mol Cell **28**(1): 159-166.

Dickson, K. S., A. Bilger, S. Ballantyne and M. P. Wickens (1999). "The cleavage and polyadenylation specificity factor in Xenopus laevis oocytes is a cytoplasmic factor involved in regulated polyadenylation." Mol Cell Biol **19**(8): 5707-5717.

Dobin, A., C. A. Davis, F. Schlesinger, J. Drenkow, C. Zaleski, S. Jha, P. Batut, M. Chaisson and T. R. Gingeras (2013). "STAR: ultrafast universal RNA-seq aligner." Bioinformatics **29**(1): 15-21.

Dolci, S., M. V. Bertolani, R. Canipari and M. De Felici (1991). "Involvement of carbohydrates in the hardening of the zona pellucida of mouse oocytes." Cell Biol Int Rep **15**(7): 571-579.

Ducibella, T. and E. Anderson (1979). "The effects of calcium deficiency on the formation of the zonula occludens and blastocoel in the mouse embryo." Dev Biol **73**(1): 46-58.

Ducibella, T. and R. Fissore (2008). "The roles of Ca2+, downstream protein kinases, and oscillatory signaling in regulating fertilization and the activation of development." Dev Biol **315**(2): 257-279.

Ducibella, T., D. Huneau, E. Angelichio, Z. Xu, R. M. Schultz, G. S. Kopf, R. Fissore, S. Madoux and J. P. Ozil (2002). "Egg-to-embryo transition is driven by differential responses to Ca(2+) oscillation number." Dev Biol **250**(2): 280-291.

Dumollard, R., M. Duchen and J. Carroll (2007). "The role of mitochondrial function in the oocyte and embryo." Curr Top Dev Biol **77**: 21-49.

Dumollard, R., M. Duchen and C. Sardet (2006). "Calcium signals and mitochondria at fertilisation." Semin Cell Dev Biol **17**(2): 314-323.

Dumollard, R., P. Marangos, G. Fitzharris, K. Swann, M. Duchen and J. Carroll (2004). "Sperm-triggered [Ca2+] oscillations and Ca2+ homeostasis in the mouse egg have an absolute requirement for mitochondrial ATP production." Development **131**(13): 3057-3067.

Dyson, N. J. (2016). "RB1: a prototype tumor suppressor and an enigma." Genes Dev **30**(13): 1492-1502.

Eaddy, A. C. and R. G. Schnellmann (2011). "Visualization and quantification of endoplasmic reticulum Ca2+ in renal cells using confocal microscopy and Fluo5F." Biochem Biophys Res Commun **404**(1): 424-427.

Eckersley-Maslin, M. A., C. Alda-Catalinas and W. Reik (2018). "Dynamics of the epigenetic landscape during the maternal-to-zygotic transition." Nat Rev Mol Cell Biol **19**(7): 436-450.

Edery, I., M. Humbelin, A. Darveau, K. A. Lee, S. Milburn, J. W. Hershey, H. Trachsel and N. Sonenberg (1983). "Involvement of eukaryotic initiation factor 4A in the cap recognition process." J Biol Chem **258**(18): 11398-11403.

Edgcomb, S. P., A. B. Carmel, S. Naji, G. Ambrus-Aikelin, J. R. Reyes, A. C. Saphire, L. Gerace and J. R. Williamson (2012). "DDX1 is an RNA-dependent ATPase involved in HIV-1 Rev function and virus replication." J Mol Biol **415**(1): 61-74.

Elvira, G., S. Wasiak, V. Blandford, X. K. Tong, A. Serrano, X. Fan, M. del Rayo Sanchez-Carbente, F. Servant, A. W. Bell, D. Boismenu, J. C. Lacaille, P. S. McPherson, L. DesGroseillers and W. S. Sossin (2006). "Characterization of an RNA granule from developing brain." Mol Cell Proteomics **5**(4): 635-651.

Eulalio, A., I. Behm-Ansmant, D. Schweizer and E. Izaurralde (2007). "P-body formation is a consequence, not the cause, of RNA-mediated gene silencing." Mol Cell Biol **27**(11): 3970-3981.

Fagerberg, L., B. M. Hallstrom, P. Oksvold, C. Kampf, D. Djureinovic, J. Odeberg, M. Habuka, S. Tahmasebpoor, A. Danielsson, K. Edlund, A. Asplund, E. Sjostedt, E. Lundberg, C. A. Szigyarto, M. Skogs, J. O. Takanen, H. Berling, H. Tegel, J. Mulder, P. Nilsson, J. M. Schwenk, C. Lindskog, F. Danielsson, A. Mardinoglu, A. Sivertsson, K. von Feilitzen, M. Forsberg, M. Zwahlen, I. Olsson, S. Navani, M. Huss, J. Nielsen, F. Ponten and M. Uhlen (2014). "Analysis of the human tissue-specific expression by genome-wide integration of transcriptomics and antibody-based proteomics." Mol Cell Proteomics **13**(2): 397-406.

Fahrenkamp, E., B. Algarra and L. Jovine (2020). "Mammalian egg coat modifications and the block to polyspermy." Mol Reprod Dev **87**(3): 326-340.

Fairman-Williams, M. E., U. P. Guenther and E. Jankowsky (2010). "SF1 and SF2 helicases: family matters." Curr Opin Struct Biol **20**(3): 313-324.

Familiari, G., R. Heyn, M. Relucenti and H. Sathananthan (2008). "Structural changes of the zona pellucida during fertilization and embryo development." Front Biosci **13**: 6730-6751.

Fang, J., E. Acheampong, R. Dave, F. Wang, M. Mukhtar and R. J. Pomerantz (2005). "The RNA helicase DDX1 is involved in restricted HIV-1 Rev function in human astrocytes." Virology **336**(2): 299-307.

Fayomi, A. P. and K. E. Orwig (2018). "Spermatogonial stem cells and spermatogenesis in mice, monkeys and men." Stem Cell Res **29**: 207-214.

Fernandes, R., C. Tsuda, A. L. Perumalsamy, T. Naranian, J. Chong, B. M. Acton, Z. B. Tong, L. M. Nelson and A. Jurisicova (2012). "NLRP5 mediates mitochondrial function in mouse oocytes and embryos." Biol Reprod **86**(5): 138, 131-110.

Fierro-Gonzalez, J. C., M. D. White, J. C. Silva and N. Plachta (2013). "Cadherin-dependent filopodia control preimplantation embryo compaction." Nat Cell Biol **15**(12): 1424-1433.

Filippakopoulos, P., A. Low, T. D. Sharpe, J. Uppenberg, S. Yao, Z. Kuang, P. Savitsky, R. S. Lewis, S. E. Nicholson, R. S. Norton and A. N. Bullock (2010). "Structural basis for Par-4 recognition by the SPRY domain- and SOCS box-containing proteins SPSB1, SPSB2, and SPSB4." J Mol Biol **401**(3): 389-402.

Fleming, T. P., J. McConnell, M. H. Johnson and B. R. Stevenson (1989). "Development of tight junctions de novo in the mouse early embryo: control of assembly of the tight junction-specific protein, ZO-1." J Cell Biol **108**(4): 1407-1418.

Flemr, M., J. Ma, R. M. Schultz and P. Svoboda (2010). "P-body loss is concomitant with formation of a messenger RNA storage domain in mouse oocytes." Biol Reprod **82**(5): 1008-1017.

Flemr, M. and P. Svoboda (2011). "Ribonucleoprotein localization in mouse oocytes." Methods **53**(2): 136-141.

Flores-Rozas, H. and J. Hurwitz (1993). "Characterization of a new RNA helicase from nuclear extracts of HeLa cells which translocates in the 5' to 3' direction." J Biol Chem **268**(28): 21372-21383.

Fox, C. A., M. D. Sheets and M. P. Wickens (1989). "Poly(A) addition during maturation of frog oocytes: distinct nuclear and cytoplasmic activities and regulation by the sequence UUUUUAU." Genes Dev **3**(12B): 2151-2162.

Franks, T. M. and J. Lykke-Andersen (2008). "The control of mRNA decapping and P-body formation." Mol Cell **32**(5): 605-615.

Fullston, T., E. M. Ohlsson-Teague, C. G. Print, L. Y. Sandeman and M. Lane (2016). "Sperm microRNA Content Is Altered in a Mouse Model of Male Obesity, but the Same Suite of microRNAs Are Not Altered in Offspring's Sperm." PLoS One **11**(11): e0166076.

Gamdzyk, M., D. M. Doycheva, C. Araujo, U. Ocak, Y. Luo, J. Tang and J. H. Zhang (2020). "cGAS/STING Pathway Activation Contributes to Delayed Neurodegeneration in Neonatal Hypoxia-Ischemia Rat Model: Possible Involvement of LINE-1." Mol Neurobiol **57**(6): 2600-2619.

Gardner, A. J. and J. P. Evans (2006). "Mammalian membrane block to polyspermy: new insights into how mammalian eggs prevent fertilisation by multiple sperm." Reprod Fertil Dev **18**(1-2): 53-61.

Gardner, A. J., C. J. Williams and J. P. Evans (2007). "Establishment of the mammalian membrane block to polyspermy: evidence for calcium-dependent and -independent regulation." Reproduction **133**(2): 383-393.

Gareau, C., E. Houssin, D. Martel, L. Coudert, S. Mellaoui, M. E. Huot, P. Laprise and R. Mazroui (2013). "Characterization of fragile X mental retardation protein recruitment and dynamics in Drosophila stress granules." PLoS One **8**(2): e55342.

Gasperin, B. G., M. H. Barreta, J. T. Santos, R. Ferreira, J. P. Neves, J. F. C. Oliveira and P. B. D. Gonçalves (2010). "Oil-Free Culture System for in Vitro Bovine Embryo Production." Italian Journal of Animal Science **9**(2): e32.

George, R. E., R. Kenyon, A. G. McGuckin, N. Kohl, P. Kogner, H. Christiansen, A. D. Pearson and J. Lunec (1997). "Analysis of candidate gene co-amplification with MYCN in neuroblastoma." Eur J Cancer **33**(12): 2037-2042.

Germain, D. R., K. Graham, D. D. Glubrecht, J. C. Hugh, J. R. Mackey and R. Godbout (2011). "DEAD box 1: a novel and independent prognostic marker for early recurrence in breast cancer." Breast Cancer Res Treat **127**(1): 53-63.

Germain, D. R., L. Li, M. R. Hildebrandt, A. J. Simmonds, S. C. Hughes and R. Godbout (2015). "Loss of the Drosophila melanogaster DEAD box protein Ddx1 leads to reduced size and aberrant gametogenesis." Dev Biol **407**(2): 232-245.

Gibbings, D. J., C. Ciaudo, M. Erhardt and O. Voinnet (2009). "Multivesicular bodies associate with components of miRNA effector complexes and modulate miRNA activity." Nat Cell Biol **11**(9): 1143-1149.

Gilbert, S. F. (2000). Developmental Biology. Sunderland (MA), Sinauer Associates.

Gilks, N., N. Kedersha, M. Ayodele, L. Shen, G. Stoecklin, L. M. Dember and P. Anderson (2004). "Stress granule assembly is mediated by prion-like aggregation of TIA-1." Mol Biol Cell **15**(12): 5383-5398.

Giorgi, C., S. Marchi and P. Pinton (2018). "The machineries, regulation and cellular functions of mitochondrial calcium." Nat Rev Mol Cell Biol **19**(11): 713-730.

Godbout, R., L. Li, R. Z. Liu and K. Roy (2007). "Role of DEAD box 1 in retinoblastoma and neuroblastoma." Future Oncol **3**(5): 575-587.

Godbout, R., M. Packer and W. Bie (1998). "Overexpression of a DEAD box protein (DDX1) in neuroblastoma and retinoblastoma cell lines." J Biol Chem **273**(33): 21161-21168.

Godbout, R., M. Packer, S. Katyal and S. Bleoo (2002). "Cloning and expression analysis of the chicken DEAD box gene DDX1." Biochim Biophys Acta **1574**(1): 63-71.

Godbout, R. and J. Squire (1993). "Amplification of a DEAD box protein gene in retinoblastoma cell lines." Proc Natl Acad Sci U S A **90**(16): 7578-7582.

Gomez-Suaga, P., S. Paillusson, R. Stoica, W. Noble, D. P. Hanger and C. C. J. Miller (2017). "The ER-Mitochondria Tethering Complex VAPB-PTPIP51 Regulates Autophagy." Curr Biol **27**(3): 371-385.

Gomez-Torres, M. J., E. M. Garcia, J. Guerrero, S. Medina, M. J. Izquierdo-Rico, A. Gil-Izquierdo, J. Orduna, M. Saviron, L. Gonzalez-Brusi, J. Ten, R. Bernabeu

and M. Aviles (2015). "Metabolites involved in cellular communication among human cumulus-oocyte-complex and sperm during in vitro fertilization." Reprod Biol Endocrinol **13**: 123.

Gorbalenya, A. E. and E. V. Koonin (1993). "Helicases: amino acid sequence comparisons and structure-function relationships." Current Opinion in Structural Biology **3**(3): 419-429.

Gordo, A. C., M. Kurokawa, H. Wu and R. A. Fissore (2002). "Modifications of the Ca2+ release mechanisms of mouse oocytes by fertilization and by sperm factor." Mol Hum Reprod **8**(7): 619-629.

Gorlach, A., P. Klappa and T. Kietzmann (2006). "The endoplasmic reticulum: folding, calcium homeostasis, signaling, and redox control." Antioxid Redox Signal **8**(9-10): 1391-1418.

Griffin, C. T., J. Brennan and T. Magnuson (2008). "The chromatin-remodeling enzyme BRG1 plays an essential role in primitive erythropoiesis and vascular development." Development **135**(3): 493-500.

Guillen-Boixet, J., V. Buzon, X. Salvatella and R. Mendez (2016). "CPEB4 is regulated during cell cycle by ERK2/Cdk1-mediated phosphorylation and its assembly into liquid-like droplets." Elife **5**.

Guli, C. L. and D. R. Smyth (1988). "UV-induced DNA repair is not detectable in pre-dictyate oocytes of the mouse." Mutat Res **208**(2): 115-119.

Gulyas, B. J. (1980). "Cortical granules of mammalian eggs." Int Rev Cytol **63**: 357-392.

Gururajan, R., L. Mathews, F. J. Longo and D. L. Weeks (1994). "An3 mRNA encodes an RNA helicase that colocalizes with nucleoli in Xenopus oocytes in a stage-specific manner." Proc Natl Acad Sci U S A **91**(6): 2056-2060.

Gustafson, E. A. and G. M. Wessel (2010). "DEAD-box helicases: posttranslational regulation and function." Biochem Biophys Res Commun **395**(1): 1-6.

Gwatkin, R. B. (1964). "Effect of Enzymes and Acidity on the Zona Pellucida of the Mouse Egg before and after Fertilization." J Reprod Fertil **7**: 99-105.

Halasz, L., Z. Karanyi, B. Boros-Olah, T. Kuik-Rozsa, E. Sipos, E. Nagy, L. A. Mosolygo, A. Mazlo, E. Rajnavolgyi, G. Halmos and L. Szekvolgyi (2017). "RNA-DNA hybrid (R-loop) immunoprecipitation mapping: an analytical workflow to evaluate inherent biases." Genome Res **27**(6): 1063-1073.

Hamatani, T., M. G. Carter, A. A. Sharov and M. S. Ko (2004). "Dynamics of global gene expression changes during mouse preimplantation development." Dev Cell **6**(1): 117-131.

Han, C., Y. Liu, G. Wan, H. J. Choi, L. Zhao, C. Ivan, X. He, A. K. Sood, X. Zhang and X. Lu (2014). "The RNA-binding protein DDX1 promotes primary microRNA maturation and inhibits ovarian tumor progression." Cell Rep **8**(5): 1447-1460.

Han, Y., S. Ishibashi, J. Iglesias-Gonzalez, Y. Chen, N. R. Love and E. Amaya (2018). "Ca(2+)-Induced Mitochondrial ROS Regulate the Early Embryonic Cell Cycle." Cell Rep **22**(1): 218-231.

Hansford, R. G. and D. Zorov (1998). "Role of mitochondrial calcium transport in the control of substrate oxidation." Mol Cell Biochem **184**(1-2): 359-369.

Haworth, R. A. and D. R. Hunter (1979). "The Ca2+-induced membrane transition in mitochondria. II. Nature of the Ca2+ trigger site." Arch Biochem Biophys **195**(2): 460-467.

Henry, J., I. H. Mather, M. F. McDermott and P. Pontarotti (1998). "B30.2-like domain proteins: update and new insights into a rapidly expanding family of proteins." Mol Biol Evol **15**(12): 1696-1705.

Herman, A. B., C. N. Vrakas, M. Ray, S. E. Kelemen, M. J. Sweredoski, A. Moradian, D. S. Haines and M. V. Autieri (2018). "FXR1 Is an IL-19-Responsive RNA-Binding Protein that Destabilizes Pro-inflammatory Transcripts in Vascular Smooth Muscle Cells." Cell Rep **24**(5): 1176-1189.

Hess, R. A. and L. Renato de Franca (2008). "Spermatogenesis and cycle of the seminiferous epithelium." Adv Exp Med Biol **636**: 1-15.

Higgs, P. G. and N. Lehman (2015). "The RNA World: molecular cooperation at the origins of life." Nat Rev Genet **16**(1): 7-17.

Hilbert, M., A. R. Karow and D. Klostermeier (2009). "The mechanism of ATP-dependent RNA unwinding by DEAD box proteins." Biol Chem **390**(12): 1237-1250.

Hildebrandt, M. R., D. R. Germain, E. A. Monckton, M. Brun and R. Godbout (2015). "Ddx1 knockout results in transgenerational wild-type lethality in mice." Sci Rep **5**: 9829.

Hildebrandt, M. R., Y. Wang, L. Li, L. Yasmin, D. D. Glubrecht and R. Godbout (2019). "Cytoplasmic aggregation of DDX1 in developing embryos: Early embryonic lethality associated with Ddx1 knockout." Dev Biol **455**(2): 420-433.

Hirling, H., M. Scheffner, T. Restle and H. Stahl (1989). "RNA helicase activity associated with the human p68 protein." Nature **339**(6225): 562-564.

Hirokawa, N. (2006). "mRNA transport in dendrites: RNA granules, motors, and tracks." J Neurosci **26**(27): 7139-7142.

Hirokawa, N. and R. Takemura (2005). "Molecular motors and mechanisms of directional transport in neurons." Nat Rev Neurosci **6**(3): 201-214.

Hivelin, C., S. Beraud-Dufour, C. Devader, A. Abderrahmani, S. Moreno, H. Moha Ou Maati, A. Djillani, C. Heurteaux, M. Borsotto, J. Mazella and T. Coppola (2016). "Potentiation of Calcium Influx and Insulin Secretion in Pancreatic Beta Cell by the Specific TREK-1 Blocker Spadin." J Diabetes Res **2016**: 3142175.

Hodgman, R., J. Tay, R. Mendez and J. D. Richter (2001). "CPEB phosphorylation and cytoplasmic polyadenylation are catalyzed by the kinase IAK1/Eg2 in maturing mouse oocytes." Development **128**(14): 2815-2822.

Hondele, M., R. Sachdev, S. Heinrich, J. Wang, P. Vallotton, B. M. A. Fontoura and K. Weis (2019). "DEAD-box ATPases are global regulators of phase-separated organelles." Nature **573**(7772): 144-148.

Honrath, B., I. Metz, N. Bendridi, J. Rieusset, C. Culmsee and A. M. Dolga (2017). "Glucose-regulated protein 75 determines ER-mitochondrial coupling and sensitivity to oxidative stress in neuronal cells." Cell Death Discov **3**: 17076.

Hoppe, U. C. (2010). "Mitochondrial calcium channels." FEBS Lett **584**(10): 1975-1981.

Horner, V. L. and M. F. Wolfner (2008). "Transitioning from egg to embryo: triggers and mechanisms of egg activation." Dev Dyn **237**(3): 527-544.

Horvath, P. M., T. Kellom, J. Caulfield and J. Boldt (1993). "Mechanistic studies of the plasma membrane block to polyspermy in mouse eggs." Mol Reprod Dev **34**(1): 65-72.

Hosken, D. J. and D. J. Hodgson (2014). "Why do sperm carry RNA? Relatedness, conflict, and control." Trends Ecol Evol **29**(8): 451-455.

Huang, Z. and D. Wells (2010). "The human oocyte and cumulus cells relationship: new insights from the cumulus cell transcriptome." Mol Hum Reprod **16**(10): 715-725.

Huarte, J., A. Stutz, M. L. O'Connell, P. Gubler, D. Belin, A. L. Darrow, S. Strickland and J. D. Vassalli (1992). "Transient translational silencing by reversible mRNA deadenylation." Cell **69**(6): 1021-1030.

Huarte, M., J. J. Sanz-Ezquerro, F. Roncal, J. Ortin and A. Nieto (2001). "PA subunit from influenza virus polymerase complex interacts with a cellular protein with homology to a family of transcriptional activators." J Virol **75**(18): 8597-8604.

Hubstenberger, A., M. Courel, M. Benard, S. Souquere, M. Ernoult-Lange, R. Chouaib, Z. Yi, J. B. Morlot, A. Munier, M. Fradet, M. Daunesse, E. Bertrand, G. Pierron, J. Mozziconacci, M. Kress and D. Weil (2017). "P-Body Purification Reveals the Condensation of Repressed mRNA Regulons." Mol Cell **68**(1): 144-157 e145.

Hyafil, F., D. Morello, C. Babinet and F. Jacob (1980). "A cell surface glycoprotein involved in the compaction of embryonal carcinoma cells and cleavage stage embryos." Cell **21**(3): 927-934.

Igusa, Y. and S. Miyazaki (1983). "Effects of altered extracellular and intracellular calcium concentration on hyperpolarizing responses of the hamster egg." J Physiol **340**: 611-632.

Ito, M. (2001). "Cerebellar long-term depression: characterization, signal transduction, and functional roles." Physiol Rev **81**(3): 1143-1195.

Iwasawa, R., A. L. Mahul-Mellier, C. Datler, E. Pazarentzos and S. Grimm (2011). "Fis1 and Bap31 bridge the mitochondria-ER interface to establish a platform for apoptosis induction." EMBO J **30**(3): 556-568.

Jachowicz, J. W., X. Bing, J. Pontabry, A. Boskovic, O. J. Rando and M. E. Torres-Padilla (2017). "LINE-1 activation after fertilization regulates global chromatin accessibility in the early mouse embryo." Nat Genet **49**(10): 1502-1510.

Jacob, M. C., M. Favre and J. C. Bensa (1991). "Membrane cell permeabilization with saponin and multiparametric analysis by flow cytometry." Cytometry **12**(6): 550-558.

Jady, B. E., X. Darzacq, K. E. Tucker, A. G. Matera, E. Bertrand and T. Kiss (2003). "Modification of Sm small nuclear RNAs occurs in the nucleoplasmic Cajal body following import from the cytoplasm." EMBO J **22**(8): 1878-1888.

Jankowsky, E. and A. Putnam (2010). "Duplex unwinding with DEAD-box proteins." Methods Mol Biol **587**: 245-264.

Jarmoskaite, I. and R. Russell (2011). "DEAD-box proteins as RNA helicases and chaperones." Wiley Interdiscip Rev RNA **2**(1): 135-152.

Jasin, M. and R. Rothstein (2013). "Repair of strand breaks by homologous recombination." Cold Spring Harb Perspect Biol **5**(11): a012740.

Jezek, J., K. F. Cooper and R. Strich (2018). "Reactive Oxygen Species and Mitochondrial Dynamics: The Yin and Yang of Mitochondrial Dysfunction and Cancer Progression." Antioxidants (Basel) **7**(1).

Jiang, C. and E. M. Schuman (2002). "Regulation and function of local protein synthesis in neuronal dendrites." Trends Biochem Sci **27**(10): 506-513.

Jiao, Z. X. and T. K. Woodruff (2013). "Detection and quantification of maternal-effect gene transcripts in mouse second polar bodies: potential markers of embryo developmental competence." Fertil Steril **99**(7): 2055-2061.

Johnson, C. M., C. S. Hill, S. Chawla, R. Treisman and H. Bading (1997). "Calcium controls gene expression via three distinct pathways that can function independently of the Ras/mitogen-activated protein kinases (ERKs) signaling cascade." J Neurosci **17**(16): 6189-6202.

Johnson, J., B. M. Bierle, G. I. Gallicano and D. G. Capco (1998). "Calcium/calmodulin-dependent protein kinase II and calmodulin: regulators of the meiotic spindle in mouse eggs." Dev Biol **204**(2): 464-477.

Johnson, M. H., B. Maro and M. Takeichi (1986). "The role of cell adhesion in the synchronization and orientation of polarization in 8-cell mouse blastomeres." J Embryol Exp Morphol **93**: 239-255.

Johnson, M. H. and C. A. Ziomek (1981). "Induction of polarity in mouse 8-cell blastomeres: specificity, geometry, and stability." J Cell Biol **91**(1): 303-308.

Jones, K. T. (2005). "Mammalian egg activation: from Ca2+ spiking to cell cycle progression." Reproduction **130**(6): 813-823.

Jones, K. T. (2007). "Intracellular calcium in the fertilization and development of mammalian eggs." Clin Exp Pharmacol Physiol **34**(10): 1084-1089.

Jongjitwimol, J., R. A. Baldock, S. J. Morley and F. Z. Watts (2016). "Sumoylation of eIF4A2 affects stress granule formation." J Cell Sci **129**(12): 2407-2415.

Joseph, S. K. and G. Hajnoczky (2007). "IP3 receptors in cell survival and apoptosis: Ca2+ release and beyond." Apoptosis **12**(5): 951-968.

Joshi, A. S., H. Zhang and W. A. Prinz (2017). "Organelle biogenesis in the endoplasmic reticulum." Nat Cell Biol **19**(8): 876-882.

Jounai, N., K. Kobiyama, F. Takeshita and K. J. Ishii (2012). "Recognition of damage-associated molecular patterns related to nucleic acids during inflammation and vaccination." Front Cell Infect Microbiol **2**: 168.

Jurkin, J., T. Henkel, A. F. Nielsen, M. Minnich, J. Popow, T. Kaufmann, K. Heindl, T. Hoffmann, M. Busslinger and J. Martinez (2014). "The mammalian tRNA ligase complex mediates splicing of XBP1 mRNA and controls antibody secretion in plasma cells." EMBO J **33**(24): 2922-2936.

Kailasan Vanaja, S., V. A. Rathinam, M. K. Atianand, P. Kalantari, B. Skehan, K. A. Fitzgerald and J. M. Leong (2014). "Bacterial RNA:DNA hybrids are activators of the NLRP3 inflammasome." Proc Natl Acad Sci U S A **111**(21): 7765-7770.

Kanai, Y., N. Dohmae and N. Hirokawa (2004). "Kinesin transports RNA: isolation and characterization of an RNA-transporting granule." Neuron **43**(4): 513-525.

Kaneda, M., M. Okano, K. Hata, T. Sado, N. Tsujimoto, E. Li and H. Sasaki (2004). "Essential role for de novo DNA methyltransferase Dnmt3a in paternal and maternal imprinting." Nature **429**(6994): 900-903.

Kaneda, M., F. Tang, D. O'Carroll, K. Lao and M. A. Surani (2009). "Essential role for Argonaute2 protein in mouse oogenesis." Epigenetics Chromatin **2**(1): 9.

Karlic, R., S. Ganesh, V. Franke, E. Svobodova, J. Urbanova, Y. Suzuki, F. Aoki, K. Vlahovicek and P. Svoboda (2017). "Long non-coding RNA exchange during the oocyte-to-embryo transition in mice." DNA Res **24**(2): 129-141.

Kashir, J., M. Konstantinidis, C. Jones, B. Lemmon, H. C. Lee, R. Hamer, B. Heindryckx, C. M. Deane, P. De Sutter, R. A. Fissore, J. Parrington, D. Wells and K. Coward (2012). "A maternally inherited autosomal point mutation in human phospholipase C zeta (PLCzeta) leads to male infertility." Hum Reprod **27**(1): 222-231.

Kaufman, R. J. and J. D. Malhotra (2014). "Calcium trafficking integrates endoplasmic reticulum function with mitochondrial bioenergetics." Biochim Biophys Acta **1843**(10): 2233-2239.

Kedersha, N. and P. Anderson (2002). "Stress granules: sites of mRNA triage that regulate mRNA stability and translatability." Biochem Soc Trans **30**(Pt 6): 963-969.

Kedersha, N. L., M. Gupta, W. Li, I. Miller and P. Anderson (1999). "RNA-binding proteins TIA-1 and TIAR link the phosphorylation of eIF-2 alpha to the assembly of mammalian stress granules." J Cell Biol **147**(7): 1431-1442.

Kellner, J. N. and A. Meinhart (2015). "Structure of the SPRY domain of the human RNA helicase DDX1, a putative interaction platform within a DEAD-box protein." Acta Crystallogr F Struct Biol Commun **71**(Pt 9): 1176-1188.

Kellner, J. N., J. Reinstein and A. Meinhart (2015). "Synergistic effects of ATP and RNA binding to human DEAD-box protein DDX1." Nucleic Acids Res **43**(5): 2813-2828.

Kidder, B. L. (2014). "In vitro maturation and in vitro fertilization of mouse oocytes and preimplantation embryo culture." Methods Mol Biol **1150**: 191-199.

Kim, B., H. J. Cooke and K. Rhee (2012). "DAZL is essential for stress granule formation implicated in germ cell survival upon heat stress." Development **139**(3): 568-578.

Kim, K. H. and K. A. Lee (2014). "Maternal effect genes: Findings and effects on mouse embryo development." Clin Exp Reprod Med **41**(2): 47-61.

Kleene, K. C. (1993). "Multiple controls over the efficiency of translation of the mRNAs encoding transition proteins, protamines, and the mitochondrial capsule selenoprotein in late spermatids in mice." Dev Biol **159**(2): 720-731.

Kline, D. and J. T. Kline (1992). "Repetitive calcium transients and the role of calcium in exocytosis and cell cycle activation in the mouse egg." Dev Biol **149**(1): 80-89.

Kline, D., L. Mehlmann, C. Fox and M. Terasaki (1999). "The cortical endoplasmic reticulum (ER) of the mouse egg: localization of ER clusters in relation to the generation of repetitive calcium waves." Dev Biol **215**(2): 431-442.

Kloc, M., S. Bilinski, A. P. Chan and L. D. Etkin (2001). "Mitochondrial ribosomal RNA in the germinal granules in Xenopus embryos revisited." Differentiation **67**(3): 80-83.

Knott, J. G., M. Kurokawa, R. A. Fissore, R. M. Schultz and C. J. Williams (2005). "Transgenic RNA interference reveals role for mouse sperm phospholipase Czeta in triggering Ca2+ oscillations during fertilization." Biol Reprod **72**(4): 992-996.

Kobayashi, S., K. Sato and Y. Hayashi (2005). "The role of mitochondrial rRNAs and nanos protein in germline formation in Drosophila embryos." Zoolog Sci **22**(9): 943-954.

Komatsu, K., A. Iwase, M. Mawatari, J. Wang, M. Yamashita and F. Kikkawa (2014). "Mitochondrial membrane potential in 2-cell stage embryos correlates with the success of preimplantation development." Reproduction **147**(5): 627-638.

Kong, Q., X. Quan, J. Du, Y. Tai, W. Liu, J. Zhang, X. Zhang, Y. Mu and Z. Liu (2019). "Endo-siRNAs regulate early embryonic development by inhibiting transcription of long terminal repeat sequence in pigdagger." Biol Reprod **100**(6): 1431-1439.

Koo, C. X., K. Kobiyama, Y. J. Shen, N. LeBert, S. Ahmad, M. Khatoo, T. Aoshi, S. Gasser and K. J. Ishii (2015). "RNA polymerase III regulates cytosolic RNA:DNA hybrids and intracellular microRNA expression." J Biol Chem **290**(12): 7463-7473.

Kulkarni, A. and C. G. Extavour (2017). "Convergent evolution of germ granule nucleators: A hypothesis." Stem Cell Res **24**: 188-194.

Kunde, S. A., L. Musante, A. Grimme, U. Fischer, E. Muller, E. E. Wanker and V. M. Kalscheuer (2011). "The X-chromosome-linked intellectual disability protein PQBP1 is a component of neuronal RNA granules and regulates the appearance of stress granules." Hum Mol Genet **20**(24): 4916-4931.

Kuroda, H., P. S. White, E. P. Sulman, C. F. Manohar, J. L. Reiter, S. L. Cohn and G. M. Brodeur (1996). "Physical mapping of the DDX1 gene to 340 kb 5' of MYCN." Oncogene **13**(7): 1561-1565.

Lai, M. C., Y. H. Lee and W. Y. Tarn (2008). "The DEAD-box RNA helicase DDX3 associates with export messenger ribonucleoproteins as well as tip-associated protein and participates in translational control." Mol Biol Cell **19**(9): 3847-3858.

Lamond, A. I. and D. L. Spector (2003). "Nuclear speckles: a model for nuclear organelles." Nat Rev Mol Cell Biol **4**(8): 605-612.

Larabell, C. A. and D. G. Capco (1988). "Role of calcium in the localization of maternal poly(A)(+)RNA and tubulin mRNA in Xenopus oocytes." Roux Arch Dev Biol **197**(3): 175-183.

Lee, B. and K. E. Kendle (1979). "The effect of reserpine, oestradiol and in-vitro perfusion on oviduct calcium levels in the mouse during egg transport." J Reprod Fertil **55**(2): 489-493.

Lee, J. W., L. Blanco, T. Zhou, M. Garcia-Diaz, K. Bebenek, T. A. Kunkel, Z. Wang and L. F. Povirk (2004). "Implication of DNA polymerase lambda in alignment-based gap filling for nonhomologous DNA end joining in human nuclear extracts." J Biol Chem **279**(1): 805-811.

Lee, S. and K. T. Min (2018). "The Interface Between ER and Mitochondria: Molecular Compositions and Functions." Mol Cells **41**(12): 1000-1007.

Letunic, I. and P. Bork (2018). "20 years of the SMART protein domain annotation resource." Nucleic Acids Res **46**(D1): D493-D496.

Letunic, I., T. Doerks and P. Bork (2015). "SMART: recent updates, new developments and status in 2015." Nucleic Acids Res **43**(Database issue): D257-260.

Levenes, C., H. Daniel and F. Crepel (1998). "Long-term depression of synaptic transmission in the cerebellum: cellular and molecular mechanisms revisited." Prog Neurobiol **55**(1): 79-91.

Li, L., B. Baibakov and J. Dean (2008). "A subcortical maternal complex essential for preimplantation mouse embryogenesis." Dev Cell **15**(3): 416-425.

Li, L., D. R. Germain, H. Y. Poon, M. R. Hildebrandt, E. A. Monckton, D. McDonald, M. J. Hendzel and R. Godbout (2016). "DEAD Box 1 Facilitates Removal of RNA and Homologous Recombination at DNA Double-Strand Breaks." Mol Cell Biol **36**(22): 2794-2810.

Li, L., E. A. Monckton and R. Godbout (2008). "A role for DEAD box 1 at DNA double-strand breaks." Mol Cell Biol **28**(20): 6413-6425.

Li, L., H. Y. Poon, M. R. Hildebrandt, E. A. Monckton, D. R. Germain, R. P. Fahlman and R. Godbout (2017). "Role for RIF1-interacting partner DDX1 in BLM recruitment to DNA double-strand breaks." DNA Repair (Amst) **55**: 47-63.

Li, L., K. Roy, S. Katyal, X. Sun, S. Bleoo and R. Godbout (2006). "Dynamic nature of cleavage bodies and their spatial relationship to DDX1 bodies, Cajal bodies, and gems." Mol Biol Cell **17**(3): 1126-1140.

Li, L., P. Zheng and J. Dean (2010). "Maternal control of early mouse development." Development **137**(6): 859-870.

Li, W., B. You, M. Hoque, D. Zheng, W. Luo, Z. Ji, J. Y. Park, S. I. Gunderson, A. Kalsotra, J. L. Manley and B. Tian (2015). "Systematic profiling of poly(A)+ transcripts modulated by core 3' end processing and splicing factors reveals regulatory rules of alternative cleavage and polyadenylation." PLoS Genet **11**(4): e1005166.

Li, Y., D. Y. Zhao, J. F. Greenblatt and Z. Zhang (2013). "RIPSeeker: a statistical package for identifying protein-associated transcripts from RIP-seq experiments." Nucleic Acids Res **41**(8): e94.

Liang, L., W. Diehl-Jones and P. Lasko (1994). "Localization of vasa protein to the Drosophila pole plasm is independent of its RNA-binding and helicase activities." Development **120**(5): 1201-1211.

Liao, Y., G. K. Smyth and W. Shi (2014). "featureCounts: an efficient general purpose program for assigning sequence reads to genomic features." Bioinformatics **30**(7): 923-930.

Liao, Y., G. K. Smyth and W. Shi (2019). "The R package Rsubread is easier, faster, cheaper and better for alignment and quantification of RNA sequencing reads." Nucleic Acids Res **47**(8): e47.

Lin, J., R. Xu, X. Wu, Y. Shen and Q. Q. Li (2017). "Role of cleavage and polyadenylation specificity factor 100: anchoring poly(A) sites and modulating transcription termination." Plant J **91**(5): 829-839.

Lin, M. H., H. Sivakumaran, A. Jones, D. Li, C. Harper, T. Wei, H. Jin, L. Rustanti, F. A. Meunier, K. Spann and D. Harrich (2014). "A HIV-1 Tat mutant protein disrupts HIV-1 Rev function by targeting the DEAD-box RNA helicase DDX1." Retrovirology **11**: 121.

Linder, P. (2006). "Dead-box proteins: a family affair--active and passive players in RNP-remodeling." Nucleic Acids Res **34**(15): 4168-4180.

Linder, P. and F. Fuller-Pace (2015). "Happy birthday: 25 years of DEAD-box proteins." Methods Mol Biol **1259**: 17-33.

Linder, P. and E. Jankowsky (2011). "From unwinding to clamping - the DEAD box RNA helicase family." Nat Rev Mol Cell Biol **12**(8): 505-516.

Linder, P., P. F. Lasko, M. Ashburner, P. Leroy, P. J. Nielsen, K. Nishi, J. Schnier and P. P. Slonimski (1989). "Birth of the D-E-A-D box." Nature **337**(6203): 121-122.

Linley, A. J., M. G. Mathieu, A. K. Miles, R. C. Rees, S. E. McArdle and T. Regad (2012). "The helicase HAGE expressed by malignant melanoma-initiating cells is required for tumor cell proliferation in vivo." J Biol Chem **287**(17): 13633-13643.

Liu, B., Q. Xu, Q. Wang, S. Feng, F. Lai, P. Wang, F. Zheng, Y. Xiang, J. Wu, J. Nie, C. Qiu, W. Xia, L. Li, G. Yu, Z. Lin, K. Xu, Z. Xiong, F. Kong, L. Liu, C. Huang, Y. Yu, J. Na and W. Xie (2020). "The landscape of RNA Pol II binding reveals a stepwise transition during ZGA." Nature **587**(7832): 139-144.

Liu, F., A. Putnam and E. Jankowsky (2008). "ATP hydrolysis is required for DEAD-box protein recycling but not for duplex unwinding." Proc Natl Acad Sci U S A **105**(51): 20209-20214.

Liu, F., A. A. Putnam and E. Jankowsky (2014). "DEAD-box helicases form nucleotide-dependent, long-lived complexes with RNA." Biochemistry **53**(2): 423-433.

Liu, J., H. Fang, Z. Chi, Z. Wu, D. Wei, D. Mo, K. Niu, A. S. Balajee, T. K. Hei, L. Nie and Y. Zhao (2015). "XPD localizes in mitochondria and protects the

mitochondrial genome from oxidative DNA damage." Nucleic Acids Res **43**(11): 5476-5488.

Liu, L., K. Hammar, P. J. Smith, S. Inoue and D. L. Keefe (2001). "Mitochondrial modulation of calcium signaling at the initiation of development." Cell Calcium **30**(6): 423-433.

Liu, L., J. R. Trimarchi and D. L. Keefe (2000). "Involvement of mitochondria in oxidative stress-induced cell death in mouse zygotes." Biol Reprod **62**(6): 1745-1753.

Liu, X., C. Wang, W. Liu, J. Li, C. Li, X. Kou, J. Chen, Y. Zhao, H. Gao, H. Wang, Y. Zhang, Y. Gao and S. Gao (2016). "Distinct features of H3K4me3 and H3K27me3 chromatin domains in pre-implantation embryos." Nature **537**(7621): 558-562.

Liu, Y., X. Lu, J. Shi, X. Yu, X. Zhang, K. Zhu, Z. Yi, E. Duan and L. Li (2016). "BTG4 is a key regulator for maternal mRNA clearance during mouse early embryogenesis." J Mol Cell Biol **8**(4): 366-368.

Liu, Y., H. Nie, H. Liu and F. Lu (2019). "Poly(A) inclusive RNA isoform sequencing (PAIso-seq) reveals wide-spread non-adenosine residues within RNA poly(A) tails." Nat Commun **10**(1): 5292.

Longo, P., R. D. Twesten and W. Lin (2014). "High Speed EELS and EFTEM Analysis across the Visual Cortex." Microscopy and Microanalysis **20**(S3): 1302-1303.

Love, M. I., W. Huber and S. Anders (2014). "Moderated estimation of fold change and dispersion for RNA-seq data with DESeq2." Genome Biol **15**(12): 550.

Lue, Y. H., A. P. Hikim, R. S. Swerdloff, P. Im, K. S. Taing, T. Bui, A. Leung and C. Wang (1999). "Single exposure to heat induces stage-specific germ cell apoptosis in rats: role of intratesticular testosterone on stage specificity." Endocrinology **140**(4): 1709-1717.

Luo, C., J. Zuniga, E. Edison, S. Palla, W. Dong and J. Parker-Thornburg (2011). "Superovulation strategies for 6 commonly used mouse strains." J Am Assoc Lab Anim Sci **50**(4): 471-478.

Lykke-Andersen, K., M. J. Gilchrist, J. B. Grabarek, P. Das, E. Miska and M. Zernicka-Goetz (2008). "Maternal Argonaute 2 is essential for early mouse development at the maternal-zygotic transition." Mol Biol Cell **19**(10): 4383-4392.

Ma, J., Y. Fukuda and R. M. Schultz (2015). "Mobilization of Dormant Cnot7 mRNA Promotes Deadenylation of Maternal Transcripts During Mouse Oocyte Maturation." Biol Reprod **93**(2): 48.

Ma, J., F. Zeng, R. M. Schultz and H. Tseng (2006). "Basonuclin: a novel mammalian maternal-effect gene." Development **133**(10): 2053-2062.

Maekawa, S., N. Imamachi, T. Irie, H. Tani, K. Matsumoto, R. Mizutani, K. Imamura, M. Kakeda, T. Yada, S. Sugano, Y. Suzuki and N. Akimitsu (2015). "Analysis of RNA decay factor mediated RNA stability contributions on RNA abundance." BMC Genomics **16**: 154.

Mahajan, K. N., S. A. Nick McElhinny, B. S. Mitchell and D. A. Ramsden (2002). "Association of DNA polymerase mu (pol mu) with Ku and ligase IV: role for pol mu in end-joining double-strand break repair." Mol Cell Biol **22**(14): 5194-5202.

Maitre, J. L., H. Turlier, R. Illukkumbura, B. Eismann, R. Niwayama, F. Nedelec and T. Hiiragi (2016). "Asymmetric division of contractile domains couples cell positioning and fate specification." Nature **536**(7616): 344-348.

Mallam, A. L., M. Del Campo, B. Gilman, D. J. Sidote and A. M. Lambowitz (2012). "Structural basis for RNA-duplex recognition and unwinding by the DEAD-box helicase Mss116p." Nature **490**(7418): 121-125.

Mandel, C. R., S. Kaneko, H. Zhang, D. Gebauer, V. Vethantham, J. L. Manley and L. Tong (2006). "Polyadenylation factor CPSF-73 is the pre-mRNA 3'-end-processing endonuclease." Nature **444**(7121): 953-956.

Manser, R. C. and F. D. Houghton (2006). "Ca2+ -linked upregulation and mitochondrial production of nitric oxide in the mouse preimplantation embryo." J Cell Sci **119**(Pt 10): 2048-2055.

Mao, Z., M. Bozzella, A. Seluanov and V. Gorbunova (2008). "DNA repair by nonhomologous end joining and homologous recombination during cell cycle in human cells." Cell Cycle **7**(18): 2902-2906.

Maragkakis, M., P. Alexiou, T. Nakaya and Z. Mourelatos (2016). "CLIPSeqTools--a novel bioinformatics CLIP-seq analysis suite." RNA **22**(1): 1-9.

Markoulaki, S., S. Matson and T. Ducibella (2004). "Fertilization stimulates long-lasting oscillations of CaMKII activity in mouse eggs." Dev Biol **272**(1): 15-25.

Marlow, F. L. (2010). Maternal Control of Development in Vertebrates: My Mother Made Me Do It! San Rafael (CA).

Mateju, D., B. Eichenberger, F. Voigt, J. Eglinger, G. Roth and J. A. Chao (2020). "Single-Molecule Imaging Reveals Translation of mRNAs Localized to Stress Granules." Cell.

Mathieu, M. G., A. K. Miles, M. Ahmad, M. E. Buczek, A. G. Pockley, R. C. Rees and T. Regad (2014). "The helicase HAGE prevents interferon-alpha-induced PML expression in ABCB5+ malignant melanoma-initiating cells by promoting the expression of SOCS1." Cell Death Dis **5**: e1061.

Matson, S., S. Markoulaki and T. Ducibella (2006). "Antagonists of myosin light chain kinase and of myosin II inhibit specific events of egg activation in fertilized mouse eggs." Biol Reprod **74**(1): 169-176.

Mauger, O., F. Lemoine and P. Scheiffele (2016). "Targeted Intron Retention and Excision for Rapid Gene Regulation in Response to Neuronal Activity." Neuron **92**(6): 1266-1278.

Mazroui, R., M. E. Huot, S. Tremblay, C. Filion, Y. Labelle and E. W. Khandjian (2002). "Trapping of messenger RNA by Fragile X Mental Retardation protein into cytoplasmic granules induces translation repression." Hum Mol Genet **11**(24): 3007-3017.

McDonald, K. K., A. Aulas, L. Destroismaisons, S. Pickles, E. Beleac, W. Camu, G. A. Rouleau and C. Vande Velde (2011). "TAR DNA-binding protein 43 (TDP-43) regulates stress granule dynamics via differential regulation of G3BP and TIA-1." Hum Mol Genet **20**(7): 1400-1410.

McGrew, L. L., E. Dworkin-Rastl, M. B. Dworkin and J. D. Richter (1989). "Poly(A) elongation during Xenopus oocyte maturation is required for translational recruitment and is mediated by a short sequence element." Genes Dev **3**(6): 803-815.

McLay, D. W. and H. J. Clarke (2003). "Remodelling the paternal chromatin at fertilization in mammals." Reproduction **125**(5): 625-633.

Mendez, R. and J. D. Richter (2001). "Translational control by CPEB: a means to the end." Nat Rev Mol Cell Biol **2**(7): 521-529.

Meshorer, E. and T. Misteli (2005). "Splicing misplaced." Cell **122**(3): 317-318.

Metzger, F. and J. P. Kapfhammer (2003). "Protein kinase C: its role in activity-dependent Purkinje cell dendritic development and plasticity." Cerebellum **2**(3): 206-214.

Mi, H., A. Muruganujan and P. D. Thomas (2013). "PANTHER in 2013: modeling the evolution of gene function, and other gene attributes, in the context of phylogenetic trees." Nucleic Acids Res **41**(Database issue): D377-386.

Miao, Y. L. and C. J. Williams (2012). "Calcium signaling in mammalian egg activation and embryo development: the influence of subcellular localization." Mol Reprod Dev **79**(11): 742-756.

Michalski, D. and M. Steiniger (2015). "In vivo characterization of the Drosophila mRNA 3' end processing core cleavage complex." RNA **21**(8): 1404-1418.

Miller, L. C., V. Blandford, R. McAdam, M. R. Sanchez-Carbente, F. Badeaux, L. DesGroseillers and W. S. Sossin (2009). "Combinations of DEAD box proteins distinguish distinct types of RNA: protein complexes in neurons." Mol Cell Neurosci **40**(4): 485-495.

Mishra, P. and D. C. Chan (2014). "Mitochondrial dynamics and inheritance during cell division, development and disease." Nat Rev Mol Cell Biol **15**(10): 634-646.

Mollet, S., N. Cougot, A. Wilczynska, F. Dautry, M. Kress, E. Bertrand and D. Weil (2008). "Translationally repressed mRNA transiently cycles through stress granules during stress." Mol Biol Cell **19**(10): 4469-4479.

Montpetit, B., N. D. Thomsen, K. J. Helmke, M. A. Seeliger, J. M. Berger and K. Weis (2011). "A conserved mechanism of DEAD-box ATPase activation by nucleoporins and InsP6 in mRNA export." Nature **472**(7342): 238-242.

Moran, Y., H. Weinberger, A. M. Reitzel, J. C. Sullivan, R. Kahn, D. Gordon, J. R. Finnerty and M. Gurevitz (2008). "Intron retention as a posttranscriptional regulatory mechanism of neurotoxin expression at early life stages of the starlet anemone Nematostella vectensis." J Mol Biol **380**(3): 437-443.

Morris, S. A., R. T. Teo, H. Li, P. Robson, D. M. Glover and M. Zernicka-Goetz (2010). "Origin and formation of the first two distinct cell types of the inner cell mass in the mouse embryo." Proc Natl Acad Sci U S A **107**(14): 6364-6369.

Mouillet, J. F., X. Yan, Q. Ou, L. Jin, L. J. Muglia, P. A. Crawford and Y. Sadovsky (2008). "DEAD-box protein-103 (DP103, Ddx20) is essential for early embryonic development and modulates ovarian morphology and function." Endocrinology **149**(5): 2168-2175.

Murchison, E. P., P. Stein, Z. Xuan, H. Pan, M. Q. Zhang, R. M. Schultz and G. J. Hannon (2007). "Critical roles for Dicer in the female germline." Genes Dev **21**(6): 682-693.

Murthy, K. G. and J. L. Manley (1992). "Characterization of the multisubunit cleavage-polyadenylation specificity factor from calf thymus." J Biol Chem **267**(21): 14804-14811.

Murthy, K. G. and J. L. Manley (1995). "The 160-kD subunit of human cleavage-polyadenylation specificity factor coordinates pre-mRNA 3'-end formation." Genes Dev **9**(21): 2672-2683.

Muto, A., S. Kume, T. Inoue, H. Okano and K. Mikoshiba (1996). "Calcium waves along the cleavage furrows in cleavage-stage Xenopus embryos and its inhibition by heparin." J Cell Biol **135**(1): 181-190.

Nadeau, J. H. (2017). "Do Gametes Woo? Evidence for Their Nonrandom Union at Fertilization." Genetics **207**(2): 369-387.

Nagaraj, R., M. S. Sharpley, F. Chi, D. Braas, Y. Zhou, R. Kim, A. T. Clark and U. Banerjee (2017). "Nuclear Localization of Mitochondrial TCA Cycle Enzymes as a Critical Step in Mammalian Zygotic Genome Activation." Cell **168**(1-2): 210-223 e211.

Naji, S., G. Ambrus, P. Cimermancic, J. R. Reyes, J. R. Johnson, R. Filbrandt, M. D. Huber, P. Vesely, N. J. Krogan, J. R. Yates, 3rd, A. C. Saphire and L. Gerace (2012). "Host cell interactome of HIV-1 Rev includes RNA helicases involved in multiple facets of virus production." Mol Cell Proteomics **11**(4): M111 015313.

Nakagawara, A. and M. Ohira (2004). "Comprehensive genomics linking between neural development and cancer: neuroblastoma as a model." Cancer Lett **204**(2): 213-224.

Nelson, J. W. and R. R. Breaker (2017). "The lost language of the RNA World." Sci Signal **10**(483).

Noguchi, T., K. Akiyama, M. Yokoyama, N. Kanda, T. Matsunaga and Y. Nishi (1996). "Amplification of a DEAD box gene (DDX1) with the MYCN gene in neuroblastomas as a result of cosegregation of sequences flanking the MYCN locus." Genes Chromosomes Cancer **15**(2): 129-133.

Nothias, J. Y., S. Majumder, K. J. Kaneko and M. L. DePamphilis (1995). "Regulation of gene expression at the beginning of mammalian development." J Biol Chem **270**(38): 22077-22080.

Nothias, J. Y., M. Miranda and M. L. DePamphilis (1996). "Uncoupling of transcription and translation during zygotic gene activation in the mouse." EMBO J **15**(20): 5715-5725.

Ogushi, S., K. Yamagata, C. Obuse, K. Furuta, T. Wakayama, M. M. Matzuk and M. Saitou (2017). "Reconstitution of the oocyte nucleolus in mice through a single nucleolar protein, NPM2." J Cell Sci **130**(14): 2416-2429.

Ohle, C., R. Tesorero, G. Schermann, N. Dobrev, I. Sinning and T. Fischer (2016). "Transient RNA-DNA Hybrids Are Required for Efficient Double-Strand Break Repair." Cell **167**(4): 1001-1013 e1007.

Ohn, T., N. Kedersha, T. Hickman, S. Tisdale and P. Anderson (2008). "A functional RNAi screen links O-GlcNAc modification of ribosomal proteins to stress granule and processing body assembly." Nat Cell Biol **10**(10): 1224-1231.

Ohsugi, M., P. Zheng, B. Baibakov, L. Li and J. Dean (2008). "Maternally derived FILIA-MATER complex localizes asymmetrically in cleavage-stage mouse embryos." Development **135**(2): 259-269.

Olszanska, B. and A. Borgul (1993). "Maternal RNA content in oocytes of several mammalian and avian species." J Exp Zool **265**(3): 317-320.

Onishi, H., Y. Kino, T. Morita, E. Futai, N. Sasagawa and S. Ishiura (2008). "MBNL1 associates with YB-1 in cytoplasmic stress granules." J Neurosci Res **86**(9): 1994-2002.

Orban, T. I. and E. Izaurralde (2005). "Decay of mRNAs targeted by RISC requires XRN1, the Ski complex, and the exosome." RNA **11**(4): 459-469.

Oshikawa, K., M. Matsumoto, K. Oyamada and K. I. Nakayama (2012). "Proteome-wide identification of ubiquitylation sites by conjugation of engineered lysine-less ubiquitin." J Proteome Res **11**(2): 796-807.

Paillard, L., D. Maniey, P. Lachaume, V. Legagneux and H. B. Osborne (2000). "Identification of a C-rich element as a novel cytoplasmic polyadenylation element in Xenopus embryos." Mech Dev **93**(1-2): 117-125.

Pan, C. and R. Russell (2010). "Roles of DEAD-box proteins in RNA and RNP Folding." RNA Biol **7**(6): 667-676.

Pandita, A., R. Godbout, M. Zielenska, P. Thorner, J. Bayani and J. A. Squire (1997). "Relational mapping of MYCN and DDXI in band 2p24 and analysis of amplicon arrays in double minute chromosomes and homogeneously staining regions by use of free chromatin FISH." Genes Chromosomes Cancer **20**(3): 243-252.

Parkening, T. A. and M. C. Chang (1976). "Effects of wheat germ agglutinin on fertilization of mouse ova in vivo and in vitro." J Exp Zool **195**(2): 215-222.

Parker, D. M., L. P. Winkenbach, S. Boyson, M. N. Saxton, C. Daidone, Z. A. Al-Mazaydeh, M. T. Nishimura, F. Mueller and E. Osborne Nishimura (2020). "mRNA localization is linked to translation regulation in the Caenorhabditis elegans germ lineage." Development **147**(13).

Patergnani, S., J. M. Suski, C. Agnoletto, A. Bononi, M. Bonora, E. De Marchi, C. Giorgi, S. Marchi, S. Missiroli, F. Poletti, A. Rimessi, J. Duszynski, M. R. Wieckowski and P. Pinton (2011). "Calcium signaling around Mitochondria Associated Membranes (MAMs)." Cell Commun Signal **9**: 19.

Pattabiraman, S., C. Baumann, D. Guisado, J. J. Eppig, J. C. Schimenti and R. De La Fuente (2015). "Mouse BRWD1 is critical for spermatid postmeiotic transcription and female meiotic chromosome stability." J Cell Biol **208**(1): 53-69.

Peng, H., B. Chang, C. Lu, J. Su, Y. Wu, P. Lv, Y. Wang, J. Liu, B. Zhang, F. Quan, Z. Guo and Y. Zhang (2012). "Nlrp2, a maternal effect gene required for early embryonic development in the mouse." PLoS One **7**(1): e30344.

Peng, T. I. and M. J. Jou (2010). "Oxidative stress caused by mitochondrial calcium overload." Ann N Y Acad Sci **1201**: 183-188.

Pepling, M. E., J. E. Wilhelm, A. L. O'Hara, G. W. Gephardt and A. C. Spradling (2007). "Mouse oocytes within germ cell cysts and primordial follicles contain a Balbiani body." Proc Natl Acad Sci U S A **104**(1): 187-192.

Perez-Gonzalez, A., A. Pazo, R. Navajas, S. Ciordia, A. Rodriguez-Frandsen and A. Nieto (2014). "hCLE/C14orf166 associates with DDX1-HSPC117-FAM98B in a novel transcription-dependent shuttling RNA-transporting complex." PLoS One **9**(3): e90957.

Philipps, D. L., K. Wigglesworth, S. A. Hartford, F. Sun, S. Pattabiraman, K. Schimenti, M. Handel, J. J. Eppig and J. C. Schimenti (2008). "The dual bromodomain and WD repeat-containing mouse protein BRWD1 is required for normal spermiogenesis and the oocyte-embryo transition." Dev Biol **317**(1): 72-82.

Piecyk, M., S. Wax, A. R. Beck, N. Kedersha, M. Gupta, B. Maritim, S. Chen, C. Gueydan, V. Kruys, M. Streuli and P. Anderson (2000). "TIA-1 is a translational silencer that selectively regulates the expression of TNF-alpha." EMBO J **19**(15): 4154-4163.

Piko, L. and K. B. Clegg (1982). "Quantitative changes in total RNA, total poly(A), and ribosomes in early mouse embryos." Dev Biol **89**(2): 362-378.

Piko, L. and L. Matsumoto (1976). "Number of mitochondria and some properties of mitochondrial DNA in the mouse egg." Dev Biol **49**(1): 1-10.

Piko, L. and K. D. Taylor (1987). "Amounts of mitochondrial DNA and abundance of some mitochondrial gene transcripts in early mouse embryos." Dev Biol **123**(2): 364-374.

Pique, M., J. M. Lopez, S. Foissac, R. Guigo and R. Mendez (2008). "A combinatorial code for CPE-mediated translational control." Cell **132**(3): 434-448.

Poenie, M., J. Alderton, R. Y. Tsien and R. A. Steinhardt (1985). "Changes of free calcium levels with stages of the cell division cycle." Nature **315**(6015): 147-149.

Ponting, C., J. Schultz and P. Bork (1997). "SPRY domains in ryanodine receptors (Ca(2+)-release channels)." Trends Biochem Sci **22**(6): 193-194.

Popow, J., M. Englert, S. Weitzer, A. Schleiffer, B. Mierzwa, K. Mechtler, S. Trowitzsch, C. L. Will, R. Luhrmann, D. Soll and J. Martinez (2011). "HSPC117 is the essential subunit of a human tRNA splicing ligase complex." Science **331**(6018): 760-764.

Popow, J., J. Jurkin, A. Schleiffer and J. Martinez (2014). "Analysis of orthologous groups reveals archease and DDX1 as tRNA splicing factors." Nature **511**(7507): 104-107.

Protter, D. S. W. and R. Parker (2016). "Principles and Properties of Stress Granules." Trends Cell Biol **26**(9): 668-679.

Proudfoot, N. J. (2011). "Ending the message: poly(A) signals then and now." Genes Dev **25**(17): 1770-1782.

Proudfoot, N. J. and G. G. Brownlee (1976). "3' non-coding region sequences in eukaryotic messenger RNA." Nature **263**(5574): 211-214.

Proudfoot, N. J., A. Furger and M. J. Dye (2002). "Integrating mRNA processing with transcription." Cell **108**(4): 501-512.

Pushpalatha, K. V. and F. Besse (2019). "Local Translation in Axons: When Membraneless RNP Granules Meet Membrane-Bound Organelles." Front Mol Biosci **6**: 129.

Pyle, A. M. (2011). "RNA helicases and remodeling proteins." Curr Opin Chem Biol **15**(5): 636-642.

Qiao, Y., C. Ren, S. Huang, J. Yuan, X. Liu, J. Fan, J. Lin, S. Wu, Q. Chen, X. Bo, X. Li, X. Huang, Z. Liu and W. Shu (2020). "High-resolution annotation of the mouse preimplantation embryo transcriptome using long-read sequencing." Nat Commun **11**(1): 2653.

Que, E. L., R. Bleher, F. E. Duncan, B. Y. Kong, S. C. Gleber, S. Vogt, S. Chen, S. A. Garwin, A. R. Bayer, V. P. Dravid, T. K. Woodruff and T. V. O'Halloran (2015). "Quantitative mapping of zinc fluxes in the mammalian egg reveals the origin of fertilization-induced zinc sparks." Nat Chem **7**(2): 130-139.

Que, E. L., F. E. Duncan, A. R. Bayer, S. J. Philips, E. W. Roth, R. Bleher, S. C. Gleber, S. Vogt, T. K. Woodruff and T. V. O'Halloran (2017). "Zinc sparks induce physiochemical changes in the egg zona pellucida that prevent polyspermy." Integr Biol (Camb) **9**(2): 135-144.

Radford, H. E., H. A. Meijer and C. H. de Moor (2008). "Translational control by cytoplasmic polyadenylation in Xenopus oocytes." Biochim Biophys Acta **1779**(4): 217-229.

Raffaello, A., C. Mammucari, G. Gherardi and R. Rizzuto (2016). "Calcium at the Center of Cell Signaling: Interplay between Endoplasmic Reticulum, Mitochondria, and Lysosomes." Trends Biochem Sci **41**(12): 1035-1049.

Ramos, S. B., D. J. Stumpo, E. A. Kennington, R. S. Phillips, C. B. Bock, F. Ribeiro-Neto and P. J. Blackshear (2004). "The CCCH tandem zinc-finger protein Zfp36l2 is crucial for female fertility and early embryonic development." Development **131**(19): 4883-4893.

Rappsilber, J., U. Ryder, A. I. Lamond and M. Mann (2002). "Large-scale proteomic analysis of the human spliceosome." Genome Res **12**(8): 1231-1245.

Reader, K. L., J. L. Stanton and J. L. Juengel (2017). "The Role of Oocyte Organelles in Determining Developmental Competence." Biology (Basel) **6**(3).

Rhodes, D. A., B. de Bono and J. Trowsdale (2005). "Relationship between SPRY and B30.2 protein domains. Evolution of a component of immune defence?" Immunology **116**(4): 411-417.

Ribeiro de Almeida, C., S. Dhir, A. Dhir, A. E. Moghaddam, Q. Sattentau, A. Meinhart and N. J. Proudfoot (2018). "RNA Helicase DDX1 Converts RNA G-Quadruplex Structures into R-Loops to Promote IgH Class Switch Recombination." Mol Cell **70**(4): 650-662 e658.

Richter, J. D. (1999). "Cytoplasmic polyadenylation in development and beyond." Microbiol Mol Biol Rev **63**(2): 446-456.

Richter, J. D. (2007). "CPEB: a life in translation." Trends Biochem Sci **32**(6): 279-285.

Rigby, R. E., L. M. Webb, K. J. Mackenzie, Y. Li, A. Leitch, M. A. Reijns, R. J. Lundie, A. Revuelta, D. J. Davidson, S. Diebold, Y. Modis, A. S. MacDonald and

A. P. Jackson (2014). "RNA:DNA hybrids are a novel molecular pattern sensed by TLR9." EMBO J **33**(6): 542-558.

Robertson-Anderson, R. M., J. Wang, S. P. Edgcomb, A. B. Carmel, J. R. Williamson and D. P. Millar (2011). "Single-molecule studies reveal that DEAD box protein DDX1 promotes oligomerization of HIV-1 Rev on the Rev response element." J Mol Biol **410**(5): 959-971.

Roest, H. P., W. M. Baarends, J. de Wit, J. W. van Klaveren, E. Wassenaar, J. W. Hoogerbrugge, W. A. van Cappellen, J. H. Hoeijmakers and J. A. Grootegoed (2004). "The ubiquitin-conjugating DNA repair enzyme HR6A is a maternal factor essential for early embryonic development in mice." Mol Cell Biol **24**(12): 5485-5495.

Rogers, G. W., Jr., N. J. Richter and W. C. Merrick (1999). "Biochemical and kinetic characterization of the RNA helicase activity of eukaryotic initiation factor 4A." J Biol Chem **274**(18): 12236-12244.

Rossler, O. G., A. Straka and H. Stahl (2001). "Rearrangement of structured RNA via branch migration structures catalysed by the highly related DEAD-box proteins p68 and p72." Nucleic Acids Res **29**(10): 2088-2096.

Rostovtseva, T. K., W. Tan and M. Colombini (2005). "On the role of VDAC in apoptosis: fact and fiction." J Bioenerg Biomembr **37**(3): 129-142.

Rozen, F., I. Edery, K. Meerovitch, T. E. Dever, W. C. Merrick and N. Sonenberg (1990). "Bidirectional RNA helicase activity of eucaryotic translation initiation factors 4A and 4F." Mol Cell Biol **10**(3): 1134-1144.

Sasaki, M., M. Ohnishi, F. Tashiro, H. Niwa, A. Suzuki, J. Miyazaki, T. Kobayashi and S. Tamura (2007). "Disruption of the mouse protein Ser/Thr phosphatase 2Cbeta gene leads to early pre-implantation lethality." Mech Dev **124**(6): 489-499.

Sato, T., J. Fukuda, K. Kawamura, H. Kodama, J. Kumagai and T. Tanaka (2008). "Dynamics of Maternal Survivin mRNA in Mouse Oocytes and Pre-implantation Embryos." Journal of Mammalian Ova Research **25**(3): 184-192.

Saunders, C. M., M. G. Larman, J. Parrington, L. J. Cox, J. Royse, L. M. Blayney, K. Swann and F. A. Lai (2002). "PLC zeta: a sperm-specific trigger of Ca(2+) oscillations in eggs and embryo development." Development **129**(15): 3533-3544.

Schmidt, E. E., E. S. Hanson and M. R. Capecchi (1999). "Sequence-independent assembly of spermatid mRNAs into messenger ribonucleoprotein particles." Mol Cell Biol **19**(5): 3904-3915.

Schonemann, L., U. Kuhn, G. Martin, P. Schafer, A. R. Gruber, W. Keller, M. Zavolan and E. Wahle (2014). "Reconstitution of CPSF active in polyadenylation: recognition of the polyadenylation signal by WDR33." Genes Dev **28**(21): 2381-2393.

Schul, W., I. van Der Kraan, A. G. Matera, R. van Driel and L. de Jong (1999). "Nuclear domains enriched in RNA 3'-processing factors associate with coiled bodies and histone genes in a cell cycle-dependent manner." Mol Biol Cell **10**(11): 3815-3824.

Schultz, R. M. (1993). "Regulation of zygotic gene activation in the mouse." Bioessays **15**(8): 531-538.

Schultz, R. M. (2002). "The molecular foundations of the maternal to zygotic transition in the preimplantation embryo." Hum Reprod Update **8**(4): 323-331.

Schutz, P., M. Bumann, A. E. Oberholzer, C. Bieniossek, H. Trachsel, M. Altmann and U. Baumann (2008). "Crystal structure of the yeast eIF4A-eIF4G complex: an RNA-helicase controlled by protein-protein interactions." Proc Natl Acad Sci U S A **105**(28): 9564-9569.

Schutz, P., T. Karlberg, S. van den Berg, R. Collins, L. Lehtio, M. Hogbom, L. Holmberg-Schiavone, W. Tempel, H. W. Park, M. Hammarstrom, M. Moche, A. G. Thorsell and H. Schuler (2010). "Comparative structural analysis of human DEAD-box RNA helicases." PLoS One **5**(9).

Seal, S. N., A. Schmidt and A. Marcus (1983). "Eukaryotic initiation factor 4A is the component that interacts with ATP in protein chain initiation." Proc Natl Acad Sci U S A **80**(21): 6562-6565.

Sengoku, T., O. Nureki, A. Nakamura, S. Kobayashi and S. Yokoyama (2006). "Structural basis for RNA unwinding by the DEAD-box protein Drosophila Vasa." Cell **125**(2): 287-300.

Sengupta, M. S. and P. R. Boag (2012). "Germ granules and the control of mRNA translation." IUBMB Life **64**(7): 586-594.

Serman, A., F. Le Roy, C. Aigueperse, M. Kress, F. Dautry and D. Weil (2007). "GW body disassembly triggered by siRNAs independently of their silencing activity." Nucleic Acids Res **35**(14): 4715-4727.

Sha, Q. Q., W. Zheng, Y. W. Wu, S. Li, L. Guo, S. Zhang, G. Lin, X. H. Ou and H. Y. Fan (2020). "Dynamics and clinical relevance of maternal mRNA clearance during the oocyte-to-embryo transition in humans." Nat Commun **11**(1): 4917.

Shi, Y. and J. L. Manley (2015). "The end of the message: multiple protein-RNA interactions define the mRNA polyadenylation site." Genes Dev **29**(9): 889-897.

Shih, J. W. and Y. H. Lee (2014). "Human DExD/H RNA helicases: emerging roles in stress survival regulation." Clin Chim Acta **436**: 45-58.

Shih, J. W., W. T. Wang, T. Y. Tsai, C. Y. Kuo, H. K. Li and Y. H. Wu Lee (2012). "Critical roles of RNA helicase DDX3 and its interactions with eIF4E/PABP1 in stress granule assembly and stress response." Biochem J **441**(1): 119-129.

Shu, J., L. L. Xing, G. L. Ding, X. M. Liu, Q. F. Yan and H. F. Huang (2015). "Effects of ovarian hyperstimulation on mitochondria in oocytes and early embryos." Reprod Fertil Dev.

Singh, A. P., J. F. Foley, M. Rubino, M. C. Boyle, A. Tandon, R. Shah and T. K. Archer (2016). "Brg1 Enables Rapid Growth of the Early Embryo by Suppressing Genes That Regulate Apoptosis and Cell Growth Arrest." Mol Cell Biol **36**(15): 1990-2010.

Song, X., F. Ma and K. Herrup (2019). "Accumulation of Cytoplasmic DNA Due to ATM Deficiency Activates the Microglial Viral Response System with Neurotoxic Consequences." J Neurosci **39**(32): 6378-6394.

Soto-Rifo, R., P. S. Rubilar, T. Limousin, S. de Breyne, D. Decimo and T. Ohlmann (2012). "DEAD-box protein DDX3 associates with eIF4F to promote translation of selected mRNAs." EMBO J **31**(18): 3745-3756.

Spiegelman, M. and D. Bennett (1973). "A light- and electron-microscopic study of primordial germ cells in the early mouse embryo." J Embryol Exp Morphol **30**(1): 97-118.

Squire, J. A., P. S. Thorner, S. Weitzman, J. D. Maggi, P. Dirks, J. Doyle, M. Hale and R. Godbout (1995). "Co-amplification of MYCN and a DEAD box gene (DDX1) in primary neuroblastoma." Oncogene **10**(7): 1417-1422.

Stein, P., N. V. Rozhkov, F. Li, F. L. Cardenas, O. Davydenko, L. E. Vandivier, B. D. Gregory, G. J. Hannon and R. M. Schultz (2015). "Essential Role for endogenous siRNAs during meiosis in mouse oocytes." PLoS Genet **11**(2): e1005013.

Steinhardt, R. A. and J. Alderton (1988). "Intracellular free calcium rise triggers nuclear envelope breakdown in the sea urchin embryo." Nature **332**(6162): 364-366.

Stephenson, R. O., Y. Yamanaka and J. Rossant (2010). "Disorganized epithelial polarity and excess trophectoderm cell fate in preimplantation embryos lacking E-cadherin." Development **137**(20): 3383-3391.

Stoecklin, G. and N. Kedersha (2013). "Relationship of GW/P-bodies with stress granules." Adv Exp Med Biol **768**: 197-211.

Story, R. M., H. Li and J. N. Abelson (2001). "Crystal structure of a DEAD box protein from the hyperthermophile Methanococcus jannaschii." Proc Natl Acad Sci U S A **98**(4): 1465-1470.

Subtelny, A. O., S. W. Eichhorn, G. R. Chen, H. Sive and D. P. Bartel (2014). "Poly(A)-tail profiling reveals an embryonic switch in translational control." Nature **508**(7494): 66-71.

Suh, N., L. Baehner, F. Moltzahn, C. Melton, A. Shenoy, J. Chen and R. Blelloch (2010). "MicroRNA function is globally suppressed in mouse oocytes and early embryos." Curr Biol **20**(3): 271-277.

Sullivan, K. D., M. Steiniger and W. F. Marzluff (2009). "A core complex of CPSF73, CPSF100, and Symplekin may form two different cleavage factors for processing of poly(A) and histone mRNAs." Mol Cell **34**(3): 322-332.

Sunden, Y., S. Semba, T. Suzuki, Y. Okada, Y. Orba, K. Nagashima, T. Umemura and H. Sawa (2007). "DDX1 promotes proliferation of the JC virus through transactivation of its promoter." Microbiol Immunol **51**(3): 339-347.

Sunden, Y., S. Semba, T. Suzuki, Y. Okada, Y. Orba, K. Nagashima, T. Umemura and H. Sawa (2007). "Identification of DDX1 as a JC virus transcriptional control region-binding protein." Microbiol Immunol **51**(3): 327-337.

Suzuki, R. and H. Shimodaira (2006). "Pvclust: an R package for assessing the uncertainty in hierarchical clustering." Bioinformatics **22**(12): 1540-1542.

Svoboda, P. (2017). "Long and small noncoding RNAs during oocyte-to-embryo transition in mammals." Biochem Soc Trans **45**(5): 1117-1124.

Szabadkai, G., K. Bianchi, P. Varnai, D. De Stefani, M. R. Wieckowski, D. Cavagna, A. I. Nagy, T. Balla and R. Rizzuto (2006). "Chaperone-mediated coupling of endoplasmic reticulum and mitochondrial Ca2+ channels." J Cell Biol **175**(6): 901-911.

Szent-Gyorgyi, A. G. (1975). "Calcium regulation of muscle contraction." Biophys J **15**(7): 707-723.

Tadros, W. and H. D. Lipshitz (2009). "The maternal-to-zygotic transition: a play in two acts." Development **136**(18): 3033-3042.

Tae, H., M. G. Casarotto and A. F. Dulhunty (2009). "Ubiquitous SPRY domains and their role in the skeletal type ryanodine receptor." Eur Biophys J **39**(1): 51-59.

Talwar, T., V. Vidhyasagar, J. Qing, M. Guo, A. Kariem, Y. Lu, R. S. Singh, K. E. Lukong and Y. Wu (2017). "The DEAD-box protein DDX43 (HAGE) is a dual RNA-DNA helicase and has a K-homology domain required for full nucleic acid unwinding activity." J Biol Chem **292**(25): 10429-10443.

Tang, F., M. Kaneda, D. O'Carroll, P. Hajkova, S. C. Barton, Y. A. Sun, C. Lee, A. Tarakhovsky, K. Lao and M. A. Surani (2007). "Maternal microRNAs are essential for mouse zygotic development." Genes Dev **21**(6): 644-648.

Tang, P. Z., C. H. Tsai-Morris and M. L. Dufau (1999). "A novel gonadotropin-regulated testicular RNA helicase. A new member of the dead-box family." J Biol Chem **274**(53): 37932-37940.

Tanner, N. K. (2003). "The newly identified Q motif of DEAD box helicases is involved in adenine recognition." Cell Cycle **2**(1): 18-19.

Tarun, S. Z., Jr., S. E. Wells, J. A. Deardorff and A. B. Sachs (1997). "Translation initiation factor eIF4G mediates in vitro poly(A) tail-dependent translation." Proc Natl Acad Sci U S A **94**(17): 9046-9051.

Tazi-Ahnini, R., J. Henry, C. Offer, C. Bouissou-Bouchouata, I. H. Mather and P. Pontarotti (1997). "Cloning, localization, and structure of new members of the butyrophilin gene family in the juxta-telomeric region of the major histocompatibility complex." Immunogenetics **47**(1): 55-63.

Telford, N. A., A. J. Watson and G. A. Schultz (1990). "Transition from maternal to embryonic control in early mammalian development: a comparison of several species." Mol Reprod Dev **26**(1): 90-100.

Theofilopoulos, A. N., D. H. Kono, B. Beutler and R. Baccala (2011). "Intracellular nucleic acid sensors and autoimmunity." J Interferon Cytokine Res **31**(12): 867-886.

Thomas, P. D., M. J. Campbell, A. Kejariwal, H. Mi, B. Karlak, R. Daverman, K. Diemer, A. Muruganujan and A. Narechania (2003). "PANTHER: a library of protein families and subfamilies indexed by function." Genome Res **13**(9): 2129-2141.

Tian, B., J. Hu, H. Zhang and C. S. Lutz (2005). "A large-scale analysis of mRNA polyadenylation of human and mouse genes." Nucleic Acids Res **33**(1): 201-212.

Tichy, D., J. M. A. Pickl, A. Benner and H. Sultmann (2018). "Experimental design and data analysis of Ago-RIP-Seq experiments for the identification of microRNA targets." Brief Bioinform **19**(5): 918-929.

Tirode, F., D. Busso, F. Coin and J. M. Egly (1999). "Reconstitution of the transcription factor TFIIH: assignment of functions for the three enzymatic subunits, XPB, XPD, and cdk7." Mol Cell **3**(1): 87-95.

Tombes, R. M., M. O. Faison and J. M. Turbeville (2003). "Organization and evolution of multifunctional Ca(2+)/CaM-dependent protein kinase genes." Gene **322**: 17-31.

Tombes, R. M., C. Simerly, G. G. Borisy and G. Schatten (1992). "Meiosis, egg activation, and nuclear envelope breakdown are differentially reliant on Ca2+, whereas germinal vesicle breakdown is Ca2+ independent in the mouse oocyte." J Cell Biol **117**(4): 799-811.

Tong, Z. B., L. Gold, K. E. Pfeifer, H. Dorward, E. Lee, C. A. Bondy, J. Dean and L. M. Nelson (2000). "Mater, a maternal effect gene required for early embryonic development in mice." Nat Genet **26**(3): 267-268.

Torres-Padilla, M. E. and M. Zernicka-Goetz (2006). "Role of TIF1alpha as a modulator of embryonic transcription in the mouse zygote." J Cell Biol **174**(3): 329-338.

Tran, E. J., Y. Zhou, A. H. Corbett and S. R. Wente (2007). "The DEAD-box protein Dbp5 controls mRNA export by triggering specific RNA:protein remodeling events." Mol Cell **28**(5): 850-859.

Tritschler, F., J. E. Braun, A. Eulalio, V. Truffault, E. Izaurralde and O. Weichenrieder (2009). "Structural basis for the mutually exclusive anchoring of P body components EDC3 and Tral to the DEAD box protein DDX6/Me31B." Mol Cell **33**(5): 661-668.

Van Blerkom, J. (2004). "Mitochondria in human oogenesis and preimplantation embryogenesis: engines of metabolism, ionic regulation and developmental competence." Reproduction **128**(3): 269-280.

Van Blerkom, J. and P. Davis (2006). "High-polarized (Delta Psi m(HIGH)) mitochondria are spatially polarized in human oocytes and early embryos in stable subplasmalemmal domains: developmental significance and the concept of vanguard mitochondria." Reprod Biomed Online **13**(2): 246-254.

Van Blerkom, J., P. Davis and S. Alexander (2003). "Inner mitochondrial membrane potential (DeltaPsim), cytoplasmic ATP content and free Ca2+ levels in metaphase II mouse oocytes." Hum Reprod **18**(11): 2429-2440.

Van Blerkom, J., P. Davis, V. Mathwig and S. Alexander (2002). "Domains of high-polarized and low-polarized mitochondria may occur in mouse and human oocytes and early embryos." Hum Reprod **17**(2): 393-406.

Van Blerkom, J. and M. N. Runner (1984). "Mitochondrial reorganization during resumption of arrested meiosis in the mouse oocyte." Am J Anat **171**(3): 335-355.

Van Vranken, J. G., D. K. Bricker, N. Dephoure, S. P. Gygi, J. E. Cox, C. S. Thummel and J. Rutter (2014). "SDHAF4 promotes mitochondrial succinate dehydrogenase activity and prevents neurodegeneration." Cell Metab **20**(2): 241-252.

Vassena, R., S. Boue, E. Gonzalez-Roca, B. Aran, H. Auer, A. Veiga and J. C. Izpisua Belmonte (2011). "Waves of early transcriptional activation and pluripotency program initiation during human preimplantation development." Development **138**(17): 3699-3709.

Vestweber, D., A. Gossler, K. Boller and R. Kemler (1987). "Expression and distribution of cell adhesion molecule uvomorulin in mouse preimplantation embryos." Dev Biol **124**(2): 451-456.

Vieux, K. F. and H. J. Clarke (2018). "CNOT6 regulates a novel pattern of mRNA deadenylation during oocyte meiotic maturation." Sci Rep **8**(1): 6812.

Vishnu, M. R., M. Sumaroka, P. S. Klein and S. A. Liebhaber (2011). "The poly(rC)-binding protein alphaCP2 is a noncanonical factor in X. laevis cytoplasmic polyadenylation." RNA **17**(5): 944-956.

Vitali, P. and T. Kiss (2019). "Cooperative 2'-O-methylation of the wobble cytidine of human elongator tRNA(Met)(CAT) by a nucleolar and a Cajal body-specific box C/D RNP." Genes Dev **33**(13-14): 741-746.

Voronina, E., G. Seydoux, P. Sassone-Corsi and I. Nagamori (2011). "RNA granules in germ cells." Cold Spring Harb Perspect Biol **3**(12).

Wakai, T., N. Zhang, P. Vangheluwe and R. A. Fissore (2013). "Regulation of endoplasmic reticulum Ca(2+) oscillations in mammalian eggs." J Cell Sci **126**(Pt 24): 5714-5724.

Wang, F., T. G. Meng, J. Li, Y. Hou, S. M. Luo, H. Schatten, Q. Y. Sun and X. H. Ou (2020). "Mitochondrial Ca(2 +) Is Related to Mitochondrial Activity and Dynamic Events in Mouse Oocytes." Front Cell Dev Biol **8**: 585932.

Wang, H., J. Luo, C. Carlton, L. K. McGinnis and W. H. Kinsey (2017). "Sperm-oocyte contact induces outside-in signaling via PYK2 activation." Dev Biol **428**(1): 52-62.

Wang, J. J., W. Ge, J. C. Liu, F. G. Klinger, P. W. Dyce, M. De Felici and W. Shen (2017). "Complete in vitro oogenesis: retrospects and prospects." Cell Death Differ **24**(11): 1845-1852.

Wang, Q. T., K. Piotrowska, M. A. Ciemerych, L. Milenkovic, M. P. Scott, R. W. Davis and M. Zernicka-Goetz (2004). "A genome-wide study of gene activity reveals developmental signaling pathways in the preimplantation mouse embryo." Dev Cell **6**(1): 133-144.

Wassarman, P., J. Chen, N. Cohen, E. Litscher, C. Liu, H. Qi and Z. Williams (1999). "Structure and function of the mammalian egg zona pellucida." J Exp Zool **285**(3): 251-258.

Wassler, M., I. Jonasson, R. Persson and E. Fries (1987). "Differential permeabilization of membranes by saponin treatment of isolated rat hepatocytes. Release of secretory proteins." Biochem J **247**(2): 407-415.

Watanabe, T., A. Thayil, A. Jesacher, K. Grieve, D. Debarre, T. Wilson, M. Booth and S. Srinivas (2010). "Characterisation of the dynamic behaviour of lipid droplets in the early mouse embryo using adaptive harmonic generation microscopy." BMC Cell Biol **11**: 38.

Weber, A., P. Imisch, E. Bergmann and H. Christiansen (2004). "Coamplification of DDX1 correlates with an improved survival probability in children with MYCN-amplified human neuroblastoma." J Clin Oncol **22**(13): 2681-2690.

Whitaker, M. (2008). "Calcium signalling in early embryos." Philos Trans R Soc Lond B Biol Sci **363**(1495): 1401-1418.

Wilson, T. E., U. Grawunder and M. R. Lieber (1997). "Yeast DNA ligase IV mediates non-homologous DNA end joining." Nature **388**(6641): 495-498.

Winata, C. L. and V. Korzh (2018). "The translational regulation of maternal mRNAs in time and space." FEBS Lett **592**(17): 3007-3023.

Winata, C. L., M. Lapinski, L. Pryszcz, C. Vaz, M. H. Bin Ismail, S. Nama, H. S. Hajan, S. G. P. Lee, V. Korzh, P. Sampath, V. Tanavde and S. Mathavan (2018). "Cytoplasmic polyadenylation-mediated translational control of maternal mRNAs directs maternal-to-zygotic transition." Development **145**(1).

Witke, W., J. D. Sutherland, A. Sharpe, M. Arai and D. J. Kwiatkowski (2001). "Profilin I is essential for cell survival and cell division in early mouse development." Proc Natl Acad Sci U S A **98**(7): 3832-3836.

Woo, J. S., H. Y. Suh, S. Y. Park and B. H. Oh (2006). "Structural basis for protein recognition by B30.2/SPRY domains." Mol Cell **24**(6): 967-976.

Worrad, D. M., P. T. Ram and R. M. Schultz (1994). "Regulation of gene expression in the mouse oocyte and early preimplantation embryo: developmental changes in Sp1 and TATA box-binding protein, TBP." Development **120**(8): 2347-2357.

Wright, W. D., S. S. Shah and W. D. Heyer (2018). "Homologous recombination and the repair of DNA double-strand breaks." J Biol Chem **293**(27): 10524-10535.

Wu, C. H., P. J. Chen and S. H. Yeh (2014). "Nucleocapsid phosphorylation and RNA helicase DDX1 recruitment enables coronavirus transition from discontinuous to continuous transcription." Cell Host Microbe **16**(4): 462-472.

Wu, X., M. M. Viveiros, J. J. Eppig, Y. Bai, S. L. Fitzpatrick and M. M. Matzuk (2003). "Zygote arrest 1 (Zar1) is a novel maternal-effect gene critical for the oocyte-to-embryo transition." Nat Genet **33**(2): 187-191.

Xie, F., K. A. Timme and J. R. Wood (2018). "Using Single Molecule mRNA Fluorescent in Situ Hybridization (RNA-FISH) to Quantify mRNAs in Individual Murine Oocytes and Embryos." Sci Rep **8**(1): 7930.

Xu, L., S. Khadijah, S. Fang, L. Wang, F. P. Tay and D. X. Liu (2010). "The cellular RNA helicase DDX1 interacts with coronavirus nonstructural protein 14 and enhances viral replication." J Virol **84**(17): 8571-8583.

Xu, Y., Y. Shi, J. Fu, M. Yu, R. Feng, Q. Sang, B. Liang, B. Chen, R. Qu, B. Li, Z. Yan, X. Mao, Y. Kuang, L. Jin, L. He, X. Sun and L. Wang (2016). "Mutations in PADI6 Cause Female Infertility Characterized by Early Embryonic Arrest." Am J Hum Genet **99**(3): 744-752.

Xu, Y. N., X. H. Shen, S. E. Lee, J. S. Kwon, D. J. Kim, Y. T. Heo, X. S. Cui and N. H. Kim (2012). "Autophagy influences maternal mRNA degradation and apoptosis in porcine parthenotes developing in vitro." J Reprod Dev **58**(5): 576-584.

Yamamoto, T. M., J. M. Cook, C. V. Kotter, T. Khat, K. D. Silva, M. Ferreyros, J. W. Holt, J. D. Knight and A. Charlesworth (2013). "Zar1 represses translation in Xenopus oocytes and binds to the TCS in maternal mRNAs with different characteristics than Zar2." Biochim Biophys Acta **1829**(10): 1034-1046.

Yan, X., J. F. Mouillet, Q. Ou and Y. Sadovsky (2003). "A novel domain within the DEAD-box protein DP103 is essential for transcriptional repression and helicase activity." Mol Cell Biol **23**(1): 414-423.

Yang, Q. and S. Doublie (2011). "Structural biology of poly(A) site definition." Wiley Interdiscip Rev RNA **2**(5): 732-747.

Yang, Q., J. Lin, M. Liu, R. Li, B. Tian, X. Zhang, B. Xu, M. Liu, X. Zhang, Y. Li, H. Shi and L. Wu (2016). "Highly sensitive sequencing reveals dynamic modifications and activities of small RNAs in mouse oocytes and early embryos." Sci Adv **2**(6): e1501482.

Yasuda-Inoue, M., M. Kuroki and Y. Ariumi (2013). "Distinct DDX DEAD-box RNA helicases cooperate to modulate the HIV-1 Rev function." Biochem Biophys Res Commun **434**(4): 803-808.

Yedavalli, V. S., C. Neuveut, Y. H. Chi, L. Kleiman and K. T. Jeang (2004). "Requirement of DDX3 DEAD box RNA helicase for HIV-1 Rev-RRE export function." Cell **119**(3): 381-392.

Yin, Y., L. Zhou and S. Yuan (2018). "Enigma of Retrotransposon Biology in Mammalian Early Embryos and Embryonic Stem Cells." Stem Cells Int **2018**: 6239245.

Yu, C., S. Y. Ji, Q. Q. Sha, Y. Dang, J. J. Zhou, Y. L. Zhang, Y. Liu, Z. W. Wang, B. Hu, Q. Y. Sun, S. C. Sun, F. Tang and H. Y. Fan (2016). "BTG4 is a meiotic cell cycle-coupled maternal-zygotic-transition licensing factor in oocytes." Nat Struct Mol Biol **23**(5): 387-394.

Yurttas, P., A. M. Vitale, R. J. Fitzhenry, L. Cohen-Gould, W. Wu, J. A. Gossen and S. A. Coonrod (2008). "Role for PADI6 and the cytoplasmic lattices in ribosomal storage in oocytes and translational control in the early mouse embryo." Development **135**(15): 2627-2636.

Zeng, F. and R. M. Schultz (2005). "RNA transcript profiling during zygotic gene activation in the preimplantation mouse embryo." Dev Biol **283**(1): 40-57.

Zhang, B., H. Zheng, B. Huang, W. Li, Y. Xiang, X. Peng, J. Ming, X. Wu, Y. Zhang, Q. Xu, W. Liu, X. Kou, Y. Zhao, W. He, C. Li, B. Chen, Y. Li, Q. Wang, J. Ma, Q. Yin, K. Kee, A. Meng, S. Gao, F. Xu, J. Na and W. Xie (2016). "Allelic reprogramming of the histone modification H3K4me3 in early mammalian development." Nature **537**(7621): 553-557.

Zhang, C. H., W. P. Qian, S. T. Qi, Z. J. Ge, L. J. Min, X. L. Zhu, X. Huang, J. P. Liu, Y. C. Ouyang, Y. Hou, H. Schatten and Q. Y. Sun (2013). "Maternal diabetes causes abnormal dynamic changes of endoplasmic reticulum during mouse oocyte maturation and early embryo development." Reprod Biol Endocrinol **11**: 31.

Zhang, D., C. Liu, H. Li and J. Jiao (2020). "Deficiency of STING Signaling in Embryonic Cerebral Cortex Leads to Neurogenic Abnormalities and Autistic-Like Behaviors." Adv Sci (Weinh) **7**(23): 2002117.

Zhang, J. M., W. B. Hou, J. W. Du, M. Zong, K. L. Zheng, W. J. Wang, J. Q. Wang, H. Zhang, Y. S. Mu, Z. Yin, C. M. Ding, Q. Y. Sun, Z. H. Liu and Q. R. Kong (2020). "Argonaute 2 is a key regulator of maternal mRNA degradation in mouse early embryos." Cell Death Discov **6**(1): 133.

Zheng, H., B. Huang, B. Zhang, Y. Xiang, Z. Du, Q. Xu, Y. Li, Q. Wang, J. Ma, X. Peng, F. Xu and W. Xie (2016). "Resetting Epigenetic Memory by Reprogramming of Histone Modifications in Mammals." Mol Cell **63**(6): 1066-1079.

Zheng, P., R. D. Schramm and K. E. Latham (2005). "Developmental regulation and in vitro culture effects on expression of DNA repair and cell cycle checkpoint control genes in rhesus monkey oocytes and embryos." Biol Reprod **72**(6): 1359-1369.

Zheng, W., Z. Zhou, Q. Sha, X. Niu, X. Sun, J. Shi, L. Zhao, S. Zhang, J. Dai, S. Cai, F. Meng, L. Hu, F. Gong, X. Li, J. Fu, R. Shi, G. Lu, B. Chen, H. Fan, L. Wang, G. Lin and Q. Sang (2020). "Homozygous Mutations in BTG4 Cause Zygotic Cleavage Failure and Female Infertility." Am J Hum Genet **107**(1): 24-33.

Zheng, X., P. Yang, B. Lackford, B. D. Bennett, L. Wang, H. Li, Y. Wang, Y. Miao, J. F. Foley, D. C. Fargo, Y. Jin, C. J. Williams, R. Jothi and G. Hu (2016). "CNOT3-Dependent mRNA Deadenylation Safeguards the Pluripotent State." Stem Cell Reports **7**(5): 897-910.

Zinder, J. C. and C. D. Lima (2017). "Targeting RNA for processing or destruction by the eukaryotic RNA exosome and its cofactors." Genes Dev **31**(2): 88-100.